VOLUME 78 JUNE 6, 1974 NUMBER 12

JPCHAx

THE JOURNAL OF PHYSICAL CHEMISTRY

PUBLISHED BIWEEKLY BY THE AMERICAN CHEMICAL SOCIETY

THE JOURNAL OF

PHYSICAL CHEMISTRY

AMERICAN CHEMICAL SOCIETY, *1155 Sixteenth St., N.W., Washington, D. C. 20036*

Books and Journals Division

JOHN K CRUM *Director*
RUTH REYNARD *Assistant to the Director*

CHARLES R. BERTSCH *Head, Editorial Processing Department*
D. H. MICHAEL BOWEN *Head, Journals Department*
BACIL GUILEY *Head, Graphics and Production Department*
SELDON W. TERRANT *Head, Research and Development Department*

All manuscripts should be sent to *The Journal of Physical Chemistry*, Department of Chemistry, University of Minnesota, Minneapolis, Minn. 55455.

Additions and Corrections are published once yearly in the final issue. See Volume 77, Number 26 for the proper form.

Extensive or unusual alterations in an article after it has been set in type are made at the author's expense, and it is understood that by requesting such alterations the author agrees to defray the cost thereof.

The American Chemical Society and the Editor of *The Journal of Physical Chemistry* assume no responsibility for the statements and opinions advanced by contributors.

Correspondence regarding accepted copy, proofs, and reprints should be directed to Editorial Processing Department, American Chemical Society, 20th and Northampton Sts., Easton, Pa. 18042. Head: CHARLES R. BERTSCH. Editorial Assistant: JOSEPH E. YURVATI.

Advertising Office: Centcom, Ltd., 50 W. State St., Westport, Conn. 06880.

Business and Subscription Information

Send all new and renewal subscriptions *with payment* to: Office of the Controller, 1155 16th Street, N.W., Washington, D. C. 20036. Subscriptions should be renewed promptly to avoid a break in your series. All correspondence and telephone calls regarding changes of address, claims for missing issues, subscription service, the status of records, and accounts should be directed to Manager, Membership and Subscription Services, American Chemical Society, P.O. Box 3337, Columbus, Ohio 43210. Telephone (614) 421-7230.

On changes of address, include both old and new addresses with ZIP code numbers, accompanied by mailing label from a recent issue. Allow four weeks for change to become effective.

Claims for missing numbers will not be allowed (1) if loss was due to failure of notice of change in address to be received before the date specified, (2) if received more than sixty days from date of issue plus time normally required for postal delivery of journal and claim, or (3) if the reason for the claim is "issue missing from files."

Subscription rates (1974): members of the American Chemical Society, $20.00 for 1 year; to nonmembers, $60.00 for 1 year. Those interested in becoming members should write to the Admissions Department, American Chemical Society, 1155 Sixteenth St., N.W., Washington, D. C. 20036. Postage to Canada and countries in the Pan-American Union, $5.00; all other countries, $6.00. Air freight rates available on request. Single copies for current year: $3.00. Rates for back issues from Volume 56 to date are available from the Special Issues Sales Department, 1155 Sixteenth St., N.W., Washington, D. C. 20036.

Subscriptions to this and the other ACS periodical publications are available on microfilm. Supplementary material not printed in this journal is now available in microfiche form on a current subscription basis. For information on microfilm or microfiche subscriptions, write Special Issues Sales Department at the address above.

Notice to Authors printed in this issue.

THE JOURNAL OF

PHYSICAL CHEMISTRY

Volume 78, Number 12 June 6, 1974

JPCHAx 78 (12) 1137-1244 (1974)

ISSN 0022-3654

COMMUNICATIONS TO THE EDITOR

■ Supplementary material for this paper is available separately, in photocopy or microfiche form. Ordering information is given in the paper.

* In papers with more than one author, the asterisk indicates the name of the author to whom inquiries about the paper should be addressed.

AUTHOR INDEX

NOTICE TO AUTHORS

I. General Considerations

The Journal of Physical Chemistry is devoted to reporting both experimental and theoretical research dealing with fundamental aspects of physical chemistry. Space limitations necessitate giving preference to research articles dealing with previously unanswered basic questions in physical chemistry. Acceptable topics are those of general interest to physical chemists, especially work involving new concepts, techniques, and interpretations. Research that may lead to reexaminations of generally accepted views is, of course, welcome.

Authors reporting data should include an interpretation of the data and its relevance to the theories of the properties of matter. However, the discussion should be concise and to the point and excessive speculation is to be discouraged. Papers reporting redeterminations of existing data will be acceptable only if there is reasonable justification for repetition: for example, if the more recent or more accurate data lead to new questions or to a reexamination of well known theories. Manuscripts that are essentially applications of chemical data or reviews of the literature are, in general, not suitable for publication in *The Journal of Physical Chemistry*. Detailed comparisons of methods of data analysis will be considered only if the paper also contains original data, or if such comparison leads to a genesis of new ideas.

Authors should include an introductory statement outlining the scientific rationale for the research. The statement should clearly specify the questions for which answers are sought and the connection of the present work with previous work in the field. All manuscripts are subject to critical review. It is to be understood that the final decision relating to a manuscript's suitability rests solely with the editors.

Symposium papers are sometimes published as a group, but only after special arrangement with the editor.

Authors' attention is called to the "Handbook for Authors," available from the Special Issues Sales Department, American Chemical Society, 1155 Sixteenth St., N.W., Washington, D. C. 20036, in which pertinent material is to be found.

II. Types of Manuscripts

The Journal of Physical Chemistry publishes two types of manuscripts: *Articles* and *Communications*.

A. Articles should cover their subjects with thoroughness, clarity, and completeness. However, authors should also strive to make their *Articles* as concise as possible, avoiding unnecessary historical background. Abstracts to *Articles* should be brief—300 words is a maximum—and should serve to summarize the significant data and conclusions. The abstract should convey the essence of the *Article* to the reader.

B. Communications are of two types, *Letters* and *Comments*. Both types are restricted to three-quarters of a page (750 words or the equivalent) including tables, figures, and text, and both types of *Communications* are subject to critical review, but special efforts will be made to expedite publication.

Letters should report preliminary results whose immediate availability to the scientific community is deemed important, and whose topic is timely enough to justify the double publication that usually results from the publication of a *Letter*.

Comments include significant remarks on the work of others. The editors will generally permit the authors of the work being discussed to reply.

The category of *Notes* has been discontinued since the handling of such manuscripts was precisely the same as that of *Articles* save for the requirement of an Abstract, and since even a short *Article* will need an Abstract ultimately, it seems as well to ask the author to provide this. Short *Articles* will of course continue to be welcome contributions.

III. Introduction

All manuscripts submitted should contain brief introductory remarks describing the purpose of the work and giving sufficient background material to allow the reader to appreciate the state-of-knowledge at the time when the work was done. The introductory remarks in an *Article* should constitute the first section of the paper and should be labeled accordingly. In *Communications*, the introductory material should not be in such a separate section. To judge the appropriateness of the manuscript for *The Journal of Physical Chemistry*, the editors will place considerable weight on the author's intentions as stated in the Introduction.

IV. Microform Material

From time to time manuscripts involve extensive tables, graphs, spectra, mathematical derivations, expanded discussions of peripheral points, or other material which, though essential to the specialized reader who needs all the data or all the detail, does not help and often hinders the effective presentation of the work being reported. Such "microform material" can be included in the *microfilm* edition of this Journal, available in many scholarly libraries, and also in the *microfiche* edition in which the microfiche accompanies the printed issue. In some instances the microform material may *also* be included in the printed issue in *miniprint*, in which the manuscript pages are reproduced directly in reduced size, nine manuscript pages to a journal page. All microform material may be obtained directly by the interested reader at nominal cost, either in full size photocopy or in microfiche (in which miniprint material appears at standard reduction, *i.e.*, one manuscript page per microfiche frame). Authors are encouraged to make use of this resource, in the interest of shorter articles (which mean more rapid publication) and clearer more readable presentation.

Microform material should accompany a manuscript at the time of its original submission to an editor. It should be clipped together and attached at the end of the manuscript, along with a slip of paper clearly indicating that the material is "microform material." Copy for microform material

should preferably be on 8½ × 11 in. paper, and in no case on sheets larger than 11 × 14 in.; if typed it should be one and one-half spaced, and in any event the smallest character should be at least one-eighth inch in size; good contrast of black characters against a white background is required for clear photoprocess reproduction.

A paragraph should appear at the end of the paper indicating the nature of the material and the means by which the interested reader may obtain copies directly. The following is an example.

Microform Material Available. A listing of structure factor amplitudes will appear following these pages in the microform editions of this volume of the Journal. Photocopies of this material from this paper only, or microfiche (105 × 148 mm, 24× reduction, negatives) containing all material for the papers in this issue, may be obtained from the Journals Department, American Chemical Society, 1155 Sixteenth Street N.W., Washington, D. C. 20036. Remit check or money order for $0.00 for photocopy or $0.00 for microfiche, referring to code number JPC-00-0000.

The amount of money to be indicated in the blanks will be filled in by the Editorial Office at Easton, Pa., after the acceptance of an article.

V. Functions of Reviewers

The editors request the scientific advice of reviewers who are active in the area of research covered by the manuscript. The reviewers act only in an advisory capacity and the final decision concerning a manuscript is the responsibility of the editors. The reviewers are asked to comment not only on the scientific content, but also on the manuscript's suitability for *The Journal of Physical Chemistry.* With respect to *Communications,* the reviewers are asked to comment specifically on the urgency of publication. **Authors are encouraged to suggest, when submitting a manuscript, names of scientists who could give a disinterested and informed and helpful evaluation of the work.** All reviews are anonymous and the reviewing process is most effective if reviewers do not reveal their identities to the authors. An exception arises in connection with a manuscript submitted for publication in the form of a comment on the work of another author. Under such circumstances the first author will, in general, be allowed to review the communication and to write a rebuttal, if he so chooses. The rebuttal and the original communication may be published together in the same issue of the journal. Revised manuscripts are generally sent back to the original reviewers, who are asked to comment on the revisions. If only minor revisions are involved, the editors examine the revised manuscript in light of the recommendations of the reviewers without seeking further opinions. For the convenience of reviewers, authors are advised to indicate clearly, either in the manuscript or in a covering letter, the specific revisions that have been made.

VI. Submission of Manuscripts

All manuscripts must be submitted in triplicate to expedite handling. Manuscripts must be typewritten, double-spaced copy, on 8½ × 11 in. paper. Legal sized paper is not acceptable. Authors should be certain that copies of the manuscript are clearly reproduced and readable. **Authors submitting figures must include the original drawings or photographs thereof, plus three xerographic copies for review purposes. These reproductions of the figures should be on 8½ × 11 in. paper.** Graphs must be in black ink on white or blue paper. Figures and tables should be held to a minimum consistent with adequate presentation of information. All original data which the author deems pertinent must be submitted along with the manuscript. For example, a paper reporting a crystal structure should include structure factor tables for use by the reviewers.

All references and explanatory notes, formerly set up as footnotes on individual pages, are now grouped at the end of the article in a section called "References and Notes." They should be numbered consecutively in the order in which they are first mentioned in the text, and the complete list of notes and literature citations should appear at the end of the manuscript. Nomenclature should conform to that used in *Chemical Abstracts* and mathematical characters should be underlined for italics, Greek letters should be annotated, and subscripts and superscripts clearly marked.

Papers should not depend for their usefulness on unpublished material, and excessive reference to material in press is discouraged. References not readily available (*e.g.*, private technical reports, preprints, or articles in press) that are necessary for a complete review of the paper must be included with the manuscript for use by the reviewers.

VII. Revised Manuscripts

A manuscript sent back to an author for revision should be returned to the editor within 6 months; otherwise it will be considered withdrawn and treated as a new manuscript when and if it is returned. Revised manuscripts returned to the editor must be submitted in triplicate and all changes should be made by typewriter. **Unless the changes are very minor, all pages affected by revision must be retyped.** If revisions are so extensive that a new typescript of the manuscript is necessary, it is requested that a copy of the original manuscript be submitted along with the revised one.

VIII. Proofs and Reprints

Galley proofs, original manuscript, cut copy, and reprint order form are sent by the printer directly to the author who submitted the manuscript. The attention of the authors is directed to the instructions which accompany the proof, especially the requirement that all corrections, revisions, and additions be entered on the proof and not on the manuscript. Proofs should be checked against the manuscript (in particular all tables, equations, and formulas, since this is not done by the editor) and returned as soon as possible. No paper is released for printing until the author's proof has been received. Alterations in an article after it has been set in type are made at the author's expense, and it is understood that by entering such alterations on proofs the author agrees to defray the cost thereof. The filled-out reprint form must be returned with the proof, and if a price quotation is required by the author's organization a request for it should accompany the proof. Since reprinting is generally done from the journal press forms, all orders must be filed before press time. None can be accepted later, unless a previous request has been made to hold the type. Reprint shipments are made a month or more after publication, and bills are issued by the printer subsequent to shipment. Neither the editors nor the Washington office keeps any supply of reprints. Therefore, only the authors can be expected to meet requests for single copies of papers.

A page charge is assessed to cover in part the cost of publication. Although payment is expected, it is not a condition for publication. Articles are accepted or rejected only on the basis of merit, and the editor's decision to publish the paper is made before the charge is assessed. The charge per journal page is $50.

THE JOURNAL OF
PHYSICAL CHEMISTRY

VOLUME 78, NUMBER 12 JUNE 6, 1974

A Flash Photolysis–Resonance Fluorescence Kinetics Study of the Reaction S(^{3}P) + OCS

R. B. Klemm*[1] and D. D. Davis

Chemistry Department, University of Maryland, College Park, Maryland 20742 *(Received November 28, 1973)*

Publication costs assisted by NASA/GSFC Astrochemistry Branch

Using the technique of flash photolysis–resonance fluorescence, the reaction of ground-state atomic sulfur with carbonyl sulfide has been investigated over the temperature range 233–445°K. Over this temperature range, the experimental data were fitted to an Arrhenius equation of the form $k_1 = (1.52 \pm 0.20) \times 10^{-12} \exp(-3.63 \pm 0.12 \text{ kcal/mol}/RT)$ cm^3 molecule^{-1} sec^{-1}. A comparison of these results with previous investigations on this reaction system is presented.

Introduction

Carbonyl sulfide, OCS, has been employed extensively as a photolytic source of atomic sulfur in kinetic studies of ground-state sulfur atom reactions.[2-19] Nevertheless, there appear to be no direct measurements of the rate constant for the reaction of S(^{3}P) with the parent molecule, *i.e.*

$$S(^3P) + OCS \longrightarrow CO + S_2(^1\Sigma) \qquad (1)$$

In a spectroscopic study reported by Basco and Pearson,[14] an effort was made to evaluate k_1 by measuring the rate of formation of $S_2(^3\Sigma)$, following the flash photolysis of OCS. However, the value obtained for k_1 was ambiguous since evidence was found which indicated that both bimolecular and termolecular reactions could have been involved in the formation of $S_2(^3\Sigma)$. In a recent product analysis study at 298°K, Breckenridge and Taube[13] estimated a lower limit for k_1 of 1.7×10^{-16} cm^3 molecule^{-1} sec^{-1}, but suggested that the actual value of the rate constant could be ten times larger (2×10^{-15} cm^3 molecule^{-1} sec^{-1}). There have also been two recent relative measurements of the rate constant for reaction 1 in which reaction 2 was taken as the reference reaction. Gunning and Strausz[6] obtained a value of 25 for k_2/k_1, while Jakubowski, *et al.*,[12] have reported a value of 83 for the rate constant ratio at 298°K.

$$S(^3P) + C_2H_4 \longrightarrow H_2C\!-\!CH_2 \quad (\text{S bridging}) \qquad (2)$$

The activation energy for reaction 1 has been estimated as ~6 kcal/mol by Kondratiev[18] in a study of the photooxidation of OCS. However, reaction 1 was not studied directly, but as part of a complex mechanism and some assumptions were made in obtaining the quoted activation energy for k_1.

In this paper we report a direct determination of the rate parameters for the reaction of S(^{3}P) with OCS using the flash photolysis–resonance fluorescence technique. Rate measurements were made over a temperature range 233–445°K and over a wide range in the experimental parameters. These included an eight- to tenfold variation in the OCS pressure, the flash intensity, and the total pressure.

Experimental Section

The experimental technique has been described in detail previously;[2-4] and hence, only a brief summary will be given here. This method involves the flash photolysis of OCS to produce atomic sulfur and subsequent monitoring of the kinetic decay of the sulfur atom concentration *via* atomic fluorescence. Typical sulfur atom concentrations were in the range of 10^{10}–10^{11} atoms/cc.[4] As before, Suprasil windows were used on both the photolytic flash lamp and the atomic sulfur resonance lamp to exclude radiation of wavelength less than about 1600 Å. A microwave discharge in a mixture of H_2S (0.1%) in He served as the source of the atomic sulfur resonance radiation.

In these experiments, sulfur atoms were generated in the central region of a reaction cell in an excess of OCS and buffer gas (Ar). Therefore, in addition to reaction with OCS, atomic sulfur was lost due to diffusion out of the reaction sampling zone. Since the OCS concentration was large compared to the initial S atom concentration,

TABLE I: Rate Data for the Reaction of S(^{3}P) with OCS

Temp, °K	OCS, mTorr	Ar, Torr	Flash energy, J	First order, $k^* \times 10^{-2}$, sec^{-1}	Bimolecular rate constant, k_1, cm^3 molecule^{-1} sec^{-1}[a]
236	100	20	31	0.29	
235	100	100	45	0.26	
233	400	100	24	0.29	
233	800	100	24	0.42	
231	100	200	29	0.33	
233	800	200	24	0.51	$(5.6 \pm 3.12) \times 10^{-16}$
298	100	20	31	0.37	
298	400	20	22	0.70	
298	800	20	24	1.10	
298	100	100	8	0.35	
298	100	100	20	0.32	
298	100	100	39	0.33	
298	100	100	80	0.35	
298	400	100	14	0.73	
298	800	100	14	1.18	
298	1000	100	14	1.40	
298	100	200	31	0.31	
298	400	200	22	0.71	
298	800	200	22	1.13	$(3.48 \pm 0.39) \times 10^{-15}$
378	100	20	34	0.72	
377	400	20	29	1.48	
378	800	20	24	2.59	
378	100	100	31	0.53	
379	400	100	22	1.34	
379	800	100	36	2.67	
378	100	200	31	0.61	
377	400	200	29	1.44	
378	800	200	24	2.75	$(1.18 \pm 0.08) \times 10^{-14}$
443	100	20	45	1.04	
445	800	20	24	4.67	
443	100	100	45	0.89	
445	400	100	36	2.52	
445	800	100	36	4.68	
443	100	200	45	0.96	
445	800	200	24	4.79	$(2.52 \pm 0.16) \times 10^{-14}$

[a] The uncertainties in these rate constants were obtained by determining the maximum and minimum slopes that could be drawn within the error bars on the individual points in Figure 1.

the decay of S(^{3}P) due to reaction 1 is given by

$$\ln [S_0]/[S] = k_1[OCS]t \quad (I)$$

The rate of diffusion is also given by a first-order law;[20] and thus, for this process

$$\ln [S_0]/[S] = k_d t \quad (II)$$

where k_d depends on the temperature, the total pressure, and the type of inert gas. Combining the above equations then yields an expression for the observed atom decay given by eq III. The quantity $\{k_1[OCS] + k_d\}$ was deter-

$$\ln [S_0]/[S] = \{k_1[OCS] + k_d\}t \quad (III)$$

mined experimentally as k^*, the pseudo-first-order rate coefficient. The bimolecular rate constant, k_1, was derived from the slope of a plot of k^* *vs.* [OCS]. The intercept of this plot gave k_d.

Results

The results of experiments carried out over a temperature range 233–445°K are given in Table I. It can be seen that, within the experimental uncertainty, the first-order rate constant is independent of the total pressure with the possible exception of the value derived at the lowest temperature studied, 233°K. Figure 1 shows a plot of k^* as a function of the OCS pressure for the four temperatures studied. The uncertainty in the individual k^* data was

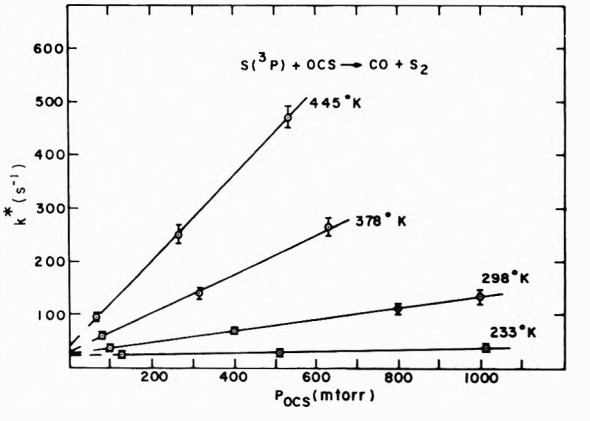

Figure 1. Plot of k^*, the pseudo-first-order rate coefficient for S(^{3}P) + OCS plus diffusion, *vs.* P_{OCS}. In this figure $P_{OCS}(T°K) = P_{OCS}(298°K) \times T°K/298°K$ to facilitate conversion of the derived rate constant to molecular units, *e.g.*, $k_{S+OCS}(T)$ = slope(T) × 1/3.21 × 10^{13} cm^3 molecule^{-1} sec^{-1}.

determined to be about ±10%.[19] The bimolecular rate constants calculated from Figure 1 are also listed in Table I. An Arrhenius plot of these data is shown in Figure 2. A least-squares fit of these data gave the following Arrhenius expression $k_1 = (1.52 \pm 0.20) \times 10^{-12} \exp(-3.63 \pm 0.12$ kcal/mol/RT) cm^3 molecule^{-1} sec^{-1}. The quoted uncer-

tainties are the standard errors[21] calculated from a weighted least-squares treatment of the data over the temperature range 233–445°K. From a consideration of the maximum and minimum slopes which could be drawn through the error bars on each data point in Figure 2, the uncertainty in A and E_{act} was determined to be $\pm 0.55 \times 10^{-12}$ and ± 0.34 kcal/mol, respectively, for the purpose of extrapolation outside the measured temperature range.

Discussion and Comparison with Previous Results

In the present study of reaction 1, atomic sulfur was produced by the flash photolysis of OCS in the vacuum uv. The photolytic light source employed for this purpose was of the spark discharge type and, as mentioned in the Experimental Section, the short wavelength cut-off was set at ~1600 Å with the use of a Suprasil window. Above this cut-off, several primary photolytic processes are energetically possible leading to the formation of S(^{3}P) as well as S(^{1}D) and S(^{1}S). It is also energetically possible to produce O(^{3}P) (+CS) above 1600 Å; however, the production of atomic oxygen from the vacuum uv photolysis of OCS has been indicated to be of negligible importance even at the LiF cut-off (~1050 Å) in recent studies by Donovan[22] and Stief, *et al.*[23] The fate of the metastable sulfur atoms has been discerned[2a,19] from calculations using recent rate data for the reaction and collisional quenching of these species.[24] For example, in the case of gas mixtures consisting of 100 mTorr of OCS and 100 Torr of Ar, the calculations indicate that the bulk (>95%) of the S(^{1}D) and about half of the S(^{1}S) formed the flash photolysis of OCS would be deactivated to S(^{3}P).[19] In addition, the lifetimes for these processes are on the order of 10 μsec, or less, and, therefore, it may be concluded that under the conditions of the present study only ground-state atomic sulfur, S(^{3}P), was of kinetic significance.

The only previous determinations of the rate constant for reaction 1 were made using either indirect techniques or relative rate measurements. In a flash photolysis–spectroscopic study, Basco and Pearson[14] attempted to determine the value of k_1 from an examination of the rate of formation of S_2. This system now appears to have been quite complex in that a negative temperature dependence was observed for the rate of formation of S_2, and the S_2 formation rate data could be fitted to an expression either first or second order in [S]. They suggested one possibility might be a mechanism involving the termolecular reaction

$$S(^3P) + OCS + M \longrightarrow OCS_2 + M \qquad (3)$$

The results of the present research, however, do not support the importance of reaction 3 since no significant effect on the S(^{3}P) decay rate due to total pressure was observed at 298°K or higher temperatures, and the temperature dependence observed in this study was positive. Indeed, Langford and Oldershaw[25] have made several arguments against the importance of reaction 3 in a recent study of S_2 formation from the flash photolysis of OCS in which they present an alternate mechanism that depends on the recombination of S(^{3}P) and reactions involving polymeric sulfur but not the OCS_2 species.

In the study of Breckenridge and Taube[13] at 298°K, reaction 1 was assumed to be in competition with the S(^{3}P) recombination reaction and a lower limit for k_1 of 1.7×10^{-16} cm^3 molecule^{-1} sec^{-1} was thus derived. However, as pointed out earlier, these authors estimated that k_1 was probably much larger, *e.g.*, $\sim 2 \times 10^{-15}$ cm^3 molecule^{-1} sec^{-1}. In two other relative rate studies, the rate

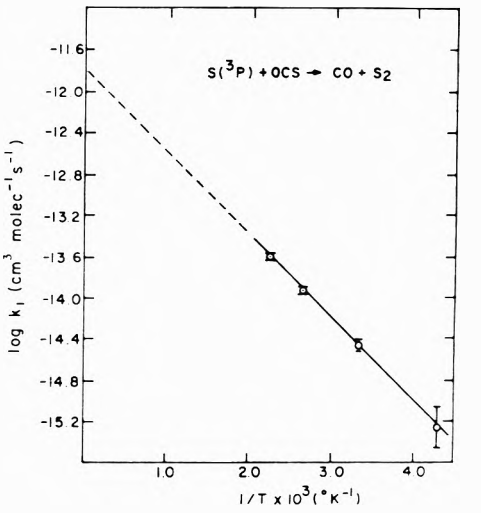

Figure 2. Arrhenius plot of the bimolecular rate constant for the reaction S(^{3}P) + OCS.

constant for reaction 1 was measured against that of reaction 2 [S(^{3}P) + C_2H_4]. Combining the value of Donovan, *et al.*,[15] for k_2 (1.2×10^{-12} cm^3 molecule^{-1} sec^{-1}) with the relative rate data of Gunning and Strausz[6] ($k_2/k_1 = 25$), one obtains a value for k_1 of 4.8×10^{-14} cm^3 molecule^{-1} sec^{-1}. Similarly, taking the relative rate data of Jakubowski, *et al.*[12] ($k_2/k_1 = 83$), a value for k_1 of 1.4×10^{-14} cm^3 molecule^{-1} sec^{-1} is obtained. The above values for k_1 are seen to be larger than the present value for k_1 at 298°K by factors of 14 and 4, respectively. On the other hand, combining the value of k_2 obtained by Davis, Klemm, and Pilling[2a] (4.97×10^{-13} cm^3 molecule^{-1} sec^{-1}) with the relative rate of Jakubowski, *et al.*,[12] leads to a value for k_1 that is within a factor of 2 of the present value. Finally, in a shock tube study by Hay and Belford,[26] the value of k_1 was estimated to be $\sim 1 \times 10^{-12}$ cm^3 molecule^{-1} sec^{-1} at 2570°K. Interestingly, this value is seen to agree to within 25% with the value of k_1 extrapolated from the Arrhenius expression derived in the present work.

The Arrhenius parameters obtained in the present study of reaction 1 are 1.52×10^{-12} cm^3 molecule^{-1} sec^{-1} for the A factor and 3.63 kcal/mol for E_{act}. This activation energy is significantly smaller than that reported by Kondratiev[18] (~6 kcal/mol); but the absence of agreement is not unreasonable considering the scheme used to derive the 6 kcal value. Much better agreement is found in the value of the activation energy calculated by Jakubowski, *et al.*,[12] who used the extended bond energy-bond order method[27] to obtain a value of ~4 kcal/mol for $E_{act}(k_1)$. The same authors also calculated the "minimum" preexponential factor to be about 10^{-11} cm^3 molecule^{-1} sec^{-1} using Benson's method.[28] However, since this method depends upon a number of assumptions concerning the geometry of the transition complex, the results of such calculations are usually considered to be "order-of-magnitude" predictions.

In summary, we have reported the first direct measurement of the activation energy for the reaction of S(^{3}P) with the reactant molecule OCS. The measured value of 3.6 kcal/mol differs significantly from the previous experimental estimate of ~6 kcal/mol. There is, however, reasonable agreement between approximate theoretical calculations, which give ~4 kcal/mol, and the present value for E_{act} (1).

Acknowledgment. Acknowledgment is made by D. D. Davis to the donors of the Petroleum Research Fund, administered by the American Chemical Society, for support of this research.

References and Notes

(1) Address correspondence to NRC/NASA Postdoctoral Research Associate, NASA/Goddard Space Flight Center, Astrochemistry Branch, Code 691, Greenbelt, Md 20771.
(2) (a) D. D. Davis, R. B. Klemm, and M. Pilling, *Int. J. Chem. Kinet.*, **4**, 367 (1972); (b) D. D. Davis, R. B. Klemm, W. Braun, and M. Pilling, *ibid.*, **4**, 383 (1972).
(3) R. B. Klemm and D. D Davis, *Int. J. Chem. Kinet.*, **5**, 149 (1973).
(4) R. B. Klemm and D. D. Davis, *Int. J. Chem. Kinet.*, **5**, 375 (1973).
(5) H. E. Gunning, *Trans. Roy. Soc. Canada II (IV)*, **293** (1964).
(6) H. E. Gunning and O. P. Strausz, *Advan. Photochem.*, **4**, 143 (1966).
(7) E. M. Lown, E. L. Dedio, O. P. Strausz, and H. E. Gunning, *J. Amer. Chem. Soc.*, **89**, 1056 (1967).
(8) P. Fowles, M. de Sorgo, A. J. Yarwood, O. P. Strausz, and H. E. Gunning, *J. Amer. Chem. Soc.*, **89**, 1352 (1967).
(9) O. P. Strausz, J. Font, E. L. Dedio, P. Kebarle, H. E. Gunning, *J. Amer. Chem. Soc.*, **89**, 4805 (1967).
(10) O. P. Strausz, W. B. O'Callaghan, E. M. Lown, H. E. Gunning, *J. Amer. Chem. Soc.*, **93**, 559 (1971).
(11) O. P. Strausz, I. Safarik, W. B. O'Calloghan, and H. E. Gunning, *J. Amer. Chem. Soc.*, **94**, 1828 (1972).
(12) E. Jakubowski, M. G. Ahmed, E. M. Lown, H. S. Sandhu, R. K. Gosavi, and O. P. Strausz, *J. Amer. Chem. Soc.*, **94**, 4094 (1972).
(13) W. H. Breckenridge and H. Taube, *J. Chem. Phys.*, **53**, 1750 (1970).
(14) N. Basco and A. E. Pearson, *Trans. Faraday Soc.*, **63**, 2684 (1967).
(15) R. J. Donovan, D. Husain, R. W. Fair, O. P. Strausz, and H. E. Gunning, *Trans. Faraday Soc.*, **66**, 1635 (1970).
(16) R. W. Fair, A. Van Roodselaar, and O. P. Strausz, *Can. J. Chem.*, **49**, 1659 (1971).
(17) R. J. Donovan and D. J. Little, *Chem. Phys. Lett.*, **13**, 488 (1972).
(18) V. N. Kondratiev, *Acta Physicochim. USSR*, **16**, 272 (1942); *cf. Chem. Abstr.*, **37**, 3348[2] (1943).
(19) R. B. Klemm, Ph.D. Thesis, University of Maryland, 1972.
(20) G. L. Pratt, "Gas Kinetics," Wiley, London, 1969, p 210.
(21) T. L. Isenhour and P. C. Jurs, "Introduction to Computer Programming for Chemists," Allyn and Bacon, Boston, Mass., 1972, pp 178–181; W. A. Wallis and H. V. Roberts, "Statistics: A New Approach," The Free Press, New York, N. Y., 1956, Chapter 17.
(22) R. J. Donovan, *Trans. Faraday Soc.*, **65**, 1419 (1969).
(23) L. J. Stief, S. Glicker, and R. B. Klemm, manuscript in preparation.
(24) R. J. Donovan and D. Husain, *Chem. Rev.*, **70**, 489 (1970).
(25) R. B. Langford and G. A. Oldershaw, *J. Chem. Soc., Faraday Trans. 1*, **69**, 1389 (1973).
(26) A. J. Hay and R. L. Belford, *J. Chem. Phys.*, **47**, 3944 (1967).
(27) S. W. Mayer, *J. Phys. Chem.*, **73**, 3941 (1969).
(28) S. W. Benson, "Thermochemical Kinetics," Wiley, New York, N. Y., 1968, pp 98–100.

Comparison of the Fluorinations of Uranium Dioxide by Bromine Trifluoride and Elemental Fluorine

Tsutomu Sakurai

Fluorine Chemistry Laboratory, Japan Atomic Energy Research Institute, Tokai-mura, Naka-gun, Ibaraki-ken, Japan

(Received September 14, 1973)

Publication costs assisted by the Japan Atomic Energy Research Institute

Uranium dioxide powder was fluorinated by gaseous BrF_3 and F_2, separately, in order to compare the characteristics of the two fluorinating agents. The BrF_3–UO_2 reaction proceeds under lower temperatures and a lower concentration of the reacting gas than the F_2–UO_2 reaction. The temperature dependence of its rate is very small; the apparent activation energy is only 1.6 kcal/mol. In the F_2–UO_2 reaction, the production of UF_6 was not observed below 390°. The rate of this reaction increases remarkably with an increase in temperature; the apparent activation energy for this reaction is 26.0 kcal/mol. In both of these reactions, UO_2F_2 is formed as an intermediate, and the further uptake of fluorine in the solid is not observed in either case. The solution from the residue of BrF_3–UO_2 reaction contains trace amounts of bromine, which possibly arises by hydrolysis of the BrF_3 chemisorbed on the solid. Oxygen fluorides were not detected in the F_2–UO_2 reaction. The diffusion rate of the reacting gas onto the solid surfaces influences the rates of both reactions. The results indicate that the physical adsorption of BrF_3 functions as the precursor to its chemisorption, and that the adsorption of fluorine is activated and dissociative.

Introduction

Bromine trifluoride (mp 8.8°, bp 127.6°) is readily prepared by direct combination of bromine and fluorine, and has been used as a liquid fluorinating agent or a solvent by many other workers.[1-4] Extensive data on its physical and chemical properties are available.[1-4]

Recently, gaseous BrF_3 has been used in the author's laboratory for the fluorination of nuclear fuels and fission products. In the series of studies,[5,6] the author has noticed that gaseous BrF_3 has higher reactivity with such inorganic materials as uranium compounds than F_2. For example, gaseous BrF_3 fluorinates UF_4 even at 55°,[5] whereas Labaton and Johnson have reported that the fluorination of UF_4 by F_2 does not proceed below 220°.[7] The reason for this has not been made clear yet. Moreover, details of their reactivities are not obtained from the literature available, because the experimental data are not sufficient or each worker used specimens with different histories of preparation.

The purpose of the present study is to obtain information on the reactivities of BrF_3 and F_2. Uranium dioxide powder was fluorinated by gaseous BrF_3 and F_2, separately, and the reaction rates and processes were studied. On the basis of the results, the difference in reactivity between the two fluorinating agents is discussed.

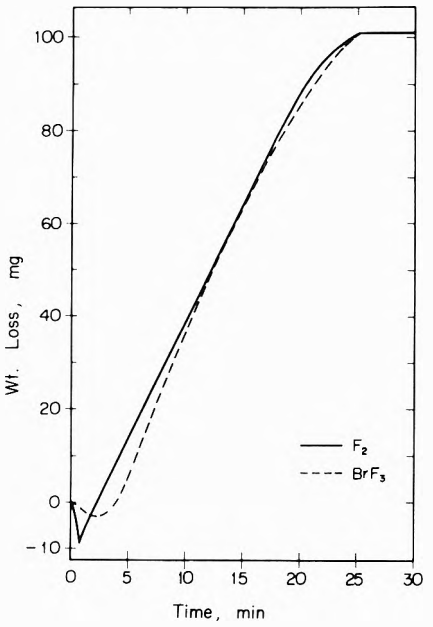

Figure 1. Examples of the weight change *vs.* time curve in the BrF_3–UO_2 and the F_2–UO_2 reaction: initial weight of UO_2 100 mg; temperature 208° for the BrF_3–UO_2 and 450° for the F_2–UO_2 reaction; BrF_3 partial pressure 15 mm; F_2 partial pressure 152 mm; helium was used as the carrier or diluent gas, the linear gas velocity being 1 cm/sec.

Experimental Section

Materials. Commercial-grade bromine trifluoride, from the Matheson Co., was purified by distillation as reported previously.[8] Fluorine, from Daikin Kogyo Co., was used after passage through a sodium fluoride column to eliminate hydrogen fluoride. Uranium dioxide powder with a purity greater than 99.9% was supplied by Mitsubishi Kinzoku Kogyo Co. Prior to the experiment the material was treated with pure hydrogen at 1050° for 10 hr; the surface area, determined by means of krypton adsorption, was 2.2 m^2/g. Argon, nitrogen, and helium, used as a diluent for F_2 and as a carrier gas for BrF_3, were of purities greater than 99.99%.

Thermogravimetric Study. The weight change of the solid phase was obtained with a thermobalance, details of which were described in a previous paper.[5] All valves and tubes in the apparatus in contact with the reacting gases and the reaction products are made of Monel, nickel, or Teflon; they were kept at 40° to prevent condensation of BrF_3 and UF_6. Leaks from the apparatus were checked with a helium leak detector; they were less than 10^{-9} atom cm^3/sec. UO_2 (100 mg) was placed in a sample pan suspended in the reaction tube. After having been evacuated, the reaction tube was filled to atmospheric pressure with an inert gas, and the sample was then heated to a specified temperature. A chromel-alumel thermocouple in a Monel sheath 0.3 cm below the sample pan sensed the reaction temperature. Subsequently, the inert gas containing BrF_3 or F_2 of a given partial pressure was passed through the reaction tube at a constant flow rate. The linear gas velocity was kept at 1 cm/sec, because the rates of both reactions were constant in the linear velocity range 0.9–2.4 cm/sec.[9,10] The partial pressure of fluorine was controlled by using a flowmeter with nickel filaments,[11] and that of BrF_3 was varied by saturating the inert gases with BrF_3 vapor at different temperatures.[5] The weight change of the solid phase with time was recorded continuously on a recording potentiometer.

Analysis of the Solid Phase. The change in composition of the solid phase with time was examined as follows. After uranium dioxide had been in contact with the reacting gas stream for a given time, the residue was taken out of the reaction tube and added to 25 ml of distilled water. The insoluble residue (UO_2) was removed by filtration, and then the amounts of fluorine, bromine, and UO_2^{2+} in the solution were determined. The alizarin complexone (ALC) photometric method was used for determination of the fluorine.[12] The UO_2^{2+} content was determined by measuring its absorbance at 425 nm. The presence of trace amounts of bromine was observed by potentiometry,[13] after the solution had been treated with sodium sulfite for reduction of BrO^- and BrO_3^- into Br^-.[8]

Analysis of the Gas Phase. The gas phase was analyzed by infrared spectroscopy, in order to see whether or not oxygen fluorides are produced in the F_2–UO_2 reaction. Uranium dioxide was treated with F_2 at various temperatures between 300 and 500°, and, before completion of the reaction, the gas in the reaction tube was quenched rapidly to −78° in order to prevent the thermal decomposition of oxygen fluorides.[14] The UF_6 produced was thus caught in the cold trap and the remainder was introduced into an absorption cell. A Shimadzu Model IR-27B spectrophotometer was used. The cell with silver chloride windows was made of Monel.

Results and Discussion

Changes in Weight and Composition of the Solid Phase. In order to compare characteristics of the two reactions, "weight change *vs.* time" curves are shown in Figure 1 for the runs in which the two reactions give similar rates. In both of the reactions, the weight of the solid phase increases slightly in the initial stage of reaction, and then decreases with time. Although both of the reactions shown in Figure 1 terminated 25 min after the start, it should be noted that the reaction temperature was 450° for the F_2–UO_2 and 208° for the BrF_3–UO_2 reaction, and the partial pressure of the reacting gas was 152 mm in the former and only 15 mm in the latter reaction. The BrF_3–UO_2 reaction thus proceeds under milder experimental conditions than the F_2–UO_2 reaction.

For the F_2–UO_2 reaction, it is known that UO_2F_2 is produced as an intermediate.[10] The change in composition of the solid phase with time was examined to obtain information on the mechanism of reaction. Table I shows the results for the runs which were carried out under the same experimental conditions as in Figure 1. The mole ratio $[F^-]/[UO_2^{2+}]$ is nearly 2 for both the reactions, except that in the initial stage. This fact indicates that UO_2F_2 is an intermediate also in the BrF_3–UO_2 reaction, and the further uptake of fluorine in the solid phase, corresponding to the formation of such intermediates as UOF_4, does not take place in either of the reactions. UO_2 may be fluorinated to UF_6 through the following two steps in both the reactions

$$UO_2 \longrightarrow UO_2F_2 \qquad \text{(step 1)}$$
$$UO_2F_2 \longrightarrow UF_6 \qquad \text{(step 2)}$$

The weight increase in the initial stage of reaction is ascribable to step 1 (see Figure 1).

Idrissi, *et al.*, reported that $(UO_2)_4F$, $(UO_2)_3F$, and $(UO_2)_xF_y$, with $x = y \leq 2$, were formed in the F_2–UO_2 reaction, preceding to the formation of UO_2F_2.[15] The low

TABLE I: Results of the Analysis of the Solutions Prepared from the Reaction Residues[a]

BrF_3–UO_2 reaction						F_2–UO_2 reaction				
Time elapsed, min	Reaction residue, mg	UO_2^{2+}, mg	F^-, mg	Mole ratio, $[F^-]/[UO_2^{2+}]$	Br^-, μg	Time elapsed, min	Reaction residue, mg	UO_2^{2+}, mg	F^-, mg	Mole ratio, $[F^-]/[UO_2^{2+}]$
4	101.6	53.3	7.1	1.89	42	2	104.5	82.3	10.8	1.86
8	80.4	35.1	5.1	2.06	28	6	82.5	67.5	9.3	1.96
10	67.7	31.7	4.6	2.06	42	11	58.9	50.0	7.0	1.99
13	48.1	18.2	2.7	2.11	28	14	43.5	36.5	5.1	1.99
19	21.7	9.8	1.4	2.03	32	19	20.2	17.7	2.6	2.09

[a] Experimental conditions of the fluorination were as follows: initial amount of UO_2 was 102 ± 1 mg, temperature was 208° for the BrF_3–UO_2 and 450° for the F_2–UO_2 reaction, BrF_3 partial pressure was 15 mm, F_2 partial pressure was 152 mm, and the carrier or diluent gas was helium, the linear gas velocity being 1 cm/sec.

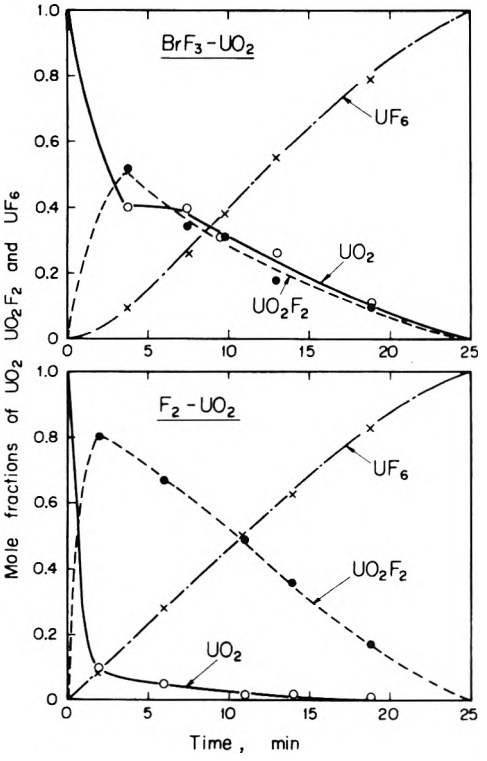

Figure 2. Changes of the mole fractions of UO_2, UO_2F_2, and UF_6 during the reactions.

values of the mole ratio $[F^-]/[UO_2^{2+}]$ in the initial stages of both the reactions, *i.e.*, 1.89 and 1.86, may be due to these intermediates.

The solution from the residue of BrF_3–UO_2 reaction contains trace amounts of bromine; the mole ratio $[Br^-]/[UO_2^{2+}]$ is in the range of 10^{-3} to 10^{-2}. The bromine in the solution is possibly produced by hydrolysis of the BrF_3 chemisorbed on the reaction residue.[8]

From Table I and Figure 1, the changes in amounts of UO_2, UO_2F_2, and UF_6 can be obtained; Figure 2 shows the results. The ordinates in the figure are the mole fractions of UO_2, UO_2F_2, and UF_6, and the abscissas the reaction time, which is the same as that in Figure 1. Elemental fluorine converts most of the UO_2 into UO_2F_2 in the first 2 min; therefore, in the F_2–UO_2 reaction the apparent weight loss of the solid phase can be regarded as the loss of UO_2F_2 due to step 2. On the other hand, in the BrF_3–UO_2 reaction, the solid phase consists of nearly equal amounts of UO_2 and UO_2F_2 throughout the reaction, and, therefore, the apparent weight loss of the solid phase is 6%, or less, smaller than the loss of UO_2F_2 due to step 2. This difference may be due to the step 1 in the

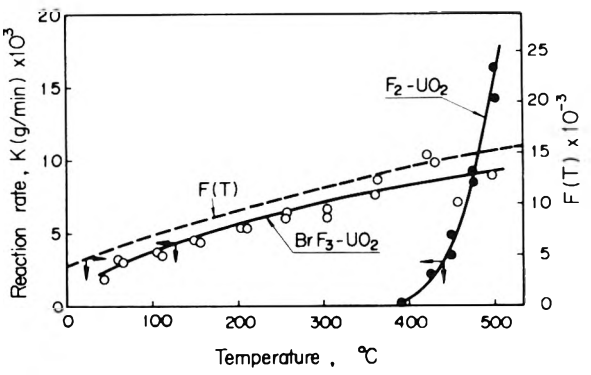

Figure 3. Temperature dependence of the rates of the two reactions and the $F(T)$ curve for $E = 2.0 \times 10^{-13}$ erg; initial weight of UO_2 100 mg; BrF_3 partial pressure 15 mm; F_2 partial pressure 152 mm; the carrier or diluent gas was helium, the linear gas velocity was 1 cm/sec. The dotted line shows a theoretical temperature function for the rate of BrF_3–UO_2 reaction, details of which are described later.

F_2–UO_2 reaction being highly exothermic; a rapid increase in the reaction temperature takes place in the beginning of this reaction, as shown later (see Figure 4).[10]

Rates of the Reactions. In many cases of gas–solid reactions in which the products are entirely gaseous, the diminishing sphere model has been used to treat the rates.[7,10,16] The final equation derived from this model is $(1 - F)^{1/3} = 1 - k't$, where F is the fraction of the solid reacted, t the reaction time, and k' a rate constant. The slope of the straight line in a graph of the value of $(1 - F)^{1/3}$ *vs.* time gives the rate constant.

However, in the present case, the plot of $(1 - F)^{1/3}$ *vs.* time did not give a straight line for either of the reactions and that of $(1 - F)$ *vs.* time was linear, except its initial and final portions, for both the reactions. This fact indicates that the thickness of the solid phase decreases with time at a constant rate, as the present author and other workers reported already for the BrF_3–UF_4 and the SF_4–UO_3 reaction, respectively.[5,16] Therefore, in the present study, the slope of the straight line approximating the middle portion of the weight change *vs.* time curve was used as a reaction rate K in g/min.

Effect of Temperature on the Reaction Rate. Temperature dependence of the reaction rate was examined by keeping both partial pressure of the reacting gas and linear gas velocity constant. The temperature was varied between 40 and 500°; the partial pressure was 152 nm for F_2 and only 15 mm for BrF_3. Figure 3 shows the results. The BrF_3–UO_2 reaction proceeds even at 40°, producing UF_6; the rate increases only slightly with temperature. In the F_2–UO_2 reaction, the weight decrease due to the produc-

tion of UF_6 was not observed up to 390°, though the sorption of fluorine was confirmed even at 300° through a pressure study. The rate of this reaction increases remarkably with increasing temperature, and beyond 480° it exceeds that of the BrF_3–UO_2 reaction. The Arrhenius plot for F_2–UO_2 reaction is linear, and gives the apparent activation energy of 26.0 kcal/mol. The least-squares method was used in the Arrhenius plot for BrF_3–UO_2 reaction, in order to determine the straight line approximating the plot; the apparent activation energy thus obtained was only 1.6 kcal/mol.

Influence of the Inert Gases on the Reaction Rate. When a gas-solid reaction is diffusion controlled, its rate is proportional to $V^{0.5}$, where V is the linear gas velocity.[17] However, the present author reported previously[9] that the BrF_3–UF_4 reaction was still diffusion controlled even in the range where the linear gas velocity little influenced the reaction rate (this phenomenon could be explained as the influence of a sample pan). Therefore, in the present study, the carrier or diluent of the reacting gas was changed in order to see the influence of the diffusion of the reacting gas on the reaction rate.

When the carrier gas was changed from helium to argon or nitrogen, the rate of BrF_3–UO_2 reaction decreased by nearly a half. This is attributed to the decrease in diffusion rate of BrF_3 in the relatively stagnant gas film between the solid phase and the main gas stream.[9]

In the F_2–UO_2 reaction, a similar decrease in reaction rate was also observed at 450° by changing the diluent of F_2. However, at higher temperatures, *e.g.*, 475°, the reaction proceeds more rapidly in argon than in helium in the initial stage. Figure 4 shows the changes in weight and in reaction temperature during the runs at 475°. The reaction temperature increases rapidly in the beginning of the F_2–UO_2 reaction, and argon keeps this high temperature for a considerably longer time than helium; the production of UF_6 is accelerated remarkably with argon during this interval. The reaction in argon then slows down as the temperature returns to the original line (475°), and becomes slower than that in helium in the final stage. This phenomenon is ascribed to the lower thermal conductivity of argon and the great temperature dependence of the rate of F_2–UO_2 reaction.

Thus, the diffusion rate of the reacting gas onto the solid surfaces influences the reaction rate in both the cases.

Study of the Reaction Products. The question has been raised whether oxygen difluoride is produced or not as a product in the fluorination of uranium oxides by F_2.[18] However, infrared spectra of the gas phase did not show any peaks corresponding to oxygen fluorides.

Difference in Mechanism between the Two Reactions. The BrF_3–UO_2 reaction proceeds under lower temperatures and a lower concentration of the reacting gas than the F_2–UO_2 reaction, and application of heat only slightly increases its rate. This reaction does not involve any activated steps. In addition, the author reported previously[19] that gaseous BrF_3 was adsorbed by ionic crystals such as sodium fluoride in the same partial pressure region as in the present experiment, *i.e.*, $P/P_s \leq 0.02$, where P_s denotes the saturated vapor pressure of BrF_3. These findings indicate that BrF_3 molecules are attracted to UO_2 surfaces by the electrostatic force between the dipole of BrF_3 molecules (μ = 1.0 D[2]) and the surface ions. Since UO_2 crystal is a semiconductor,[18] the fluorine atoms of the

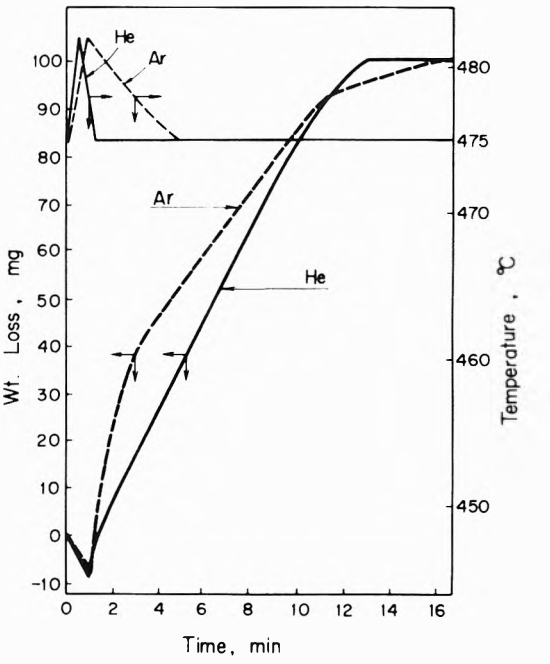

Figure 4. Changes in weight and temperature during F_2–UO_2 reactions at 475° in different diluents: diluent of F_2 helium or argon; initial weight of UO_2 100 mg; F_2 partial pressure 152 mm; linear gas velocity 1 cm/sec.

BrF_3 molecules adsorbed form acceptor bonds with uranium ions on the surfaces by trapping surface electrons of the semiconductor.[20,21] This process may correspond to the case that the potential energy curve for chemisorption crosses that for physical adsorption while the van der Waals force is still attractive, and no activation energy is required for the chemisorption.[21]

Small temperature dependence of the rate of BrF_3–UO_2 reaction, in Figure 3, may be explained as follows. Of the BrF_3 molecules in the gas phase, only a fraction with total translational energies less than the heat of adsorption, E erg, will be attracted to UO_2 surfaces by the electrostatic force. On the assumption that the distribution law is applicable to the BrF_3 molecules in the inert gas, the fraction, $f(E,T)$, described above is given as[22]

$$f(E,T) = \mathrm{erf}[(E/kT)^{1/2}] - 2/\pi^{1/2}(E/kT)^{1/2} \exp(-E/kT)$$

where k is Boltzmann's constant, T the temperature in °K, and erf(x) the error function. The rate of a gas-solid reaction is proportional to $D_{12}(C_b - C_s)$,[23] where D_{12} is the diffusion coefficient in the binary gas system, and C_b and C_s are the concentration of the reactant in the main gas stream and in the gas phase at the solid surface, respectively. In the present case, C_s can be taken as $C_b[1 - f(E,T)]$. In theoretical equations,[24] D_{12} is related to temperature as $T^{3/2}$. The temperature function of the reaction rate, $F(T)$, is thus expressed as

$$F(T) = T^{3/2} f(E,T)$$

Since $f(E,T)$ decreases with an increase in temperature, $F(T)$ increases slightly or decreases, depending upon the value of E, when temperature is increased. The results of calculation show that the $F(T)$ curves for $E = 1.0 \times 10^{-13} \sim 3.0 \times 10^{-13}$ erg are similar in shape to the temperature-dependence curve for the BrF_3–UO_2 reaction rate shown in Figure 3. The $F(T)$ curve for $E = 2.0 \times 10^{-13}$ erg is shown in Figure 3 by the dotted line; the values of $f(E,T)$ for $E = 2.0 \times 10^{-13}$ erg are 0.94 at 400°K, 0.82 at 600°K, and 0.70 at 800°K.

On the other hand, characteristics of the F_2–UO_2 reaction are as follows: (i) heating is necessary for its initiation, and (ii) the rate increases remarkably with increasing temperature. Similar characteristics are also observed in other reactions of fluorine: the F_2–MoO_3 and the F_2–UF_4 reaction proceed at temperature above 250 and 220°, respectively,[6,7] and the apparent activation energy is 36.8 kcal/mol for the former and in the range 15.5–19.9 kcal/mol for the latter reaction.

The facts described above indicate that the F_2–UO_2 reaction involves the activated and dissociative adsorption of fluorine. The heating, necessary for the initiation of this reaction, may be attributed to the energy of stretching the interatomic distance of fluorine molecules so as to match the distances between uranium sites on the surfaces.[21,25]

Acknowledgment. The author wishes to thank Mr. S. Tsujimura and Dr. M. Iwasaki for their discussion, and Dr. H. Hashitani for the analysis of the solid phase. Thanks are also due to Messrs. G. Fujisawa, N. Ishikawa, and A. Takahashi for their assistance in the performance of the experiments.

References and Notes

(1) W. K. R. Musgrave, *Advan. Fluorine Chem.*, **1**, 10 (1960).
(2) R. D. W. Kemmitt and D. W. A. Sharp, *Advan. Fluorine Chem.*, **4**, 244 (1960).
(3) H. L. Leech, "Mellor's Comprehensive Treatise on Inorganic and Theoretical Chemistry," Suppl. II, Part I, J. W. Mellor, Ed., Longmans, Green and Co, London, 1956, pp 160–171.
(4) E. H. Wiebenga, E. E. Havinga, and K. H. Boswijk, *Advan. Inorg. Chem. Radiochem.*, **3**, 133 (1961).
(5) T. Sakurai and M. Iwasaki, *J. Phys. Chem.*, **72**, 1491 (1968).
(6) M. Iwasaki and T. Sakurai, *J. Inorg. Nucl. Chem.*, **34**, 2189 (1972); T. Sakurai, *J. Nucl. Sci. Technol.*, **10**, 130 (1973).
(7) V. Y. Labaton and K. D. B. Johnson, *J. Inorg. Nucl. Chem.*, **10**, 74 (1959).
(8) T. Sakurai, Y. Kobayashi, and M. Iwasaki, *J. Nucl. Sci. Technol.*, **3**, 10 (1966).
(9) T. Sakurai, *J. Nucl. Sci. Technol.*, **7**, 176 (1970).
(10) T. Yahata and M. Iwasaki, *J. Inorg. Nucl. Chem.*, **26**, 1863 (1964).
(11) S. Tsujimura, G. Fujisawa, and A. Takahashi *J. Nucl. Sci. Technol.*, **4**, 244 (1967).
(12) H. Hashitani and H. Muto, *Jap. Anal.*, **14**, 1114 (1965).
(13) H. Hashitani and K. Katsuyama, unpublished.
(14) M. Schmeisser and K. Brandle, *Advan. Inorg. Chem. Radiochem.*, **5**, 41 (1963); A. G. Streng, *Chem. Rev.*, **63**, 607 (1963).
(15) R. Idrissi, T. Kikindai, B. Auguin, and D. Vigner, *C. R. Acad. Sci., Ser. C*, **270**, 765 (1970).
(16) C. E. Johnson and J. Fischer, *J. Phys. Chem.*, **65**, 1849 (1961).
(17) P. L. Walker, Jr., F. Rusinko, Jr., and L. G. Austin, *Advan. Catal.*, **11**, 173 (1959).
(18) J. J. Katz and E. Rabinowitch, "The Chemistry of Uranium," Dover Publications, New York, N. Y., 1961, pp 246–567.
(19) T. Sakurai, *Inorg. Chem.*, **11**, 3110 (1972).
(20) F. F. Vol'kenshtein, "The Electronic Theory of Catalysis on Semiconductor," Pergamon Press, London, 1963, pp 1–95.
(21) D. O. Hayward and B. M. W. Trapnell, "Chemisorption," Butterworths, London, 1964, pp 88–91.
(22) S. W. Benson, "The Foundation of Chemical Kinetics," McGraw-Hill, New York, N. Y., 1960, pp 135–148.
(23) J. M. Smith, "Chemical Engineering Kinetics," McGraw-Hill, New York, N. Y., 1970, p 275.
(24) R. C. Reid and T. K. Sherwood, "The Properties of Gases and Liquids," McGraw-Hill, New York, N. Y., 1966, pp 520–570.
(25) A. W. Adamson, "Physical Chemistry of Surfaces," Interscience, New York, N. Y., 1967, pp 658–659; S. Glasstone, K. J. Laidler, and H. Eyring, "The Theory of Rate Processes," McGraw-Hill, New York, N. Y., 1941, pp 356–359.

Photochemistry of Rhodium(III) Complexes. Ligand Field Excitation of Hexaamminerhodium(III) and Characteristics of Nonradiative Deactivation Paths[1]

John D. Petersen and Peter C. Ford*[2]

Department of Chemistry, University of California, Santa Barbara, California 93106 *(Received October 29, 1973)*

Publication costs assisted by the National Science Foundation

Ligand field excitation of hexaamminerhodium(III), $Rh(NH_3)_6^{3+}$, in aqueous solution results in the photoaquation of one coordinated NH_3. The measured quantum yields at 23° are 0.075 mol/einstein for 313-nm excitation of the $^1A_{1g} \rightarrow {}^1T_{1g}$ transition and 0.07 for 254-nm excitation of the $^1A_{1g} \rightarrow {}^1T_{2g}$ transition, suggesting efficient interconversion of the higher energy state to a common reactive excited state. Under similar conditions, the quantum yield for the perdeuterated complex $Rh(ND_3)_6^{3+}$ is about twice as large (0.14 in H_2O, 0.15 in D_2O, 313-nm excitation). However, the temperature dependence of the photoaquation quantum yields is measurably greater for the perprotio complex than for the perdeuterio complex. To explain these results, it is proposed that temperature-independent weak coupling and temperature-dependent strong coupling mechanisms are competitive in the nonradiative deactivation of the reactive excited state of $Rh(NH_3)_6^{3+}$.

Introduction

In the past several years, interest[3,4] in the photoreactivities of d^6 metal ion complexes has been extended to quantitative studies of the ammine complexes of ruthenium(II)[5] and rhodium(III).[6-10] The rhodium(III)–ammine complexes whose photochemistry reported to date have been halide complexes such as $Rh(NH_3)_5X^{2+}$ or $Rh(en)_2X_2^+$ (X = Cl^-, Br^-, or I^-), for which perturbations of the ligand field involve the stereochemistry of the bis(ethylenediamine) complexes or the identity of the halide ion. In order to consider more subtle differences, we have been examining the photochemistry[1,11] and lumines-

cence spectroscopy[12] of complexes of the type $Rh(NH_3)_5L^{3+}$, where L is one of a series of uncharged nitrogen bases such as NH_3, a substituted pyridine py-X, or an organonitrile RCN. During these studies the dramatic effects[13,14] that perdeuteration of the coordinated ammines has on the luminescent lifetimes at 77°K of the complex ions $Rh(NH_3)_5X^{2+}$ and $Rh(NH_3)_6^{3+}$ came to our attention. These deuteration effects provide insight into the nonradiative deactivation mechanisms of the emitting states[14] and, conceivably, studies of similar effects under photochemically significant conditions might improve our understanding of processes deactivating chemically reactive excited states. Since $Rh(NH_3)_6^{3+}$, a member of the $Rh(NH_3)_5L^{3+}$ series, displays the greatest effect of deuteration on its phosphorescence lifetime,[14] it was decided to examine in some detail the photoreactions of this ion and its perdeuterated analog in aqueous solution. Kelly and Endicott[7] have studied the photoaquation of the ions $Rh(ND_3)_5X^{2+}$ and found that quantum yields were identical with those of the perprotio analogs for X^- = Br^- or I^-, but for X^- = Cl^- perdeuteration led to a small enhancement (~40%) of the quantum yield. A larger effect is seen for the hexaammine complexes whose photochemistry is presented here.

Experimental Section

Materials and Syntheses. The hexaammine complex $[Rh(NH_3)_6]Cl_3$ was prepared by the procedure of Thomas and Crosby.[13] The perdeuterated hexaammine complex $[Rh(ND_3)_6]Cl_3$ was prepared by heating the perprotio complex in D_2O. Initially, $[Rh(NH_3)_6]Cl_3$ (0.25 g) was dissolved in 5 ml of D_2O (Thompson-Packard, 99.8% D) and heated (in a system isolated from atmospheric water by drying tubes) for a period of 5 hr. The solution was then cooled to ice temperatures and diethyl ether (5 ml) added to form a heterogeneous liquid mixture. To this was added ethanol (10 ml) leading to immediate precipitation of the rhodium salt. This material was collected by filtration, washed with ethanol–ether mixtures, and dried in a vacuum desiccator. An infrared spectrum was taken to determine the approximate amount of deuteration. The procedure was repeated three times to give a highly deuterated hexaammine sample in an overall yield of 68%. Per cent deuteration was examined by a published nmr method[7] on a Varian T-60. According to this analysis, no protons were shown to be present in the perdeuterated hexaammine salt; however, experimental uncertainties established an upper limit of 0.8 protons per rhodium, or, in other words, deuteration was at least 95.5% complete.

Photolysis Procedures. Photolyses at 313 nm were carried out on an optical train utilizing a PEK 200-W high-pressure mercury short arc lamp as a light source, an infrared filter and a 313-nm interference filter (Oriel) for wavelength selection, and a thermostated cell holder. Photolyses were carried out in aqueous perchloric acid solutions (pH 2–4) in 2-cm pathlength cylindrical quartz cells (volume = 6.0 ml). Irradiation beam intensities (band pass = 12 nm for the interference filter) averaged 1 × 10^{-6} einstein/min as determined by ferrioxalate actinometry.[15] Beam intensities were monitored continuously with a YSI-Kettering Model 65A radiometer to ensure stability. Solutions irradiated were relatively optically dense (OD ~ 1.5); however, quantum yields are based on einsteins of quanta absorbed as determined by a computational method. Proceeding reactions were monitored periodically by recording the electronic spectrum on a Cary 14 spectrophotometer. Analogous solutions allowed to react in the dark displayed no spectral changes at any of the temperatures studied. On the basis of spectral changes, quantum yields were calculated as moles of reaction per einstein of light absorbed during a particular photolysis interval. As the reaction proceeded, these values dropped off slowly owing to the secondary involvement of the reaction product. For this reason, the interval quantum yields were plotted as a function of per cent reaction, and the resulting plots were extrapolated to zero time to obtain the quantum yield for photolysis of the starting complex. Values obtained in this manner were equivalent within experimental uncertainty to those obtained by plotting overall quantum yield as a function of irradiation time or per cent reaction according to the method of Chaisson, *et al.*[5] Aquation of NH_3 was also examined by measuring pH changes of the photolysis solution during the course of the reaction. A Sargent-Welch Model NX digital pH meter calibrated against commercial buffers was employed for pH measurements.

Photolyses at 254 nm were carried out on an optical train utilizing a 90-W medium-pressure Philips "spectral" lamp as source, an Oriel 254-nm interference filter to isolate the desired wavelength region, and a thermostated cell compartment. Reactions were carried out in a 2-cm pathlength cylindrical cell. Irradiation beam intensities (2 × 10^{-7} einstein/min) were determined by ferrioxalate actinometry and reactions were followed by spectral and pH changes.

Sensitization. Sensitization experiments were carried out with two sensitizers, biacetyl (Aldrich, vacuum redistilled) and pyrazine (Aldrich). Solutions were prepared with the appropriate sensitizer and sufficient 1 *M* $HClO_4$ to give the desired pH (~3.1) in redistilled H_2O and were carefully deaerated in all cases using chromous scrubbed argon. Care was taken to ensure that solutions to which $[Rh(NH_3)_6]Cl_3$ had been added were entrained for the same period of time as control solutions to which no substrate had been added. Optical densities of the solutions at the excitation wavelength (405 nm for biacetyl, 254 nm for pyrazine) fell in the range 1–2 and direct absorption by $Rh(NH_3)_6^{3+}$ accounted for less than 1% of this for biacetyl sensitization and less than 5% for pyrazine sensitization. Reaction yields for ammonia aquation were determined at the conclusion of photolysis by measuring the pH change on a Radiometer model 26 pH meter. Emission spectra of solutions were obtained in a Perkin-Elmer MPF-3 fluorescence spectrophotometer. Photolyses at 405 nm were carried out using the PEK high-pressure mercury lamp with a 405-nm interference filter (beam intensity ~ 4 × 10^{-6} einstein/min) and at 254 nm using the apparatus described above.

Results

The spectrum of $Rh(NH_3)_6^{3+}$ in aqueous solution displays two absorption bands at 305 (ϵ 134 M^{-1} cm^{-1}) and 255 nm (ϵ 101) (Figure 1) which can be assigned to the $^1A_{1g} \rightarrow {}^1T_{1g}$ and $^1A_{1g} \rightarrow {}^1T_{2g}$ ligand field transitions, respectively. Continuous photolysis with 313- or 254-nm light, corresponding to excitation of these transitions, results in substitutional behavior as the only observed photochemical reaction of this complex in acidic aqueous solution (eq 1). Reactions were monitored by examining the

$$Rh(NH_3)_6^{3+} + H_2O \xrightarrow[(313 \text{ or } 254 \text{ nm})]{h\nu} Rh(NH_3)_5H_2O^{3+} + NH \quad (1)$$

spectral changes in the solution after photolysis intervals

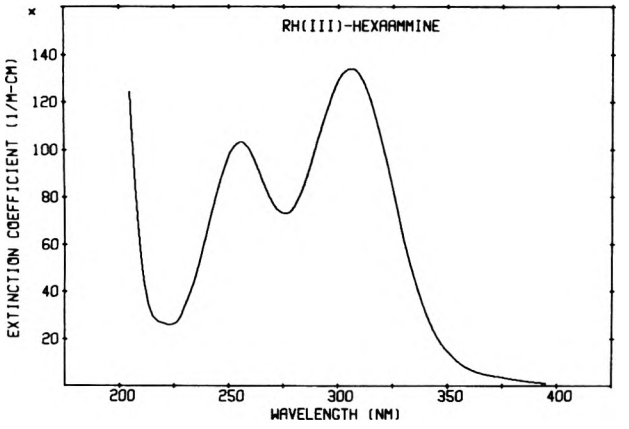

Figure 1. Spectrum of $Ru(NH_3)_6^{3+}$ in aqueous solution.

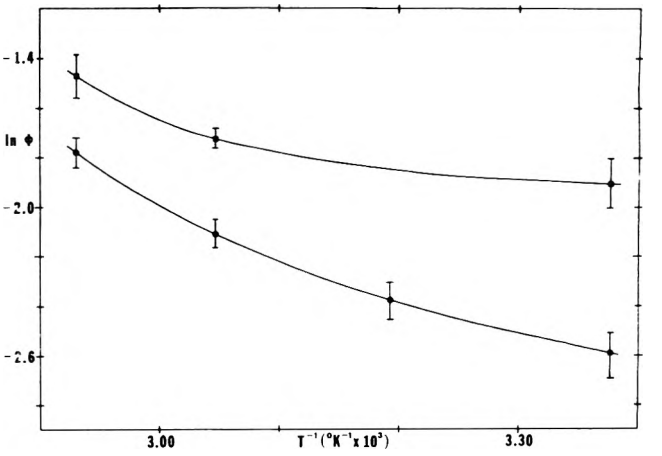

Figure 2. "Activation energy" plots of the temperature-dependent quantum yield for photoaquation of hexaamminerhodium(III) in aqueous solution: upper curve shows data for $Rh(ND_3)_6^{3+}$ in D_2O; lower curve data for $Rh(NH_3)_6^{3+}$ in H_2O.

and by measuring the difference in the solution pH between the initial solution and the product solution at the conclusion of the photolysis experiment (usually carried to approximately 20% reaction as determined by the spectral changes). An increase in pH indicates the photolysis caused release of NH_3 into the weakly acidic photolysis solution (pH 2-4). Quantum yields determined by the two methods were comparable. Photolysis of $Rh(NH_3)_6^{3+}$ to greater than 90% completion in the acidic perchlorate solutions gave product solutions with λ_{max} (316 nm) and optical densities essentially identical with those predicted for $Rh(NH_3)_5H_2O^{3+}$ as the sole reaction product. Under these experimental conditions the product $Rh(NH_3)_5H_2O^{3+}$ has the appearance of being essentially photolysis insensitive, and no spectral changes are observed when this complex is photolyzed with 313-nm light.

During each photochemical experiment a parallel dark reaction was carried out with another sample of the same solution under comparable conditions. For all the temperatures used in this study, no reaction was detected by either spectral or pH measurements for solutions not irradiated. Photolysis experiments were carried out both on solutions which had been carefully entrained with deoxygenated argon and on solutions saturated with air. However, no differences in quantum yield measurements were detected, indicating that the photoreactions are not sensitive to the presence of dissolved oxygen. A similar observation was made for the halopentaamminerhodium(III) complexes.[7]

Quantum Yields. Table I summarizes the quantum yields for 313-nm photolysis of aqueous $Rh(NH_3)_6^{3+}$ at four temperatures. Considering the values for $\Phi(NH_3)$ at 23 and at 68° only, an apparent activation energy, E_a(apparent), of 3.6 ± 0.3 kcal/mol can be calculated for the NH_3 photoaquation. Also listed in Table I is the $\Phi(NH_3)$ value measured at 23° for 254-nm irradiation. Within experimental uncertainty this quantum yield is indistinguishable from $\Phi(NH_3)$ measured for 313-nm photolysis under comparable conditions.

The quantum yields measured for photoaquation of $Rh(ND_3)_6^{3+}$ are also listed in Table I. In each case studied here, photoaquation of $Rh(ND_3)_6^{3+}$ occurred with a higher quantum yield than for the perprotio analog. However, the photoreactivity of the perdeuterio complex is not as temperature sensitive with an E_a(apparent) value of only 1.9 ± 0.4 kcal/mol between the values measured at 23 and 68°. Plots of ln (Φ) *vs.* T^{-1} (Arrhenius type activation plot) are shown in Figure 2 for the perdeuterio hexaammine complex and for the perprotio complex. Neither plot appears to be linear, but it is evident that over the range the perprotio system is the more temperature sensitive.

TABLE I: Quantum Yields for the Photoaquation of Hexaamminerhodium(III)

Complex	T, °C	λ_{irr}, nm	Φ^a	$\Phi(ND_3)/\Phi(NH_3)^b$
$Rh(NH_3)_6^{3+}$	23	313[c]	0.075 ± 0.007 (19)[d]	
		313	0.07 ± 0.01 (2)[e]	
		254[c]	0.07 ± 0.02 (4)[d]	
	40	313	0.093 ± 0.007 (6)[d]	
	55	313	0.122 ± 0.007 (6)[d]	
	68	313	0.169 ± 0.010 (4)[d]	
$Rh(ND_3)_6^{3+}$	23	313	0.150 ± 0.005 (4)[e]	2.00
		313	0.14 ± 0.02 (6)[d]	1.87
	55	313	0.179 ± 0.007 (3)[e]	1.47
	68	313	0.23 ± 0.02 (3)[e]	1.36

[a] Quantum yield (initial) for NH_3 or ND_3 aquation, mean value and average deviation reported with number of determinations in parentheses. [b] Ratio of quantum yields for perdeuterio *vs.* perprotio systems. [c] 313-nm irradiation corresponds to $^1A_{1g} \rightarrow {}^1T_{1g}$ excitation, 254-nm irradiation to $^1A_{1g} \rightarrow {}^1T_{2g}$ excitation. [d] In H_2O solution, $HClO_4 \sim 10^{-3}$ *M*. [e] In D_2O solution, $D_2SO_4 \sim 10^{-3}$ *M*.

Quantum yields for photoaquation of $Rh(ND_3)_6^{3+}$ were determined both in D_2O solution and in H_2O solution (Table I). A slightly higher quantum yield was found for the deuterated solvent, although the differences fall into the ranges of experimental uncertainty. Similarly, photolysis of $Rh(NH_3)_6^{3+}$ in D_2O solution gives quantum yields essentially indistinguishable from those values measured in H_2O solution (Table I).

Sensitization Studies. No net photochemical reaction was observed when deaerated solutions of biacetyl (~0.2 *M*) and 2×10^{-3} *M* $Rh(NH_3)_6^{3+}$ in pH 3.1 water were photolyzed extensively at 405 nm. Similarly a solution with 1.2×10^{-2} *M* $Rh(NH_3)_6^{3+}$ gave a small pH change on irradiation, but this could be attributed entirely to direct photolysis of the rhodium(III) substrate. Thus, it appears that no biacetyl sensitization of $Rh(NH_3)_6^{3+}$ photochemistry occurs. Emission studies demonstrated that the failure to see sensitized photochemistry was not the result of impurity quenching of biacetyl. Solutions containing $Rh(NH_3)_6^{3+}$ and control solutions without Rh(III) both displayed the biacetyl phosphorescence and fluorescence

emission bands at 510 and 465 nm, respectively, with peak height ratios ranging from ~5:1 to ~10:1. Rh(III) and control solutions prepared identically (including deaeration procedures, etc.) have similar phosphorescence/fluorescence ratios, but for each pair the solution containing Rh(III) showed a smaller ratio by about 10–20%. Greater variations were observed between different pairs of solutions indicating that impurity quenching (presumably O_2 quenching of phosphorescence) was playing some role.

Unlike biacetyl, pyrazine appears to sensitize the photochemistry of $Rh(NH_3)_6^{3+}$. Solutions containing ~2×10^{-4} M pyrazine and 7.0×10^{-4} M $Rh(NH_3)_6^{3+}$ displayed pH changes sufficient to give an overall quantum yield of 0.012 based on the total light absorbed by the solution. A maximum upper limit of 40–45% of this reaction can be attributed to direct photolysis of the complex, thus the quantum yield for sensitized photolysis is about 0.006 to 0.007 mol per einstein absorbed by pyrazine. A lower concentration of Rh(III) (4.7×10^{-4} M) led to a smaller sensitized photolysis quantum yield (~0.004). Pyrazine does not display a phosphorescence band in its room temperature emission spectrum, so quenching efficiency cannot be compared to sensitized photolysis yields. However, the presence of Rh(III) does not affect the fluorescence intensity of pyrazine at 342 nm, so the photochemistry observed apparently is not due to energy transfer to the singlet state of $Rh(NH_3)_6^{3+}$ but to energy transfer from the pyrazine triplet. Intersystem crossing for pyrazine occurs with less than unitary efficiency (Φ_{ISC} = 0.33 in hexane),[16] thus the observed quantum yields of sensitized photochemistry (not under limiting concentration) are in fact closer to the direct photolysis value of 0.075 than immediately obvious.

Discussion

Aquation of NH_3 (eq 1) is the sole photoreaction observed for aqueous $Rh(NH_3)_6^{3+}$ when ligand field transitions $^1A_{1g} \rightarrow {}^1T_{1g}$ or $^1A_{1g} \rightarrow {}^1T_{2g}$ are excited in acidic aqueous solution. The quantum yields are independent of the ligand field state initially populated by irradiation, suggesting that the higher state undergoes efficient interconversion to a reactive state common to that reached by excitation directly into the lower state.

The failure to see biacetyl triplet sensitization of $Rh(NH_3)_6^{3+}$ photoaquation contrasts to the behavior of the halopentaammine complexes[7] but is not surprising. The energy of the biacetyl triplet is 19.2 kK[17] compared to the estimated $Rh(NH_3)_6^{3+}$ triplet energy of 20.3 kK;[13] thus, energy transfer in this case would be endothermic. The modest quenching (10–20%) of biacetyl phosphorescence in the presence of $Rh(NH_3)_6^{3+}$ does not appear significant and may be due to impurities, most likely O_2. However, such quenching conceivably may result from significant perturbation of biacetyl nonradiative deactivation pathways owing to "exiplex" formation with the Rh(III) in solution. Energy transfer from the pyrazine lowest triplet (26.2 kK)[16] to $Rh(NH_3)_6^{3+}$ would be significantly exothermic. Energy transfer from the pyrazine singlet (30.1 kK)[16] to give the $Rh(NH_3)_6^{3+}$ $^1T_{1g}$ state (29.3 kK, estimated from spectral data of ref 13) also would be exothermic but may be slow owing to Franck–Condon effects. The failure to detect any Rh(III) quenching of pyrazine fluorescence indicates that neither direct energy transfer nor "trivial" sensitization (absorption by Rh(III) of emitted radiation) is an important process under the experimental conditions. Thus, observation of photoreaction exceeding the small direct photolysis suggests triplet sensitization of $Rh(NH_3)_6^{3+}$.

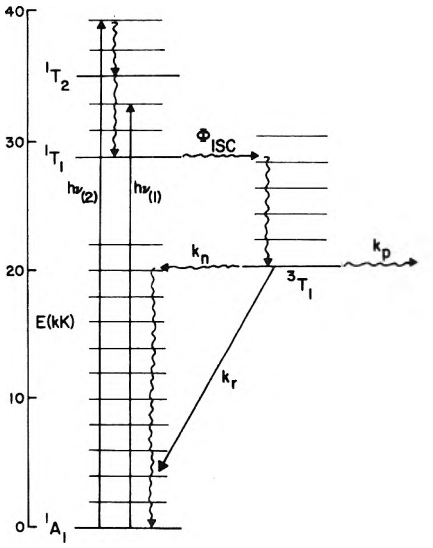

Figure 3. Energy level diagram for photoreaction of $Rh(NH_3)_6^{3+}$: $h\nu(1)$ and $h\nu(2)$ represent excitation into the $^1T_1$ and $^1T_2$ states, respectively, k_p is aquation of excited state $^3T_1$ to give photoproducts, and k_n and k_r represent nonradiative and radiative deactivation to ground state, respectively.

In the absence of quantitative photophysical data for the pyrazine sensitizer in aqueous solution, the limiting quantum yield for reaction of the $Rh(NH_3)_6^{3+}$ triplet excited state cannot be established from the current data. However, our data indicate that this state is reactive toward aquation. This conclusion is consistent with the holopentaammine complexes[7] where it was concluded using biacetyl as a photosensitizer that intersystem crossing from ligand field singlet states populated by initial excitation to reactive triplet states occurred with unitary efficiency. Highly efficient intersystem crossing from ligand field singlets to triplet emitting states has also been concluded[13,14] from studies of the low-temperature (77°K) emission spectra of rhodium(III)-ammine complexes including $Rh(NH_3)_6^{3+}$. Such high rates of intersystem crossing can be in large part attributed[18] to the sizeable spin orbit coupling of the rhodium atom. For these reasons, we will assume for sake of the present discussion that like the halopentaammine complexes, higher energy ligand field excited states of $Rh(NH_3)_6^{3+}$ undergo very efficient internal conversion/intersystem crossing to a reactive lowest energy triplet state.

An electronic state diagram for $Rh(NH_3)_6^{3+}$ illustrating relevant photochemical and photophysical processes is shown in Figure 3. Implicit are the assumptions that internal conversion, intersystem crossing, and vibrational relaxation are rapid relative to the processes responsible for deactivation of the reactive triplet state ($^3T_1$) and that the chemically relevant form of this species is thermally equilibrated (a "thexi" state).[4] The processes depleting the reactive state are chemical reactions leading to substitution of H_2O for NH_3 in the Rh(III) coordination sphere (k_p), radiative deactivation (phosphorescence) to ground state (k_r), or nonradiative deactivation to ground state (k_n). Based on the earlier stated assumptions, the lifetimes (τ) of the reactive state and the quantum yield of the photochemical reaction (Φ_p) can be expressed in terms of the rate constants k_p, k_n, and k_r

$$\tau = (k_p + k_n + k_r)^{-1} \quad (2)$$

$$\Phi_p = k_p/(k_p + k_n + k_r) \quad (3)$$

Attempts to observe luminescence from $Rh(NH_3)_6^{3+}$ at room temperature were unsuccessful[12,13] and under these conditions k_r is apparently much smaller than k_n or k_p. Thus eq 3 can be rewritten as

$$\Phi_p = k_p/(k_p + k_n) \quad (4)$$

and rearrangement of eq 4 gives the ratio of the rate constants

$$k_n/k_p = (1 - \Phi_p)/\Phi_p \quad (5)$$

The importance of the nonradiative deactivation pathway is illustrated by considering the photoaquation of $Rh(NH_3)_6^{3+}$ at 23° (Table I) where the quantum yield of 0.075 mol/einstein can be translated into a k_n/k_p ratio of 12.3. Thus it should be clear that any interpretative discussion of photoreaction quantum yields should consider other deactivation pathways as well.

Kelly and Endicott,[7,8] in discussing the photochemistry of the haloammine complexes of rhodium(III), have focused attention on the theories of radiationless deactivation mechanisms proposed by Robinson and Frosch[19] for excited organic compounds and extended by others.[20-23] The low-temperature (77–110°K) luminescence of certain Rh(III) amines has been subject[14,24] to similar theoretical considerations. For large molecules, the nonradiative deactivation rate constant k_n is primarily determined by intramolecular processes and is the product of vibrational and electronic factors. Vibronic coupling between two states has been analyzed in terms of two limiting cases.[21,22] The *strong coupling limit* is one for which there is large displacement of the potential surface (at least one normal mode) of one state with respect to the other and for which the surfaces are expected to cross not far from the minimum of the higher state. The *weak coupling limit* represents the case where relative displacement of potential energy surfaces is small. For the limiting weak coupling case, it is predicted that k_n will increase exponentially as the difference in energy between the ground and excited state decreases and that k_n is dominated by the highest frequency vibrational modes of the molecule.[21] The presence of high frequency modes allows an isoenergetic transition from the thermally equilibrated excited state to an electronic ground state vibrational level of relatively low quantum number thus increasing the probability of such a transition. In the strong coupling limit, k_n increases exponentially as the energy gap ($\Delta E'$) between the lowest vibrational level of the excited state and the intersection of the ground and excited state surfaces[22] decreases. In this case, the nonradiative deactivation rate depends on the mean vibrational frequency[21] and is relatively insensitive to the highest frequency vibrational modes. In gross simplification, it might be said that in the weak coupling limit for metal–ammine complexes, the radiationless transition from $^3T_1$ to the $^1A_1$ ground state primarily involves activation of the N–H vibrations of the coordinated ammonias[25] (the highest frequency modes) while in the strong coupling limit radiationless deactivation involves major distortion (and activation) of the metal–ligand bond framework as well.

Interpretation of luminescence data for the rhodium(III) –ammine complexes has led to some disagreement.[14,24] For example, it appears that large energy differences between the estimated maxima of the triplet absorption bands and the phosphorescence bands are the rule.[12-14,24] The estimated Stokes shift for $Rh(NH_3)_6^{3+}$ is 4 kK,[13] and this is easily rationalized in terms of metal–ligand bond lengthening in the $^3T_1$ state (electronic configuration $(t_{2g})^5(e_g)^1$) given that the e_g orbital is σ antibonding. Nonetheless, comparisons of luminescence lifetimes and quantum yields at 77–110°K for $Rh(NH_3)_6^{3+}$ and the halopentaammine ions and the perdeuterated analogs in methanol–water glasses[14] show that replacing the high-frequency N–H modes with lower frequency N–D modes leads to very large decreases in nonradiative deactivation rate constants. For example, k_n is 62 times larger for $Rh(NH_3)_6^{3+}$ than for $Rh(ND_3)_6^{3+}$ at 77°K. Such sensitivity to perdeuteration of the high-frequency, nitrogen–hydrogen bonds is considered diagnostic of a dominating weak coupling mechanism for nonradiative deactivation.

Under the conditions of the luminescence experiments (rigid glasses at 77–110°K) no photochemical reactions of the Rh(III) ammine complexes are observed.[13] However, in aqueous solution at ambient temperatures, ligand field excitation of these species results in photosubstitution processes with total quantum yields ranging from the 0.075 for $Rh(NH_3)_6^{3+}$ to near unity[7] for aquation of trans NH_3 from $Rh(NH_3)_5I^{2+}$. Aquation (k_p) is one path for deactivation of the reactive excited state. If this process occurs by unimolecular dissociation of the Rh–L bond, it is clear that the k_p path would be closely related to a strong coupling process for nonradiative deactivation, and it appears a valid assumption[7] that such a path should be important under photochemically significant conditions. Nonetheless, photoaquation of the hexaammine complex shows a significant deuterium isotope effect (Table I). The effect of carrying out the photolysis in D_2O rather than H_2O is small; hence, the principal isotope effect is a unimolecular property of the hexaammine ion.

Deuterium isotope effects have been studied[26-28] for the thermal aquations of the cobalt(III) complexes $CoA_4Cl_2^+$ (where A = perprotio- or perdeuterioammonia or (ethylenediamine)$_{1/2}$). In each case deuteration of the ammine function led to decreases in the chloride aquation rates. Aquations in D_2O solution also proved to be slower than the analogous reactions in H_2O. These results suggest that ammine perdeuteration would decrease the rate of ligand aquation (k_p) from the excited state, if it has any effect at all. However, since Φ_p is *larger* for the perdeuterated hexaammine, the dominant effect of perdeuteration must be to decrease the rate of nonradiative deactivation k_n instead. If perdeuteration has no effect on k_p, then the ratio of k_n for $Rh(ND_3)_6^{3+}$ in D_2O to k_n for $Rh(NH_3)_6^{3+}$ in H_2O at 23° can be calculated to be 0.46. In other words, perdeuteration reduces the nonradiative deactivation rate by at least a factor of 2 thus indicating that weak coupling is apparently an important mechanism for deactivation of $Rh(NH_3)_6^{3+}$ from $^3T_1$ to the ground state at 23°.

If for a particular case, strong and weak coupling were competitive, independent mechanisms for nonradiative deactivation, we might rewrite k_n as the sum of the rates of the competitive processes

$$k_n = k_s + k_w \quad (6)$$

where k_s represents the rate of deactivation by the strong coupling path(s) and k_w by the weak coupling path(s). Therefore

$$\Phi_p = k_p/(k_p + k_s + k_w) \quad (7)$$

The temperature dependence of the quantum yield Φ_p will be a composite of the temperature dependences of the independent terms k_p, k_s, and k_w. If k_p is simply a chemical reaction of the thexi state, its temperature dependence might be expected to follow Arrhenius behavior, *i.e.*, $k_p = A_p \exp(-E_a/RT)$. The temperature dependence of the deactivation processes are not so simple; however, strong coupling has been suggested to have an Arrhenius-type behavior and weak coupling to be essentially temperature independent.[23,29] Thus for sake of illustration we might rewrite eq 7 as

$$\Phi_p = \frac{A_p \exp(-E_a/RT)}{A_p \exp(-E_a/RT) + A_s \exp(-\Delta E'/RT) + k_w} \quad (8)$$

where the energy difference $\Delta E'$ may or may not be closely related to E_a and where k_w is independent of temperature. Given this form of the equation for the limiting case where k_w is much larger at all temperatures than either $A_p \exp(-E_a/RT)$ or $A_s \exp(-\Delta E'/RT)$, then Φ_p would follow a simple Arrhenius relationship and E_a(apparent) would equal E_a for both the perprotio and perdeuterio cases. On the other extreme, if k_w were small compared to $A_s \exp(-\Delta E'/RT)$ at all temperatures studied and if $\Delta E'$ were comparable to E_a, then eq 8 would predict Φ_p to be essentially temperature independent regardless of its magnitude. Neither limiting behavior is observed for $Rh(NH_3)_6^{3+}$ and $Rh(ND_3)_6^{3+}$ (Figure 2), and it is apparent that $\Phi_p(D)$ is less temperature sensitive than is $\Phi_p(H)$.[30] This observation implies that the temperature independent contribution (*e.g.*, k_w) to $k_n(H)$ is a smaller fraction of $k_n(D)$ and, also, that a temperature dependent term not greatly sensitive to perdeuteration (*e.g.*, k_s) is an important contribution to both $k_n(H)$ and $k_n(D)$.

In conclusion, we feel that the data for the hexaammine complex can be explained on the basis of a potential energy surface where the values of $\Delta E'$ for the strong coupling mechanism and E_a for ligand aquation are sufficiently large that weak coupling deactivation is the overwhelmingly dominant nonradiative process when kT is small (*e.g.*, at 77°K). However, at larger values of kT, the three processes appear to be competitive, at least for $Rh(NH_3)_6^{3+}$ at ambient temperature. Although the relationship between the strong coupling contribution to k_n and photoaquation is unclear, the observation of an activation energy (apparent) for $\Phi(NH_3)$ of about 4 kcal indicates that the potential well for the reactive excited state of $Rh(NH_3)_6^{3+}$ is reasonably defined.

Acknowledgment. This work was supported by the National Science Foundation (GP-26199 and GP-36643X). We are indebted to Professor R. J. Watts of this Department for helpful discussion and for providing a copy of ref 14 prior to publication.

References and Notes

(1) Reported in part at the 165th National Meeting of the American Chemical Society, Dallas, Tex., April 1973, INOR 39.
(2) Camille and Henry Dreyfus Foundation Teacher-Scholar, 1971–1976.
(3) V. Balzani and V. Carassiti, "Photochemistry of Coordination Compounds," Academic Press, London, 1970.
(4) P. D. Fleischauer, A. W. Adamson, and G. Satori, *Progr. Inorg. Chem.*, **17**, 1 (1972).
(5) D. A. Chaisson, R. E. Hintze, D. H. Stuermer, J. D. Petersen, D. P. McDonald, and P. C. Ford, *J. Amer. Chem. Soc.*, **94**, 6665 (1972).
(6) L. Moggi, *Gazz. Chim. Ital.*, **97**, 1089 (1967).
(7) T. L. Kelly and J. F. Endicott, *J. Phys. Chem.*, **76**, 1937 (1972).
(8) T. L. Kelly and J. F. Endicott, *J. Amer. Chem. Soc.*, **94**, 1797 (1972).
(9) C. Kutal and A. W. Adamson, *Inorg. Chem.*, **12**, 1454 (1973).
(10) M. M. Muir and W. L. Huang, *Inorg. Chem.*, **12**, 1831 (1973).
(11) J. D. Petersen and P. C. Ford, to be submitted for publication.
(12) J. D. Petersen, R. J. Watts, and P. C. Ford, work in progress.
(13) T. R. Thomas and G. A. Crosby, *J. Mol. Spectrosc.*, **38**, 118 (1971).
(14) T. R. Thomas, R. J. Watts, and G. A. Crosby, *J. Chem. Phys.*, **59**, 2123 (1973).
(15) J. G. Calvert and J. N. Pitts, Jr., "Photochemistry," Wiley, New York, N. Y., 1966, Chapter 7.
(16) B. J. Cohen and L. Goodman, *J. Chem. Phys.*, **46**, 713 (1967).
(17) N. J. Turro, "Molecular Photochemistry," W. A. Benjamin, New York, N. Y., 1967, p 132.
(18) (a) J. N. Demas and G. A. Crosby, *J. Amer. Chem. Soc.*, **92**, 7262 (1970). (b) *Note.* A recent communication [G. A. Crosby, K. W. Hipps, and W. H. Elfring, Jr., *J. Amer. Chem. Soc.*, **96**, 629 (1974)] has drawn renewed attention to the point that the spin orbit coupling constants of the heavier transition metals are of such a magnitude that spin multiplicity levels may no longer be meaningful for certain excited states of these metals' complexes. For the Rh(III)–ammine complexes, evidence in this paper and ref 7 points to the presence of a reactive, lowest energy excited state which is populated by energy transfer from an excited organic molecule (*e.g.*, biacetyl or pyrazine) in the triplet state but not from the corresponding singlet excited state. Whether this reactive state is in fact a "triplet" does not affect significantly the conclusions of this paper; however, by describing this state as a triplet our discussion has remained consistent with other recent studies (ref 7, 13, 14) of the excited states of these complexes.
(19) G. W. Robinson and R. P. Frosch, *J. Chem. Phys.*, **37**, 1962 (1962); **38**, 1187 (1963).
(20) B. R. Henry and M. Kasha, *Ann. Rev. Phys. Chem.*, **19**, 161 (1968).
(21) R. Englman and J. Jortner, *Mol. Phys.*, **18**, 145 (1970).
(22) W. M. Gelbart, K. F. Freed, and S. A. Rice, *J. Chem. Phys.*, **52**, 2460 (1970).
(23) E. W. Schlag, S. Schneider, and S. F. Fischer, *Ann. Rev. Phys. Chem.*, **22**, 465 (1971).
(24) J. E. Hillis and M. K. DeArmond, *J. Luminescence*, **4**, 273 (1971).
(25) D. J. Robbins and A. J. Thomson, *Mol. Phys.*, **25**, 1103 (1973).
(26) R. G. Pearson, N. Stellwagen, and F. Basolo, *J. Amer. Chem. Soc.*, **82**, 1077 (1960).
(27) S. C. Chan and F. Leh, *J. Chem. Soc. A*, 2010 (1967).
(28) S. G. Zipp and S. K. Madan, *Inorg. Chem. Acta*, **6**, 401 (1972).
(29) The term k_w could show temperature dependence if it represented the composite of several weak coupling deactivation pathways having different rates and occurring from different vibrational states of the electronic excited state. Thus the weak coupling rate could be temperature dependent owing to changes in the Boltzmann distribution between the various vibration states. However, given the criterion that weak coupling mechanisms are largely suppressed by perdeuteration, this possibility alone cannot explain the differing temperature dependences of quantum yields in the perprotio and perdeuterio cases.
(30) Not only is $\Phi_p(D)$ less temperature sensitive than $\Phi_p(H)$ but also the ratio k_n/k_p is less temperature sensitive for the deuterated complexes. For example, between 23 and 55°, k_r/k_p falls from 12.3 to 7.2 for the perprotio case and from 5.7 to 4.6 for the perdeuterio case.

On the Mechanism of Ion Exchange in Crystalline Zirconium Phosphates. XI. The Variation in Unit Cell Dimensions and Sodium Ion/Hydrogen Ion Exchange Behavior in Highly Crystalline α-Zirconium Phosphates[1]

A. Clearfield,*

Department of Chemistry, Clippinger Graduate Pesearch Laboratories, Ohio University, Athens, Ohio 45701

L. Kullberg, and Å. Oskarsson

Department of Chemistry, University of Lund, Lund, Sweden *(Received August 22, 1973)*

Publication costs assisted by the National Science Foundation

The Na^+/H^+ exchange behavior of highly crystalline samples of α-zirconium phosphate were examined. It was found that the greater the degree of crystallinity, as measured by the time of digestion of α-ZrP in 12 *M* H_3PO_4, the greater was the preference of the exchanger for sodium ion relative to hydrogen ion. However, under all conditions examined, hydrogen ion was greatly preferred. Precise determination of the unit cell dimensions of the several exchangers showed a systematic variation in their values. This variation is attributed to structure differences arising from the digestion process. A qualitative explanation of the observed ion-exchange behavior of α-ZrP is presented based on the proposed variations in structure of the exchanger samples.

Introduction

In paper VI of this series it was shown that the ion-exchange behavior of α-zirconium phosphate (α-ZrP) preparations is strongly dependent upon the degree of crystallinity of the preparation.[2a] In that study portions of amorphous zirconium phosphate were refluxed in progressively stronger concentrations of phosphoric acid. This produced exchangers with average crystallite sizes ranging from 70 to greater than 1000 Å. The most crystalline of these exchangers was one prepared by refluxing the amorphous gel in 12 *M* H_3PO_4 for 48 hr (12:48).[2b] Its ion-exchange behavior differed significantly from a preparation described earlier which had been refluxed for 336 hr.[2c] X-Ray powder patterns of the two zirconium phosphates showed no evidence of line broadening and their interplanar spacings were identical to three significant figures. Therefore, it was of interest to determine whether the observed differences in behavior really did depend upon the time of refluxing. In this paper we report upon additional experiments with highly crystalline samples of α-ZrP.

Experimental Section

The crystalline samples of α-ZrP were prepared as described earlier.[2a] The reflux medium was 12 *M* H_3PO_4 and the reflux times were 48 (identified as 12:48) 96 (12:96), 190 (12:190), and 336 hr (12:336). X-Ray diffraction patterns confirmed that all of the samples were α-ZrP with no measurable line broadening or extraneous reflections. The titration curves were also carried out as described previously.[2a]

Accurate unit cell dimensions of the crystalline exchangers were obtained at 22 ± 1° with a Guinier-Hagg focusing camera, equipped with a quartz monochromator. Cu Kα radiation (λ 1.54051 Å) was used. Aluminum powder (cubic, a = 4.04962 Å) was taken as a standard to check the errors of measurement. A scale graduated in units of 0.1 mm was photographed onto each film before processing to facilitate the measurements.

Calculations. Approximate unit cell dimensions, determined by Ahrland and Albertsson,[3] were employed for the initial indexing of the powder patterns. More accurate unit cell dimensions were then obtained from the indexed powder data and these were refined by the method of least squares. The function minimized was $\Sigma w(\sin^2\theta_o - \sin^2\theta_c)^2$ where θ_o and θ_c represent the values of observed and calculated Bragg angles, respectively. The weights were obtained from the function $w = 1/\sin^2 2\theta$.

X-Ray powder patterns of the exchangers, taken at different levels of exchange, were obtained as described before with a Norelco wide-angle goniometer.[2a]

Results

The potentiometric titration curves, obtained using a mixed NaCl + NaOH solution as titrant, are shown in Figure 1. It is seen that the longer the reflux time used to prepare the exchanger, the greater is its preference for sodium ion relative to hydrogen ion. X-Ray diffraction patterns of the solids, taken at various levels of exchange, showed that the exchange phases are similar to those reported for the fully crystalline α-ZrP. That is, up to 50% of exchange the X-ray pattern is that of a mixture of α-ZrP and $ZrNaH(PO_4)_2 \cdot 5H_2O$ [termed phase $A(Na^+ \cdot 5H_2O)$] and from 50 to 100% of exchange this latter phase converts to $Zr(NaPO_4)_2 \cdot 3H_2O$ [phase $D(Na^+ \cdot 3H_2O)$].[4] However, it should be noted that all the curves except the one for 12:336 exhibit definite nonzero slopes. The occurrence of these nonzero slopes is evidence for the presence of one or more solid solution phases with a variable composition in the solid exchanger.[2a,c] An even larger positive slope is exhibited by the titration curve for a sample refluxed for 24 hr in 12 *M* H_3PO_4.[5] These results follow the general trend reported earlier,[2a] *viz.*, that the less crystalline the exchanger, the greater the slope in the titration curve.

The degree of crystallinity of α-ZrP exchangers less crystalline than those examined in the present study

TABLE I: Unit Cell Dimensions of α-ZrP Samples[a]

Dimension	α-ZrP exchanger				
	12:24[b]	12:48	12:96	12:190	∞
a, Å	9.097 (5)	9.0523 (21)	9.0401 (10)	9.0491 (13)	9.0540 (20)
b, Å	5.307 (1)	5.2853 (16)	5.2775 (7)	5.2845 (9)	5.2843 (15)
c, Å	16.284 (3)	16.2508 (65)	16.2125 (25)	16.1938 (35)	16.1908 (65)
β, deg	111.38 (1)	111.369 (27)	111.414 (11)	111.447 (15)	111.440 (30)
$a \times b$, Å^2	48.278 (27)	47.844 (17)	47.709 (8)	47.820 (10)	47.844 17)
V, Å^3	732.0 (5)	724.1 (4)	720.1 (2)	720.8 (2)	721.0 (4)

[a] Estimated standard deviations in the last significant figures are given in parentheses. [b] Data taken from ref 3.

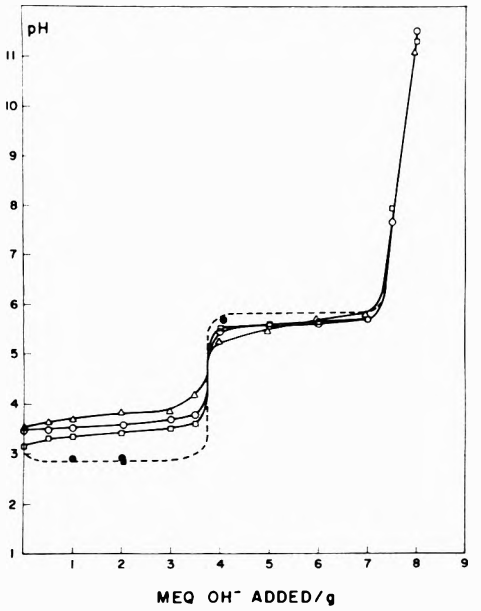

Figure 1. Potentiometric titration curves for crystalline α-ZrP preparations: titrant 0.1 M NaCl + 0.1 M NaOH; reflux time of sample 48 hr (△), 96 hr (○), 190 hr (□), 336 hr dashed line taken from data in ref 2c, solid points determined in present study.

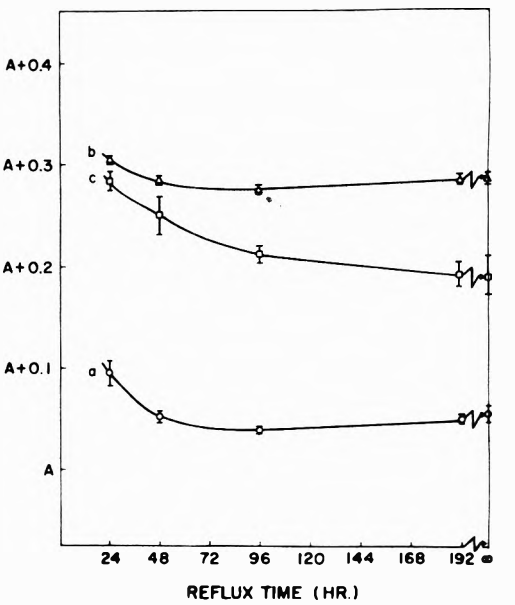

Figure 2. Variation in unit cell dimensions of α-ZrP with reflux time (in 12 M H_3PO_4) used to prepare samples. A represents the integer closest to the value of the respective unit cel dimension. The error bars represent $\pm 3\sigma$ where σ is the estimated standard deviation listed in Table I.

could be determined by X-ray line broadening measurements.[2a] However, the X-ray patterns of the exchanger samples exhibiting the titration curves of Figure 1 showed no evidence of line broadening. Thus, the crystallite size must be greater than 1000 Å in each of these exchangers. Still, the variation in ion-exchange behavior of the highly crystalline α-ZrP exchangers must have their origin in some subtle structural differences. With this in mind we determined the unit cell dimensions of the different samples. The results are given in Table I and plotted in Figures 2 and 3. For a complete indexing of one of the powder patterns the reader may consult ref 3. The sample chosen as ∞ was prepared by heating a gel in 12 M H_3PO_4 at 160–170° for 5 weeks. The resultant crystals ranged in size from 10 to 300 μ compared to ~0.1–1 μ obtained by the refluxing procedure. It is seen from the plots that the variation of the unit cell parameters are larger than 3σ and therefore real.

Discussion

In seeking reasons for the variation in ion-exchange behavior exhibited by the highly crystalline α-ZrP samples, differences in composition must be considered as a possible factor. However, accumulated analytical data presented previously show that within fairly narrow limits the composition of the highly crystalline samples corresponds to the formula $Zr(HPO_4)_2 \cdot H_2O$.[2a,c,5-7] What is more important is that no systematic variation of composition with crystallinity is observed for these more crystalline exchangers. This is corroborated by the titration results. All of the samples examined in this work exhibit end points at identical levels of added sodium hydroxide (Figure 1). These end points occur after the addition of 3.77 ± 0.02 and 7.54 ± 0.03 mequiv of sodium hydroxide per gram of exchanger which correspond to the replacement of 1 and 2 mol of hydrogen ion per formula weight of exchanger. Thus the differences in the titration curves are not due to variations in the phosphate content of the exchangers and must be structural in origin. This is also the case for the less crystalline zirconium phosphates examined previously.[2a]

Taking the present results in conjunction with those for less crystalline α-ZrP exchangers permits a fuller explanation of the exchange process. Three types of exchange behavior can be distinguished. With the amorphous or nearly amorphous exchanger (0.5:48) a single solid solution is obtained over the entire composition range of sodium and hydrogen ions. At the other extreme the exchanger which had been refluxed for 336 hr in 12 M H_3PO_4 formed pure sodium containing phases of composition $ZrNaH(PO_4)_2 \cdot 5H_2O$ (phase A) and $Zr(NaPO_4)_2 \cdot 3H_2O$ (phase D).[2c] Exchangers of intermediate crystallinity form a complicated series of solid solutions.[2a] However, the more crystalline ones (starting with 3.5:48) yield phases whose

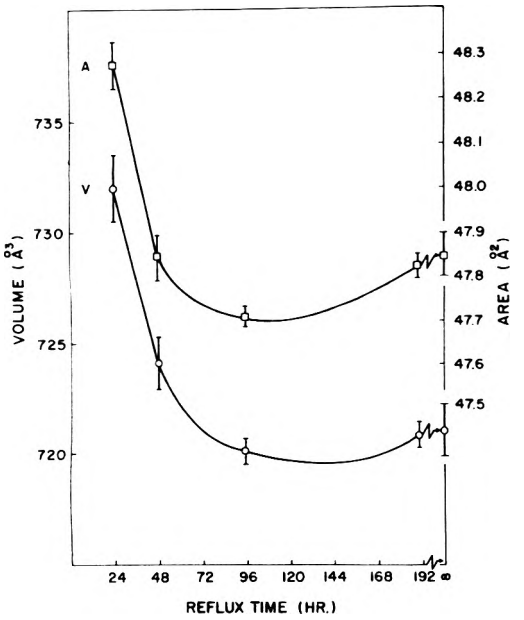

Figure 3. Variation in unit cell volume and area of *ab* plane of α-ZrP with reflux time. Error bars are $\pm 3\sigma$.

X-ray patterns resemble those of phase A and phase D. That these are in actuality solid solutions and not pure phases is clear from the fact that they exist over a range of compositions. They are therefore referred to as phase A (Na-H) and phase D (2Na-H), respectively.[2a] For example, with the exchanger 4.5:48 phase A (Na-H) was the only one present from 38 to 50% of exchange and phase D (2Na-H) from 90 to 100%. These ranges are considerably reduced in the case of the more crystalline exchanger 9:48. Phase A (Na-H) was found to exist by itself in the narrow range of 46–50% of loading and phase D (2Na-H) at about 97–100%. These results indicate that the difference in the titration curves of the two exchangers stems from the composition (Na^+ and H^+ content) of the solid phases in equilibrium with the exchanging solution.

All the titration curves in Figure 1 exhibit positive slopes, except for exchanger 12:336 for which the slopes are zero. Phase rule arguments can be invoked to show that a nonzero slope requires that at least one solid phase present during the titration must have a variable composition.[2c] Thus, even in the highly crystalline exchangers examined in this study, the exchanged phases must have variable composition even if only over a small composition range. They are thus distinguished from the sample 12:336 which exhibits zero slope in its titration curve and constant composition solid phases. It was pointed out that the range of variable composition of the exchanged phases decreased drastically with increased crystallinity as represented by the results for samples 4.5:48 and 9:48. It is then reasonable to suppose that this process of narrowing of the solubility range continues as the crystallinity, taken to be proportional to the time of reflux in 12 *M* H_3PO_4, of the exchanger improves. The end member of the series is then the fully crystalline exchanger (as represented by sample 12:336) which yields the titration curve with zero slopes. Thus between 9:48 and 12:336 the crystallinity of the samples must be less than complete and continue to improve during the refluxing even though the changes are small. However, their differences in crystallinity are reflected in the changing unit cell dimensions and in the different pH values of their titration curves. The underlying reason for the pH differences is then the narrowing of the composition ranges over which the solid solutions exist. Thus, the solids present during exchange would have slightly different compositions and be in equilibrium with solutions having different H^+/Na^+ ratios.

Structural arguments can be brought to bear in developing an explanation for the observed experimental results. Rapid precipitation of zirconium phosphate leads to the formation of an amorphous gel.[6] However, as already stated, single crystals about 0.1 mm in length can be grown in 4–6 weeks at 150–180° in sealed quartz tubes containing the gel and 12 *M* H_3PO_4.[7] These crystals of α-ZrP consist of layers.[7] Within the layers the zirconium atoms lie in a plane at the corners of parallelograms and are linked together through phosphate groups. The parallelograms can be divided into two equilateral triangles with zirconium atoms at their apices. The phosphate groups are situated such that the phosphorus atoms are nearly on the perpendiculars to the planes through the centers of the triangles and are alternately above and below the plane in any two adjacent triangles. Three oxygens of the phosphate are then bonded to the three zirconium atoms forming a triangle and the fourth bears the hydrogen and points away from the metal atom plane. Each metal atom is octahedrally coordinated by oxygen atoms from six different phosphate groups. The layers are staggered in such a way that hexagonal-shaped cavities are formed between the layers.[4,7] The sides of the cavity are formed by P-OH groups, three from the layer above and three from the layer below. In the fully exchanged ammonium ion form the layers remain intact although spread further apart with the NH_4^+ ions taking up positions between the layers.[8] Four NH_4^+ groups surround each negative oxygen and each positive ion is in turn surrounded by four negative oxygens. Presumably equally ordered structures are obtained with the sodium exchanged phases.

Apparently, under conditions of rapid precipitation, the complex stereochemical requirements of crystal formation cannot be achieved. In the gel, the phosphate and metal atoms are pictured as being randomly displaced from their equilibrium crystal lattice sites.[6] On refluxing the gels in phosphoric acid an ordering process occurs through a digestion mechanism.[9] The process is slow requiring hundreds of hours in strong phosphoric acid at reflux temperature to produce single crystals. In these crystals the cavities are sufficiently regular so as to appear identical with the incoming ions during exchange. Thus, the sodium ions arrange themselves in adjacent cavities even at very low uptake, with the formation of a new phase of composition $ZrNaH(PO_4)_2 \cdot 5H_2O$ (phase A). Thus phase A and unexchanged α-ZrP exist together until 50% of exchange.

In exchangers of intermediate crystallinity all degrees of order between the crystals and amorphous gels are possible. Consider a highly ordered (but not fully crystalline) exchanger such as those examined in this study. The solid phase may be thought of as essentially α-ZrP crystals but with small regions where the phosphate and zirconium atoms are shifted away from their normal lattice positions. If the phosphate groups forming a cavity shift or tilt toward each other, the cavity becomes more restricted and at the same time adjacent cavities become larger since each phosphate group is common to three cavities. On the average some of these cavities (presumeably the larger ones) are more favorable for occupation by the sodi-

um ions than the ordered cavities of the ideal crystal and others less favorable. Thus the sodium ions would initially distribute themselves randomly in those sites which are more favorable for exchange than the ordered ones. The ordered sites retain the α-ZrP structure so that the resultant solid phase would be α-ZrP in which some Na^+ is randomly distributed. When all of these favored sites are occupied the Na^+ then enters the ordered sites producing a phase change to phase A (Na–H). Filling all of the ordered sites converts the solid completely to phase A (Na–H) but this phase still contains exchangable hydrogens in the less favorable sites, *i.e.*, the more restricted ones. Thus, phase A can have a variable composition in these cases. The solubility limits of the ions in the phases (or the composition ranges) then would depend upon the type and number of cavities in the original exchanger which deviate from the ideal size. Thus, as the crystallinity of the exchanger decreases the number of nonregular cavities increases with attendent increase in the composition range over which a particular phase can exist. In the case of exchangers which are nearly amorphous (0.5:48) only a single solid solution is obtained for the entire range of sodium ion uptake. This is consistent with the idea that in the amorphous gel there is a random distribution of cavities sizes and that sites of equivalent preference for an ion are statistically distributed. In such a structure there should be a steady decrease in preference for the incoming sodium ion with increase load as the more favorable cavities are occupied first. This phenomenon is actually observed.[2a]

We interpret the variation in unit cell dimensions of the highly crystalline zirconium phosphates as resulting from the displacements of metal and/or phosphate groups as described above. A fully crystalline exchanger then is one which has been refluxed long enough so that its structure is sufficiently regular that all the cavities have the same preference for sodium ion. This exchanger has the cell dimensions listed in Table I under the heading ∞.

The a and b unit cell dimensions lie within the plane of the layers while the $c \cos \beta$ direction is perpendicular to the layers. Thus the interlayer distance $\frac{1}{2}c \cos \beta$, varies from 7.582 Å in 12:24 to 7.5352 Å in the larger crystals. This represents a 0.62% change compared to a 0.47 and 0.43% change for the a and b dimensions, respectively. Since the forces between layers are weak relative to the bonding forces within the layers,[7] this result is not unexpected. Furthermore, the interlayer distance is the only parameter which continually decreases. The others pass through a minimum. However, a strict correlation between the magnitude of the interlayer distance and the position of the titration curve on the pH scale is not to be expected since, as has been pointed out, the pH depends upon the composition and nature of the solid phase(s).

Alberti and coworkers have found that α-ZrP, prepared by direct precipitation, yields phases of different composition in the Li^+/H^+ and Ca^{2+}/H^+ exchange systems than does α-ZrP crystals prepared by the reflux method.[10] Similarly, Horsley and Nowell observed significant differences in the dehydration, thermal behavior, and surface properties of crystalline α-ZrP prepared in several different ways.[11,12] Torracca has also found that several highly crystalline α-ZrP samples prepared by refluxing in strong H_3PO_4 yielded different pH values during titration.[13] It is quite likely that these behaviors are also due to the type of structural disorder described above. Thus, a more detailed study of the nature of this disorder must be forthcoming before a quantitative explanation for the behavior of α-ZrP can be formulated.

References and Notes

(1) This work is part of a cooperative research program jointly sponsored by the National Science Foundation under Grant No. GP 8108 and the Swedish Natural Science Research Council. The Swecish portion is under the Direction of Professor Sten Ahrland, Lund University, Lund, Sweden.

(2) (a) A. Clearfield, Å. Oskarsson, and C. Oskarsson, *Ion Exchange Membranes*, 1, 91 (1972). (b) The exchangers will be referred to by two numbers separated by a colon. The first number gives the concentration of H_3PO_4 in which the gel was refluxed and the second number the time of reflux in hours. The characterization of the samples as to crystallinity, composition, etc. is given in ref 2a. (c) A. Clearfield and A. S. Medina, *J. Phys. Chem.*, **75**, 3750 (1971).

(3) S. Ahrland and J. Albertsson, *Acta Chem. Scand.*, **23**, 1446 (1969).

(4) A. Clearfield, W. L. Duax, A. S. Medina, G. D. Smith, and J. R. Thomas, *J. Phys. Chem.*, **73**, 3424 (1969).

(5) J. Albertsson, *Acta Chem. Scand.*, **29**, 1689 (1966).

(6) A. Clearfield and J. A. Stynes, *J. Inorg. Nucl. Chem.*, **26**, 117 (1964).

(7) A. Clearfield and G. D. Smith, *Inorg. Chem.*, **7**, 431 (1969).

(8) A. Clearfield and J. M. Troup, *J. Phys. Chem.*, **77**, 243 (1973).

(9) A. Clearfield and J. R. Thomas, *Inorg. Nucl. Chem. Lett.*, **5**, 775 (1969).

(10) G. Alberti, U. Constantino, S. Allulli, M. A. Massucci, and M. Pellicčioni, *J. Inorg. Nucl. Chem.*, **35**, 1347 (1973).

(11) S. E. Horsley and D. V. Nowell, *Thermal Anal.*, **2**, 611 (1971).

(12) S. E. Horsley and D. V. Nowell, *J. Appl. Chem. Biotechnol.*, **23**, 215 (1973).

(13) E. Torracca, private communication.

Predicted Observable Fluorescent Lifetimes of Several Cyanines

Nancy J. L. Roth and Arnold C. Craig*

Department of Chemistry, Montana State University, Bozeman, Montana 59715 *(Received January 2, 1974)*

Predicted observable fluorescent lifetimes of six cyanine dyes have been obtained from intrinsic fluorescent lifetime and quantum yield measurements. The predicted lifetimes vary by nearly three orders of magnitude, from 1 nsec to 1.7 psec, and appear to be more sensitive to chain length variation than heteroatom differences. In particular the shortest chain cyanines appear to have a facile nonradiative pathway from the excited singlet.

Introduction

The determination of fluorescence lifetimes is critical to the understanding of the "energy-handling" properties of excited states. Although there have been recent advances in measuring short lifetimes by pulse distortion,[1] single-photon counting,[2] and picosecond pulse lasers,[3] they are not readily applicable to all compounds. It would be desirable to be able to determine indirectly, but with a good degree of confidence, observable fluorescent lifetimes. Such determinations can be made if the intrinsic fluorescent lifetimes and fluorescent quantum yields are measured with reasonable accuracy.

Because cyanine dyes are of current interest as photographic sensitizers,[4] dye lasers, and mode locks for lasers[3] and can be readily obtained in various structural modifications with respect, for example, to chain length, heterocyclic nuclei, and ring and chain substitution,[4] we proposed to obtain predicted observable fluorescent lifetimes for several series of cyanines. The results for the first two such series are reported here. The lifetime of dye 3 has been measured by two photon absorption and subsequent fluorescence decay analysis as 1.6 ± 0.1 nsec.[5] Even though the experimental conditions were not identical with the present work the agreement is rather good. Another group has estimated the observable fluorescent lifetime of 3 as 1.24 nsec using a similar analysis.[6] Their data for ϕ (0.49) and τ_{intr} (2.54 nsec) compare favorably with our data.

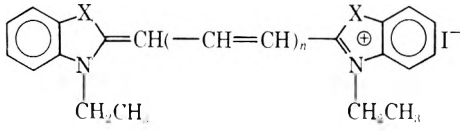

1, X = O; n = 0 4, X = S; n = 0
2, X = O; n = 1 5, X = S; n = 1
3, X = O; n = 2 6, X = S; n = 2

Experimental Section

The dyes 1-6 were prepared by standard methods[4] and were analytically pure. Determination of absorption spectra were made on a Cary Model 14 spectrophotometer. Fluorescent spectra and quantum yields were determined on a custom apparatus utilizing a tungsten source, two Bausch & Lomb 500-mm monochromators, and an EMI 9558Q photomultiplier tube.[7] Predicted observable lifetimes (τ_{pred}) were calculated from intrinsic fluorescent lifetimes (τ_{intr}) and fluorescent quantum yields (ϕ) by

$$\tau_{pred} = \tau_{intr}\phi$$

Intrinsic lifetimes were calculated from absorption and fluorescent parameters by the Birks and Dyson modification of the Strickler-Berg relationship.[8,9]

$$1/\tau_{intr} = 2.880 \times 10^{-9} n_{u_0-1}{}^3/n_{l_0-u} \times \langle \bar{\nu}_f^{-3} \rangle_{av}^{-1} g_l/g_u \int \epsilon_{(\bar{\nu}_{l_0-u})} \, d \ln \bar{\nu}_{l_0-u}$$

Fluorescent quantum yields were determined by comparison with known standards,[10] by methods generally described by Parker.[11]

The fluorescent standards used were quinine bisulfate, 3-aminophthalimide, 3-nitro-*N*,*N*-dimethylaniline, 4-dimethylamino-4′-nitrostilbene, and Rhodamine B.

The cyanine dyes were dissolved in absolute methanol; 10^{-6} to 10^{-5} *M* for absorption and fluorescence spectra and 10^{-4} to 10^{-3} *M* for quantum yield measurements. All measurements were carried out at room temperature. Action spectra for fluorescence of the cyanine dyes indicated the main species was responsible for emission.

Results and Discussion

The predicted observable fluorescent lifetimes of several cyanine dyes are presented in Table I. We believe they represent a realistic assessment of the observable fluorescent lifetimes of these dyes.

The data show differences in τ_{pred} of almost three orders of magnitude. The most striking observation is that the shortest chain length compounds, both the monomethine oxygen and sulfur cyanines, 1 and 4, have extremely short predicted lifetimes, 6.4 and 1.7 psec, respectively. A facile nonradiative pathway from excited singlet must exist for these two dyes. That the counterion, iodide, is not providing that pathway is supported by the high (0.43

TABLE I: Luminescence Properties of Six Cyanine Dyes

Dye	ϕ	$\tau_{intr}(10^9)$, sec	$\tau_{pred}(10^{10})$, sec
1	0.0037	1.72	0.064
2	0.053	2.02	1.1
3	0.43	2.37	10
4	0.00059	2.94	0.017
5	0.048	3.09	1.5
6	0.33	2.87	9.5

and 0.33) fluorescent quantum yields of the longest chain pair, 3 and 6.

The somewhat longer intrinsic lifetimes of the sulfur compounds are almost compensated by their lower fluorescent quantum yields so that the oxygen and sulfur compounds of comparable chain length have nearly the same predicted lifetimes.

Since these predicted observable lifetimes were determined in dilute solutions without the presence of obvious quenchers or energy receptors and since the composite rate of all decay processes from the excited state is the inverse of the observable lifetime, a minimum may be placed on the rate of energy transfer from the first excited singlet state of these dyes to quenchers or acceptor molecules. Investigation of the energy transfer rates to acceptors in dilute solutions is a logical step which we plan to investigate.

References and Notes

(1) K. Osada, *Rev. Sci. Instrum.*, **44**, 656 (1973).
(2) (a) R. Schuyler, I. Isenberg, and R. D. Dyson, *Photochem. Photobiol.*, **15**, 395 (1972); (b) W. R. Ware, L. J. Doemeny, and T. L. Nemzek, *J. Phys. Chem.*, **77**, 2038 (1973); (c) C. Lewis, W. R. Ware, L. J. Doemeny, and T. L. Nemzek, *Rev. Sci. Instrum.*, **44**, 107 (1973).
(3) (a) P. M. Rentzepis, *Advan. Chem. Phys.*, **23**, 189 (1973); (b) T. A. Erdmann, H. Figger, and H. Walther, *Opt. Commun.*, **6**, 166 (1972).
(4) L. G. S. Brooker in "The Theory of the Photographic Process," 3rd ed, C. E. K. Mees and T. H. James, Ed., MacMillan, New York, N. Y., 1966, Chapter 11 and references cited therein.
(5) H. Cirkel, L. Ringwelski, and F. P. Schaeffer, *Z. Phys. Chem. (Frankfurt am Main)*, **81**, 158 (1972).
(6) D. N. Dempster, T. Morrow, R. Rankin, and G. F. Thompson, *J. Chem. Soc., Faraday Trans. 2*, **68**, 1479 (1972).
(7) The authors wish to thank Dr. Patrik R. Callis for use of his equipment and for helpful discussions.
(8) (a) S. J. Strickler and R. A. Berg, *J. Chem. Phys.*, **37**, 814 (1962); (b) J. B. Birks and D. J. Dyson, *Proc. Roy. Soc., Ser. A*, **275**, 135 (1963).
(9) The cyanines meet very nicely the criterion established by Strickler and Berg[8a] for those compounds for which the equation would give good predictions.
(10) (a) E. Lippert, W. Nägele, I. Seibold-Blankenstein, U. Staiger, and W. Voss, *Z. Anal. Chem.*, **170**, 1 (1954); (b) R. J. Argauer and C. E. White, *Anal. Chem.*, **36**, 368 (1964); (c) R. J. Argauer, Ph.D. Thesis, University of Maryland, June 1963, pp 12–42.
(11) C. A. Parker, "Photoluminescence of Solutions," Elsevier, New York, N. Y., 1968, pp 252–261.

Theory of Saturation and Double Resonance in Electron Spin Resonance Spectra. VI. Saturation Recovery[1]

Jack H. Freed

Department of Chemistry, Cornell University, Ithaca, New York 14850

(Received December 27, 1973)

Publication costs assisted by the Petroleum Research Fund

The general theory of Freed for steady-state saturation and double resonance in esr spectra of free radicals is extended to cover time-dependent experiments. The solution is again found to depend on the same matrix representations developed in the earlier work. Particular attention is paid to saturation recovery in the light of recent such experiments. It is shown that while the general solutions yield sums of many exponential decays, the dominant observation may, to a first approximation in many cases, be described in terms of single $T_1 = \frac{1}{2}W_e$, where W_e is the electron-spin flip rate, in agreement with recent observations. This T_1 is characteristically the slowest decay constant, and is either well separated from the much faster decays (due to nuclear spin flip, exchange, and/or reorientational effects), or may be difficult to distinguish from decay constants of comparable magnitude (due to the same type of effects). Both conventional saturation recovery and eldor-type recoveries are discussed from this point of view. The general approach given is equally adaptable to cases of esr spectra in the motional narrowing region as well as esr spectra characteristic of slow tumbling. Both cases are discussed in detail with several examples given. In particular, in the slow tumbling region for the case of a radical with hyperfine structure (*e.g.*, a nitroxide), it is shown that, in general, both direct reorientational effects as well as nuclear spin flip processes contribute directly to the relaxation modes. The analysis given emphasizes analytic aspects although the general expressions, appropriate for accurate computer simulation, are given.

I. Introduction

Recently, there has been growing interest in pulsed esr experiments on free radicals in liquids, in particular, saturation recovery-type experiments.[2] The relaxation behavior of such systems is, in general, rather complex, and has been the subject of a series of papers (I–V) analyzing steady-state saturation and double resonance behavior.[3-9] A review of some of these aspects has recently been given.[10] In the future, one may expect to see an increase in importance of pulsed techniques, so it was deemed ap-

propriate to adapt the steady-state saturation theory to such techniques, and this is the main objective of the present paper. Our main emphasis is on saturation recovery, but we also include some comments on pulsed eldor,[9] which, in principle, may be thought of as a saturation recovery, but with observation at a frequency displaced from the high-power pulse frequency. Our methods, however, could be extended to free-induction decay and echo-type experiments for the free-radical systems.

In developing our analysis, we are struck by the close similarity between the values of W_e obtained by steady-state saturation techniques involving an analysis of the complex relaxation paths[6,11-14] and $(2T_1)^{-1}$ obtained (but not analyzed) from the saturation recovery experiments for similar systems also involving complex relaxation.[2] Thus, another objective of the present work is to demonstrate that over a wide range of types of systems, the saturation recovery experiment is simply interpreted. In this context we emphasize analytic results, but we also give the general expressions which are amenable to computer methods already developed.

Also, recent theoretical and experimental work, which has focused on esr spectra in the slow-tumbling region, has (1) extended the range of motional reorientation times over which accurate analyses could be made of these motions and (2) demonstrated that interesting features of the motion (*i.e.*, deviations from Brownian motion) could be obtained.[15] There have been some studies of saturation effects in such cases[12,15-17] and a theoretical framework has been developed.[12,18-21] It is another objective of the present work to show how slow-motional saturation-recovery (and eldor-type) experiments may be analyzed by an extension of the theories already developed. We are able to take advantage of a number of *formal* similarities between a motional-narrowing theory and a slow motional theory to cast both in a single general framework. We are then able to establish analogies to clarify the more complex slow motional analysis.

We give in section II the extensions of the general formalism to time-dependent experiments. Our discussion here borrows heavily from the previous notation and methods[3-8,12,18-21] and the reader is referred to these sources for more complete discussion. Motional narrowing examples are discussed in section III, while slow tumbling is discussed in section IV. A summary is given in section V.

II. General Formulation

We start with the usual density-matrix equation of motion for $\sigma(t)$[3-8,10,22]

$$\dot{\sigma} = -(\mathcal{H}_0^{\times} + \epsilon(t)^{\times} + iR)(\sigma - \sigma_0) \tag{2.1}$$

where $\mathcal{H}_0$ is the zero-order Hamiltonian, $\epsilon(t)$ the interaction with the radiation field, R the relaxation matrix, σ_0 the equilibrium value, and the superscript times sign implies that for two operators A and B, $A^{\times}B = [A,B]$.

This is the usual expression one obtains for the motional narrowing region, where rotational modulation of the perturbing Hamiltonian $\mathcal{H}_1(\Omega)$ is sufficiently rapid that $|\mathcal{H}_1(\Omega)^2|\tau_R^2 \ll 1$. More generally, we may write a stochastic Liouville expression for $\sigma(\Omega,t)$ wherein the assumption of motional narrowing need not be made[10,18,21]

$$\dot{\sigma}(\Omega,t) = -i(\mathcal{H}_0^{\times} + \epsilon(t)^{\times} + \mathcal{H}_1(\Omega)^{\times} + iR' - i\Gamma_\Omega)(\sigma(\Omega,t) - \sigma_0(\Omega)) \tag{2.2}$$

Here Γ_Ω is the Markov operator for the rotational tumbling, R' is that part of the relaxation matrix which is orientation independent, while

$$\sigma(t) = \int d\Omega \sigma(\Omega,t) P_0(\Omega) \equiv \langle P_0(\Omega)|\sigma(\Omega,t)|P_0(\Omega)\rangle \tag{2.3}$$

where the convenient bra-ket notation is introduced. When $|\mathcal{H}_1(\Omega)|/|\Gamma_\Omega| \ll 1$ eq 2.2 again becomes eq 2.1.

We first study the general approach to the time-dependent solution of eq 2.1, and then we generalize to cover eq 2.2. Thus we introduce the definitions

$$(\sigma(t) - \sigma_0)_{\lambda_j} \equiv \chi(t)_{\lambda_j} \tag{2.4a}$$

$$\chi(t)_{\lambda_j} = \sum_{n=-\infty}^{\infty} e^{in\omega t} Z(t)_{\lambda_j}^{(n)} \tag{2.4b}$$

and

$$Z(t)_{\lambda_j}^{(n)} = Z(t)_{\lambda_j}^{(n)'} + iZ(t)_{\lambda_j}^{(n)''} \tag{2.4c}$$

for the λ_jth transition. Then by analogy with the steady-state solutions,[3-8,10] we obtain the coupled partitioned-matrix equations

$$\begin{bmatrix} \frac{1}{\sqrt{2}}\dot{\mathbf{Z}}(t) \\ \frac{1}{\sqrt{2}}\dot{\mathbf{Z}}^*(t) \\ \frac{1}{2}\dot{\hat{\mathbf{X}}}(t) \\ \frac{1}{2}\dot{\tilde{\mathbf{X}}}(t) \end{bmatrix} = \begin{bmatrix} \mathbf{R} - i\mathbf{K} & 0 & \sqrt{2}i\hat{\mathbf{d}} & \sqrt{2}i\tilde{\mathbf{d}} \\ 0 & \mathbf{R} + i\mathbf{K} & -\sqrt{2}i\hat{\mathbf{d}} & -\sqrt{2}i\tilde{\mathbf{d}} \\ \sqrt{2}i\hat{\mathbf{d}}^{tr} & -\sqrt{2}i\hat{\mathbf{d}}^{tr} & -\hat{\mathbf{W}} & -\mathbb{W} \\ \sqrt{2}i\tilde{\mathbf{d}}^{tr} & -\sqrt{2}i\tilde{\mathbf{d}}^{tr} & -\mathbb{W}^{tr} & -\tilde{\mathbf{W}} \end{bmatrix} \times \begin{bmatrix} \frac{1}{\sqrt{2}}\mathbf{Z}(t) \\ \frac{1}{\sqrt{2}}\mathbf{Z}^*(t) \\ \frac{1}{2}\hat{\mathbf{X}}(t) \\ \frac{1}{2}\tilde{\mathbf{X}}(t) \end{bmatrix} + \begin{bmatrix} i\mathbf{Q}/\sqrt{2} \\ -i\mathbf{Q}/\sqrt{2} \\ 0 \\ 0 \end{bmatrix} \tag{2.5}$$

where we have introduced the definitions

$$\hat{X}_{\lambda_j} \equiv X_{\lambda_j^+} - X_{\lambda_j^-} \tag{2.6a}$$

and

$$\tilde{X}_{\lambda_j} \equiv X_{\lambda_j^+} + X_{\lambda_j^-} \tag{2.6b}$$

(where $\lambda_j^{\pm}$ are the $m_s = \pm$ states corresponding to the λ_jth transition) with the matrices $\hat{\mathbf{d}}, \tilde{\mathbf{d}}$, the transition probability matrices, $\hat{\mathbf{W}}$, $\tilde{\mathbf{W}}$, and $\mathbb{W}$, the width matrix $\mathbf{R}$, the coherence matrix $\mathbf{K}$, and the $\mathbf{Q}$ vector defined elsewhere.[6,7] Equation 2.5 is of the form of a complex symmetric matrix, which may therefore be solved by first diagonalizing the matrix of matrices (*i.e.*, partitioned matrix) on the right-hand side.

The steady-state solutions to eq 2.5 may be calculated by the methods already developed in I–V. In particular, the form of eq 2.5 is

$$\dot{\mathbf{M}}(t) = \mathbf{L}\mathbf{M} + \mathbf{Q}' \tag{2.7}$$

Then the steady-state solution $\mathbf{M}^{ss}$ is formally given as

$$\mathbf{M}^{ss} = -\mathbf{L}^{-1}\mathbf{Q}' \tag{2.8}$$

If we define

$$\Delta\mathbf{Z}(t) \equiv \mathbf{Z}(t) - \mathbf{Z}^{ss} \tag{2.9a}$$

etc. or

$$\Delta\mathbf{M}(t) \equiv \mathbf{M}(t) - \mathbf{M}^{ss} \tag{2.9b}$$

then eq 2.7 may be written in terms of these deviations from steady-state value as

$$\Delta\dot{\mathbf{M}}(t) = \mathbf{L}\Delta\mathbf{M}(t) \tag{2.7a}$$

or

$$\Delta\mathbf{M}(t) = e^{\mathbf{L}t}\Delta\mathbf{M}(o) \tag{2.10}$$

so as $t \rightarrow \infty$, $\Delta\mathbf{M}(t) \rightarrow 0$.

We now assume that we may let $\mathcal{W} = 0$. This is so when the matrix elements of $\mathbf{W}$ obey

$$W_{\alpha\pm,\beta\mp} = W_{\alpha\mp,\beta\pm} \tag{2.11a}$$

$$W_{\alpha\pm,\beta\pm} = W_{\alpha\mp,\beta\mp} \tag{2.11b}$$

(where α and β represent any nuclear spin configurations and the $\pm$ signs refer to m_s) which is a common situation.[6,7] We further assume that only esr tranitions are excited, so that $\hat{\mathbf{d}} = 0$ (For endor $\hat{d} \neq 0$) and the $\hat{\chi}(t)$ may now be decoupled from the relevant part of the solution, *i.e.*, eq 2.5 becomes

$$\begin{bmatrix} \frac{1}{\sqrt{2}}\dot{\hat{\mathbf{Z}}}(t) \\ \frac{1}{\sqrt{2}}\dot{\hat{\mathbf{Z}}}(t) \\ \frac{1}{2}\dot{\hat{\mathbf{X}}}(t) \end{bmatrix} = \begin{bmatrix} \mathbf{R} - i\mathbf{K} & 0 & \sqrt{2}i\hat{\mathbf{d}} \\ 0 & \mathbf{R} + i\mathbf{K} & -\sqrt{2}i\hat{\mathbf{d}} \\ \sqrt{2}i\hat{\mathbf{d}}^{tr} & -\sqrt{2}i\hat{\mathbf{d}}^{tr} & -\hat{\mathbf{W}} \end{bmatrix} \times \begin{bmatrix} \frac{1}{\sqrt{2}}\hat{\mathbf{Z}}(t) \\ \frac{1}{\sqrt{2}}\mathbf{Z}^*(t) \\ \frac{1}{2}\hat{\mathbf{X}}(t) \end{bmatrix} + \begin{bmatrix} iQ/\sqrt{2} \\ -iQ/\sqrt{2} \\ 0 \end{bmatrix} \tag{2.12}$$

In the simple two-level, one-line case, the substitutions $\mathbf{K} \rightarrow \Delta\omega_\lambda$, $-\mathbf{R} \rightarrow T_2^{-1}$, $2\hat{\mathbf{d}} \rightarrow -\omega_1$, $\hat{\mathbf{W}} \rightarrow T_1^{-1}$, $\mathbf{Z} \rightarrow M_x$, $\mathbf{Z}'' \rightarrow M_y$, $\frac{1}{2}\hat{X} \rightarrow (M_0 - M_z)$ yield the familiar Bloch equations, which may be solved by standard methods (*e.g.*, Laplace transforms).[23] However the more general eq 2.12 in operator form are more conveniently handled by diagonalization methods. (The $\mathbf{R}$ and $\mathbf{K}$ matrices are $M \times M$ square matrices in the "space" of induced transitions while $\mathbf{W}$ is an $\frac{1}{2}M \times \frac{1}{2}N$ square matrix in the "eigenstate-pair" space; thus $\mathbf{d}$ is an $M \times \frac{1}{2}N$ rectangular matrix.) Note that since the $\mathbf{Z}''$ elements are typically detected, we shall need the unitary transformation

$$\begin{bmatrix} \mathbf{Z}' \\ i\mathbf{Z}'' \\ \frac{1}{2}\hat{\mathbf{X}} \end{bmatrix} = \begin{bmatrix} \frac{1}{\sqrt{2}}\mathbf{1} & \frac{1}{\sqrt{2}}\mathbf{1} & 0 \\ \frac{1}{\sqrt{2}}\mathbf{1} & -\frac{1}{\sqrt{2}}\mathbf{1} & 0 \\ 0 & 0 & 1 \end{bmatrix} \begin{bmatrix} \frac{1}{\sqrt{2}}\mathbf{Z} \\ \frac{1}{\sqrt{2}}\mathbf{Z}^* \\ \frac{1}{2}\hat{\mathbf{X}} \end{bmatrix} = \mathbf{u} \begin{bmatrix} \frac{1}{\sqrt{2}}\mathbf{Z} \\ \frac{1}{\sqrt{2}}\mathbf{Z}^* \\ \frac{1}{2}\hat{\mathbf{X}} \end{bmatrix} \tag{2.13}$$

which transforms eq 2.12 into

$$\begin{bmatrix} \mathbf{Z}'(t) \\ i\mathbf{Z}''(t) \\ \frac{1}{2}\dot{\hat{\mathbf{X}}}(t) \end{bmatrix} = \begin{bmatrix} \mathbf{R} & -i\mathbf{K} & 0 \\ -i\mathbf{K} & \mathbf{R} & 2i\hat{\mathbf{d}} \\ 0 & 2i\hat{\mathbf{d}}^{tr} & -\hat{\mathbf{W}} \end{bmatrix} \begin{bmatrix} \mathbf{Z}'(t) \\ i\mathbf{Z}''(t) \\ \frac{1}{2}\hat{\mathbf{X}}(t) \end{bmatrix} + \begin{bmatrix} 0 \\ iQ \\ 0 \end{bmatrix} \tag{2.14}$$

with the new symmetric matrix on the right-hand side of eq 2.14.

We now particularize the solutions to saturation recovery-type experiments, such that observations are made only for small d. We thus wish to develop a perturbation scheme to lowest order in d. For this purpose, the matrix of eq 2.12 is more satisfactory than that of eq 2.14, since it lacks the two degenerate submatrices ($\mathbf{R}$) along the partitioned-diagonal which appear in eq 2.14. Note, however, that for $K_\lambda = 0$, *i.e.*, λth line is on resonance, that if $-R_\lambda \equiv T_{2,\lambda}^{-1} = T_{1,\lambda}^{-1}$ then a triple degeneracy occurs with respect to the λth transition which is lifted by $d_\lambda \neq 0$. We must consider the case of $T_{2,\lambda} \neq T_{1,\lambda}$ separately from that for $T_{2,\lambda} = T_{1,\lambda}$. We develop the perturbation scheme by a generalization of the Van-Vleck transformation procedure.[24] We first introduce the partitioned matrices

$$\mathbf{A} = \begin{bmatrix} \mathbf{R} - i\mathbf{K} & 0 & 0 \\ 0 & \mathbf{R} + i\mathbf{K} & 0 \\ 0 & 0 & -\hat{\mathbf{W}} \end{bmatrix}$$

$$\mathbf{B} = i\sqrt{2} \begin{bmatrix} 0 & 0 & \hat{\mathbf{d}} \\ 0 & 0 & -\hat{\mathbf{d}} \\ \hat{\mathbf{d}}^{tr} & -\hat{\mathbf{d}}^{tr} & 0 \end{bmatrix} \tag{2.15b}$$

where $\mathbf{L} = \mathbf{A} + \mathbf{B}$ and consider a vector $\mathbf{M}$ (*cf.* eq 2.7) and solve for

$$\mathbf{OAO}^{-1}(\mathbf{OM}) + \mathbf{OBO}^{-1}(\mathbf{OM}) \cong (\mathbf{A} + \mathbf{b})\mathbf{M}' \tag{2.16}$$

where the partitioned matrix $\mathbf{B}$ is transformed approximately to the form of $\mathbf{A}$, (*i.e.*, partitioned matrices along the diagonal) by the (complex) orthogonal transformation $\mathbf{O}$ to lowest order in d. That is we let

$$\mathbf{M}' = e^{iS}\mathbf{M} \cong (1 + i\mathbf{S})\mathbf{M} \tag{2.17}$$

where $\mathbf{S}$ is found to be the (complex) antisymmetric operator

$$\mathbf{S} = +i(\mathbf{A}^\times)^{-1}\mathbf{B} \tag{2.18}$$

and

$$\mathbf{b} = \tfrac{1}{2}\mathbf{B}^\times\mathbf{S} = -\tfrac{1}{2}\mathbf{B}^\times[(\mathbf{A}^\times)^{-1}\mathbf{B}] \tag{2.19}$$

That is

$$\mathbf{S} = \begin{bmatrix} 0 & 0 & -(\mathbf{A}^{0,d\times})^{-1}\sqrt{2}\hat{\mathbf{d}} \\ 0 & 0 & (\mathbf{A}^{c,d\times})^{-1}\sqrt{2}\hat{\mathbf{d}} \\ -(\mathbf{A}^{d,0\times})^{-1}\sqrt{2}\hat{\mathbf{d}}^{tr} & (\mathbf{A}^{d,c\times})^{-1}\sqrt{2}\hat{\mathbf{d}}^{tr} & 0 \end{bmatrix} \tag{2.20}$$

Here the inverse operator $(\mathbf{A}^{j,k\times})^{-1}$ for $j,k = o,c,d$ may be conveniently defined by the prescription

$$(\mathbf{A}^{j,d\times})^{-1}\hat{\mathbf{d}} = \lim_{\epsilon\to 0_+} -\int_0^\infty d\tau \exp[-\epsilon\tau]\exp[\mathbf{A}^j\tau]\hat{\mathbf{d}}\exp[-\mathbf{A}^d\tau] \qquad j = o \text{ or } c \quad (2.21a)$$

and

$$(\mathbf{A}^{d,j\times})^{-1}\mathbf{d}^{tr} = \lim_{\epsilon\to 0_+} -\int_0^\infty \hat{\mathbf{d}}\tau \exp[-\epsilon\tau]\exp[\mathbf{A}^d\tau]\hat{\mathbf{d}}^{tr}\exp[-\mathbf{A}^j\tau] \qquad j = o \text{ or } c \quad (2.21b)$$

where

$$\mathbf{A}^o = \mathbf{R} - i\mathbf{K},\ \mathbf{A}^c = \mathbf{R} + i\mathbf{K} = \mathbf{A}^{o*},\ \mathbf{A}^d = -\hat{W} \quad (2.22)$$

(The convergence factor $\epsilon > 0$ is always taken as large enough to guarantee vanishing of the integrand as $\tau \to \infty$, and the limit is taken only after performing the integration.) Thus in an M dimensional basis set $a, b \ldots$ in which $\mathbf{A}^o$ (or $\mathbf{A}^c$) is diagonal and an $N/2$ dimensional basis set $\alpha,\beta \ldots$ in which $\mathbf{A}^d$ is diagonal, one has, for example

$$[(\mathbf{A}^{o,d\times})^{-1}]_{a\alpha b\beta} = \frac{\delta_{ab}\delta_{\alpha\beta}}{A_{aa}{}^o - A_{\alpha\alpha}{}^d} = \frac{\delta_{ab}\delta_{\alpha\beta}}{(-R_{aa}) - \hat{W}_{\alpha\alpha} + iK_{aa}} \quad (2.23)$$

Thus the expansion is in terms of

$$|\sqrt{2}\hat{d}_{a\alpha}|/|(-R_{aa}) - \hat{W}_{\alpha\alpha} + iK_{aa})| \ll 1 \quad (2.24)$$

for any nonvanishing $\hat{d}_{an}$, or more simply for a simple line

$$|\frac{\sqrt{2}}{2}\omega_1|/|T_2^{-1} - T_1^{-1} + i\Delta\omega| \ll 1 \quad (2.24a)$$

One finds, utilizing the fact that the $\mathbf{A}^j$ are symmetric matrices, that

$$[(\mathbf{A}^{j,d\times})^{-1}\hat{\mathbf{d}}]^{tr} = -[(\mathbf{A}^{d,j\times})^{-1}\hat{\mathbf{d}}^{tr}] \qquad j = o,c \quad (2.25)$$

from which it follows that $\mathbf{S}$ is antisymmetric, as required. Also we have

$$\mathbf{b} = \begin{bmatrix} \mathbf{C}+\mathbf{C}^{tr} & -(\mathbf{C}^{tr}+\mathbf{C}^*) & 0 \\ -(\mathbf{C}+\mathbf{C}^{tr*}) & \mathbf{C}^*+\mathbf{C}^{tr*} & 0 \\ 0 & 0 & \mathbf{E}+\mathbf{E}^{tr} \end{bmatrix} \quad (2.26)$$

where

$$\mathbf{C} = \hat{\mathbf{d}}(\mathbf{A}^{d,o\times})^{-1}\hat{\mathbf{d}}^{tr} \quad (2.27a)$$

$$\mathbf{E} = 2\hat{\mathbf{d}}^{tr}\,\mathrm{Re}[(\mathbf{A}^{o,d\times})^{-1}]\hat{\mathbf{d}} \quad (2.27b)$$

When the transformation of eq 2.13 is utilized, then in the basis of $\mathbf{Z}'$, $i\mathbf{Z}''$, $\frac{1}{2}\hat{\mathbf{X}}$ one has

$$\mathbf{S} = 2\begin{bmatrix} 0 & 0 & -i[\mathrm{Im}\,(\mathbf{A}^{d,o\times})^{-1}]\hat{\mathbf{d}}^{tr} \\ 0 & 0 & -[\mathrm{Re}\,(\mathbf{A}^{d,o\times})^{-1}]\hat{\mathbf{d}}^{tr} \\ -i[\mathrm{Im}\,(\mathbf{A}^{o,d\times})^{-1}]\hat{\mathbf{d}} & -[\mathrm{Re}(\mathbf{A}^{o,d\times})^{-1}]\hat{\mathbf{d}} & 0 \end{bmatrix} \quad (2.28)$$

while

$$\mathbf{b} = 2\begin{bmatrix} 0 & 2i\,\mathrm{Im}\,\mathbf{C}^{tr} & 0 \\ 2i\,\mathrm{Im}\,\mathbf{C} & 2\mathrm{Re}\,(\mathbf{C}+\mathbf{C}^{tr}) & 0 \\ 0 & 0 & \mathbf{E}+\mathbf{E}^{tr} \end{bmatrix} \quad (2.29)$$

Thus one may solve either eq 2.12 or 2.14 in the approximations used as

$$\Delta\dot{\mathbf{M}}'(t) \cong (\mathbf{A}+\mathbf{b})\Delta\mathbf{M}'(t) \quad (2.30a)$$

so

$$\Delta\mathbf{M}'(t) \cong \exp[-(\mathbf{A}+\mathbf{b})t]\Delta\mathbf{M}'(0) \quad (2.30b)$$

and

$$\Delta\mathbf{M}(t) \cong (1-i\mathbf{S})\exp[-(\mathbf{A}+\mathbf{b})t](1+i\mathbf{S})\Delta\mathbf{M}(0) \quad (2.30c)$$

Note that $\mathbf{A} + \mathbf{b}$ given either by eq 2.15a plus eq 2.26 (in the representation of eq 2.12) or by $\mathbf{uAu}^{tr}$ plus eq 2.29 (in the representation of eq 2.14) have the eigenstate-pair space (represented by superscript d) (approximately) uncoupled from the transition space (o and c superscripts) so $-\dot{\mathbf{W}}' + (\mathbf{E} + \mathbf{E}^{tr})$ may be diagonalized separately. However

$$\begin{bmatrix} \mathbf{R} & -i(\mathbf{K} - 4\,\mathrm{Im}\,\mathbf{C}^{tr}) \\ -i(\mathbf{K} - 4\,\mathrm{Im}\,\mathbf{C}) & \mathbf{R} + 4\,\mathrm{Re}\,(\mathbf{C}+\mathbf{C}^{tr}) \end{bmatrix}$$

will in general couple $\mathbf{Z}'$ to $\mathbf{Z}''$ (or alternatively the coupling can be written for $\mathbf{Z}$ and $\mathbf{Z}''$ from eq 2.15a and eq 2.26).

We note here that it is always possible to choose basis sets $a,b \ldots$ for transition space and $\alpha,\beta \ldots$ for eigenstate-pair space such that $\hat{\mathbf{d}}$ has a simple structure with $\hat{d}_{i,\hat{j}} = \hat{d}_{i,i}\delta_{\hat{i},j}$ where $\hat{j}$ refers to the eigenstate-pair corresponding to the jth esr transition. Several examples appear below.[24b] However, this choice will not, in general, simultaneously diagonalize $\mathbf{A}^o$ and $\mathbf{A}^d$. In those cases where it does, and if $\hat{d}_{i,\hat{i}} = d$ independent of i, it then follows from the above definitions that $\mathbf{U}^d = \mathbf{U}^o$ (see below), $\mathbf{C}^{tr} = \mathbf{C}$, and $\mathbf{E}^{tr} = \mathbf{E}$. Also the mixing of the $\mathbf{Z}$ and $\mathbf{Z}^*$ components by the terms in $\mathbf{b}$ is, in general, not easily simplified. This mixing becomes important as elements $K_{i,i} \to 0$ representing resonances.

(*A*) *Simple One Line Case.* We illustrate the above formalism for the simple one line case, which is otherwise well known, in preparation for the more complex cases given below. In this case we have $\mathbf{C} = \mathbf{C}^{tr}$, $\mathbf{E} = \mathbf{E}^{tr}$ and

$$\mathbf{S} = \frac{+\omega_1}{(T_2^{-1} - T_1^{-1})^2 + \Delta\omega^2} \times \begin{bmatrix} 0 & 0 & -i\Delta\omega \\ 0 & 0 & (T_2^{-1} - T_1^{-1}) \\ i\Delta\omega & -(T_2^{-1} - T_1^{-1}) & 0 \end{bmatrix} \quad (2.31a)$$

and

$$\mathbf{b} = \frac{\omega_1^2}{(T_2^{-1} - T_1^{-1})^2 + \Delta\omega^2} \times \begin{bmatrix} 0 & -i\Delta\omega & 0 \\ -i\Delta\omega & (T_2^{-1} - T_1^{-1}) & 0 \\ 0 & 0 & -(T_2^{-1} - T_1^{-1}) \end{bmatrix} \quad (2.31b)$$

in the Z', iZ'', $\frac{1}{2}\hat{X}$, representation. When we neglect terms of order $\omega_1^2/[(T_2^{-1} - T_1^{-1})^2 + \Delta\omega^2]$ compared to unity, one has

$$\mathbf{A}+\mathbf{b} \cong \begin{bmatrix} -T_2^{-1} & -i\Delta\omega & 0 \\ -i\Delta\omega & -T_2^{-1}+\delta & 0 \\ 0 & 0 & -T_1^{-1}-\delta \end{bmatrix} \tag{2.32}$$

where

$$\delta = \omega_1^2(T_2^{-1}-T_1^{-1})/[(T_2^{-1}-T_1^{-1})^2+\Delta\omega^2] \tag{2.32a}$$

The 2 × 2 submatrix may be diagonalized by the orthogonal transformation **U**

$$\mathbf{U} = \begin{bmatrix} [1-a_+]^{-1/2} & [1-a_+^{-1}]^{-1/2} \\ [1-a_-]^{-1/2} & -[1-a_-^{-1}]^{-1/2} \end{bmatrix} \tag{2.33a}$$

such that

$$\mathbf{U}[\mathbf{A}+\mathbf{b}]\mathbf{U}^{-1} = \begin{bmatrix} E_+ & O \\ O & E_- \end{bmatrix} \tag{2.33b}$$

where

$$a_\pm = (\delta \pm \sqrt{\delta^2-4\Delta\omega^2})^2/4\Delta\omega^2 \tag{2.33c}$$

and

$$E_\pm = -T_2^{-1}+\delta/2 \pm \tfrac{1}{2}\sqrt{\delta^2-4\Delta\omega^2} \tag{2.33d}$$

For $|\delta^2/\Delta\omega^2| \ll 1$, *i.e.*, a line off-resonance, one has complex eigenvalues of eq 2.33 of $\lambda \cong -T_2^{-1} + (\delta/2) \mp i\Delta\omega$ corresponding to the eigen solutions $(1/\sqrt{2})Z$ and $(1/\sqrt{2})Z^*$ (*cf.* eq 2.15a); while for $|\delta^2/\Delta\omega^2| \gg 1$, *i.e.*, a line close to resonance, one has simple decaying solutions $\lambda \cong -T_2^{-1}$ and $-T_2^{-1} + \delta$ for eigen solutions $\mathbf{Z}'$ and $i\mathbf{Z}''$, respectively (*cf.* eq 2.32). It then follows from the above equations that the complete solution is

$$\begin{bmatrix} \Delta Z' \\ \Delta Z'' \\ \frac{1}{2}\Delta\hat{X}(t) \end{bmatrix} = (1-i\mathbf{S})\mathbf{U}^{tr} \begin{bmatrix} e^{-E_+t} & & \\ & e^{-E_-t} & \\ & & e^{-(T_1^{-1}+\delta)t} \end{bmatrix} \times \mathbf{U}(1+i\mathbf{S}) \begin{bmatrix} \Delta Z'(0) \\ \Delta Z''(0) \\ \frac{1}{2}\Delta\hat{X}(0) \end{bmatrix} \tag{2.34}$$

where only terms linear in **S** are kept. Some simple and well-known limiting cases are[25]

(1) $\Delta\omega = 0$. Then

$$\Delta Z''(t) = e^{-t(T_2^{-1}-\delta)}\Delta Z''(0) + \frac{\omega_1}{(T_2^{-1}-T_1^{-1})}(e^{-t(T_2^{-1}-\delta)}-e^{-t(T_1^{-1}+\delta)})\Delta\tfrac{1}{2}\hat{X}(0) \tag{2.35}$$

(2) $T_2^{-1} \gg T_1^{-1}$, then for $t > T_2^{-1}$

$$\Delta Z''(t) \cong \frac{-\omega_1 T_2^{-1}}{T_2^{-2}+\Delta\omega^2} e^{-t(T_1^{-1}+\delta)} \left[\tfrac{1}{2}\Delta\hat{X}(0)\right] \tag{2.36}$$

If we use conditions of partial saturation such that $M_z(0) = \alpha M_0$, $0 \le \alpha \le 1$, with M_0 the equilibrium magnetization, then

$$\begin{aligned} M_x(0) &= \alpha\Delta\omega\omega_1 T_2^{\,2} M_0 \\ M_y(0) &= \alpha\omega_1 T_2 M_0 \\ M_z(0) &= \alpha M_0 \end{aligned} \tag{2.37}$$

and

$$\begin{aligned} \Delta Z'(0) = \Delta M_x(0) = \Delta\omega T_2 \Delta M_y(0) = \Delta\omega T_2^{\,2}\omega_1(\alpha-1)M_0 \\ \Delta Z''(0) = \Delta M_y(0) = (\alpha-1)\omega_1 T_2 M_0 \\ -\Delta\tfrac{1}{2}\hat{X} = \Delta M_z(0) = (\alpha-1)M_0 \end{aligned} \tag{2.38}$$

Then for case 1 we have

$$\Delta Z''(t) \cong \frac{-(1-\alpha)\omega_1 T_2 M_0}{(T_2^{-1}-T_1^{-1})}[T_2^{-1}e^{-t(T_2^{-1}+\delta)} - T_1^{-1}e^{-t(T_1^{-1}-\delta)}] \tag{2.39}$$

while for case 2 we have

$$\Delta Z''(t) \cong \frac{-(1-\alpha)\omega_1 T_2^{-1} M_0}{T_2^{-2}+\Delta\omega^2} e^{-t(T_1^{-1}+\delta)} \tag{2.40}$$

B. General Case for $T_2 \ll T_1$. The formalism given above permits the solution of a variety of situations involving saturation recovery for which eq 2.34 is immediately generalized, and the general expression of eq 2.5 may be used for more general cases. We will now, however, particularize our solutions to the case for $T_2 \ll T_1$ or, more generally, $|\mathbf{R}| \gg |\mathbf{W}|$. This is a useful case, especially in the slow-tumbling region, and also one for which some relatively simple analytic solutions may be obtained even for spectra which otherwise appear complex to describe. In this case we have from eq 2.14, 2.15, 2.28, and 2.29 that for

$$|\mathbf{R}|t > 1 \tag{2.41}$$

$$\Delta\mathbf{Z}''(t) \cong [\mathrm{Re}(\mathbf{A}^{\alpha,d^\times})^{-1}2\mathbf{d}]e^{-\hat{\mathbf{W}}t}\Delta\tfrac{1}{2}\hat{\mathbf{X}}(0) \tag{2.42}$$

In eq 2.42, we have dropped the small correction $\mathbf{E} + \mathbf{E}^{tr}$ of eq 2.29 to $\hat{\mathbf{W}}$. In the simple line case, this is just the neglect of δ of eq 2.32a compared to T_1^{-1}, which is valid since for $T_2^{-1} > T_1^{-1}$

$$\delta T_1 \cong \frac{\omega_1^2 T_1 T_2^*}{1+T_2^{*2}\Delta\omega^2} \le \omega_1^2 T_1 T_2^* \ll 1 \tag{2.43}$$

(where $T_2^{*-1} = T_2^{-1} - T_1^{-1}$). The last inequality is a consequence of the no-saturation condition during the recovery. Now if $\mathbf{U}_o$, $\mathbf{U}_c$, and $\mathbf{U}_d$ are the orthogonal transformations which diagonalize $\mathbf{A}^o$, $\mathbf{A}^c$, and $\mathbf{A}^d$, respectively, we may rewrite eq 2.42 as

$$\Delta\mathbf{Z}''(t) \cong -\int_0^\infty d\tau\{\mathbf{U}_0^{tr}\exp[\tau\mathbf{U}_0(\mathbf{R}-i\mathbf{K})\mathbf{U}_0^{tr}]\mathbf{U}_0 + \mathbf{U}_c^{tr}\exp[\tau\mathbf{U}_c(\mathbf{R}+i\mathbf{K})\mathbf{U}_c^{tr}]\mathbf{U}_c\}\hat{\mathbf{d}}\mathbf{U}_d^{tr} \times \exp[\tau\mathbf{U}_d(+\hat{\mathbf{W}})\mathbf{U}_d^{tr}]\exp[\mathbf{U}_d^{tr}(-\hat{\mathbf{W}}t)\mathbf{U}_d^{tr}]\mathbf{U}_d\Delta\tfrac{1}{2}\hat{\mathbf{X}}(0) \tag{2.44}$$

(The convergence factor has been dropped in eq 2.44 since $|\mathbf{R}| > |\mathbf{W}|$ implies satisfactory behavior of the integrals.) Note, however, by the functional properties $\mathbf{U}_o = \mathbf{U}_o\{\mathbf{R}, -\mathbf{ik}\}$ and $\mathbf{U}_c = \mathbf{U}_c\{\mathbf{R}, +\mathbf{iK}\}$ it follows that $\mathbf{U}_c = \mathbf{U}_o^*$. Then if we let

$$\mathbf{r}-i\mathbf{k} \equiv \mathbf{U}_0(\mathbf{R}-i\mathbf{K})\mathbf{U}_0^{tr} \tag{2.45a}$$

and

$$\mathbf{w} \equiv \mathbf{U}_d(\hat{\mathbf{W}})\mathbf{U}_d^{tr} \tag{2.45b}$$

eq 2.44 may be written more simply as

$$\Delta\mathbf{Z}''(t) \cong -\int_0^\infty d\tau\,\mathrm{Re}\{\mathbf{U}_0^{tr}\exp[\tau(\mathbf{r}-i\mathbf{k})]\mathbf{U}_0\}(2\hat{\mathbf{d}})\mathbf{U}_d^{tr} \times \exp[(\tau-t)\mathbf{w}]\mathbf{U}_d\Delta\tfrac{1}{2}\hat{\mathbf{X}}(0) \tag{2.46}$$

We now consider specific examples.

III. Motional Narrowing Examples

(A) *Well-Separated Hyperfine Lines (Nitroxide).* We first illustrate the application of our expression to a nitroxide in the motional narrowing region when the three Lorentzian hyperfine lines are well separated. If we consider just pure electron spin flip transitions or W_e, pseudo-secular END terms (bW_e), and spin exchange ($b''W_e$), we have[3-8]

$$\hat{\mathbf{W}} = 2W_e \begin{bmatrix} 1+2b''+b & -b''-b & -b' \\ -b''-b & 1+2b''+2b & -b''-b \\ -b'' & -b''-b & 1+2b''+b \end{bmatrix} \quad (3.1)$$

Then

$$\mathbf{U}_d = \begin{bmatrix} 1/\sqrt{3} & 1/\sqrt{3} & 1/\sqrt{3} \\ 1/\sqrt{2} & 0 & -1/\sqrt{2} \\ 1/\sqrt{6} & -2/\sqrt{6} & 1/\sqrt{6} \end{bmatrix} \quad (3.2)$$

and

$$\mathbf{w} = 2W_e \begin{bmatrix} 1 & 0 & 0 \\ 0 & 1+3b''+b & 0 \\ 0 & 0 & 1+3b''+3b \end{bmatrix} \quad (3.3)$$

We also have

$$-R_{i,j} = T'_{2,i}{}^{-1}\delta_{i,j} + (\hat{W}_{i,j} - W_e\delta_{i,j}) \quad (3.4)$$

where the $T'_{2i}{}^{-1}$ give the purely secular contributions to the ith hyperfine line. Also

$$K_{i,j} = \Delta\omega_i\delta_{i,j} \quad (3.5)$$

and

$$-\hat{d}_{i,j} = \tfrac{1}{2}\omega_1\delta_{i,j} = \tfrac{1}{2}\gamma_e B_1 \quad (3.5a)$$

where j refers to the eigenstate pair associated with the jth transition.

For the general spectrum of well-separated lines we have for $i \neq j$[7]

$$|-R_{i,j}| = |\hat{W}_{i,j}| \ll |\omega_i - \omega_j| \qquad i \neq j \quad (3.6)$$

Thus $\mathbf{R} \pm i\mathbf{K} = \mathbf{r} \pm i\mathbf{k}$ is diagonal in the basis of the separate transitions, and $\mathbf{U}_0 = \mathbf{1}$ (except for higher-order terms in $2W_eb''$ and $2W_eb$ *vs.* $(\omega_i - \omega_j)$). Then elements of eq 2.46 are

$$\Delta Z''_i(t) = -\sum_{j,\beta}\int_0^\infty d\tau\, \mathrm{Re}\exp[\tau(r_{i,i} - ik_{i,i})]\omega_1(U_d{}^{tr})_{i,\beta} \times \exp[(\tau - t)w_{\beta\beta}](U_d)_{\beta j}\Delta\tfrac{1}{2}\hat{X}_j(0) =$$

$$+\omega_1\,\mathrm{Re}\sum_{j,\beta}\frac{e^{-w_{\beta\beta}t}}{r_{i,i} + w_{\beta\beta} - i\Delta\omega_i}(U_d{}^{tr})_{i\beta}(U_d)_{\beta\hat{j}}\Delta\tfrac{1}{2}X_{\hat{j}}(0) \quad (3.7)$$

It is necessary, in order to complete the solution, to specify the initial condition

$$\tfrac{1}{2}\hat{X}_j(0) = -(M_{z,j}(0) - M_{0,\hat{j}}) = (1-\alpha_j)M_{0,\hat{j}} \quad (3.8)$$

or

$$\alpha_{\hat{j}} = M_{z,j}(0)/M_{0,\hat{j}} \quad (3.8a)$$

It is now convenient to consider two limiting cases depending upon whether b, $b'' \ll 1$ or $\gg 1$.

(1) *Uncoupled Relaxation. b, $b'' \ll 1$.* For this case a saturating pulse on the jth transition leading to $\alpha_j \neq 0$ will not appreciably affect the $i \neq j$ lines (except for terms higher order in b, b'' see below). Furthermore

$$w_{\beta\beta} \cong 2W_e = T_1{}^{-1} \quad \text{all } \beta \quad (3.9)$$

Then, since $\Sigma_\beta(U_d{}^{tr})_{\hat{i}\beta}(U_d)_{\beta\hat{j}} = \delta_{i,j}$, eq 3.7 becomes

$$\cong -\mathrm{Re}\,\frac{\omega_1(1-\alpha_{\hat{i}})M_{0,\hat{j}}}{T'_{2i,j}{}^{-1} + i\Delta\omega_i}e^{-t/T_1}\delta_{i,j} \quad (3.10)$$

which is just eq 2.40 for each line.

(2) *Coupled Relaxation. b', $b'' \gg 1$.* For this case, a saturating pulse on the jth transition will have its effects transmitted equally to all the eigenstate pairs so that $\alpha_{\hat{i}} = \alpha_{\hat{j}} = \alpha = \frac{1}{3}\alpha_{\text{total}}) \neq 0$. Then since $\Sigma_j(U_d)_{\beta\hat{j}} = \delta_{\beta,1}\sqrt{3}$ eq 3.7 becomes

$$\Delta Z''_i(t) = -\mathrm{Re}\,\omega_1(1-\alpha)M_{0,\hat{i}}\,\frac{e^{-t/T_1}}{(-R_{i,i})^{-1} - T_1{}^{-1} + i\Delta\omega_i} \quad (3.11)$$

for $i = 1$, 2, or 3 (corresponding to transitions with nuclear spin of -1, 0, and $+1$). Thus only one of the eigenvalues of $\mathbf{w}$ (*i.e.*, $2W_e = T_1{}^{-1}$) is seen.

If it were possible to saturate one of the lines relative to the other two, then one could obtain a superposition of three decay terms each decaying by one of the eigenvalues of $\mathbf{w}$. Such would be the case if b and/or b'' is of order of magnitude unity. But then the three eigenvalues of $\mathbf{w}$ would not be much different, so that the superposition of three decay terms would not differ much from a single average exponential decay. A rigorous solution of this intermediate region would require a calculation from eq 2.12 of the values of $\hat{\mathbf{X}}$ resulting from a pulse of finite duration, $\Delta t'$. However if $\Delta t' \geq w_{\beta\beta}{}^{-1} \leq T_1 = (2W_e)^{-1}$, then one may use as the ratios $\alpha_{\hat{j}}/\alpha_{\hat{i}} \cong \hat{\mathbf{X}}_{\hat{j}}{}^{ss}/\hat{\mathbf{X}}_{\hat{i}}{}^{ss}$, *i.e.*, the steady-state values obtained in the presence of the saturating field. Thus for case 3, the steady-state approximation on the pulse duration, one has

$$\hat{\mathbf{X}}^{satd} = -2\hat{\mathbf{W}}^{-1}\mathbf{d}_{satd}{}^{tr}\mathbf{Z}''^{satd} \quad (3.12)$$

with $\mathbf{Z}''^{satd}$ calculated by standard means.[3-8] Then we can use the relation (appropriate when only pure esr transitions are generated) for the saturation parameters $\Omega_{i,j}$[7]

$$4(\hat{W}^{-1})_{i,j} = \Omega_{i,j} \quad (3.12a)$$

to rewrite eq 3.7 as (with $\hat{d}_{i,\hat{j}}\,\text{satd} \equiv \frac{1}{2}\omega_1{}^s$).

$$\Delta Z''_i(t) = \omega_1\,\mathrm{Re}\sum_{j,\beta,k}\frac{e^{-w_{\beta\beta}t}}{r_{i,i} + w_{\beta\beta} - i\Delta\omega_i}(U_d)_{\hat{i}\beta}{}^{tr}(U_d)_{\beta\hat{j}} \times \frac{\Omega_{j,k}}{4}\frac{Z''_k{}^{satd}}{2}\omega_1{}^s = \omega_1\,\mathrm{Re}\sum_{k,\beta}\frac{e^{-w_{\beta\beta}t}}{r_{i,i} + w_{\beta\beta} - i\Delta\omega_i}\frac{1}{w_{\beta\beta}} \times (U_d)_{\hat{i}\beta}{}^{tr}(U_d)_{\beta\hat{k}}\frac{Z''_k{}^{satd}}{2}\omega_1{}^s \quad (3.13)$$

where the second equality follows because

$$\mathbf{w}^{-1} = \mathbf{U}_d\hat{\mathbf{W}}^{-1}\mathbf{U}_d{}^{tr} \quad (3.14)$$

Case 1 is obtained from the second form of eq 3.13 by setting only one $Z''_k{}^{satd}$ unequal to zero and then using eq 3.9. Case 2 is obtained from the first form of eq 3.13 by recognizing that for b and/or $b'' \gg 1$, $\Omega_{j,k}$ becomes independent of j and k, *i.e.*, $\Omega_{j,k} \to 2/(N/2)W_e$.[6] (These $\Omega_{j,k}$ are given explicitly for the nitroxide case in Table V of ref 8.) Then one may use $\Sigma_j(U_d)_{\beta\hat{j}} = \delta_{\beta,1}\sqrt{N/2}$. (Recall, however, that our original derivations of cases 1 and 2 did not require the "steady-state pulse" approximation.) Cases

intermediate between (1) and (2) exhibiting effects of all three decay constants are also obtained from eq 3.13. (Note that eq 3.13 also covers eldor-type situations.) It follows from eq 3.13 that the exponential decays of larger $w_{\beta\beta}$ have the weaker amplitudes.[26]

In particular, let us assume that the $w_{\beta\beta}$ are nearly equal so $b,b'' \ll 1$. Then if the line observed is $i = 1$, while $k = 1$ has been saturated (simple saturation recovery), one obtains from eq 3.13

$$\Delta Z''_1(t) \cong T_1\omega_1 \mathrm{Re}\,(r_{1,1} + T_1^{-1} - i\Delta\omega_1)^{-1} e^{-t/T_1} \times [1-(2b''+b)(1+t/T_1)] Z''_1{}^{\mathrm{satd}}\omega_1{}^{\mathrm{s}} \quad (3.15)$$

However, if we let $k = 2$ (an eldor case)

$$\Delta Z''_1(t) \cong \frac{b+b''}{1+b+b''} e^{-t/T_1} T_1\omega_1 \mathrm{Re}\,(r_{1,1} + T_1^{-1} - i\Delta\omega_1)^{-1} \times (1+t/T_1) Z''_2{}^{\mathrm{satd}}\omega_1{}^{\mathrm{s}} \quad (3.16)$$

This emphasizes how the relaxation is dominated by T_1, and how an eldor effect would be weak (but potentially noticeable) compared to the direct saturation recovery effect for this case.

(*B*) *Single Average Hyperfine Line (Nitroxide).* Here we assume the opposite of eq 3.6, *i.e.*

$$|-R_{i,j}| = |\hat{W}_{i,j}| \gg |\omega_i - \omega_j| \qquad i \neq j \quad (3.17)$$

or

$$2W_e b \text{ and/or } 2W_e b'' \gg |\omega_i - \omega_j| \sim a_N \quad (3.17a)$$

so the original three-line spectrum has collapsed into a single average Lorentzian. If we also assume $|T_{2,i}^{-1} - T_{2,j}^{-1}| \ll 2W_e b$ and/or $2W_e b''$ then $\mathbf{U}_o \cong \mathbf{U}_d$ of eq 3.2 and eq 2.46 becomes

$$\sum_{i=1}^{3} \Delta Z''_i(t) \cong -\sum_{i,\alpha,k,m,\beta} \int_0^\infty d\tau\, \mathrm{Re}\{U_{0i,\alpha}{}^{\mathrm{tr}} \times \exp[\tau(r_{\alpha,\alpha} - k_{\alpha,\alpha})] U_{0\alpha k}(2\hat{d})_{k,\hat{k}} U_{\hat{k},\beta}{}^{\mathrm{tr}}\} \times \exp[(\tau - t)w_{\beta\beta}](U_d)_{\beta\hat{m}} \Delta\tfrac{1}{2}\hat{X}_{\hat{m}}(0) \quad (3.18)$$

But since $d_{k,\hat{k}}$ is independent of k and $\Sigma_k U_{o\alpha\hat{k}} U_{dk,\beta}{}^{\mathrm{tr}} \cong \delta_{\alpha\beta}$, while $\Sigma_i U_{oi,\alpha}{}^{\mathrm{tr}} = \Sigma_i U_{o\alpha,i} = \sqrt{3}\delta_{\alpha,1}$ and $X_{\hat{m}}(0) = \alpha$ independent of m, one has

$$\sum_{i=1}^{3} \Delta Z''_i(t) \cong 3\omega_1 \mathrm{Re} \frac{e^{-w_{11}t}}{r_{11} + w_{11} - i\Delta\omega_{11}} \alpha \quad (3.19)$$

where $w_{11} = 2W_e$

$$r_{11} = T'_{2\,av}{}^{-1} + 2W_e \quad \text{with } T'_{2\,av}{}^{-1} = \frac{1}{3}\sum_{i=1}^{3} T'_{2,(i)}{}^{-1}$$

and

$$\Delta\omega_{11} = \frac{1}{3}\sum_{i=1}^{3} \Delta\omega_i \quad (3.20)$$

Corrections due to the incomplete averaging of effects of the b and b'' terms can be obtained by perturbation methods in the usual fashion. Again the relaxation is dominated by $T_1 = 1/2W_e$. (Note that eq 3.17 does not violate the validity of the perturbation approach as long as $T_2'^{-1} > 2W_e$.)

(*C*) *General Case.* The discussion given above in terms of the example of a nitroxide in the motional narrowing region is seen to apply quite generally to the case of any hyperfine spectrum in the motional narrowing region. That is, eq 3.7 is still applicable in the well-resolved spectral region as are the discussions and conclusions of cases 1, 2, and 3; also eq 3.18 applies in the limit of a single average hyperfine line. When there are degenerate hyperfine lines, it is only necessary to replace the vectors (*e.g.*, **Z**, $\hat{\mathbf{X}}$) and matrices (*e.g.*, **R**, $\hat{\boldsymbol{W}}$) by their appropriate symmetrized forms as given in V, which then properly include the degeneracy factors. (Care must be exercised in describing the (coupled) relaxation of the components of the degenerate line, but the methods of I–V are applicable.)

Note that in the diagonalization of $\hat{\boldsymbol{W}}$ (and **R**), one can take advantage of the symmetries of these matrices. Thus the feature of spin exchange for *nondegenerate* transitions, *viz.* that it leads to equal transition probabilities among *all* the eigenstate pairs (*i.e.*, $-\hat{W}_{i,j}{}^{\mathrm{ex}} = 2W_e b''$, $i \neq j$),[4] means that $\hat{\boldsymbol{W}}$ in the presence of exchange (but absence of END terms) is invariant to all permutations of the $N/2$ nondegenerate eigenstate pairs, *i.e.*, it commutes with the permutation group $P_{N/2}$. It is then a simple matter to show from the properties of this group that there is one eigenvalue.

$$w_{11} = T_1^{-1} = 2W_e \quad (3.20)$$

corresponding to $U_{i1} = 1/\sqrt{N/2}$ (for all i) or the totally symmetric linear combination of eigenstate pairs. Furthermore, all the other eigenvalues are found to be degenerate (belonging to an $(N/2 - 1$ dimensional representation of $P_{N/2}$) and equal to

$$w_{ii} = 2W_e\left(1 + \frac{N}{2}b''\right) \qquad i \neq 1 \quad (3.21)$$

The END interaction shows less symmetry. However, for the eigenstate pairs of a single nucleus of I (or for the $J^{(\kappa)\mathrm{th}}$ set of eigenstate pairs corresponding to n completely equivalent nuclei with $J = \Sigma_{i=r} I_i$ and κ refers to a particular partner[3]) the $W_{i,j}{}^{\mathrm{END}}$ are symmetric in the quantum number M. Thus the only symmetry operation involves $W_{M,M\pm1} \rightarrow W_{-M,-M\pm1}$, and $\hat{X}_M \rightarrow \hat{X}_{-M}$. However, one may also take advantage of the structure of $\hat{\boldsymbol{W}}$[7]

$$\hat{W}_{i,j} = 2W_e\delta_{i,j} + \hat{W}(\mathrm{END})_{i,j} \quad (3.22)$$

so only $\hat{W}(\mathrm{END})_{i,j}$ the END contribution, needs to be diagonalized. Then since[7]

$$\hat{W}(\mathrm{END})_{\hat{i}\hat{i}} = -\sum_{j\neq i}\hat{W}(\mathrm{END})_{\hat{i}\hat{j}} = -\sum_{j\neq 1}\hat{W}(\mathrm{END})_{\hat{j}\hat{i}} \quad (3.23)$$

the matrix $\hat{\mathbf{W}}$(END) must have a single eigenvalue of zero corresponding to the eigenvector $\Sigma_i \hat{X}_i$ (by analogy with the equivalent property of symmetric **W** matrices corresponding to the conservation of probability). Thus one again has

$$w_{11} = T_1^{-1} = 2W_e$$

corresponding to $U_{i1} = 1/\sqrt{N/2}$ with $w_{ii} = 2W_e[1 + f_i(b)] > 2W_e$ for $i \neq 1$ where the function $f_i(b)$ is of form seen in eq 3.3. (The above symmetry considerations are sufficient to determine the w_{ii} for the nitroxide.)

When both END and exchange are present, then the lower symmetry of the END interaction is to be used. Also, if the hyperfine pattern is degenerate with different degeneracies for the different lines, then the $\hat{\mathbf{W}}^{\mathrm{s}}$ matrix (the symmetrized form, *cf.* V), in the presence of exchange only, one no longer has $P_{N/2}$ symmetry but usually symmetry such as $\hat{\mathbf{W}}$(END), since, $D(\lambda)$, the degeneracy of the λth transition, is symmetric about the center of the spectrum.

One can further generalize the problem to include a $\hat{\boldsymbol{W}}$ which depends upon M (*i.e.*, effects of the cross term between g and dipolar tensors). This will, however, destroy

the symmetries discussed above. When cross transitions are not negligible, then the $\mathcal{W}$ matrix is nonzero and one must return to eq 2.5, but perturbation methods comparable to those of section II may still be employed.

On Contributions of T_2-Type Decays. We now wish to discuss the validity of the neglect of the terms appropriate when $|\mathbf{R}| \gg |\hat{\mathbf{W}}|$ *cf.* eq 2.41–2.42. Such an approximation is valid, for example, for dilute solutions of semiquinones where the secular g tensor broadening dominates the widths, except at higher temperatures when spin rotation is most important and $T_1 \approx T_2$.[14] In the latter case, each hyperfine line is uncoupled from the others, and one treats each such line separately.[12] This latter case is also the case for the nitroxides at low viscosity; at higher viscosity the secular g tensor broadening is, however, not dominant, and $T_{2'i}^{-1} \sim W_n$ in eq 3.4, so $T_{2,i}^{-1}$ is only somewhat larger than W_n. However, $b \equiv W_n/W_e$ is then usually substantially greater than unity. Thus, while $w_{11} = 2W_e \ll T_{2,i}^{-1}$ in this case, the w_{22} and w_{33} of eq 3 3 are of comparable order of magnitude to $T_{2,i}^{-1}$. We have already seen that for $b \gg 1$ we can neglect the effects of w_{22} and w_{33} in the saturation recovery, and for the same reason of rapid decay we can neglect terms decaying with time constant of order T_2. A similar argument applies when exchange makes a major contribution to the widths. However, in that region where W_e and W_n (or $\omega_{EX} \equiv Nb''W_e$) are of the same order, and $T_{2'i}^{-1}$ is not large, then the complicating effects of the decay of T_2-type terms from the complete solution of eq 2.30 might become important to consider. Note further, that in the well-resolved region, where only a single hyperfine line is observed, this solution may be achieved fairly simply utilizing the techniques given above, since $\mathbf{U}_o = \mathbf{1}$ (even though $\mathbf{U}_d$ is not so simple).

IV. Slow Tumbling Examples

(*A*) *Simple Line.* By means of the eigenfunction expansion method of FBP,[18] one obtains from eq 2.2

$$\frac{1}{\sqrt{2}}\dot{C}_m(t) = \sum_n (R_{m,n} - iK_{m,n})\frac{1}{\sqrt{2}}C_n(t) - i\sqrt{2}d_{m,\hat{m}} \times \left(\frac{1}{2}b_{\hat{m}}(t)\right) + i\frac{1}{\sqrt{2}}Q_m \quad (4.1)$$

as well as the complex-conjugate form of eq 4.1, and

$$\frac{1}{2}\dot{b}_{\hat{m}}(t) = i\sqrt{2}\hat{d}^{\mathrm{tr}}_{\hat{m},m}\left(\frac{1}{\sqrt{2}}C_m(t) - \frac{1}{\sqrt{2}}C_m^*(t)\right) - \sum_n \hat{W}_{\hat{m},\hat{n}}\left(\frac{1}{2}b_{\hat{m}}(t)\right) \quad (4.2)$$

where the absorption is proportional to Im $C_o \equiv C_o''$. Equations 4.1 and 4.2 have been obtained by expanding the orientation-dependent terms

$$Z(\Omega,t)_{\lambda_j} = \sum_m C_m(t)|G_m(\Omega)\rangle \quad (4.3a)$$

and

$$X(\Omega,t)_{\lambda_j} = \Sigma b_{\hat{m}}(t)|G_{\hat{m}}(\Omega)\rangle \quad (4.3b)$$

in eigenfunctions $G_m(\Omega)$ of the Markov operator Γ_Ω

$$\Gamma_\Omega G_m(\Omega) = E_m G_m(\Omega) \quad (4.4)$$

and in this section we drop the λ_j subscript, since only a simple line is being considered. (We also let $\hat{m} \rightarrow m$.) These eigenfunctions $G_n(\Omega)$ may be written for Brownian rotation in isotropic liquids as the normalized Wigner rotation matrices

$$G_n(\Omega) \longrightarrow \sqrt{\frac{(2L+1)}{8\pi^2}}\,\mathfrak{D}_{KM}^{L}(\Omega) \quad (4.5)$$

with eigenvalues E_n for isotropic motion

$$E_n \longrightarrow E_{L,K,M} = L(L+1)\mathfrak{R} \quad (4.6)$$

where $\mathfrak{R}$ is the rotational diffusion coefficient.[10,18] For models involving reorientation by appreciable jumps, it is found that the functions of eq 4.5 are still good eigenfunctions, and eq 4.6 becomes

$$E_n \longrightarrow E_{K,M}^{L} = B_L L(L+1)\mathfrak{R} \quad (4.6')$$

where the model parameter, B_L ranges from unity for Brownian motion to $B_L = [L(L+1)]^{-1}$, $L \neq 0$ (and $B_L = 1$ for $L = 0$) for a strong collision model. It is discussed in detail elsewhere.[19,21,23] (We note that there is a simple analog between Brownian rotational diffusion with an END mechanism on the one hand and strong jump diffusion with a Heisenberg exchange mechanism on the other hand. The former pair have significant "selection rules" while the latter have none.)

In particular, if we assume the orientation-dependent perturbation in eq 2.2 is an axially symmetric g tensor, one finds only the $C_{0,0}^{L}(t)$ and the $b_{0,0}^{L}(t)$ for L even affect the observed signals (*cf.* eq 4.8b below). For this case the terms in eq 4.1 and 4.2 are[18]

$$R_{L,L'} = r_{L,L}\delta_{L,L'} = -(T_2^{-1} + E_L)\delta_{L,L'} \quad (4.7a)$$

$$K_{L,L'} = \Delta\omega + \kappa_{L,L'} \quad (4.8a)$$

with

$$\kappa_{L,L'} = [(2L+1)(2L'+1)]^{1/2}\begin{pmatrix} L & 2 & L' \\ 0 & 0 & 0 \end{pmatrix}^2 \mathfrak{F} \quad (4.8b)$$

$$\mathfrak{F} = \frac{2}{3}\hbar^{-1}\beta_e B_0(g_\parallel - g_\perp) \quad (4.8c)$$

These expressions include only the secular contribution of the axially symmetric g tensor. (The nonsecular contributions have been omitted in eq 4.1 and 4.2 (*cf.* FBP section IIIB1).) Also

$$\hat{W}_{L,L'} = w_{L,L}\delta_{L,L'} = (2W_e + E_L)\delta_{L,L'} \quad (4.9)$$

and

$$Q_L = q\omega_\lambda d_\lambda \delta_{L,0} \quad (4.10)$$

We have introduced an orientation-independent width T_2^{-1} and $T_1^{-1} = 2W_e$ into eq 4.7a and 4.9, respectively. Equations 4.1 and 4.2 are seen to be of the same matrix form as eq 2.12 (with the matrices $\hat{\mathbf{d}}$ and $\hat{\mathbf{d}}^{\mathrm{tr}}$ defined by eq 4.1 and 4.7. So, provided the inequality of eq 2.24 for the present case applies, then the same perturbation treatment in d_λ utilized for solving eq 2.12 may be utilized for the present case.

We wish to point out at this stage, that the eigenfunction expansion method immediately yields $R_{m,n}$ and $\hat{W}_{m,n}$ in *diagonal* form. Thus, when $E_m/\mathfrak{F} \gg 1$ corresponding to motional narrowing, the $\mathbf{R} \pm i\mathbf{K}$ is approximately diagonal in this representation. However, κ, which arises from $\mathfrak{K}_1(\Omega)$, is diagonal in the space of orientational unit vectors $|\delta(\Omega - \Omega_0)\rangle$.[15] We note that from the representation of the δ function

$$|\delta(\Omega - \Omega_0)\rangle = \sum_n G_n^*(\Omega_0)|G_n(\Omega)\rangle \quad (4.11a)$$

where, here, $|G_n(\Omega)\rangle$ are any complete *O.N.* set of functions, one has

$$|G_n(\Omega)\rangle = \int d\Omega_0 G_n(\Omega_0)|\delta(\Omega-\Omega_0)\rangle \quad (4.11b)$$

and, if they are also eigenfunctions of Γ_Ω, then

$$\langle\delta(\Omega-\Omega_1)|\Gamma_\Omega|\delta(\Omega-\Omega_0)\rangle = \sum_n G_n^*(\Omega_0)G_n(\Omega_1)E_n \quad (4.12)$$

Equations 4.11 define the unitary transformation

$$U_{n,\Omega_0} = G_n(\Omega_0) \quad (4.13a)$$

$$(U^{-1})_{\Omega_0,n} = U_{n,\Omega_0}^* = G_n^*(\Omega_0) \quad (4.13b)$$

between the two sets of basis vectors. It is often the case, however, that the real linear combinations of the $G_n(\Omega)$ can be used so $\mathbf{U}$ becomes an orthogonal transformation.

When $E_L/\mathfrak{F} \ll 1$, corresponding to the very slowly tumbling region, then $\mathbf{R} \pm i\mathbf{K}$ is approximately diagonal in the $|\delta(\Omega-\Omega_0)\rangle$ representation, with

$$K_{\Omega_j,\Omega_j} \equiv k(\Omega_j) = \Delta\omega_\lambda - \omega'(\Omega_j) \quad (4.14a)$$

where

$$\omega'(\Omega_j) = \mathfrak{F}\,\mathfrak{D}_{00}^2(\Omega_j) = \mathfrak{F}\,P_2(\beta_j) \quad (4.14b)$$

with $P_2(\beta)$ the second rank Legendre polynomial. (Of course, actual calculations are performed using finite grid points on the unit sphere.)

Again the solution may be written in the form of eq 2.46, with an equation such as eq 3.7 appropriate when $E_L/\mathfrak{F} \lll 1$, except that $\mathbf{U}_0 \cong (\mathbf{U}^{-1})$ are defined by eq 4.13b while $\mathbf{U}_d = \mathbf{1}$ (since the initial basis sets are the eigenfunctions of Γ and not the individual orientational component; whereas in the motional-narrowing case of section III the individual hyperfine components are utilized). When $E_L/\mathfrak{F} \lesssim 1$, defining the slow tumbling region where the spectrum is intermediate between the motional narrowing and rigid limit ones, the matrix $\mathbf{U}_0$ may be obtained by diagonalizing $(\mathbf{R} - i\mathbf{K})$ following methods already well described[12,15,18,19] while $\mathbf{U}_d = \mathbf{1}$. Thus we may write from eq 2.46

$$\Delta C_0''(t,\omega) = \omega_1 \mathrm{Re}\sum_{L,j}\frac{e^{-w_{LL}t}}{(R-ik)_{jj}+w_{LL}}(U_0^{tr})_{0,j}\times (U_0)_{j,L}\frac{1}{2}\Delta b_L(0) \quad (4.15')$$

and when $E_L \ll \mathfrak{F}$, this may be rewritten as

$$\Delta C_0''(t,\omega) \cong \frac{\omega_1 \mathrm{Re}}{\sqrt{8\pi^2}}\sum_L \int d\Omega_j \frac{e^{-w_{LL}t}}{r(\Omega_j)-ik(\Omega_j)+w_{LL}} G_L(\Omega_j)\Delta\frac{1}{2}b_L(0) \quad (4.15)$$

In both cases, it follows from eq 4.8b that only even values of L are required. Note that in eq 4.15, it is never really necessary to take an infinite sum over L. This is because in the integration over Ω_i, the $G_L(\Omega_i)$ for large L have rapid oscillations compared to the rest of the integrand, so that they average to zero. That is, we do not need values of L so large that $G_L(\Omega_i)$ varies much faster in Ω_i than $[r(\Omega_i) - ik(\Omega_i) + w_{LL}]^{-1}$. The effect of a large T_2^{-1} in $r(\Omega_i)$ is to broaden out the features of the near-rigid spectrum, thus decreasing the maximum value of L required. The approximate equality of eq 4.15 reflects the fact that we have taken $\mathbf{R} - i\mathbf{K}$ as diagonal in the $|\delta(\Omega-\Omega_0)\rangle$ representation, with the dominant part of $r(\Omega_i)$ being $-T_2^{-1}$ (with any small residual motional broadening calculated using the correct representation which diagonalizes $\mathbf{R} - i\mathbf{K}$ which, for practical purposes involves finite difference methods.) We can also rewrite eq 4.15 in a form more closely resembling eq 3.7

$$\Delta Z''(\Omega_i,t,\omega) = \omega_1 \mathrm{Re}\sum_{L\,\mathrm{even}}\frac{e^{-w_{LL}t}}{r_{i,i}-ik_{i,i}+w_{LL}}\int d\Omega_j G_L(\Omega_i)G_L^*(\Omega_j)\Delta\frac{1}{2}\hat{X}(\Omega_j,0) \quad (4.16)$$

First suppose that $E_L \ll W_e$, so that $w_{LL} \cong 2W_e$ for all values of L which contribute appreciably to the sum (since as already noted the sum may be truncated, but also the $b_L(0)$ may be negligible for large L), then eq 4.16 becomes

$$\Delta Z''(\Omega_i,t) \approx \omega_1 e^{-t/T_1}\frac{1}{r_{i,i}-ik_{i,i}+2W_e}\Delta\frac{1}{2}\hat{X}(\Omega_i,0) \quad (4.17)$$

representing the fact that the spin packet at Ω_i is uncoupled to the other orientations (compare with eq 3.10) and

$$\Delta C_0''(t,\omega) = \frac{1}{\sqrt{8\pi^2}}\int d\Omega_i \Delta Z''(\Omega_i,t,\omega) \quad (4.17a)$$

(Note that it is $\Delta C_0''(t,\omega)$ which is observed in an experiment.) Now suppose that $E_L \gg W_e$ for $L > 0$ such that $w_{LL} \gg 2W_e$ for $L > 0$. Then a saturating pulse will have its effects transmitted by the rotational diffusion equally to all parts of the line, *i.e.*, only $b_0(0)$ is normally saturated, so only $\Delta\frac{1}{2}b_0(0) \neq 0$, and eq 4.15 becomes (with an equivalent form for the more general eq 4.15')

$$\Delta C_0''(t,\omega) = \frac{\omega_1}{8\pi^2}e^{-t/T_1}\times \mathrm{Re}\left[\int d\Omega_i \frac{1}{r(\Omega_i)-ik(\Omega_i,\omega)+2W_e}\right]\frac{1}{2}\Delta b_0(0) \quad (4.18)$$

again giving relaxation with a simple $T_1 = 1/2W_e$ (compare with eq 3.11).

We can, again, introduce the "steady-state approximation on the pulse duration" and the analog of eq 3.12 becomes

$$\frac{1}{2}\hat{X}(\Omega_i)^{\mathrm{satd}} = -\int d\Omega_j \hat{W}_{\Omega_i\Omega_j}^{-1}\hat{d}_{\Omega_j,\Omega_j}^{\mathrm{tr\,satd}}Z''(\Omega_j)^{\mathrm{satd}} \quad (4.19)$$

where

$$\hat{W}_{\Omega_i\Omega_j}^{-1} = \sum_m G_m(\Omega_i)w_{mm}^{-1}G_m^*(\Omega_j) = \sum_{L,K,M}\left(\frac{2L+1}{8\pi^2}\right)\mathfrak{D}_{KM}^L(\Omega_i)w_{KM}^{L-1}\mathfrak{D}_{KM}^{L*}(\Omega_j) \quad (4.19a)$$

and for an orientation-independent transition moment we may write $d(\Omega_i,\Omega_j)^{\mathrm{tr\,satd}} = -\frac{1}{2}\omega_1^s\delta_{i,j}$. While, in principle, the sum in eq 4.19a includes a complete sum over the *O.N.* set, the nature of $Z''(\Omega_j)$ for the present case, as determined by eq 4.8, again means that only the restricted sum of L even and $K = M = 0$ need be used in eq 4.19. An alternative form of eq 4.19 is

$$b_L^{\mathrm{satd}} = \omega_1^s w_{LL}^{-1}C_L''^{\mathrm{satd}} \quad (4.19b)$$

In general, the b_L^{satd} will be nonnegligible only for those L such that the $C_L''^{\mathrm{satd}}$ are strongly coupled into the problem by the term in $\mathfrak{F}$ of eq 4.14b *and* for which $4d^{\mathrm{satd}2}w_{LL}^{-1} \gtrsim (-\mathrm{R}_{L,L})$, *i.e.*, the $C_L''^{\mathrm{satd}}$ are indeed being saturated. It is usually the latter condition which is limiting, since one has

$$T_2^{-1}/E_L,\ W_e/E_L \ll |\mathfrak{F}|/E_L$$

and usually

$$(\omega_1^s)^2 \gtrsim (2W_e)^{-1}T_2$$

(but not very much greater). Note also that the C^{satd} are obtained from eq 4.1 to 4.8 once $C_L(t)$ and $b_L(t)$ are set equal to zero. We now obtain from eq 4.15'

$$\Delta C_0''(t) = +\omega_1 \mathrm{Re}\sum_{L,j}\frac{e^{-w_{LL}t}}{(R-iK)_{j,j}+w_{LL}}\left(\frac{1}{w_{LL}}\right)(U_0^{tr})_{0,j}(U_0)_{j,m}$$
$$C_L''^{(satd)}\frac{1}{2}\omega_1^s \quad (4.20)$$

with the obvious modification when eq 4.15 is appropriate. Equation 4.16 may be rewritten as

$$\Delta Z''(\Omega_i,\omega,t) = \omega_1 \mathrm{Re}\sum_L \frac{e^{-w_{i,L}t}}{r(\Omega_i)-ik(\Omega_i)+w_{L,L}} \times$$
$$\int \frac{G_L(\Omega_i)G_L^*(\Omega_j)}{w_{L,L}} Z''^{satd}(\Omega_j)\frac{\omega_1^s}{2}d\Omega_j \quad (4.21)$$

where it is again clear that only w_{00} and those $w_{L,L}$ comparable to w_{00} would contribute substantially. And the saturation recovery spectrum given by $\Delta C''(\omega,t)$ is obtained by integrating eq 4.21 over Ω_i, and utilizing $\langle G_L(\Omega_j)|Z''(\Omega_j)\rangle = C_L$. The case of $w_{L,L}$ comparable to $w_{0,0}$ for all L contributing appreciably to eq 4.21 may be dealt with in the manner of eq 3.13 to yield

$$\Delta Z''(\Omega_i,\omega,t) \cong \omega_1 \mathrm{Re}\frac{e^{-w_{00}t}}{r(\Omega_i)-ik(\Omega_i)+w_{0,0}}\int d\Omega_j \times$$
$$[\delta(\Omega_i-\Omega_j)-\overline{\gamma(\Omega_i,\Omega_j)}(1+w_{00}t)]w_{00}^{-1}Z''(\Omega_j)^{satd}\frac{1}{2}\omega_1^s \quad (4.22)$$

where

$$\overline{\gamma(\Omega_i,\Omega_j)} = \sum_{L\neq 0}{}'\gamma_L G_L^*(\Omega_i)G_L(\Omega_j) \quad (4.22a)$$

and γ_L is defined by $w_{LL} = w_{00}\gamma_L$ with $\gamma_L \ll 1$ for all values of L contributing appreciably to eq 4.21. (The prime on eq 4.22a indicates it may be calculated over this restricted set of L values.) Note also that $\Sigma_L' G^L(\Omega_i)G^{L*}(\Omega_j) \approx \delta(\Omega_i - \Omega_j)$ compared to the much slower variation of $Z''(\Omega_j)$ with Ω_j. For Brownian diffusion $\gamma_L = L(L+1)\mathcal{R}/2W_e$; while for the limit of strong jumps

$$\overline{\gamma(\Omega_i,\Omega_j)} = \left[\delta(\Omega_i-\Omega_j)-\frac{1}{8\pi^2}\right]\mathcal{R}/2W_e \quad (4.23)$$

Equation 4.22 again emphasizes how the dominant relaxation is *via* $T_1 = 1/2W_e$, and it shows how one may calculate the magnitude of the weak recovery signal for an eldor experiment in this case when Ω_i and Ω_j are quite different. Equation 4.23 substituted into eq 4.22 gives the simple orientation-independent result expected for a strong-collision model (for $\Omega_i \neq \Omega_j$). For this model, the more general expression, eq 4.21, takes on the simpler form

$$\Delta Z''(\Omega_i,\omega,t) = \omega_1 \mathrm{Re}\left[\frac{e^{-w_{00}t}}{r(\Omega_i)-ik(\Omega_i)+w_{0,0}}\frac{C_0''^{satd}}{w_{00}\sqrt{8\pi^2}}+\right.$$
$$\left.\frac{e^{-w't}}{r(\Omega_i)-ik(\Omega_i)+w'}\left(\frac{1}{w'}\right)\left(Z''(\Omega_i)^{satd}-\frac{C_0''^{satd}}{\sqrt{8\pi^2}}\right)\right]\frac{1}{2}\omega_1^s \quad (4.24)$$

where $w' = w_{00} + \mathcal{R}$.

Other Aspects of a Simple Line. (1) Orientation-Dependent T_1 and T_2. Near the rigid limit, it is possible that orientation-dependent effects of T_1 and T_2 begin to show up. We can examine such effects by introducing terms $T_{1,\Omega}^{-1}\,{}_{00}^2(\Omega)$ and $T_{2,\Omega}^{-1}\mathfrak{D}_{00}^2(\Omega)$. Then

$$R_{L,L'} = -(T_2^{-1}+E_L)\delta_{L,L'} -$$
$$T_{2,\Omega}^{-1}[(2L+1)(2L'+1)]^{1/2}\begin{pmatrix} L & 2 & L' \\ 0 & 0 & 0\end{pmatrix}^2 \quad (4.25)$$

and

$$\hat{W}_{L,L'} = (T_1^{-1}+E_L)\delta_{L,L'} +$$
$$T_{1,\Omega}^{-1}[(2L+1)(2L'+1)]^{1/2}\begin{pmatrix} L & 2 & L' \\ 0 & 0 & 0\end{pmatrix}^2 \quad (4.26)$$

When eq 4.25 is compared with eq 4.7 and 4.8, it is seen that its only effect on the previous results is to change $\mathfrak{F} \rightarrow \mathfrak{F} - iT_{2,\Omega}^{-1}$, but eq 4.26 renders $\hat{W}_{L,L}$ nondiagonal. When $T_{1,\Omega}E_L \gg 1$ (or more precisely $T_{1,\Omega}E_2 \gg 1$) then these orientation-dependent effects may be neglected, but for very slow motions it would be necessary to diagonalize $\hat{W}_{L,L}$ (where, in the limit $E_L \rightarrow 0$, one would obtain the $|\delta(\Omega - \Omega_i)\rangle$ representation).

(2) Asymmetric g Tensor. The correct expressions may be obtained for this case by direct comparison of the above expressions with the steady-state case given by FBP. The main feature to note is that the $\mathfrak{D}_{K0}^L(\Omega)$ for even L and nonzero K appear in the problem, so effects of anisotropic rotational diffusion can appear.[12] Otherwise the discussion is analagous to that given for symmetric g tensors.

(3) Contribution from T_2-Type Decaying Terms. In general, one finds that T_2^{-1} is significantly larger than $2W_e$ in the slow motional region, so the T_2-type decaying terms should decay much faster. However, it is possible for $E_L = \mathcal{R}L(L+1)$ to play a dominant role for large L in eq 4.7a and 4.9, *i.e.*, $\mathcal{R}L(L+1) \gg T_1^{-1}$ and T_2^{-1}. But this is the case where these terms of large L decay too rapidly in $e^{-\hat{W}t}$ to be important compared to the $w_{0,0}$ case, and similar comments would apply to the T_2-type decaying terms. Again one can return to the complete eq 2.30 for a detailed examination of such effects. We note that in the slow tumbling region, the $K_{L,L}$ of eq 4.8 will result in contributions from slightly off-resonant components of the line, and their T_2-type decay (but not T_1-type decays) will have some oscillatory character, *cf.* eq 2.32-2.33. Our analysis given above can be further refined by distinguishing between that portion of the line broadening which is homogeneous, and that which is inhomogeneous (assumed Lorentzian). This is unimportant for unsaturated effects, but is important when considering saturation.[12,22,23]

(B) Complex Spectra. E.g., Nitroxides. Very often, a slow tumbling spectrum is not just describable as a simple line, but is rather a complex one involving the coupling of the different transitions. Methods for solving the steady-state spectra in such cases are given in detail in FBP[18] and Goldman, *et al.*,[12,19] and in Bruno's thesis.[21] However, the partitioned-matrix concept of eq 2.12 may again be applied in a manner analogous to the simple line case treated in the previous section. The important generalizations are just to regard each of the coefficients $C_{KM}^L(t)$ and $b_{KM}^L(t)$ as vectors in spin space,[18] such that $C_{KM}^L(t,i)$ refers to the component representing the ith esr transition. For the particular case of nitroxides, one need only consider the three allowed transitions (i = 1, 2, or 3) and three (mixed) forbidden transitions.[12,19,21]

These forbidden transitions are coupled into the (high-field motional narrowing) allowed transitions by the pseudo-secular terms in $\mathfrak{K}_1(\Omega)$ which induce nuclear spin flips and, as the motion slows, they also affect the actual resonance frequencies. (For very slow motions, one achieves the rigid-limit resonance frequencies, which may, to a good approximation, be described by three allowed transitions, for each orientation.)

Similarly there are six components $b_{KM}^L(t,i)$ representing population differences between pairs of eigenstates: *i.e.*, three for the allowed transitions (i = 1, 2, or 3) and three which are really (mixed) nmr transitions. These latter arise from the pseudo-secular terms in $\mathfrak{K}_1(\Omega)$, and thus play a role closely analogous to the three forbidden

transitions for the $C_{KM}^{L}(i)$. As the rigid limit is approached (in particular for $|\mathcal{K}_1(\Omega)|/\mathcal{R} \gg 1$) they become equivalent to representing the diagonalized eigenstates characteristic of the rigid limit.

One may thus generalize all our above procedures to such cases wherein the vector spaces of eq 2.12 include the product space of the $C_{KM}^{L}(t)$ for the different L, K, M (or alternatively the $|\delta(\Omega - \Omega_i)\rangle$ representation) with the appropriate spin space as just described. In the slow tumbling region where

$$|\mathcal{K}_1(\Omega)|\ \mathcal{R} \gtrsim 1$$

i.e., the unsaturated slow tumbling spectra still show important motional effects, the detailed diagonalizations required for eq 2.46 for example are complex although tractable.[12,18,19,21] However, this is typically the region where

$$2W_e \ll \mathcal{R}$$

and any saturation effects are transmitted throughout the spectrum. In this event, we again have a case where the $\tilde{\mathbf{W}}$ matrix is characterized by a $w_{00} = (2W_e)$ and $w_{LL} \gg w_{00}$ for $L \neq 0$, and the dominant (slow) decay will again give just $T_1^{-1} = 2W_e$.

A more careful analysis of the slow tumbling region shows that two types of saturation transmission effects are operative: (1) the motional effect, which contributes terms of type $B_L L(L+1)\mathcal{R}$ to the $w_{L,L}$ and (2) nuclear spin flip processes, which in the fast motional case depend on b (*cf.* section III). For $|\mathcal{K}_1(\Omega)|/\mathcal{R} \lesssim 1$ (*i.e.*, $\tau_R \lesssim 10^{-9}$ sec) one gets values of $b \sim 20$–40 representing strong coupling of the hyperfine lines.[12,13] But when $|\mathcal{K}_1(\Omega)|/\mathcal{R} \gg 1$, and only residual motional effects are important, one must examine their effects more carefully.

In order to obtain some insight into the nuclear spin flip aspect of the problem, we consider a "quasi-nitroxide" case, such that for an axial hyperfine tensor one has $\sqrt{3/10}$ $(A_\parallel - a_N)$ being considerably smaller than a_N (see eq below) where a_N is the isotropic hyperfine splitting and A is the rigid limit value of $A_{z'z'}$, (in reality $a_N \approx 15$ G and $\sqrt{3/10}(A - a_N) \approx 11$ G).[13,19] For this "quasi-nitroxide" case, one may effectively decouple the $C_{KM}^{L}(t,i)$ for the three allowed transitions from the three (mixed) forbidden transitions and the $b_{KM}^{L}(t,i)$ representing the three eigenstate pairs from the three (mixed) nmr transition terms, by means of a perturbation theory approach which is closely equivalent to that discussed in Appendix A of ref 23 for the $C_{KM}^{L}(t,i)$ and to that plus the general perturbational approach given here in section II for the $b_{KM}^{L}(t,i)$.[27] In the limit of fast motion, *i.e.*, $|\mathcal{K}_1(\Omega)|\tau_R \ll 1$, the results are indeed quite general (independent of the smallness of $|A - a_N|$) and are just the familiar END terms discussed in section III. For slow motions, however, the nuclear spin flips persist and our axial "quasi-nitroxide" calculation gives an idea of their effects. In particular, one obtains a nuclear spin flip rate coupling $b_{00}^{L}(t,i)$ with $b_{0,0}^{L}(t,i \pm 1)$ where $i = 1, 2$, or 3 given by

$$W_n'(i,L,0,0 \longleftrightarrow i \pm 1, L'', 0, 0) \equiv W_n'(i,L;i \pm 1, L'') = \frac{D^2}{2} \sum_{\text{even } L', L''} (2L'+1)[(2L+1)(2L''+1)]^{1/2} \times \begin{pmatrix} L & 2 & L' \\ 0 & 0 & 0 \end{pmatrix}\begin{pmatrix} L' & 2 & L'' \\ 0 & 0 & 0 \end{pmatrix}\begin{pmatrix} L & 2 & L' \\ 0 & 1 & -1 \end{pmatrix}\begin{pmatrix} L' & 2 & L'' \\ 1 & -1 & 0 \end{pmatrix} \times [V(L,L') + V(L''+L')] \quad (4.27)$$

where

$$V(L,L') = \frac{E_{L'} - E_L - 2W_e + T_{2,n}^{-1}}{\tilde{b}_{L'}^{\,2} + (E_{L'} - E_L - 2W_e + T_{2,n}^{-1})^2} \quad (4.28)$$

with

$$D = -|\gamma_e| \left(\frac{3}{2}\right) 6^{-1/2}(A_\parallel - a_N) \quad (4.29a)$$

and

$$\tilde{b}_L = -\frac{|\gamma_e|}{2}\left[a_N + D'(2L+1)\begin{pmatrix} L & 2 & L \\ 0 & 0 & 0 \end{pmatrix}\begin{pmatrix} L & 2 & L \\ -1 & 0 & 1 \end{pmatrix}\right] \quad (4.30)$$

with

$$D' = -(8/3)^{1/2} D \quad (4.29b)$$

and E_L is given by eq 4.6 (or 4.6′) with $T_{2,n}^{-1}$ being the orientation-independent width component for the nmr transition.[3,5,7] This result for the nuclear spin flip rate is to be compared with the relaxation term for $b_{KM}^{L}(i)$ itself of $2W_e + E_L$. In particular, the diagonal contribution to the $L = 0$ term is just (when we drop $2W_e^{-1} - T_{2,n}^{-1}$)

$$W_n'(i,o;i \pm 1,0)\frac{D^2}{5}\frac{E_2}{\tilde{b}_2^{\,2} + E_2^{\,2}} = \frac{D^2}{5}\frac{\tau_R}{\tilde{b}_2^{\,2}\tau_R^{\,2} + 1} \quad (4.31)$$

with

$$\tilde{b}_2 = -\frac{1}{2}|\gamma_e|\left[a_N + \frac{1}{7}(A_\parallel - a_N)\right] \quad (4.30a)$$

or essentially the fast-motional result, but it is correct for slow motion (for the quasi-nitroxide) where its asymptotic behavior goes as $(D^2/5)\tilde{b}_2^{-2}\tau_R^{-1}$. Note that we can define a term in this limit

$$b = \frac{1}{2}\frac{D^2}{5}\tilde{b}_2^{-2}\tau_R^{-1}/W_e$$

which for $\mathcal{R}/W_e \gg 1$ will still allow $b \gtrsim 1$, and nuclear spin flips are an important part of the problem. For $\mathcal{R}/W_e \lesssim 1$, then the contribution of nuclear spin flips decreases relative to effects of W_e.

The analysis of this case would thus appear to be a generalization and combination of our previous discussions of a simple line in slow tumbling, *e.g.*, eq 4.9 and the fast motional nitroxide case, *e.g.*, eq 3.3 for an END mechanism. We must thus consider a $\hat{\mathbf{W}}$ matrix of type

$$\hat{W}(i,L;j,L'') = \left(2W_e + E_L + \sum_k W_n(i,k)\right)\delta_{i,j}\delta_{L,L''} + \sum_k W_n'(i,L;k,L'')\delta_{i,j} - [W_n(i,j)\delta_{L,L''} + W_n'(i,L;j,L'')]\delta_{j,i\pm1} \quad (4.32)$$

Note that this introduces off-diagonal terms between different L values of the type similar to eq 4.26 (*e.g.*, $W_n'(i,o;i \pm 1,2) = W_n'(i,o;i \pm 1, 0)$ $(\sqrt{5/14})$). Thus the diagonalization of the $\mathbf{W}$ matrix of form of eq 4.32 is not, in general, trivial. When W_n type terms are neglected, each of the three allowed transitions behave independently as simple lines, while the W_n type terms couple the relaxation of all three lines, and mix L values. Our general arguments apply for $R \gg W_e$, such that the whole spectrum relaxes together. In our quasi-nitroxide model $W_n'/\mathcal{R}$ is of order of $D_2/\tilde{b}_2^{\,2} \ll 1$, so W_n' becomes small sooner than E_L, but for a true nitroxide where $D_2/b_2^{\,2}$ is *not* much smaller than unity, our perturbation analysis is not quantitative but suggests that the importance of nuclear spin flip terms persists roughly almost as long as the terms in E_L.

Some other comments about the application of eq 2.46

to nitroxides are appropriate. First we note that $\tilde{\mathbf{d}}$ just couples $C_{KM}{}^{L}(i)$ with $b_{KM}{}^{L}(i)$. The diagonalization of the $\mathbf{R}$-$i\mathbf{K}$ matrix in the vector space of the $C_{KM}{}^{L}(i)$ may be performed as discussed elsewhere, but for the "quasi-nitroxide" model, the perturbational decoupling of the forbidden transitions renders the three allowed transitions separable, with the pseudosecular contribution between $C_{KM}{}^{L}(j)$ and $C_{KM}{}^{L''}(j)$ for $\mathbf{R}$-$i\mathbf{K}$ given by

$$D^2 \sum_{\substack{\text{even} \\ L,L''}} (2L'+1)[2L+1][2L''+1)]^{1/2} \times \begin{pmatrix} L & 2 & L' \\ 0 & 0 & 0 \end{pmatrix} \begin{pmatrix} L' & 2 & L'' \\ 0 & 0 & 0 \end{pmatrix} \begin{pmatrix} L & 2 & L' \\ 0 & 1 & -1 \end{pmatrix} \begin{pmatrix} L' & 2 & L'' \\ 0 & -1 & 0 \end{pmatrix} \times \frac{1}{2}[\pm i\tilde{b}_{L'} - (E_{L'} - E_L)]^{-1} + [\pm i b_{L'} - (E_{L'} - E_{L''})]^{-1} \quad (4.33)$$

where the plus and minus signs are for $j = 1$ and 3 respectively, and for $j = 2$ one uses the sum of the two expressions for $j = 1$ and 3. Equation 4.33 is of closely similar form to eq 4.27, but it includes the frequency shifts due to the pseudo-secular terms as well as the line-broadening effects due to the nuclear spin flips. Secular g tensor contributions have been neglected for simplicity, but they can readily be added in. (One also takes the terms in eq 4.33 as small compared to $\tilde{b}_0$ in decoupling the transitions for the "quasi-nitroxide" and we have neglected the small effects of weakly mixing in allowed character into the forbidden transitions).

We note that in a pulsed eldor experiment, if the observing and pulsed pumping modes are set at different frequencies corresponding to the same hyperfine transition, one may approximate the analysis in terms similar to those discussed for eq 4.22, etc. However, when they are set to different hyperfine transitions, the combined effects of reorientation and spin flip will, in general, be seen.

V. Summary

We have shown how our general methods applicable to steady-state saturation experiments in both the motional narrowing and slow tumbling region may also be generally applied to time-dependent experiments such as saturation recovery. The solution is again dependent upon the same matrix representations including the relaxation matrix $\mathbf{R}$, the coherence matrix $\mathbf{K}$, the transition-probability matrix $\mathbf{W}$ (or $\tilde{\mathbf{W}}$), and the transition moment matrix $\mathbf{d}$ which have already been extensively discussed. The complex coupled differential equations are most effectively solved in terms of separate diagonalizations in transition space (in which $\mathbf{R}$ and $\mathbf{K}$ are defined) and in eigenstate (or eigenstate-pair) space (in which $\mathbf{W}$ (or $\tilde{\mathbf{W}}$) is defined). This is because of a general feature of these problems, such that usually the different eigenstates (pairs) exhibit coupled relaxation even while their associated transitions are uncoupled.

Particular attention has been given to the saturation-recovery-type experiment, which also includes pulsed eldor with a weak observing mode. A general procedure, based on having a weak nonsaturating observing mode, has been developed, which permits convenient solutions. The procedure is illustrated with examples of the well-known case of a single line.

The analysis of spectra with hyperfine lines exhibiting coupled relaxation (with a nitroxide being a particular example) has shown that quite generally, the saturation recovery signal is dominated by a single exponential decay of time constant $T_1 = (2W_e)^{-1}$ despite the complexities of coupled relaxation which may exist. Simply stated, this is because when W_n or ω_{EX} are much greater than W_e, so as to strongly couple the relaxation of the eigenstate pairs, then the whole spectrum first rapidly adjusts to a common level of saturation with time constants $\sim W_n{}^{-1}$ or $\omega_{EX}{}^{-1}$, and then proceeds to relax to equilibrium more slowly with T_1, which is the slow decay observed experimentally. When a steady-state pulse approximation (*i.e.*, the saturating pulse is on for times $\geq$ the T_1's) is applicable, then one finds the fast decays also have much weaker amplitudes (proportional to their decay time constants). For W_n, $\omega_{EX} \ll W_e$, the lines are essentially uncoupled and all decays are $\sim T_1$. However, when W_n, $\omega_{EX} \sim W_e$, then more complex behavior may be seen with several (not very different) decay constants, which are weighted differently for eldor *vs.* direct observation. Thus eldor would be helpful in deciphering the different decays. When W_n, $\omega_{EX} \ll W_e$, it is still possible to observe eldor-recovery effects with time constant $\approx T_1$, but with a signal attenuated by factors of the order of $b = W_n/W_e$ or $Nb'' = \omega_{HF}/W_e$. T_2-type decays (including oscillatory effects) were not considered in detail in the examples, but, in those special cases where they could be important, the general methods given may be satisfactorily employed.

The slow motional case has been discussed from the point of view of examples of (1) a simple line and (2) a nitroxide (also a "quasi-nitroxide" in which the pseudo-secular terms are taken as small but not negligible). Here the important comparison is between $\mathfrak{R}$ *vs.* W_e, where $\mathfrak{R}$ is the rotational diffusion constant. For $\mathfrak{R} \gg W_e$ (a frequent situation even in the slow motional region), the rotational reorientation spreads the saturation over the whole spectrum, and the observed slow decay is again given by $T_1 \cong 2W_e$. For $\mathfrak{R} \ll W_e$ each component of the spectrum is separately saturated and it relaxes with $T_1 \cong 2W_e$. The region of $6\mathfrak{R} \sim W_e$ allows for the superposition of several decays of comparable order of magnitude which might be effectively explored by a combination of direct and eldor-observational techniques. Effects of model dependence on the reorientational motion are also given. The nitroxide case involves a combination of reorientational, and nuclear-spin-flip effects. Advantage is taken of the simplicity of the quasi-nitroxide model to analyze effects of the latter, showing their importance even when the pseudo-secular terms are small, thus implying their importance for real nitroxides. (The comments given for effects of W_n in the motional narrowing case apply here in a qualitative sense.) Computational techniques already well developed for computer simulation are fully applicable to a more thorough analysis of this case.

References and Notes

(1) Supported in part by grants from the National Science Foundation (Grant No. GP-13780), the Petroleum Research Fund, administered by the American Chemical Society, and by the Cornell University Materials Science Center.
(2) (a) K. V. Lingam, P. G. Nair, and B. Venkataraman, *Proc. Indian Acad. Sci. A*, **76**, 207 (1972); (b) M. Huisjen and J. S. Hyde, *J. Chem. Phys.*, **60**, 1682 (1974).
(3) J. H. Freed, *J. Chem. Phys.*, **43**, 2312 (1965). Referred to as I.
(4) J. H. Freed, *J. Phys. Chem.*, **71**, 38 (1967). Referred to as II.
(5) J. H. Freed, D. S. Leniart, and J. S. Hyde, *J. Chem. Phys.*, **47**, 2762 (1967). Referred to as III.
(6) M. P. Eastman, R. G. Kooser, M. R. Das, and J. H. Freed, *J. Chem. Phys.*, **51**, 2690 (1969). Referred to as IV.
(7) J. H. Freed, D. S. Leniart, and H. D. Connor, *J. Chem. Phys.*, **58**, 3089 (1973). Referred to as V.
(8) J. S. Hyde, J. C. W. Chien, and J. H. Freed, *J. Chem. Phys.*, **48**, 4211 (1968).
(9) M. Nechtschein and J. S. Hyde, *Phys. Rev. Lett.*, **24**, 672 (1970).

(10) J. H. Freed, *Ann. Rev. Phys. Chem.*, **23**, 265 (1972).
(11) R. G. Kooser, W. V. Volland, and J. H. Freed, *J. Chem. Phys.*, **50**, 5243 (1969).
(12) S. A. Goldman, G. V. Bruno, and J. H. Freed, *J. Chem. Phys.*, **59**, 3071 (1973).
(13) J. S. Hwang, R. P. Mason, and J. H. Freed, to be submitted for publication.
(14) D. S. Leniart, Ph.D. Thesis, Cornell University, 1971; H. D. Connor, Ph.D. Thesis, Cornell University, 1972; H. D. Connor, D. S. Leniart, and J. H. Freed, to be submitted for publication.
(15) See ref 10 for a review and references through 1971.
(16) J. S. Hyde, L. E. G. Eriksson, and A. Ehrenberg, *Biochim. Biophys. Acta*, **222**, 688 (1970).
(17) J. S. Hyde and L. S. Dalton, *Chem. Phys. Lett.*, **16**, 568 (1972).
(18) J. H. Freed, G. V. Bruno, and C. F. Polnaszek, *J. Phys. Chem.*, **75**, 3385 (1971).
(19) S. A. Goldman, G. V. Bruno, C. F. Polnaszek, and J. H. Freed, *J. Chem. Phys.*, **56**, 716 (1972).
(20) G. V. Bruno and J. H. Freed, *Chem. Phys. Lett.*, **25**, 328 (1974)
(21) G. V. Bruno, Ph.D. Thesis, Cornell University, 1973.
(22) A. Abragam, "The Principles of Nuclear Magnetism," Oxford University Press, New York, N. Y., 1961.
(23) H. C. Torrey, *Phys. Rev.*, **76**, 1059 (1949).
(24) (a) C. F. Polnaszek, G. V. Bruno, and J. H. Freed, *J. Chem. Phys.*, **58**, 3185 (1973). (b) This is based on a rigorous definition of **d** as a transition moment. However, in previous usage we have set $d_{i,j}$ = 0 for any transition which is not excited even though it is allowed.[3-8] Such a usage is a convenience for well-separated lines, but it breaks down for overlapping lines or in the slow tumbling region, so we return here to the rigorous definition of **d** for general discussions.
(25) The special case of $\Delta\omega = 0$ and $T_1 = T_2 \equiv T$, which, as noted, represents a breakdown of the expansion eq 2.24a, results in $\Delta Z'(t)$ decaying as $e^{-t/T}$, while the coupled modes $[\Delta Z''(t) \pm \frac{1}{2}\Delta X(t)]$ decay as $e^{-t(T^{-1} \pm i\omega_1)}$. Since we are assuming $\omega_1^2 T_1 T_2 = (\omega_1 T)^2 \ll 1$, it follows that $e^{-t(T^{-1} \pm i\omega_1)} \cong e^{-t/T}(1 \pm i\omega_1 t)$, essentially an exponential decay in T_1.
(26) When the $w_{\beta\beta}$ are very different, *e.g.*, b and/or $b'' \gg 1$, such that w_{22}, $w_{33} \gg w_{11}$, then other steady-state approximations appropriate to pulses of duration Δt fulfilling w_{22}^{-1}, $w_{33}^{-1} \ll w_{11}^{-1} = 2T_1$ may be used by solving for the steady-state solutions appropriate for $W_e \approx 0$ but W_n and/or $\omega_{EX} \neq 0$. This steady-state solution yields equal degrees of saturation of all the eigenstate pairs, and thus gives comparable results to that for case (2) above. [Note, however, that for a steady-state approximation to apply here, $\Delta t \gtrsim 2(T_1^{-1} + T_2^{-1})^{-1}$ and $\omega_1^2 \gtrsim (T_1^{-1} - T_2^{-1})$.[22,23]
(27) This perturbation approach was first used by FBP in ref 18 to discuss effects of nonsecular g tensor contributions to saturation behavior. There are some minor errors in eq 60 of that reference, due to a use of nonsymmetric matrices (*i.e.*, the unnormalized $\mathfrak{D}_{KML}$ were used as the basis), but this has no effect on the discussion which follows, nor on the final result of eq 61.

A Molecular Orbital Study of the Addition of Singlet Methylene to Butadiene

Hiroshi Fujimoto and Roald Hoffmann*

Department of Chemistry, Cornell University, Ithaca, New York 14850 *(Received January 24, 1974)*

Publication costs assisted by the Petroleum Research Fund and the National Science Foundation

A simple molecular orbital method is proposed to deal with chemically reacting systems in terms of the molecular orbitals of two isolated reactants. The electron population of a reacting system is partitioned into several orbital interaction terms, allowing a tracing of the origin of intermolecular bond formation and of the intramolecular reorganization of the electron distribution. The method is applied to the interaction between singlet methylene and butadiene. Both 1,2- and 1,4 addition are electronically allowed, but the 1,4 addition is discriminated against by excessive closed-shell repulsive interactions.

Introduction

The interpretation of chemical interactions between two systems in terms of the electronic structures of isolated reactants is a problem of crucial importance to chemistry. Some useful reactivity indices and generalized stereoselection rules have been derived by rather simplified molecular orbital (MO) methods.[1-8] There perturbation theory and orbital correlation diagrams have been found to be quite powerful. Several more detailed MO theoretical methods have been proposed in order to calculate the interaction energy and the electron distribution of chemically interacting systems from the wave functions of two isolated reactants.[9-17] Although the application of the "isolated-molecule-approximation"[18] is limited to the case of relatively weak interactions, *e.g.*, the early stage of chemical reactions, it can often be very informative in disclosing the governing factors of complicated chemical reactions.

The typical reactions of methylenes, namely, addition to a double bond, insertion into a single bond, and dimerization, have proven a useful testing ground for approximate calculations of bimolecular potential energy surfaces and reaction coordinates.[19,20] In the present work we continue our study of methylene reactions, returning to the addition reaction. We seek to understand a negative result; experiments on the reaction of singlet methylene with dienes have given no direct evidence of 1,4 concerted addition.[21] Normal 1,2 addition apparently prevails as the initial step.[22] This is so despite the least-motion cheletropic reaction of 1,4 addition clearly being a symmetry allowed process.[7]

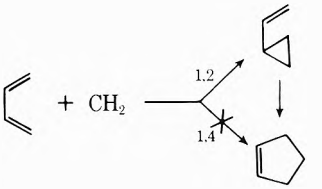

In this paper we first present a simple way of discussing the reorganization of the electronic distributions of two interacting molecules, and then apply our formalism to the reaction of singlet methylene and butadiene.

Population Analysis of Chemically Reacting Systems

Let us consider an interaction between two molecular systems, A and B. The MO's of A and B in their isolated states are given by linear combinations of atomic orbitals (AO's) as

$$a_i = \sum_r^{A} c_{ir}\chi_r \qquad \text{for the system A}$$

$$b_l = \sum_s^{B} c_{ls}\chi_s \qquad \text{for the system B}$$

The MO's of the composite system A–B of the two reactants, retaining the nuclear configurations they possessed when isolated, are given by

$$\psi_n = \sum_l^{A-B} c_{nl}\chi_l$$

ψ_n can be rewritten in terms of the a_i's and b_l's as a linear combination of MO's

$$\psi_n = \sum_i^{occ} k_{ni}a_i + \sum_j^{unocc} k_{nj}a_j + \sum_l^{occ} k_{nl}b_l + \sum_m^{unocc} k_{nm}b_m \quad (1)$$

where Σ^{occ} and Σ^{unocc} imply summation over all the occupied MO's and over all the unoccupied MO's, respectively. The coefficients k can be obtained exactly, for example, by solving the secular equation, or approximately, by the use of perturbation theory. It should be noted here that the a's form an orthonormal set, the b's another orthonormal set, and that a's and b's are not in general mutually orthogonal. All the functions are assumed to be taken as real.

The spin-free electron density of the systems A and B in their isolated states is defined by

$$\rho_A{}^0 = 2\sum_i^{occ}(a_i)^2 \quad (2)$$

and

$$\rho_B{}^0 = 2\sum_l^{occ}(b_l)^2 \quad (3)$$

The electron density of the system A–B is given by

$$\rho = 2\sum_n^{occ}(\psi_n)^2 = \rho_A + \rho_B + \rho_{A\text{-}B} \quad (4)$$

where

$$\rho_A = 2\sum_n^{occ}\Bigg[\sum_i^{occ}(k_{ni}a_i)^2 + \sum_j^{unocc}(k_{nj}a_j)^2 + \sum_i^{occ}\sum_{i'\neq i}^{occ}(k_{ni}k_{ni'}a_ia_{i'}) + \sum_j^{unocc}\sum_{j'\neq j}^{unocc}(k_{nj}k_{nj'}a_ja_{j'}) + \sum_i^{occ}\sum_j^{unocc}k_{ni}k_{nj}(a_ia_j + a_ja_i)\Bigg] \quad (5)$$

and

$$\rho_{A\text{-}B} = \Bigg[\sum_i^{occ}\sum_l^{occ}\rho_{A\text{-}B,il} + \sum_i^{occ}\sum_n^{unocc}\rho_{A\text{-}B,in} + \sum_j^{unocc}\sum_l^{occ}\rho_{A\text{-}B,jl} + \sum_j^{unocc}\sum_n^{unocc}\rho_{A\text{-}B,jn}\Bigg] \quad (6)$$

$$\rho_{A\text{-}B,il} = 4\sum_n^{occ}k_{ni}k_{nl}a_ib_l \quad \text{etc.}$$

The first and the second terms in eq 5 reflect the strength of the charge transfer and local excitation in the course of reaction, and the last three terms give the electron reorganization, *i.e.*, polarization, in the system A. The density $\rho_{A\text{-}B}$ measures the changes in the electron densities of the intermolecular region and is responsible for the formation of chemical bonds between A and B.

The distortion of the electron density distribution due to the interaction of the two systems is given by

$$\Delta\rho = \Delta\rho_A + \Delta\rho_B + \rho_{A\text{-}B} \quad (7)$$

where

$$\Delta\rho_A = \rho_A - \rho_A{}^0 \quad \text{etc.}$$

From the condition of the conservation of the total number of electrons throughout the reaction, we have

$$\int\Delta\rho\ d\upsilon = 0 \quad (8)$$

That is, the intermolecular bond is formed at the cost of electron densities in the neighborhood of the two reactants.

The intermolecular electron density $\rho_{A\text{-}B}$ can be expanded in terms of the AO's of A and AO's of B

$$\int\rho_{A\text{-}B,il}\ d\upsilon = 4\sum_n^{occ}k_{ni}k_{nl}S_{il} = 4\sum_r^{A}\sum_s^{B}\Bigg(\sum_n^{occ}k_{ni}k_{nl}c_{ir}c_{ls}s_{rs}\Bigg) = V_{A\text{-}B,il} \quad (9)$$

where

$$S_{il} = \int a_ib_l\ d\upsilon \quad \text{and} \quad s_{rs} = \int\chi_r\chi_s\ d\upsilon$$

The quantity $V_{A\text{-}B,il}$ gives the overlap population between A and B as a result of interaction of MO a_i with MO b_l. The total overlap population is given by

$$V_{A\text{-}B} = \sum_i^{occ}\sum_l^{occ}V_{A\text{-}B,il} + \sum_i^{occ}\sum_m^{unocc}V_{A\text{-}B,im} + \sum_j^{unocc}\sum_l^{occ}V_{A\text{-}B,jl} + \sum_j^{unocc}\sum_n^{unocc}V_{A\text{-}B,jn} \quad (10)$$

According to the Mulliken population analysis scheme,[23] the overlap population between AO r and AO s is divided evenly into two parts, one of which contributes to the gross population of AO r and the other to that of AO s. The overlap population $V_{A\text{-}B,il}$ arises from the interaction between MO a_i and MO b_l. Therefore, it is natural to divide this quantity into two parts, one belonging to MO a_i and the other to MO b_l. Thus, we may define the number of electrons occupying MO a_i in the interacting state by

$$\nu_i = 2\sum_n^{occ}(k_{ni})^2 + 2\sum_n^{occ}\sum_l^{B}k_{ni}k_{nl}S_{il} \quad (11)$$

We can thus see the complete analogy between ν_i and the Mulliken gross population and between $V_{A\text{-}B,il}$ and the Mulliken overlap population.[23]

ν and $V_{A\text{-}B}$ may be useful in analyzing what happens in a given chemical interaction. When the reactants are separated, isolated, the overlap population $V_{A\text{-}B}$ is zero. In the framework of a single-electron-configuration approximation the numbers of electrons occupying the originally occupied MO's a_i's and b_l's are two and those occupying the originally unoccupied MO's a_j's and b_m's are zero. As the interaction grows, the originally occupied MO's will lose some fraction of their electron pairs and the originally unoccupied MO's will correspondingly gain electrons. This process, of course, will be accompanied by an energy destabilization, except for the case of some strong donor-acceptor interactions in which the zero- and/or first-order perturbation stabilizes a charge-transferred configuration. However, this destabilization will be overcome or partly compensated by the stabilization originating from intermolecular bond formation. The situation is very similar to the promotion of electrons from an atomic state to a valence state, familiar to us for the case of molecule forma-

tion from atoms. The question is then how to diminish the unnecessary destabilization due to electron promotion in the course of reaction, so as to facilitate the progress of the reaction. The distinction between so-called "allowed" and "forbidden"[7] reaction paths is clearly related to this problem.

By introducing the MO's ψ_n which are expanded in terms of the MO's of A and B into the total wave function Ψ of the composite system, we can analyze Ψ as a linear combination of various electron configurations of two reactants, *e.g.*, the original, charge-transferred, locally excited configuration and so on.[24,25] Such a configuration analysis can also furnish us with a clearer perception of the factors influencing chemical interaction.

Orbital Crossing and Correlation Diagrams

Before proceeding to the discussion of our calculation on the interaction of singlet methylene and butadiene, it may be worth mentioning here briefly how orbital correlation diagrams[7] relate to our present MO treatment. The expansion coefficients k provide much the same information that is contained in correlation diagrams, which interrelate the orbitals of reactants with products, or in simple orbital interaction diagrams.

To make the correspondence clear we first examine the addition of singlet methylene to ethylene. This reaction is an excellent example of an orbital symmetry directed preference for a non-least-motion path of low symmetry over a least-motion approach of higher symmetry. It also forms an obvious departure point for analysis of the interaction of methylene with butadiene.

Consider two configurations of a methylene and an ethylene (Figure 1). The first, marked A, represents a waypoint in the orbital symmetry allowed approach of the two molecules.[19a,d] The second, marked B, is a higher symmetry, C_{2v}, geometry, corresponding to the least-motion, forbidden approach.[26] π and π^* are the usual ethylene orbitals, σ the highest occupied molecular orbital (HOMO) of a singlet methylene, p the lowest unoccupied molecular orbital (LUMO) of the methylene, in reality a 2p orbital on carbon.[27]

The numbers of electrons occupying the various orbitals in geometry A are the following: $\nu_{\pi^*} = 0.040$, $\nu_p = 0.427$, $\nu_\sigma = 1.909$, $\nu_\pi = 1.629$. Charge transfer has clearly taken place primarily from π to p. This, of course, is in agreement with the experimental results on the polarity developed in the transition state for methylene addition.[28]

In a complementary analysis,[25] one can expand the total wave function of the composite system in terms of various states of the components

$$\Psi = 0.718\Psi_0 + 0.445\Psi_{\pi\to p} + 0.135\Psi_{\pi\to p,\pi\to p} + 0.122\Psi_{\sigma\to\pi^*} + 0.179\Psi_{\sigma\to p} + \cdots$$

where Ψ_0 is the original state ($\pi^2\sigma^2$), $\Psi_{\pi\to p}$ the one-electron transferred state, with an electron moving from π to p ($\pi^1\sigma^2p^1$), $\Psi_{\sigma\to p}$ the locally-one-electron-excited state, σ to p ($\pi^2\sigma^1p^1$), and so on.[29,30] The magnitude of the various coefficients shows again the important role of the charge transfer from π to p.

The population analysis we have developed allows an informative partitioning of the total overlap population between ethylene and methylene: $V_{\pi\sigma} = -0.026$, $V_{\pi p} = 0.167$, $V_{\pi^*\sigma} = 0.028$, and $V_{\pi^* p} = -0.002$. Note the antibonding character of the closed-shell interaction between π and σ, and once again the dominant bonding interaction between π and p.

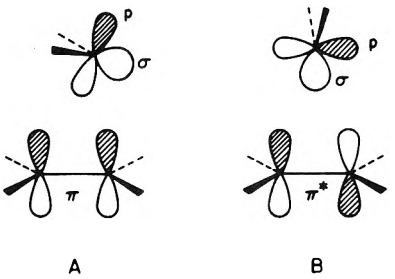

Figure 1. Geometries of two approaches of methylene to ethylene: A, non-least-motion allowed; B, least-motion forbidden. The two illustrations also show the shape of the σ and p orbitals of methylene and π and π^* levels of ethylene.

The above results are to be contrasted with the least-motion approach B. The occupation numbers in that case are $\nu_{\pi^*} = 0.059$, $\nu_p = 1.940$, $\nu_\sigma = 0.743$, and $\nu_\pi = 1.270$. Decomposition of the state wave function gives

$$\Psi = 0.292\Psi_{\pi\to p,\pi\to p} + 0.545\Psi_{\sigma\to p,\sigma\to p} + 0.570\Psi_{\pi\to p,\sigma\to p} + 0.116\Psi_{\sigma\to\pi^*,\sigma\to p} + \cdots$$

In the isolated state, four electrons occupy π and σ. Therefore, it is clear from examining the occupation numbers that a level crossing had taken place at $R > 2.5$ Å. Indeed, if the calculation is repeated at $R = 3.0$ Å, prior to that crossing, $\nu_\sigma = 1.999$, $\nu_\pi = 2.000$.[31]

The above example demonstrates how the ν's can show the type of electron shift, *i.e.*, transfer and/or excitation, which accompanies the orbital crossing. By expanding the wave function of the composite system as a linear combination of various electron configurations, one can define still more clearly the type of reorganization of electrons required to facilitate the occurrence of a reaction. It should be noted that neither the changes in the occupation numbers, nor the transfer from one electron configuration to another will take place discontinuously. An electronic state can and does interact with other states of the same spatial symmetry and the same spin multiplicity. Such configuration interaction is of particular importance when one is dealing with nearly degenerate levels, and may endow a system with biradical character.[32]

Addition of Singlet Methylene to Butadiene

As mentioned in the Introduction, there is no convincing evidence that singlet methylene can add in a concerted fashion to the termini of a butadiene. Instead 1,2 addition to a single double bond appears to be favored. This is so despite the 1,4 addition being a symmetry-allowed least-motion process. The problem at hand is thus to analyze how in this system a choice is made between two allowed reactions.

To study the difference between 1,2 and 1,4 addition we set up two reaction models for a methylene interacting with an *s-cis*-butadiene, as shown in Figure 2. In mode I, suited to 1,4 addition, C_s symmetry is maintained. The methylene is allowed to move in the mirror plane of butadiene orthogonal to the molecular plane. The separation of the two molecules was measured by the distance R from the methylene carbon to the midpoint of the line joining C_1 and C_4 of butadiene. The constraint to a plane allowed two angular degrees of freedom in addition to R. No particular symmetry constraint was used in mode II. The separation R here was measured from the midpoint of the $C_1{=}C_2$ double bond. The full six degrees of freedom were studied. For both modes the geometries of the buta-

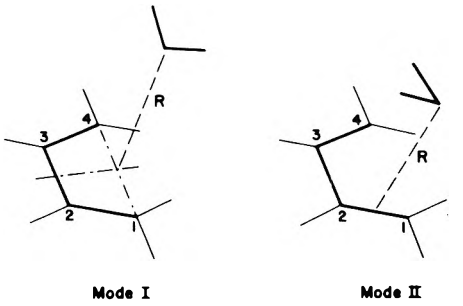

Figure 2. Two modes of approach of methylene to butadiene

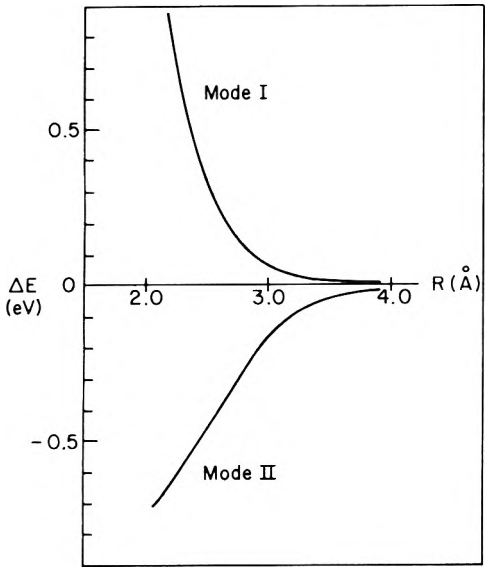

Figure 3. Energy as a function of R for modes I and II. Note that R is measured from a different origin (Figure 2) for the two modes.

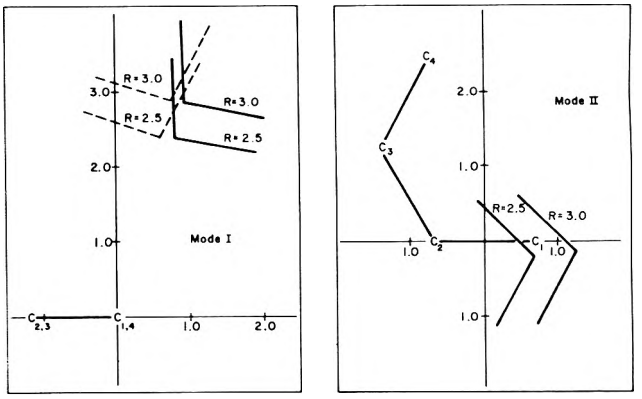

Figure 4. Projections of two optimized geometries along the modes of approach of methylene to butadiene. See text for a description of this drawing. The projection for mode I is on the vertical mirror plane of butadiene, and for mode II on the horizontal mirror plane containing the butadiene. Reference 34 explains the dashed geometries for mode I.

TABLE I: Partitioned Overlap Populations between Butadiene and Methylene

	Mode I		Mode II	
	R = 3.0 Å	R = 2.5 Å	R = 3.0 Å	R = 2.5 Å
$\sum_{i}^{\text{occ}}\sum_{l}^{\text{occ}} V_{\text{A-B},il}$	−0.0146	−0.0752	−0.0173	−0.0537
$\sum_{i}^{\text{occ}}\sum_{m}^{\text{unocc}} V_{\text{A-B},im}$	0.0086	0.0478	0.0699	0.1816
$\sum_{j}^{\text{unocc}}\sum_{l}^{\text{occ}} V_{\text{A-B},jl}$	0.0041	0.0180	0.0057	0.0351
$\sum_{j}^{\text{unocc}}\sum_{m}^{\text{unocc}} V_{\text{A-B},jm}$	0.0000	0.0001	0.0005	−0.0029
Total	−0.0019	−0.0094	0.0587	0.1601

diene and the methylene were frozen throughout the optimization.[33]

At a given R all the angular degrees of freedom were optimized. Figure 3 shows the energy as a function of R for both modes. The energy goes up along mode I, uniformly down along mode II in the region shown in Figure 3. Apparently mode I is not a real local minimum. When an optimized mode I geometry is used as a starting point for a mode II optimization (R measured from midpoint of $C_1{=}C_2$ instead of the C_1C_4 line), it moves smoothly over to a type II geometry. The preference for 1,2 addition is confirmed, though it must be noted that we did not allow full freedom to the reaction partners to relax their internal geometries in the course of the reaction.

We next turn to the analysis of what makes the mode II approach preferred over mode I. Figure 4 gives two projections of a pair of "snapshots" of angularly optimized geometries along the two reaction paths,[34] and Table I lists partitioned intermolecular overlap populations.

In both modes the sum of the overlap populations between occupied MO's of butadiene and occupied MO's of methylene is negative, as noted before for ethylene and methylene and as would be expected for the interaction between two closed-shell systems.[14b,23,35] The sum of the overlap populations between the occupied MO's of butadiene and the unoccupied MO's of methylene, and the converse, is positive, mainly coming from mutual charge-transfer interactions. Interactions between the unoccupied MO's are not important. Of all the combinations of the MO's of the two species, the interaction between the HOMO of butadiene and the LUMO of methylene plays the dominant role in intermolecular bond formation. As R gets smaller, the total overlap population between butadiene and methylene, however, becomes more negative in mode I, while it becomes more positive in mode II.

The calculation further showed that the σ electronic system of butadiene remained almost unaffected at distances of R = 2.5 Å and greater. It is thus sufficient to consider interactions with the π orbitals of butadiene, here labeled π_1 through π_4. Table II gives the numbers of electrons occupying the π MO's of butadiene and σ and p of methylene at R = 2.5 Å. The values in parentheses indicate the contributions from the second term of eq 11, *i.e.*, the intermolecular part. It is interesting to note that the HOMO of diene, π_2, donates more electrons than the lower orbital π_1, and that the LUMO, π_3, accepts more electrons than the higher orbital π_4. Moreover, the contribution from the intermolecular term in π_2 is about four times as large as that in π_1. The same is true with respect to π_3 and π_4. These results show quantitatively the important role of the frontier orbitals π_2 and π_3.

Returning to an examination of Tables I and II, we can first confirm that both reaction modes are symmetry allowed. This follows from the uniform increase with decreasing separation in the charge transfer part of the overlap populations, and the corresponding smooth depopulation of bonding levels and population of antibonding ones. There are no pathological features similar to those en-

TABLE II: Number of Electrons Occupying the MO's of Interacting Butadiene and Methylene at R = 2.5 Å

MO	Mode 1	Mode 2
Butadiene		
π_4	0.000	0.008(0.003)
π_3	0.038	0.044(0.012)
π_2	1.836	1.586(0.065)
π_1	1.998	1.918(0.016)
Methylene		
p	0.170	0.562(0.088)
σ	1.966	1.891(0.016)

countered in the least-motion approach of methylene to ethylene.

Nevertheless, there is a significant and obvious differential between the two modes. The charge transfer in mode I, the 1,4 addition, is considerably smaller than in mode II. The corresponding positive overlap population arising from the interaction between the occupied MO's of one component and unoccupied MO's of the other is, in mode I, insufficient to compensate for the negative, antibonding population arising from closed-shell interactions. At R = 2.5 Å the net overlap population between methylene and butadiene is in fact slightly negative.

A decomposition of the wave functions at R = 2.5 Å yields[36]

$$\Psi_I = 0.881\Psi_0 + 0.350\Psi_{\pi_2 \rightarrow p} + 0.144\Psi_{\sigma \rightarrow \pi_3} + 0.026\Psi_{\pi_1 \rightarrow \pi_3} + 0.008\Psi_{\pi_2 \rightarrow \pi_3} + \ldots$$

and

$$\Psi_{II} = 0.644\Psi_0 + 0.184\Psi_{\pi_1 \rightarrow p} + 0.457\Psi_{\pi_2 \rightarrow p} + 0.116\Psi_{\sigma \rightarrow \pi_3} + 0.045\Psi_{\sigma \rightarrow \pi_4} + 0.003\Psi_{\pi_1 \rightarrow \pi_3} + 0.001\Psi_{\pi_1 \rightarrow \pi_4} + 0.022\Psi_{\pi_2 \rightarrow \pi_3} + 0.004\Psi_{\pi_2 \rightarrow \pi_4} + 0.185\Psi_{\sigma \rightarrow p} + \ldots$$

We observe that the original state Ψ_0 is still dominant. The $\pi_1 \rightarrow$ p and $\pi_2 \rightarrow$ p transfers in II are considerably more important than the $\pi_2 \rightarrow$ p transfer in I. This indeed is the crux of the difference between modes I and II. In any reaction of methylene the crucial orbital is its acceptor orbital, p. The primary interaction is between that acceptor, LUMO, p and whatever donor orbital is offered up by the substrate. In the 1,2 addition both π_1 and π_2 serve as donors, with the latter dominating. In the 1,4 addition mode by symmetry only π_2 can interact with p. And that overlap, shown schematically in 1 is basically inefficient. The methylene has to approach very close to the butadiene to make that overlap significant, and in doing so it encounters excessive closed-shell repulsions.

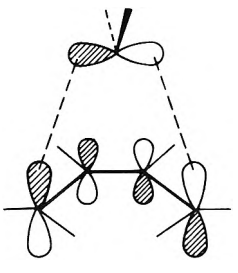

1

Charge Transfer and Polarization

It is worthwhile to analyze in somewhat greater detail the reorganization, in course of the favored 1,2 addition, of the π electrons in butadiene and the mixing of σ and p orbitals in the attacking methylene. As seen in the preceding section, the donation of electrons from the HOMO of butadiene to the LUMO of methylene is the dominant term. Such donation will weaken the 1,2 and (equally) the 3,4 bonds of the diene, and strengthen the 2,3 bond, because π_2, the HOMO, has a node between carbons 2 and 3. The effect would appear to be symmetric with respect to the bond being attacked, $C_1{=}C_2$, and its untouched partner, $C_3{=}C_4$. But, of course, there is a differential between the two ends of the molecule, set by polarization terms. The π-electron density of the butadiene in the interacting state is given by[37]

$$\rho_\pi = 1.9015\pi_1^2 + 1.5206\pi_2^2 + 0.0325\pi_3^2 + 0.0047\pi_4^2 - 0.2241(\pi_1\pi_2 + \pi_2\pi_1) - 0.0053(\pi_1\pi_3 + \pi_3\pi_1) - 0.0009(\pi_1\pi_4 + \pi_4\pi_1) + 0.0502(\pi_2\pi_3 + \pi_3\pi_2) + 0.0112(\pi_2\pi_4 + \pi_4\pi_2) + 0.0122(\pi_3\pi_4 + \pi_4\pi_3)$$

Here we note that the number of electrons occupying the π MO's is calculated to be less than four in the interacting state, because a part is transferred to methylene and another part is consumed in bond formation. The cross terms are the ones which yield the polarization.[38]

The effect of polarization may be seen by the changes in electron densities and overlap populations specified in **2**. A positive sign implies an increase in electronic density or overlap population due to polarization. An electron flow from the 1,2 bond region to the 2,3 and 3,4 bond regions will be observed. The interaction weakens the 1,2 π bonding and strengthens somewhat the 3,4 bond.

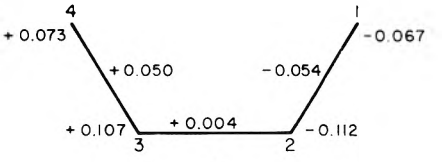

2

Another interesting effect may be seen at the attacking methylene. The σ and p orbitals of the methylene, which are orthogonal in the isolated state, will be intermixed through their interaction with butadiene orbitals. Figure 5 shows the electron density of methylene, ρ_{CH_2}, in the x'-z' plane at $y' = 0$. The coordinate axes are defined in the figure. They refer to a local coordinate frame fixed in the methylene. It is most interesting to see that spatial rearrangement of electron density takes place in such a way that the maximum electron distribution in methylene is almost parallel to the molecular plane of butadiene. Qualitatively it may be said that the repulsive nature of the closed-shell interaction between σ and π is "remembered" to the extent that even when the primary attack of the methylene is through its p orbital, it still attempts to remove the σ electron pair as far as possible from possible interaction. In another way of thinking, the bonding situation, shown in **3**, represents a transition from the symmetry-enforced σ-p picture of methylene bonding to a hybridized state associated with the product cyclopropane.

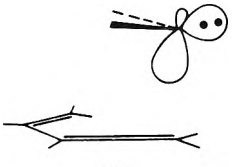

3

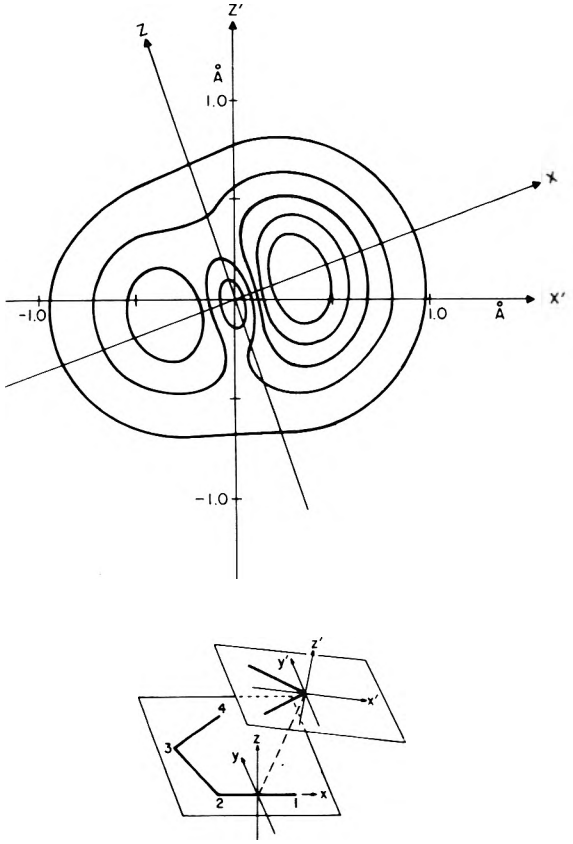

Figure 5. The electronic density of methylene is shown at top. The coordinate system is specified in detail in the small figure at bottom. Primed axes refer to a coordinate system fixed in the methylene, unprimed axes to one fixed at the midpoint of $C_1{=}C_2$.

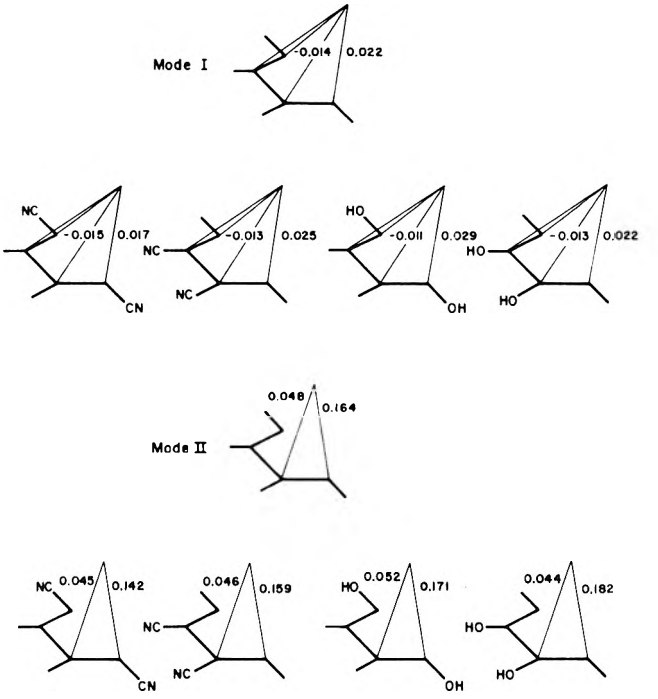

Figure 6. Overlap populations for some substituted butadienes in mode I and II geometries at R = 2.5 Å.

Effect of Substituents

We conclude by examining the effect of electron-donating and accepting substituents on the relative merits of 1,2 and 1,4 addition. Taking the R = 2.5 Å geometry for modes I and II, we substituted the 1 and 4 or 2 and 3 positions with sample donors, hydroxyl groups, or sample acceptors, cyano groups. Though a comparison of energetics can be made, we have found it illuminating to examine the methylene–butadiene overlap populations in the substituted compounds relative to the unsubstituted case. This is done in Figure 6. Donor substituents, either at the terminal or central carbons, increase the intermolecular overlap populations for mode II. Acceptor substituents, on the contrary, make for weaker interaction. It is easy to trace this effect to the perturbation of the HOMO of the diene, π_2, by the substituents.

The overall effect on mode I, the model for 1,4 addition, is disappointingly small. The placement of electron accepting groups at the 2 and 3 positions increases slightly the intermolecular overlap populations. This can be traced to increased charge transfer from methylene σ to π_3 of diene. One strategy to bring about a preference of 1,4 over 1,2 addition might then be the placement of π-electron accepting groups at the 2 and 3 positions of the diene, coupled with substitution by σ-electron-releasing groups at the methylene carbon. However, we are pessimistic whether a reversal of the preference can be achieved; the calculated substituent effects are so small.[39]

To summarize we have analyzed in detail the origins of the preference for 1,2 addition of methylene to butadiene over 1,4 addition. Both processes are allowed, but the stabilizing charge transfer interaction in the 1,2 addition is much more efficient. The simple methodology of intermolecular population analysis and orbital decomposition which we have developed here covers and connects the perturbation, orbital and state correlation, configuration interaction, and frontier orbital approaches to chemical interactions. The method may be extended easily to open-shell systems and the interaction of more than two reagents.

Acknowledgment. We are grateful to the donors of the Petroleum Research Fund, administered by the American Chemical Society, and the National Science Foundation (GP28137X) for support of this research.

References and Notes

(1) C. A. Coulson and H. C. Longuet-Higgins, *Proc. Roy. Soc., Ser. A*, **192**, 16 (1947).
(2) F. H. Burkitt, C. A. Coulson, and H. C. Longuet-Higgins, *Trans. Faraday Soc.*, **47**, 553 (1951).
(3) G. W. Wheland, *J. Amer. Chem. Soc.*, **64**, 900 (1940).
(4) (a) M. J. S. Dewar, *J. Amer. Chem. Soc.*, **74**, 3341, 3345, 3350, 3353, 3355 (1952). (b) M. J. S. Dewar, "The Molecular Orbital Theory of Organic Chemistry," McGraw-Hill, New York, N. Y., 1969.
(5) (a) K. Fukui, T. Yonezawa, and H. Shingu, *J. Chem. Phys.*, **20**, 722 (1952); (b) K. Fukui, T. Yonezawa, and C. Nagata, *Bull. Chem. Soc. Jap.*, **27**, 423 (1954); (c) K. Fukui in "Molecular Orbitals in Chemistry, Physics and Biology," P.-O. Lowdin and B. Pullman, Ed., Academic Press, New York, N. Y., 1964.
(6) R. D. Brown, *J. Chem. Soc.*, 2232 (1959).
(7) (a) R. B. Woodward and R. Hoffmann, *J. Amer. Chem. Soc.*, **87**, 395, 2511 (1965); (b) R. Hoffmann and R. B. Woodward, *ibid.*, **87**, 2046, 4388, 4389 (1965); (c) *Accounts Chem. Res.*, **1**, 17 (1968); (d) R. B. Woodward and R. Hoffmann, *Angew. Chem.*, **81**, 797 (1969).
(8) R. F. Hudson, *Angew. Chem., Int. Ed. Engl.*, **12**, 36 (1973).
(9) J. N. Murrell, M. Randić, and D. R. Williams, *Proc. Roy. Soc., Ser. A*, **284**, 566 (1965).
(10) G. Klopman and R. F. Hudson, *Theor. Chim. Acta*, **8**, 165 (1967).
(11) G. Klopman, *J. Amer. Chem. Soc.*, **90**, 223 (1968).

(12) A. Imamura, *Mol. Phys.*, **15**, 225 (1968).
(13) L. Salem, *J. Amer. Chem. Soc.*, **90**, 543, 553 (1968).
(14) (a) K. Fukui and H. Fujimoto, *Bull. Chem. Soc. Jap.*, **41**, 1989 (1968); **42**, 3399 (1969); (b) H. Fujimoto, S. Yamabe, and K. Fukui, *ibid.*, **44**, 2936 (1971).
(15) L. Salem and A. Devaquet, *J. Amer. Chem. Soc.*, **91**, 3793 (1969).
(16) A. Devaquet, *Mol. Phys.*, **18**, 233 (1970).
(17) R. Sustmann and G. Binsch, *Mol. Phys.*, **20**, 1, 9 (1971).
(18) R. D. Brown, *Quart. Rev., Chem. Soc.*, **6**, 63 (1952).
(19) (a) R. Hoffmann, *J. Amer. Chem. Soc.*, **90**, 1475 (1968); (b) R. Hoffmann, R. Gleiter, and F. B. Mallory, *ibid.*, **92**, 1460 (1970); (c) R. C. Dobson, D. Hayes, and R. Hoffmann, *ibid.*, **93**, 6188 (1971); (d) R. Hoffmann, D. M. Hayes, and P. S. Skell, *J. Phys. Chem.*, **76**, 664 (1972).
(20) (a) H. Kollmar, *Tetrahedron Lett.*, 3337 (1970); *Tetrahedron*, **28**, 5893 (1972); (b) M. J. S. Dewar, E. Haselbach, and M. Shanshal, *J. Amer. Chem. Soc.*, **92**, 3505 (1970); N. Bodor, M. J. S. Dewar, and J. S. Wasson, *ibid.*, **94**, 9095 (1972); (c) H. Basch, *J. Chem. Phys.*, **55**, 1700 (1971); *Theor. Chim. Acta*, **28**, 151 (1973); (d) I. S. Y. Wang and M. Karplus, *J. Amer. Chem. Soc.*, **95**, 8160 (1973); (e) J. P. Snyder, R. J. Boyd, and M. A. Whitehead, *Tetrahedron Lett.*, 4347 (1972); (f) J. E. Del Bene, *J. Amer. Chem. Soc.*, **94**, 3713 (1972); (g) G. F. Tantardini and M. Simonetta, *Isr. J. Chem.*, **10**, 581 (1972); (h) J. N. Murrell, J. B. Pedley, and S. Durmat, *J. Chem. Soc., Faraday Trans. 2*, 1370 (1973); (i) S. P. Kolesnikov, A. I. Ioffe, and O. M. Nefedov, *Izv. Akad. Nauk SSSR, Ser. Khim.*, 2622 (1973).
(21) (a) The literature contains several cases of possible 1,4 addition: B. Grzybowska, J. H. Knox, and A. F. Trotman-Dickinson, *J. Chem. Soc.*, 4402 (1961); 3826 (1962); V. Franzen, *Chem. Ber.*, **95**, 571 (1962); J. A. Berson and E. S. Hand, *J. Amer. Chem. Soc.*, **86**, 1978 (1964); T. V. Domareva-Mandelshtam and I. A. Dyakonov, *Zh. Obsch. Khim.*, **34**, 3844 (1964); H. Nozaki, M. Yamabe, and R. Noyori, *Tetrahedron*, **21**, 1657 (1965); E. Müller and H. Kessler, *Justus Liebigs Ann. Chem.*, **692**, 58 (1966); P. Hodge, J. A. Edwards, and J. H. Fried, *Tetrahedron Lett.*, 5175 (1966). (b) The 1,4 addition of triplet dicyanocarbene to cyclooctatetraene is discussed by A. G. Anastassiou, R. P. Cellura, and E. Ciganek, *Tetrahedron Lett.*, 5267 (1970). The related additions of triplet cyanonitrene have been treated in detail by A. G. Anastassiou, *J. Amer. Chem. Soc.*, **87**, 5512 (1955); **90**, 1527 (1968). (c) See the recent discussion of C. W. Jefford, nT. Kabengele, J. Kovacs, and U. Burger, *Tetrahedron Lett.*, 257 (1974); *Helv. Chim. Acta*, **57**, 104 (1974).
(22) A careful analysis of the parent system of methylene and butadiene has been carried out by H. M. Frey, *Trans. Faraday Soc.*, **58**, 516 (1972).
(23) R. S. Mulliken, *J. Chem. Phys.*, **23**, 1833, 1841 (1955).
(24) H. Baba, S. Suzuki, and T. Takemura, *J. Chem. Phys.*, **50**, 2078 (1969).
(25) S. Yamabe, S. Kato, H. Fujimoto, and K. Fukui, *Theor. Chim. Acta*, **30**, 327 (1973).
(26) In both A and B, R, the distance from the carbene carbon to the midpoint of the C=C bond is the same and equal to 2.5 Å. For further details see ref 19a and 19d. The molecular orbitals in this paper were calculated by the extended Hückel method: R. Hoffmann, *J. Chem. Phys.*, **39**, 1397 (1963); R. Hoffmann and W. N. Lipscomb, *ibid.*, **36**, 2179, 3489 (1962); **37**, 2872 (1962).
(27) For a discussion of the electronic structure of methylenes see J. F. Harrison in W. Kirmse, "Carbene Chemistry," 2nd ed, Academic Press, New York, N. Y., 1971, p 159; R. Hoffmann, G. D. Zeiss, and G. W. Van Dine, *J. Amer. Chem. Soc.*, **90**, 1485 (1968).
(28) P. S. Skell and A. Y. Garner, *J. Amer. Chem. Soc.*, **78**, 3409 (1956).
(29) In this type of analysis the wave functions are given by the proper antisymmetrized products of molecular orbitals.
(30) The locally excited state $\Psi_{\sigma\rightarrow p}$ can also be regarded as a successive charge-transfer process, *e.g.*, $\Psi_{\sigma\rightarrow\pi^*,\pi^*\rightarrow p}$. Such a forward and backward charge-transfer interaction may be important in strong donor–acceptor interactions. On this point, see the discussion by Epiotis [N. D. Epiotis, *J. Amer. Chem. Soc.*, **94**, 1924 (1972); **95**, 1191 (1973)]. In that case, however, the charge-transferred state, $\Psi(A^-D^+)$ or $\Psi(A^{2-}D^{2+})$, should be the dominant term in the wave function. We think this is rarely so, even when the reactants are highly polar.
(31) In an interesting approach to concerted reactions, E. B. Wilson and P. S. C. Wong, *Chem. Phys. Lett.*, **15**, 400 (1972), have suggested following the change in occupation numbers of natural orbitals as a criterion of allowedness. At large separation $\Psi = \Psi_0$. If we form the wave function Ψ' for the doubly excited state (two electrons shifted from HOMO to LUMO) at R = 2.5 Å, we get $\Psi' = 0.994\Psi_0 + \ldots$. The corresponding occupation numbers for this Ψ' state are $\nu_\pi = 1.999$, $\nu_{\pi^*} = 0.000$, $\nu_\sigma = 1.994$, $\nu_p = 0.002$. Thus the crossing is confirmed in another way.
(32) (a) L. Salem, *Chem. Commun.*, 981 (1970); (b) E. F. Hayes and A. K. Q. Siu, *J. Amer. Chem. Soc.*, **93**, 2090 (1971); (c) L. Salem and C. Rowland, *Angew. Chem., Int. Ed. Engl.*, **11**, 92 (1971); (d) H. Fukutome, *Progr. Theor. Phys.*, **47**, 1156 (1972).
(33) The following geometrical assumptions were made: C_1=C_2 1.35 Å, C_2–C_3 1.46 Å, all C–H 1.10 Å. The HCH angle in methylene was taken as 102°, all valence angles in butadiene at 120°.
(34) Within the constraints of a type I approach we actually locate two local energy minima at a given value of R. They are both shown in Figure 4. The two minima differ only in the cant of the methylene group, they possess virtually identical energies and yield nearly identical population partitions. In the subsequent discussion we use the geometries corresponding to one of these minima, the one drawn in solid in Figure 4.
(35) (a) L. Salem, *Proc. Roy. Soc., Ser. A*, **264**, 379 (1961); (b) V. Magnasco, *Theor. Chim. Acta.*, **21**, 267 (1971).
(36) Only singly transferred and singly excited electron configurations are shown, in order to simplify the representation of Ψ. The contributions of highly transferred and highly excited electron configurations are not necessarily small. The doubly transferred configuration from π_2 of butadiene to p of methylene $\Psi_{\pi_2\rightarrow p,\pi_2\rightarrow p}$, for example, has a coefficient of 0.075 in Ψ_I and 0.161 in Ψ_{II}.
(37) The σ–π separability does not hold in the interacting state. Here the π electron density means the distribution of electrons occupying those levels which, in the isolated butadiene, were strictly π levels.
(38) For a further discussion of polarization see L. Libit and R. Hoffmann, *J. Amer. Chem. Soc.*, **96**, 1370 (1974).
(39) One might note the negative overlap populations in mode I between the methylene carbon and C_2 or C_3 of butadiene. These can be traced to the σ–π_3 interaction and the nature of π_3, that it has a different phase of the wave function at C_2 and C_3 relative to C_1 and C_4. The σ–π_3 interaction, governed by σ overlap with butadiene p orbitals at C_1 and C_4, thus has a destablizing secondary interaction with C_2 and C_3. This is still another component of the troubles with the 1,4 addition.

An Infrared and Electron Paramagnetic Resonance Study of Some Silver–Nitric Oxide Complexes in Y Type Zeolites

Chien-Chung Chao and Jack H. Lunsford*[1]

Department of Chemistry, Texas A & M University, College Station, Texas 77843 *(Received October 19, 1973)*

Publication costs assisted by The Robert A. Welch Foundation

Nitric oxide was allowed to react with Ag^+ ions in silver-exchanged zeolites, yielding two paramagnetic complexes. One complex, attributed to $[Ag(I)NO]^+$, was formed upon adsorption of NO at pressures less than 50 Torr. This species is characterized by an epr spectrum with $g_\perp = 2.000$, $g_\parallel = 1.934$, $A_\perp = 65$ G, and $A_\parallel = 72$ G. An infrared band at 1884 cm^{-1} appears to be associated with the $[Ag(I)NO]^+$ ion. The second, more stable complex became the dominant species after adsorption of NO at pressures in excess of 300 Torr. The partially resolved epr spectrum has been interpreted in terms of an $[Ag(I)_2NO]^{2+}$ complex in which the nitrosyl group is in a bridging position between two silver ions located in the sodalite unit. An infrared band at 1876 cm^{-1} is associated with this species.

Introduction

A considerable amount of research has been devoted to the preparation and characterization of nitrosyl compounds of transition metals.[2] From the viewpoint of surface chemistry these nitrosyl compounds may be important intermediates in the catalytic reduction or dissociation of nitric oxide. Both CuY and AgY zeolites are active as catalysts for the reduction of NO; yet, little is known concerning the mechanism for this reaction.[3] By comparing the structure, stability, and reactivity of surface nitrosyl complexes with other nitrosyl compounds one might gain some insight into the nature of these surface species.

Recently the authors observed that a $[Cu(I)NO]^+$ complex could be formed in a Cu(I)Y zeolite.[4] In the present work two complexes have been observed for NO in a AgY zeolite. The $[Ag(I)NO]^+$ complex which is analogous to $[Cu(I)NO]^+$ was observed, as well as a stable NO–silver radical which is inert to molecular oxygen. The infrared data clearly show that this new radical is not some other oxide of nitrogen produced by a disproportionation reaction. According to the electron paramagnetic resonance and infrared data a tentative structure of $[Ag(I)_2NO]^{2+}$ is proposed. Here the Ag^+ is also attached to the framework oxygen atoms of the zeolite.

Experimental Section

The AgY was prepared by exchanging 5 g of a NaY type zeolite supplied by the Linde Co. (Lot No. 11007-73) in 100 ml of 0.2 *M* $AgNO_3$ solution. The exchange was repeated three times, and each time the sample was stirred in the dark at room temperature for 12 hr. The exchange was essentially complete. For infrared measurements, the samples were pressed into plates. The procedure for sample preparation and a description of the infrared cell were given in an early paper.[5] For the epr measurements, the zeolite was broken into chips and dehydrated in a conventional cell having a 2- or 4-mm o.d. quartz side arm which could be inserted into a microwave cavity.[6] All samples were degassed to 500° under vacuum (5×10^{-6} Torr). The temperature was raised hourly in 100° increments. Purified NO was admitted into the cell containing the degassed samples at pressures which varied from 5 to 400 Torr. After degassing some of the samples were treated in 400 Torr of O_2 at 500° for 3 hr; however, the oxygen treatment did not alter the results.

A Beckman IR-12 spectrophotometer was used for the infrared measurements, which were carried out at room temperature. The slit widths were such that a resolution better than 3 cm^{-1} was maintained. A Varian 4502 and an E6S spectrometer were employed for the epr measurements. A rectangular TE_{102} mode cavity and a cylindrical TE_{011} mode cavity were used for X band and Q band, respectively. For X band measurements samples were cooled by immersing the sample tube in liquid nitrogen, but for the Q band measurements the samples were cooled by the gas boiled off from liquid nitrogen. In the latter case the sample temperature was about 90°K. The g values were determined relative to a DPPH standard (g = 2.0039) or a phosphorus-doped silicon standard (g = 1.9987).

Results

1. Infrared Spectra. The fundamental band for free NO is at 1876 cm^{-1}. At low NO pressures (<50 Torr), two peaks due to adsorbed NO were observed for the AgY zeolite. One appears at a slightly higher frequency (1884 cm^{-1}) and the other one appears at a slightly lower frequency (1844 cm^{-1}) than free NO. The peaks developed immediately upon exposure to NO and remained essentially constant over several hours. Both peaks could be removed by degassing the sample at room temperature. At higher NO pressures, though the initially observed spectra were the same, new features developed upon allowing the sample to stand at room temperature for several hours. A new peak at 1876 cm^{-1} grew at the expense of the 1884-cm^{-1} peak. This new peak could not be removed by degassing the sample at room temperature. Approximately 0.5 hr was required to remove the peak completely, even with the sample at 200°. After the excess NO was removed at room temperature, the introduction of oxygen or air into the cell did not cause any change in the 1876-cm^{-1} peak.

Some of the typical spectra are depicted in Figure 1. Curve 1 is the spectrum of an AgY sample which was degassed to 500°, heated in 400 Torr of O_2 at 500° for 40 min, and then degassed at 250° for 10 min. Curve 2 shows the

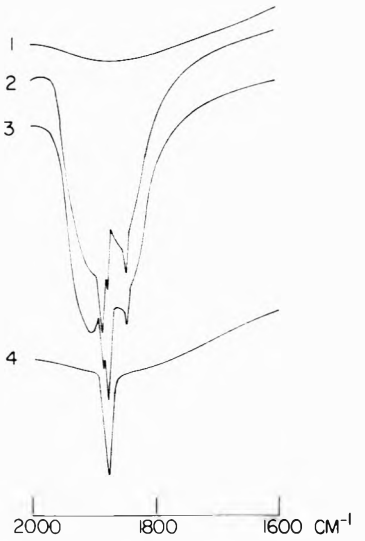

Figure 1. Infrared spectra of an AgY zeolite: (1) after oxygen treatment and degassing at 500°, (2) 5 min after introducing 320 Torr of NO in the cell, (3) 12 hr after introducing 320 Torr of NO into the cell, (4) after evacuating the cell for 1 hr at 25°.

spectrum of the sample 5 min after 320 Torr of NO was introduced. In addition to the peaks at 1884 and 1844 cm^{-1} which are due to adsorbed NO, the strong absorption of gas-phase NO may be observed. In this spectrum the sharp peak at 1876 cm^{-1} is mainly due to the Q branch of free NO. Curve 3 shows the spectrum of the sample after standing at room temperature for 12 hr. It is clear that the peak at 1876 cm^{-1} increased while the peak at 1884 cm^{-1} decreased in amplitude. Here, a new type of adsorbed NO is contributing to the intensity of the 1876-cm^{-1} peak. Curve 4 shows the spectrum after evacuation of the cell at room temperature for 1 hr. Every peak but the one at 1876 cm^{-1} disappeared.

2. *Epr Spectra.* Basically, the epr and ir observations were parallel to each other in that a relatively unstable species is formed at lower pressures and a more stable complex is formed at higher pressures. When the adsorption was carried out under low NO pressures (<50 Torr), the X band spectrum depicted in Figure 2 was observed. This spectrum also developed immediately upon exposure to NO and remained constant over a period of several hours. The species responsible for the signal could be removed very easily by degassing the sample at room temperature. The spectrum can be reasonably interpreted

$$\mathcal{H} = g_{\parallel}\beta H_z S_z + g_{\perp}\beta(H_x S_x + H_y S_y) + A_{\parallel}^{N} I_z^{N} S_z + A_{\perp}^{N}(I_x^{N} S_x + I_y^{N} S_y) + A_{\parallel}^{Ag} I_z^{Ag} S_z + A_{\perp}^{Ag}(I_x^{Ag} S_x + I_y^{Ag} S_y) \quad (1)$$

Here we assume that the principal axes of the g tensor and the A tensors are parallel to each other. In analyzing the spectrum the nitrogen hyperfine lines are not resolved, hence, the splitting constants have to be estimated from the observed line width. A computer program was written to simulate the powder spectrum and to determine the nitrogen hyperfine splitting. The spectrum in the Q band region is in complete agreement with the data in Table I. For comparison purposes the magnetic parameters for NO in NaY and Cu(I) are also given in Table I.

When higher NO pressures were used and the sample was maintained in the NO atmosphere at room temperature or at −78° for 12 hr, a completely new spectrum emerged and the previous spectrum diminished significantly. The new spectrum was also observed using a crushed ir sample plate which gave the stable 1876-cm^{-1} ir peak. The samples which were cooled to −78° gave better resolved spectra. Four spectra of this species are depicted in Figure 3. Curves 1 and 2 are the X band spectra produced by adsorbing ^{14}NO and ^{15}NO, respectively; curves 1 and 2 of Figure 4 are their Q band counterparts. In an analysis of these spectra several observations must be reconciled. First, the spreading of spectrum changes only slightly when one switches from X band to Q band. This implies that the anisotropy of the g values is small.

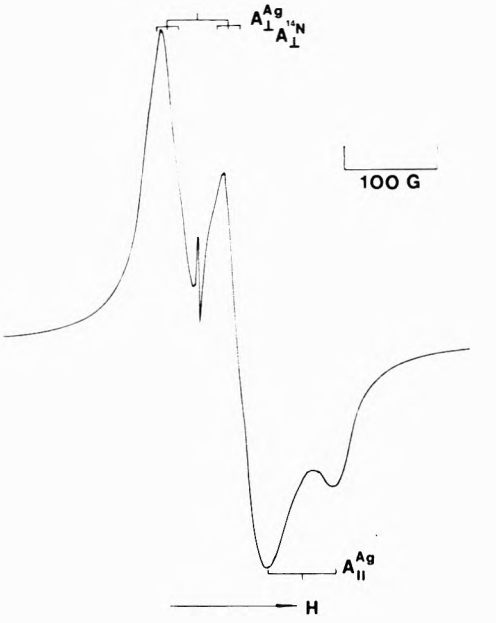

Figure 2. X-band epr spectrum of the $[Ag(I)NO]^{+}$ complex at 77°K. The sharp peak is due to phosphorus-doped silicon.

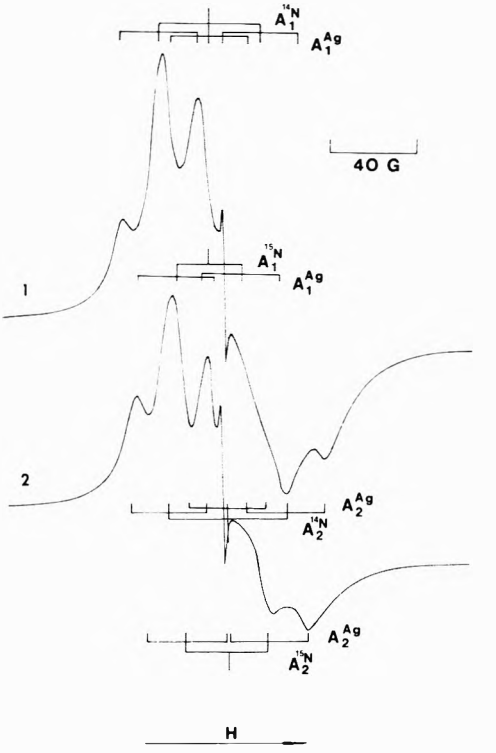

Figure 3. X-band epr spectrum of $[Ag(I)_2NO]^{2+}$ at 77°K: (1) formed from ^{14}NO, (2) formed from ^{15}NO. The sharp peak is due to phosphorus-doped silicon.

TABLE I: Epr Parameters and Ir Absorption Peaks for NO Complexes in Y-Type Zeolites

Centers	g_1	g_2	g_3	Ag $\|A_1\|$, G	Ag $\|A_2\|$, G	Ag $\|A_3\|$, G	N $\|A_1\|$, G	N $\|A_2\|$, G	N $\|A_3\|$, G	Ir peak, cm^{-1}	Ref
$(Ag^{14}NO)^+$ in Ag(I)Y	1.934	2.000	2.000	72	65	65	1	12[a]	12[a]	1884	This work
$(Ag_2{}^{14}NO)^{2+}$ in Ag(I)Y	1.998	2.004		18	18		26.8	23.5		1876	This work
$(Ag_2{}^{15}NO)^{2+}$ in Ag(I)Y	1.998	2.004		18	18		37.6	29.7			This work
$(Cu^{14}NO)^+$ in Cu(I)Y	1.89	2.009	2.009	240[b]	190[b]			25			4
^{14}NO in NaY	1.86	1.989	1.989					28			6

[a] Parameters used in computer simulation. [b] Copper hyperfine splitting.

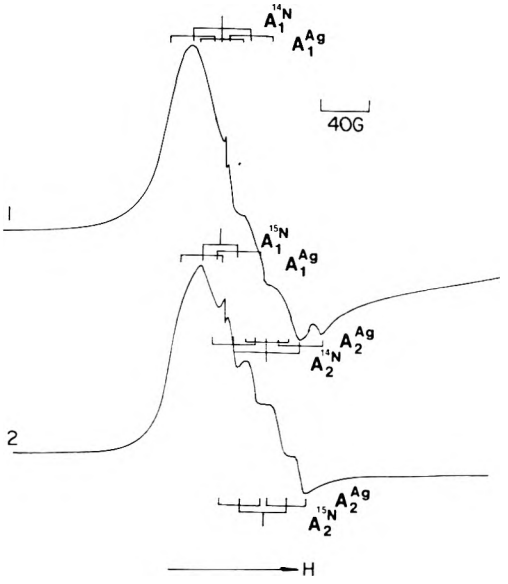

Figure 4. Q-band epr spectrum of $[Ag(I)_2NO]^{2+}$ at 77°K: (1) formed from ^{14}NO, (2) formed from ^{15}NO. The sharp peak is due to DPPH.

It is obvious then that there must be a severe overlap among hyperfine lines. Furthermore, when one changes from ^{14}NO ($I = 1$) to ^{15}NO ($I = \frac{1}{2}$) the number of resolved peaks is unchanged; only the spread of spectrum decreased. This implies that both nitrogen and silver ($I = \frac{1}{2}$) atoms have significant hyperfine splitting and the total number of unresolved lines in the spectrum might be very large.

The parameters of the spectra are extracted by first assuming that the right most resolved lines in the X band and Q band spectra correspond to the same line. Starting from the expression $H = (h\nu/g\beta) - m(A/g\beta)$ with some algebraic manipulation one can obtain the expression

$$g = (g_r)\frac{H_r - H_r'}{H - H'} \qquad (2)$$

Here g and g_r are the g values of the center in one principal direction and that of the DPPH standard; H_r and H_r' are the resonance fields of the standard at Q band and X band, respectively; and H and H' are the resonance fields of one particular hyperfine line at the two frequencies. A value of $g_1 = 1.998$ is thus determined from the right most hyperfine line. It is important to notice that the ^{14}NO and ^{15}NO spectra gave identical values. Ideally, a second g value could be determined from the low-field hyperfine components in the X band and Q band spectra. Since the low-field hyperfine structure is not resolved at Q band, it was assumed that second low-field hyperfine line corresponds to the maximum in Figures 3c and 3d. This results in a value of $g_2 = 2.0042$.

Based on these g values and the ratio of the nuclear magnetic moments for ^{14}N and ^{15}N ($\mu^{15}N/\mu^{14}N = 1.403$), consistent sets of hyperfine splittings were determined from the X band spectra. The most reasonable values are given in Table I, and stick figures indicating these values are shown in Figure 3. These parameters yielded a comparable simulated spectrum except in the region corresponding to the baseline crossover, where an extra line appeared. This feature could probably be eliminated by including a third g value and a third set of hyperfine constants in the calculation; however, the complexity of the polycrystalline spectrum and the arbitrary assignments that would be required probably do not merit this approach. Nevertheless, according to the model proposed in the next section, there is justification for nonaxial symmetry.

The epr signal from the latter species exhibited only moderate line broadening upon exposure of the sample to molecular oxygen. This of course means that the paramagnetic ion is removed from the supercage by a distance of several Ångstroms.

3. Desorption Products. The formation of $[Ag(I)NO]^+$ is completely reversible and there is no evidence of a disproportionation reaction. The ir spectrum of the gas removed from the sample showed only the presence of nitric oxide. Gas removed from samples showing the $[Ag(I)_2NO]^{2+}$ signal were collected in two fractions; one at room temperature and another at temperatures higher than 100°. Infrared and mass spectrometry showed that only nitric oxide was present in both fractions.

Discussion

It appears reasonable to assign the ir peak at 1884 cm^{-1} and the spectrum of Figure 2 to the same species. This assignment is based mainly on the intensity correlation: as the pressure of NO and the time of interaction between the AgY zeolite and NO increased, the intensity of both the epr signal and the 1884-cm^{-1} line decreased. No corresponding intensity change was observed for the ir peak at 1884 cm^{-1}. This peak is due to adsorbed NO, but the adsorption site is unknown.

The hyperfine structure indicates that the paramagnetic complex contains one nucleus with $I = \frac{1}{2}$, which is the nuclear spin of silver. Before adsorption all silver atoms in AgY were in their univalent state, since no epr signal of Ag^{2+} or Ag^0 was detected. Most AgY samples were treated with oxygen to remove Ag^0. The adsorption of NO does not formally seem to change the valence of the silver. It is

possible for $(NO)^+$ to absorb in the region of 1884 cm^{-1},[7] but if this were the case, the silver would be reduced to Ag^0. The observed epr spectrum is totally unlike that of Ag^0.[8-10] Also, it is highly unlikely that $[NO]^-$ would absorb in the 1884-cm^{-1} region. Therefore, we concluded that after complex formation the silver is still in its univalent state, and propose that the paramagnetic center is $[Ag(I)NO]^+$. Although no spin concentration measurements were carried out, it is evident from the spectra that <20% of the silver ions were involved in complex formation.

If one assumes that the unpaired electron on the Ag^+ ion is localized in a hybridized $4d_{z^2}5s$ orbital, then it is possible to calculate the spin density in this orbital using the procedure previously adopted for the $[Cu(I)NO]^+$ complex.[4] The Fermi contact term, $g_e\beta_e g_N\beta_N{}^8/_3\pi|\psi_{5s}(O)|^2$, is 1713 MHz as determined from atomic beam measurements for ^{107}Ag.[11] The value of $g_e\beta_e g_N\beta_N\langle r^{-3}\rangle_{4d}$ for a $4d^9$ electron on Ag^{107} is 180 MHz.[12] From these values and the experimental hyperfine coupling constants one may show that the wave function on the silver ion has 13% $4d_{z^2}$ and 11% 5s character. The unpaired electron is approximately 24% on the Ag+ ion, which is very similar to the results obtained for the $[Cu(I)NO]^+$ complex.

The 1876-cm^{-1} infrared peak and the epr spectra of Figure 3 are assigned to the same species for the samples which received extended exposure to a high pressure of NO. Based on the infrared spectrum and the fact that the only gas obtained upon desorption was nitric oxide, it seems probable that this center is a nitrosyl silver complex. The number of hyperfine lines and the g values suggest this center has the composition of $[Ag(I)_2NO]^{2+}$. The small silver hyperfine splitting constants confirm that there is little delocalization of the paramagnetic electron onto this ion; they are certainly much less than in the $[Ag(I)NO]^+$ complex. Hence, the stabilization of the complex is not due to electron delocalization.

The presence of nitrogen hyperfine splitting along at least two principal directions and the absence of a large g tensor anisotropy must mean that the molecular orbitals of the nitric oxide are significantly different from those of the molecule in a NaY zeolite.[6] The bonding with the silver ions may induce sp hybridization into the NO molecule such as that proposed for $[Fr(II)(CN)_5NO]^{3-}$.[13] A more detailed model of the complex is not warranted on the basis of the available hyperfine data.

The secluded location of the $[Ag(I)_2NO]^{2+}$ ion suggests that the NO molecule enters the sodalite unit where it bonds with two silver ions which are probably located at site I′ positions.[14] The extended exposure at higher pressures of NO maybe required for the gas molecules to diffuse into the sodalite cages. The decrease in the concentration of $[Ag(I)NO]^+$, which accompanied the formation of $[Ag(I)_2NO]^{2+}$, indicates that the former complex may have been transformed into the latter.

Acknowledgment. The authors acknowledge the support of this work by The Robert A. Welch Foundation under Grant No. A-257.

References and Notes

(1) Author to whom correspondence should be addressed.
(2) B. F. G. Johnson and J. W. McCleverty, *Progr. Inorg. Chem.*, 7, 277 (1966).
(3) S. Z. Roginskii, O. V. Al'tshuler, O. M. Vinogradova, V. A. Seleznev, and I. L. Isitovskaya, *Dokl. Akad. Nauk USSR*, **196**, 872 (1972).
(4) C. Chao and J. H. Lunsford, *J. Phys. Chem.*, **76**, 1546 (1972).
(5) C. Chao and J. H. Lunsford, *J. Amer. Chem. Soc.*, **93**, 6794 (1971).
(6) J. H. Lunsford, *J. Phys. Chem.*, **72**, 4163 (1968).
(7) K. Nakamoto, "Infrared Spectra of Inorganic and Coordination Compounds," 2nd ed., Interscience, New York, N. Y., 1970.
(8) R. S. Eachus and M. C. R. Symons, *J. Chem. Soc. A*, 1329 (1970).
(9) B. L. Bales and L. Kevan, *J. Chem. Phys.*, **55**, 1327 (1971).
(10) P. H. Kasai and D. McLeod, Jr., *J. Chem. Phys.*, **55**, 1566 (1971).
(11) G. Wessel and H. Lew, *Phys. Rev.*, **92**, 641 (1953).
(12) A. J. Freeman and R. E. Watson in "Magnetism," G. T. Rado and H. Sahl, Ed., Vol. IIA, Academic Press, New York, N. Y., 1965, p 167.
(13) M. B. D. Bloom, J. B. Raynor, and M. C. R. Symons, *J. Chem. Soc. A*, 3843 (1971).
(14) For a discussion of the structure and cation positions in a Y-type zeolite see J. V. Smith, *Advan. Chem. Ser.*, **No. 101**, 171 (1971).

Wetting under Chemical Equilibrium and Nonequilibrium Conditions

İlhan A. Aksay, Carl E. Hoge, and Joseph A. Pask*[1]

Inorganic Materials Research Division, Lawrence Berkeley Laboratory and Department of Materials Science and Engineering, College of Engineering, University of California, Berkeley, California 94720 *(Received October 17, 1973)*

Publication costs assisted by U. S. Atomic Energy Commission

The thermodynamics of a solid-liquid-vapor system both under chemical equilibrium and nonequilibrium conditions, based on the model of Gibbs, is discussed. Under chemical equilibrium conditions, the degree of wetting or nonwetting of a flat and nondeformable solid by the liquid is defined by Young's equation in terms of the static interfacial tensions. Under chemical nonequilibrium conditions, mass transfer across an interface results in a transient decrease in the corresponding specific interfacial free energy and the interfacial tension by an amount equal to the free energy of the effective chemical reaction per area at that interface. When the reaction is between the solid and the liquid, this transient lowering of the interfacial tension can cause the liquid drop to spread on the solid substrate if the interfacial energy reduction is large enough and also if the diffusion rates of the reacting components in the solid phase are slow enough relative to the flow rate of the liquid to cause the liquid at the periphery of the drop to be in dynamic contact with unreacted solid.

I. Introduction

The degree of wetting of a solid by a liquid in a solid-liquid-vapor system is characterized by the conditions of thermodynamic equilibrium. Young,[2] from a mechanistic approach, expressed the relationship between the horizontal components of the three interfacial tensions of such a system at the three-phase contact as

$$\gamma_{sv} - \gamma_{sl} = \gamma_{lv} \cos\theta \qquad (1)$$

where γ is the interfacial tension between solid-vapor (sv), solid-liquid (sl), and liquid-vapor (lv) phases, and θ is the contact angle measured through the liquid phase as shown in Figure 1.

The first exact treatment of the thermodynamics of a solid-liquid-vapor system is due to Gibbs[3] who derived Young's equation for the nongravitational case and outlined its derivation for a system in a gravitational field. A more rigorous treatment of the thermodynamics of a solid-liquid-vapor system, using the method of Gibbs, has more recently been provided by Johnson.[4] In both Gibbs' and Johnson's treatment of the conditions of mechanical equilibrium, the system was assumed to be at chemical equilibrium, *i.e.*, no mass transport across the interfaces. Johnson explicitly defined the conditions for mechanical equilibrium in a solid-liquid-vapor system and emphasized that Young's equation is not the only requirement for total mechanical equilibrium and that the effect of the gravitational field and of curvature on pressure also has to be considered.

In wetting studies at elevated temperatures, the phases of a solid-liquid-vapor system are not often at chemical equilibrium prior to an experiment. Under chemical nonequilibrium conditions, the effect of chemical reactions on the interfacial tensions have to be considered. It has frequently been suggested[5-13] that an interfacial reaction or diffusion of a component from one bulk phase to the other results in the lowering of the corresponding interfacial tensions. Attempts have consequently been made[6,9,12] to correlate the wetting tendency with the free energy of interfacial reactions. This suggestion has been refused by others[14] on the grounds that interfacial reactions do not necessarily correlate with changes in wetting behavior.

The objectives of this study are to expand on the thermodynamic treatment of Gibbs and Johnson in order (i) to establish the correlation between the degree of wetting and the corresponding interfacial tensions under total thermodynamic equilibrium conditions (section II) and (ii) to establish the effect of interfacial chemical reactions on the wetting mechanics under chemical nonequilibrium conditions (section III).

II. Mechanics of Wetting under Chemical Equilibrium Conditions

Let us consider a solid-liquid-vapor system as presented in Figure 1, where the effect of the gravitational field is neglected. The total differential of the free energy of this three-phase system[15,16] (at constant temperature and pressure, after neglecting the effect of curvature on the pressure and assuming that interfacial tensions are independent of orientation) is

$$dG = \sum_i \mu_i^s\, dn_i^s + \sum_i \mu_i^l\, dn_i^l + \sum_i \mu_i^v\, dn_i^v + \gamma_{sl}\, dA_{sl} + \gamma_{sv}\, dA_{sv} + \gamma_{lv}\, dA_{lv} + \sum_{\alpha,\beta}\left\{\sum_i \left(\frac{\partial G^{\alpha\beta}}{\partial n_i^{\alpha}}\right) dn_i^{\alpha} + \sum_i \left(\frac{\partial G^{\alpha\beta}}{\partial n_i^{\beta}}\right) dn_i^{\beta} + \sum_i \left(\frac{\partial G^{\alpha\beta}}{\partial n_i^{\alpha\beta}}\right) dn_i^{\alpha\beta}\right\} \qquad (2)$$

where μ_i is the chemical potential of component i in the designated phases; n_i is the total number of moles of component i in the designated phase obtained by multiplying the concentration of component i in the homogeneous region of the phase by its volume, *i.e.*, $C_i^{\alpha}V^{\alpha}$ or $C_i^{\beta}V^{\beta}$ or by multiplying the adsorption of component i at an interface by the corresponding interfacial area, *i.e.*, $\Gamma_i^{\alpha\beta}A^{\alpha\beta}$; G is the total free energy of the designated phase obtained by multiplying the free energy of a unit volume in the homogeneous region of the phases by the volume of the corresponding phase, *i.e.*, $g^{\alpha}V^{\alpha}$ or $g^{\beta}V^{\beta}$ or by multiplying the specific interfacial free energy by the corresponding interfacial area, *i.e.*, $g^{\alpha\beta}A^{\alpha\beta}$, and where the subscripts of the

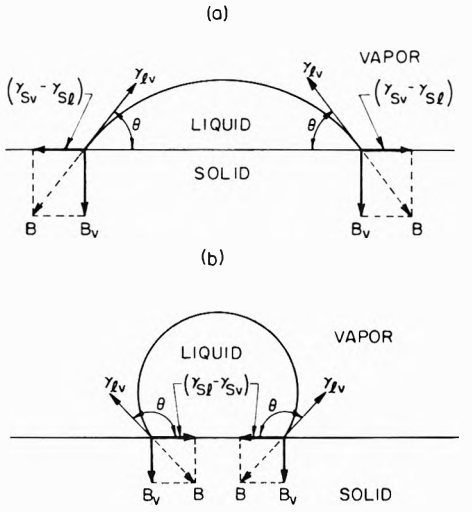

Figure 1. Equilibrium of forces on the periphery of a sessile drop of an (a) acute contact angle and (b) obtuse contact angle. B is the resultant balancing force equal and of opposite direction to γ_{lv}, and B_v is the vertical component. The liquid drops are small enough to neglect gravitational forces.

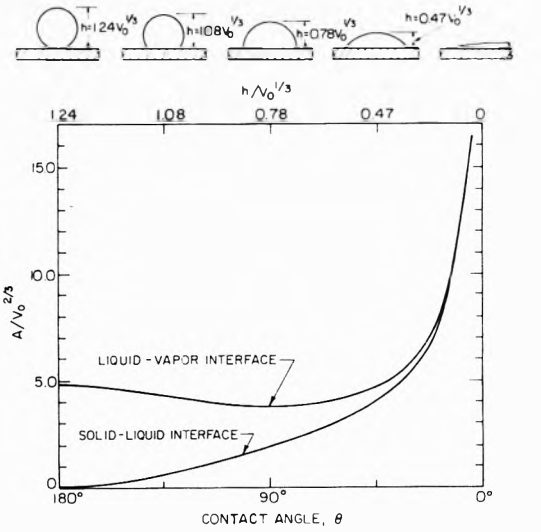

Figure 2. Variation of the solid–liquid and the liquid–vapor interfacial areas *vs.* decreasing contact angle, θ, or the height of the drop, h. V_0 is the volume of the liquid drop.

partial derivatives are omitted for brevity and the summation $\Sigma_{\alpha,\beta}$ is taken over all three interfaces.

At total thermodynamic equilibrium, $dG = 0$; then since the variations of mass are independent of the variations of area

$$\gamma_{sl}\,dA_{sl} + \gamma_{sv}\,dA_{sv} + \gamma_{lv}\,dA_{lv} = 0 \qquad (3)$$

and

$$\sum_i \mu_i^{s}\,dn_i^{s} + \sum_i \mu_i^{l}\,dn_i^{l} + \sum_i \mu_i^{v}\,dn_i^{v} + \sum_{\alpha,\beta}\left\{\sum_i \left(\frac{\partial G^{\alpha\beta}}{\partial n_i^{\alpha}}\right) dn_i^{\alpha} + \sum_i \left(\frac{\partial G^{\alpha\beta}}{\partial n_i^{\beta}}\right) dn_i^{\beta} + \sum_i \left(\frac{\partial G^{\alpha\beta}}{\partial n_i^{\alpha\beta}}\right) dn_i^{\alpha\beta}\right\} = 0 \qquad (4)$$

These two equations outline the conditions for mechanical and chemical equilibrium of the system, respectively; at chemical equilibrium eq 4 is satisfied and γ has a static value. Now, let us assume that the liquid is a small enough drop so that its equilibrium configuration in the absence of attractive forces is spherical due to negligible gravitational effects. If such a drop is placed on a flat and rigid solid surface, a solid–liquid interface will form if

$$\delta G = \delta \int_{sl} \gamma_{sl}\,dA_{sl} + \delta \int_{sv} \gamma_{sv}\,dA_{sv} + \delta \int_{lv} \gamma_{lv}\,dA_{lv} < 0 \qquad (5)$$

This free-energy decrease results in a driving force for the deformation of the liquid drop. The solid–liquid interfacial area increases, and the deformation continues until the minimum energy state is reached as defined by eq 3. Thus, for a given system, when the bulk volumes are nonreactive, the free-energy changes for the system are only associated with changes in the interfacial areas.

Several progressive geometric configurations of the drop and the change in the areas of the liquid–vapor and the solid–liquid interfaces *vs.* the contact angle, θ (or the height of the drop, h), are shown in Figure 2. It should be noted that the liquid–vapor interfacial area decreases from 180 to 90° and then increases as the contact angle decreases to 0°, whereas the solid–liquid interface increases continuously. Since $dA_{sl} = -dA_{sv}$, eq 5 becomes

$$\delta G = \delta \int_{sl} (\gamma_{sl} - \gamma_{sv})\,dA_{sl} + \delta \int_{lv} \gamma_{lv}\,dA_{lv} \qquad (6)$$

TABLE I: The Sign of the Terms in Eq 7 for Possible γ Relationships

γ relationship	First term	Second term
For contact angles of 180° → 90°		
(a) $\gamma_{sv} < \gamma_{sl} > \gamma_{lv}$	(+)	(−)
(b) $\gamma_{sv} < \gamma_{sl} < \gamma_{lv}$	(+)	(−)
(c) $\gamma_{sv} > \gamma_{sl} > \gamma_{lv}$	(−)	(−)
(d) $\gamma_{sv} > \gamma_{sl} < \gamma_{lv}$	(−)	(−)
For contact angles of 90° → 0°		
(a) $\gamma_{sv} < \gamma_{sl} > \gamma_{lv}$	(+)	(+)
(b) $\gamma_{sv} < \gamma_{sl} < \gamma_{lv}$	(+)	(+)
(c) $\gamma_{sv} > \gamma_{sl} > \gamma_{lv}$	(−)	(+)
(d) $\gamma_{sv} > \gamma_{sl} < \gamma_{lv}$	(−)	(+)

or

$$\frac{dG}{dh} = (\gamma_{sl} - \gamma_{sv})\frac{dA_{sl}}{dh} + \gamma_{lv}\frac{dA_{lv}}{dh} \qquad (7)$$

It is now possible by use of eq 7 to determine whether the contact angle will be acute or obtuse for any combination of relative interfacial tensions as shown in Table I which gives the sign of the terms of the equation. A net negative dG/dh indicates that the solid–liquid interface will continue to form and the contact angle will continue to decrease; the minimum energy configuration is obtained when dG/dh is zero which is realized when a balance is achieved between the two terms of the equation. It thus can be seen that when $\gamma_{sv} > \gamma_{sl} > \gamma_{lv}$ (case c), the contact angle is always acute; and when $\gamma_{sv} < \gamma_{sl} < \gamma_{lv}$ (case b), the contact angle is always obtuse. When $\gamma_{sv} < \gamma_{sl} > \gamma_{lv}$ (case a) and $\gamma_{sl} < \gamma_{sv} + \gamma_{lv}$, regardless of whether $\gamma_{sv} >$ or $< \gamma_{lv}$, the contact angle is obtuse; but when $\gamma_{sl} = \gamma_{sv} + \gamma_{lv}$, no interface forms and the measured contact angle is 180°. When $\gamma_{sv} > \gamma_{sl} < \gamma_{lv}$ (case d), regardless of whether $\gamma_{sv} >$ or $< \gamma_{lv}$, the contact angle is acute. When $\gamma_{sv} - \gamma_{sl} > \gamma_{lv}$, an equilibrium contact angle is not obtained since the free-energy decrease on wetting the rigid solid is greater than the increase due to the extension of the liquid surface; spreading, a dynamic condition, then continues as long as the bulk liquid is available. A reduction of the total surface energy of the

solid by the liquid ($\gamma_{sv} > \gamma_{sl}$) is defined as wetting; a condition of $\gamma_{sl} > \gamma_{sv}$ is defined as nonwetting of the solid. Then, $\gamma_{sv} - \gamma_{sl}$ can be considered as the driving force for wetting.

The formation of a solid-liquid interface due to the wetting of the solid results in forces acting on the liquid drop that, because of the rigid nature of the solid, result in resisting forces generated by the liquid because of the imposed deformation of the liquid drop whose minimum energy state is a spherical shape. From the viewpoint of mechanics, there must be a balance of forces acting on the liquid drop at its periphery, as shown in Figure 1. If an unbalance of these forces occurs, due to unequal chemical conditions around the periphery of the drop, the drop will move, as has been observed.[17] Likewise, there must be a balance of all the forces acting at any point; a balance of the horizontal forces at the "triple point" (solid, liquid, and vapor in equilibrium) provides the familiar Young's equation directly from mechanics (eq 1). A balance of the vertical forces acting at the triple point also occurs: the magnitude of the attractive forces exerted by the solid, B_v, is determined[18] by the vertical component of the surface tension of the liquid at the triple point, which does not exceed the bonding force at the interface and normally does not distort the solid. The resultant of the horizontal and vertical forces exerted by the solid becomes a balancing force, B, equal and opposite to the surface tension force of the liquid at the triple point (Figure 1).

The formation of a solid-liquid interface due to minimum energy requirements but with no wetting of the solid becomes possible because of a reduction of the surface energy, $\int \gamma_{lv}\, dA$, of the liquid in contact with the solid ($\gamma_{sv} < \gamma_{sl} < \gamma_{lv}$). Again, there is a balancing force equal and opposite to the surface tension of the liquid, which is the resultant of the vertical attractive force (equal and opposite to the vertical component of γ_{lv}) and the force developed due to $\gamma_{sl} - \gamma_{sv}$, as seen in Figure 1b.

It is now worthwhile to consider the boundary conditions which are not indicated by the mathematical analysis just employed. Under chemical equilibrium conditions, the formation of a true interface can be considered to be analogous to the formation of a solution and corresponds to an adjustment of surface structures to form some intermediate interfacial structure whose interfacial tension (γ_{sl}) then is between γ_{sv} and γ_{lv} (cases b and c). The actual magnitude of γ_{sl}, however, is dependent upon the degree of chemical bonding or minimization of structural discontinuity across the interface developed in the system; γ_{sl} thus becomes smaller with increasing chemical bonding at the interface. For $\gamma_{lv} > \gamma_{sv}$, then, γ_{sl} approaches γ_{sv} with the development of chemical bonding, resulting in a limiting contact angle of 90°. For $\gamma_{sv} > \gamma_{lv}$, γ_{sl} approaches γ_{lv}; experimental evidence,[17,19] however, suggests that the maximum reduction of γ_{sv} by the liquid is by an amount equal to γ_{lv} resulting in a limiting nominal zero contact angle as long as $\gamma_{sv} - \gamma_{lv} \geq \gamma_{lv}$, as can be seen from eq 1.

If γ_{sl} is greater than both γ_{sv} and γ_{lv} (case a), a true interface actually has not formed. It is visualized that the two surfaces are actually attracted to reduce the total interfacial energy but that they have not lost their individual identity; the contact angle approaches 180° with decreasing attraction. If γ_{sl} is less than both γ_{sv} and γ_{lv} (case d), a transient condition involving chemical reactions exists (section III).

III. Mechanics of Wetting under Chemical Nonequilibrium Conditions

The conditions of chemical equilibrium at constant temperature and pressure are given by eq 4. When the conditions of eq 4 are not satisfied throughout the system, the phases of the solid-liquid-vapor system will react with each other through the interfaces to achieve a state of chemical equilibrium. During these nonequilibrium dynamic conditions, the interfacial tensions and thus the contact angle will be continuously changing until the system reaches a state of chemical equilibrium. Volume changes occurring during the reactions, if significant, will affect the physical configuration of the system.

Transfer of mass across the interfaces can be regarded as absorption from one phase to the other in the interfacial region. This process is more critical than adsorption (no mass transfer across the interfaces when the bulk phases are at equilibrium) since the degree of compositional and corresponding volume changes both in the bulk phases and the interphase could be substantially higher than the changes observed during adsorption. Volume changes of the condensed phases during adsorption can normally be neglected.

Mass transfer across the interfaces must result in a net decrease of the free energy of the system at any time, for the reaction, otherwise, will not proceed. At the first instant of formation of an interface, however, only the interfacial region is involved in the chemical reaction, and thus the corresponding initial decrease in the free energy of the system is totally attributed to the decrease in the free energy of the interfacial region. The magnitude of the decrease in the specific interfacial free energy, $(-)\Delta g^{\alpha\beta}$, then is directly equal to $(-\Delta G^{\alpha\beta}/A)$. The corresponding interfacial tension is similarly reduced by an amount equal to $(-)\Delta g^{\alpha\beta}$ since[15]

$$\gamma_{\alpha\beta} = g^{\alpha\beta} - \sum_i \mu_i^{\alpha\beta} \Gamma_i \qquad (8)$$

as schematically shown in Figure 3. If it is assumed that the free energy of the reaction between the phases in the interfacial region is comparable but not necessarily equal to that between the bulk phases, the value of $(-\Delta G^{\alpha\beta}/A)$ could be substantially high, and for an approximate interfacial region thickness of 20 Å, a decrease of as much as 1000 erg/cm^2 (see Appendix A) could be realized in the magnitude of the specific interfacial energy and thus the interfacial tension. Experimentally, negative interfacial tensions are often measured during such chemical reactions that result in spontaneous spreading[5-9,12,20] or emulsification phenomena.[13]

Under chemical equilibrium conditions, however, specific interfacial free energies and static interfacial tensions are always positive since the bulk phases are more stable than the interfaces. Thus, after the completion of the reaction at the interface followed by its continuation into the bulk regions by diffusion, the incremental contributions of the $\Sigma_i(\partial G^{\alpha\beta}/\partial n_i^{\alpha})\, dn_i^{\alpha}$ and $\Sigma_i(\partial G^{\alpha\beta}/\partial n_i^{\beta})\, dn_i^{\beta}$ terms in eq 2 must be such that $\gamma_{\alpha\beta}$ increases toward a static interfacial tension value. With time, the contributions of these terms will decrease and become minimal because of the decrease in the chemical potential or composition gradient from the interface into the bulk phases. Therefore, after the initial decrease, $\gamma_{\alpha\beta}$ increases and gradually approaches the static interfacial tension of the reacted bulk phases (Figure 3). In comparison, Figure 3 also

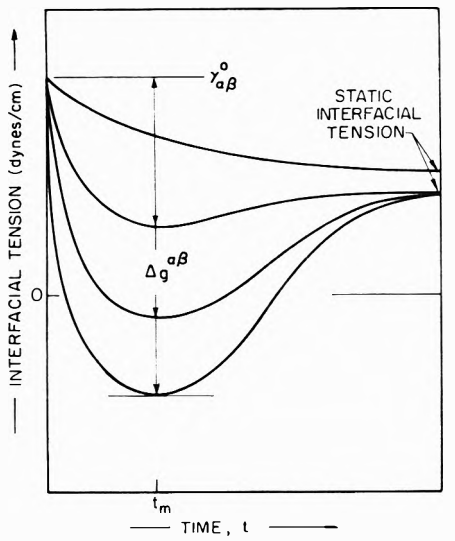

Figure 3. Variation of dynamic interfacial tension with time during a chemical reaction between two phases. The initial or pure dynamic interfacial tension is indicated by $\gamma_{\alpha\beta}{}^{0}$. The degree of minimization of the interfacial tension at t_m is proportional to $\Delta g^{\alpha\beta}$ (see Appendix A). In case of a pure adsorption process, no transient minimum is observed (top curve).

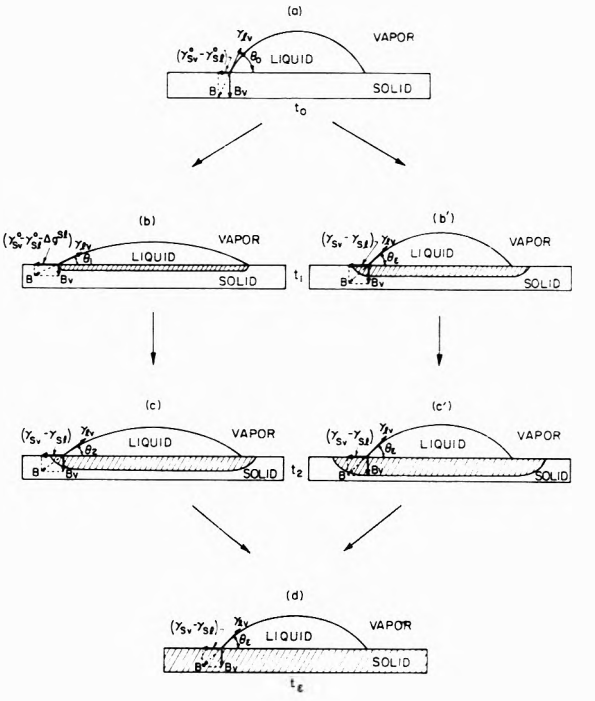

Figure 4. Schematic representation of the various dynamic stages of a sessile drop when the initial solid is not saturated with some or all of the components of the liquid. The path abcd corresponds to the case where the growth rate of the reaction product is slower than the flow rate of the liquid drop; and path ab'c'd corresponds to the case where the growth rate of the reaction product is faster than the flow rate of the liquid drop.

shows the variation of the interfacial tension with time for a pure adsorption process which differs from that for a mass transfer across the interface since a transient minimization of the interfacial tension is not realized with adsorption.

Let us now consider the specific effects of several types of reactions on the solid-liquid-vapor system of Figure 1, assuming that chemical equilibrium exists between the vapor and the condensed phases but not between the solid and the liquid. The reactions to be considered are those that result because (i) only the solid is not saturated with some or all of the components of the liquid, (ii) only the liquid is not saturated with some or all of the components of the solid, (iii) both phases are unsaturated with respect to the other, and (iv) a compound forms at the interface.

Several dynamic stages associated with the first type of reaction are shown schematically in Figure 4. At the time t_0, Figure 4a illustrates the instantaneous quasichemical equilibrium involving no interfacial reaction between the liquid and the solid. Young's equation (eq 1) may then be expressed only in terms of the initial dynamic surface tensions. Now, as the solid solution reaction proceeds at the interface, the dynamic specific interfacial free energy, $g^{0,sl}$, will change by an amount Δg^{sl} due to the free energy of the reaction; a corresponding change in $\gamma_{sl} = \gamma_{sl}{}^{0} + \Delta g^{sl}$ with time occurs, as shown in Figure 3. When the diffusion rates of the reacting components and thus the growth rate of the reaction product are slow enough relative to the flow rate of the liquid drop (see Appendix B), the liquid at the periphery of the drop will remain in contact with unreacted solid that has an unaltered $\gamma_{sv}{}^{0}$ as long as ΔA_{sl} is positive; the driving force for wetting $\gamma_{sv}{}^{0} - (\gamma_{sl}{}^{0} + \Delta g^{sl})$ which is increased by the amount $(-)\Delta g^{sl}$ remains constant. If the maximum driving force at t_m (Figure 3) exceeds γ_{lv}, then spreading occurs;[20] and if the force does not exceed γ_{lv}, the contact angle continues to decrease until a transient mechanical equilibrium is reached as represented by t_1 in Figure 4b. At this point, however, diffusion in the solid continues as shown schematically in Figure 4c; $\gamma_{sv}{}^{0}$ ahead of the liquid periphery then is also decreased by an amount $\approx (-)\Delta g^{sl}$.[21] The driving force for wetting therefore decreases, and the contact angle increases to a new value of θ_ℓ corresponding to the one for mechanical and chemical equilibria for the system (Figure 4d). During this pull-back stage, the drop may break into isolated smaller drops if the thickness of the original drop decreases considerably during the transient spreading stage.[20]

On the other hand, when the diffusion rates of the reacting components in the solid are fast relative to the flow rate of the liquid drop (see Appendix B), both $\gamma_{sv}{}^{0}$ and $\gamma_{sl}{}^{0}$ will simultaneously decrease by an amount $(-)\Delta g^{sl}$, and the liquid at the periphery of the drop will remain in contact with reacted solid, as represented schematically in Figure 4b'. The driving force for wetting in this case does not change drastically from that due to the initial dynamic surface tensions (Figure 4a) and remains essentially constant while the system moves to chemical equilibrium (Figures 4b', 4c', and 4d).

Throughout these entire sequences, and in Figure 4, the amount of material dissolved by the solid was considered to be small enough to be neglected so that the solid surface remained flat. However, if the specific volume of the solid solution phase at the interface differs appreciably from that of the unreacted solid, analysis by use of Young's equation as applied to experimentally measured contact angles could be misinterpreted because of the resulting nonexistence of a flat solid surface.

Several dynamic stages associated with a reaction of type ii, where only the liquid is not saturated with the solid, are shown schematically in Figure 5. Figure 5a shows the configuration at t_0 when the liquid phase first comes into contact with the solid and Young's equation may be used to express the conditions for mechanical

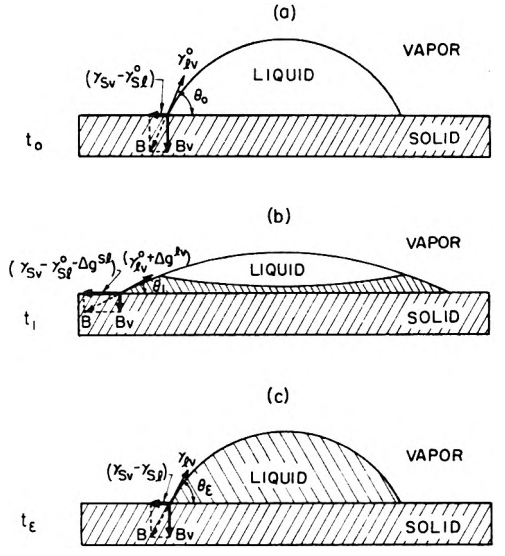

Figure 5. Schematic representation of the dynamic stages of a sessile drop when the initial liquid is not saturated with some or all of the components of the solid.

equilibrium in terms of the dynamic interfacial tensions. After the initial reaction the composition of the liquid around the periphery and at the solid-liquid interface rapidly approaches equilibrium compositions relative to the solid; correspondingly, γ_{sl}^0 and γ_{lv}^0 decrease because of the free-energy contribution of the reaction, but then they rapidly approach their static interfacial tension values γ_{sl} and γ_{lv} (Figure 3). During the initial reaction stage, thus, an instantaneous lowering of the contact angle or spreading may be observed[20] which is immediately followed by the drop pulling back to an equilibrium contact angle θ_ϵ which is retained until the system reaches equilibrium (Figures 5b and 5c). With high-viscosity liquids and fast diffusion rates, however, the initial spreading may not be realized because the static interfacial tensions are attained faster than the liquid can spread. Again, as in the previous case, the amount of solid dissolved by the liquid was considered to be small enough to be neglected. In actual fact, however, as the reaction proceeds, the solid-liquid interface will drop below the solid-vapor surface,[22] complicating the analysis of mechanical equilibrium.

The same sequences would occur in the case of a sessile drop with an obtuse contact angle, $\gamma_{sl}^0 > \gamma_{sv}^0$, experiencing reactions. If the Δg^{sl} contribution is large enough to reduce γ_{sl} to a value smaller than γ_{sv}, an initial acute angle will form; and if Δg^{sl} is large enough to increase $\gamma_{sv}^0 - \gamma_{sl}^0 - \Delta g^{sl}$ to a value larger than γ_{lv}, initial spreading will occur.

A type iii reaction is expected to be similar in behavior either to type i or ii reaction depending on whether an increase or decrease of volume of the solid occurs at the interface, but the kinetic analysis of the reaction and determination of the nature of the physical configuration become more complicated. The formation of a compound at the interface (type iv reaction) is also expected to cause the mechanical behavior of the system to be similar to that for one with type i reaction. The analysis in this case could be even more complicated, particularly if the compound should isolate the liquid from direct contact with the reacting solid.

IV. Conclusions

The conditions of thermodynamic equilibrium, *i.e.*, the minimization of the free energy, of a solid-liquid-vapor system define the degree of wetting of the solid by the liquid phase. When chemical equilibrium exists throughout the system, the free-energy changes for the system are associated only with changes in the interfacial areas. The equilibrium contact angle of a liquid drop on a flat and rigid solid surface, then, is determined by Young's equation in terms of the static interfacial tension values. The relative magnitudes of the interfacial tensions indicate whether the contact angle will be acute or obtuse: (i) when $\gamma_{sv} > \gamma_{sl} <$ or $> \gamma_{lv}$, the contact angle is always acute (the condition of wetting of the solid), and (ii) when $\gamma_{sv} < \gamma_{sl} <$ or $> \gamma_{lv}$, the contact angle is always obtuse (the condition of nonwetting of the solid). Experimental observations, however, indicate that, under chemical equilibrium conditions, γ_{sl} is always in between γ_{sv} and γ_{lv}. With increasing degree of chemical bonding at the interface, γ_{sl} approaches the lower value of the two, γ_{sv} or γ_{lv}.

Under chemical nonequilibrium conditions, the free-energy changes for the system are associated not only with changes in the interfacial areas but also with changes in mass. Mass transfer across an interface initially results in a decrease in the corresponding specific interfacial free energy and the interfacial tension by an amount equal to the magnitude of $(-\Delta G/A)$ for the effective chemical reaction at the interface. However, after the completion of the reaction at the interface followed by its continuation into the bulk regions by diffusion, the specific interfacial free energy and the interfacial tension gradually increase toward their static values. When the reaction is between the solid and the liquid, this transient lowering of the interfacial tension can cause the liquid drop to spread on the solid substrate if the interfacial tension reduction is large enough and if the diffusion rates of the reacting components, and thus the growth rate of the reaction product, are slow enough relative to the flow rate of the liquid.

Acknowledgments. Discussions with Leo Brewer and David J. Meschi are gratefully acknowledged.

This work was supported by the United States Atomic Energy Commission.

Appendix A. Effective Free Energy of Reaction at an Interface

Consider a solid-liquid-vapor system[20] where an interfacial reaction

$$MgO(s) + R_2O_3(\text{in liquid}) \rightarrow MgR_2O_4(\text{in MgO}) \quad (A1)$$

takes place at the solid (MgO)-liquid interface that results in the formation of an MgO solid solution with MgR_2O_4, where R_2O_3 denotes a sesquioxide Al_2O_3, Cr_2O_3, or Fe_2O_3. At 1673 K, an average value for the standard free energy of this reaction,[23] $\Delta G°$, is −8000 cal/mol. The free energy of the reaction (A1), then, is

$$\Delta G = RT \ln \frac{a(MgR_2O_4)}{a(R_2O_3)} - 8000 \quad (A2)$$

where R is the gas constant. Assuming that Raoult's law is applicable, $a(MgR_2O_4)$ is equal to the concentration of MgR_2O_4 in the MgR_2O_4 solid solution at equilibrium with the MgO solid solution. A typical value[20] for $a(MgR_2O_4)$

is ≈0.9. Similarly, $a(R_2O_3)$ depends on the concentration of R_2O_3 in the liquid phase. Assuming a value of 0.5 for $a(R_2O_3)$, $\Delta G = -6050$ cal/mol. The effective contribution of this reaction at the solid–liquid interface depends on the volume of the effective interfacial region and the extent of the solid solution in MgO. Consider a liquid drop of 0.5 cm in diameter on an MgO substrate. Assume the effective thickness of the interfacial region at the solid–liquid interface to be ≈20 Å. The volume of this interfacial disk is 3.94×10^{-8} cm^3. The number of moles of MgR_2O_4 going into solution in MgO in this volume depends on the extent of the solubility of MgR_2O_4 in MgO. The density and the molecular weight of this solid solution can be estimated assuming that the molar volumes of the pure components are equal to the partial molal volumes and thus the molar volumes of the pure components are additive. The molecular weight of an MgO solid solution with 50 mol % $MgFe_2O_4$, then, is 120.16 g. Similarly, the density, ρ, of this solid solution is 4.04 g/cm^3 based on the $\rho(MgO) = 3.58$ and $\rho(MgFe_2O_4) \cong 4.5$ g/cm^3 values.[24] Therefore, the number of moles of the MgO ($MgFe_2O_4$) solid solution forming in the interfacial volume is 1.32×10^{-9}, and thus the number of moles of $MgFe_2O_4$ going into solution is 6.6×10^{-10}. The ΔG of the interfacial reaction becomes -4×10^{-6} cal or -167 erg; and in terms of unit area, $\Delta g^{sl} = -850$ erg/cm^2.

In case of the formation of the compound MgR_2O_4 at the interface, Δg^{sl} is higher due to the higher number of moles of MgR_2O_4 forming in the interfacial region. The number of moles of $MgFe_2O_4$ solid solution forming in the same interfacial region is then 8.86×10^{-10}, and Δg^{sl} becomes -1140 erg/cm^2.

Appendix B. Kinetics of Spreading

The kinetics of spreading of a spherical liquid droplet on a flat and rigid solid surface has been discussed by Yin[25] based on the assumption that spreading is impelled by the horizontal components of the surface tensions at the three-phase boundary and retarded by the viscous flow of the droplet. Yin showed that the instantaneous rate of spreading, in terms of area per unit time, is

$$dA/dt = K(S_0 I_1 + \gamma_{lv} I_2) \tag{B1}$$

with

$$K = \left(\frac{4\pi}{\eta}\right)\left(\frac{3V_0}{\pi}\right)^{1/3} \tag{B2}$$

where η is the viscosity of the liquid (Poise), V_0 is the volume of the droplet (cm^3), $S_0 = \gamma_{sv} - \gamma_{sl} - \gamma_{lv}$ is the spreading coefficient, and I_1 and I_2 are definite integrals as functions of the instantaneous contact angle only. For the system shown in Figure 4, when an original instantaneous contact angle of 50° is assumed $I_1 = 0.5$ and $I_2 = 0.05$.[25] Furthermore, when values of $V_0 = 0.03$ cm^3, $\gamma_{lv} = 500$, $\gamma_{sv} = 1000$, $\gamma_{sl} \cong 0$ dyn/cm (chemical reaction case), are assumed, $S_0 = 500$ dyn/cm, and

$$\frac{dA}{dt} = \frac{107}{\eta}(\text{cm}^2/\text{sec}) \text{ or } \frac{dr}{dt} = \frac{51.2}{\eta}(\text{cm/sec}) \tag{B3}$$

Now, let us consider the spreading of an R_2O_3 containing silicate liquid on an MgO substrate which is unsaturated with respect to MgR_2O_4. When R_2O_3 diffuses into MgO, in order for the reaction product to grow ahead of the liquid periphery, *i.e.*, into the solid–vapor interface, the flow rate of the drop has to be slower than the growth rate of the diffusion product. The concentration, C, of a component diffusing rapidly in the surface region of a substrate, from a stationary cylindrical source, is[26]

$$C(r,t) = \frac{C_0 r_0}{r(D_s t)^{1/2}} \operatorname{erfc}\left\{\frac{r - r_0}{(D_s t)^{1/2}}\right\} \tag{B4}$$

where C_0 is the concentration of the diffusing component in the surface region of the substrate beneath the circular source, r_0 is the radius of the source, D_s is the surface diffusion coefficient, and erfc is the complementary error function. For an instantaneous contact angle of 50° and $V_0 = 0.03$ cm^3, $r_0 = 0.33$ cm. Taking $D_s = 10^{-6}$ cm^2/sec,[27] the concentration front of $C/C_0 = 0.9$ at $t = 1.0$ sec is at $r = 0.332$, and $\Delta r = 2.35 \times 10^{-3}$ cm. In order for the liquid to spread faster than the diffusion product can grow, a liquid viscosity of $< 2.56 \times 10^4$ P is required (eq B3). Thus, when dealing with high-viscosity liquids (silicates), lowering of the contact angle or spreading may not necessarily be observed during an interfacial reaction.

References and Notes

(1) Author to whom correspondence should be addressed.
(2) T. Young, *Phil. Trans. Roy. Soc. London*, **95**, 65 (1805).
(3) J. W. Gibbs, *Trans. Conn. Acad.*, **3**, 343 (1878); also included in "Scientific Papers of J. W. Gibbs," Vol. 1, Dover Publications, New York, N. Y., 1961, p 314.
(4) R. E. Johnson, Jr., *J. Phys. Chem.*, **63**, 1655 (1959).
(5) A. A. Leont'eva, *Kolloid. Zh.*, **11**, 176 (1949).
(6) M. Humenik, Jr., and W. D. Kingery, *J. Amer. Ceram. Soc.*, **37**, 18 (1954).
(7) P. Kozakevitch, G. Urbain, and M. Sage, *Rev. Met.*, **52**, 161 (1955).
(8) S. I. Popel, O. A. Esin, G. F. Konovalov, and N. S. Smirnov, *Dokl. Akad. Nauk SSSR*, **112**, 104 (1957), or *Proc. Acad. Sci. USSR, Phys. Chem.*, **112**, 27 (1957).
(9) W. M. Armstrong, A. C. D. Chaklader, and M. L. A. DeCleene, *J. Amer. Ceram. Soc.*, **45**, 407 (1962); W. M. Armstrong, A. C. D. Chaklader, and D. J. Rose, *Trans. AIME*, **227**, 1109 (1963); and A. C. D. Chaklader, A. M. Armstrong, and S. K. Misra, *J. Amer. Ceram. Soc.*, **51**, 630 (1968).
(10) A. A. Zhukhovitskii, V. A. Grigorian, and E. Mikhalik, *Dokl. Akad. Nauk SSSR*, **155**, 392 (1964), or *Proc. Acad. Sci. USSR, Phys. Chem.*, **155**, 255 (1964).
(11) J. E. McDonald and J. G. Eberhart, *Trans. AIME*, **233**, 512 (1965).
(12) V. I. Kostikov and B. S. Mitin, *Sb. Mosk. Inst. Stali Splavov*, **No. 49**, 114 (1968).
(13) The phenomenon of spontaneous emulsification is also often explained as a consequence of diffusion of a component from one bulk phase to the other or lowering of the interfacial tension between the bulk phases. A review of this topic is provided by J. T. Davies and E. K. Rideal, "Interfacial Phenomena," 2nd ed, Academic Press, New York, N. Y., 1963, p 360.
(14) D. A. Mortimer and M. Nicholas, *J. Mater. Sci.*, **5**, 149 (1970).
(15) R. Defay, I. Prigogine, A. Bellemans, and D. H. Everett, "Surface Tension and Adsorption," Wiley, New York, N. Y., 1966.
(16) D. A. Netzel, G. Hoch, and T. I. Marx, *J. Colloid Sci.*, **19**, 774 (1964).
(17) R. W. Cline, R. M. Fulrath, and J. A. Pask, *J. Amer. Ceram. Soc.*, **44**, 423 (1961).
(18) G. R. Lester, *J. Colloid Sci.*, **16**, 315 (1961).
(19) J. A. Pask, "Modern Aspects of the Vitreous State," Vol. 3, J. D. MacKenzie, Ed., Butterworths, Washington, D. C., 1964, p 1.
(20) I. A. Aksay, A. P. Raju, and J. A. Pask, *J. Amer. Ceram. Soc.*, submitted for publication.
(21) The free energy change at the solid–vapor interface is designated as Δg^{sl} instead of Δg^{sv} since, assuming that the composition of the liquid at the interface remains essentially constant, compositional variations are only in the solid due to components diffusing from the liquid and thus the nature of the reactions at the solid–vapor and the solid–liquid interfaces do not differ appreciably.
(22) R. D. Carnahan, T. L. Johnston, and C. H. Li, *J. Amer. Ceram. Soc.*, **41**, 343 (1958); J. A. Champion, B. J. Keene, and J. M. Sillwood, *J. Mater. Sci.*, **4**, 39 (1969).
(23) A. Navrotsky and O. J. Kleppa, *J. Inorg. Nucl. Chem.*, **30**, 479 (1968).
(24) R. C. Weast, Ed., "Handbook of Chemistry and Physics," 53 ed, The Chemical Rubber Publishing Co., Cleveland, Ohio, 1973.
(25) T. P. Yin, *J. Phys. Chem.*, **73**, 2413 (1969).
(26) J. B. Drew and J. J. Pye, *Trans. AIME*, **227**, 99 (1963); J. C. Jaeger, *J. Math. Phys.*, **34**, 316 (1956).
(27) W. M. Robertson, *J. Nucl. Mater.*, **30**, 36 (1969).

Ion–Molecule Reactions in Disilane[1]

T. M. H. Cheng, T-Y. Yu, and F. W. Lampe*

Davey Laboratory, Department of Chemistry, The Pennsylvania State University, University Park, Pennsylvania 16802
(Received September 24, 1973; Revised Manuscript Received March 11, 1974)

Publication costs assisted by the U. S. Atomic Energy Commission

The ion–molecule reactions occurring in ionized disilane have been studied by tandem and high-pressure mass spectrometry. All primary ions react with the parent molecule. Phenomenological cross sections and rate constants have been measured for reactant ion energies of 2 eV in the laboratory system. The chemical conversion initiated by ionization of disilane is shown by high-pressure mass spectrometry to be a polymerization to higher silicon hydrides that is carried mainly by $Si_nH_{2n-2}^+$, $Si_nH_{2n}^+$, $Si_nH_{2n+1}^+$, and $Si_nH_{2n+3}^+$ ions. A number of endothermic reactions have been detected and in some cases threshold energies of these processes have been determined.

Introduction

The reactions of low-energy ions with molecules play a centrally important role in radiation chemistry,[2,3] flames,[4] and electric discharges.[5] In accord with this importance numerous studies of the elementary ion–molecule occurring in ionized paraffin hydrocarbons have appeared in the literature[6] with methane, ethane, and propane being particularly well studied. Ion–molecule reactions in the structurally similar silanes have, however, received relatively little attention, studies in monosilane[7-10] and its admixtures with methane,[11-14] acetylene,[15] ethylene,[16] and benzene,[17] being apparently the only such work reported.

As part of a general program involving the effects of ionizing radiation on volatile silicon compounds, we have identified and studied the ion–molecule reactions occurring in disilane when this molecule is subjected to electron impact ionization and dissociation. This paper is a report of our results.

Experimental Section

Reaction identification and measurement of reaction cross sections and rate constants were carried out in a tandem mass spectrometer which permits the injection of mass-selected reactant ions, having kinetic energies variable down to about 1 eV, into a collision chamber containing the neutral reactant molecule. The apparatus, which has been described previously,[9] consists of two quadrupole mass filters separated by the collision chamber and ion lenses. In all experiments the mass filters were mounted in the "in-line" configuration. The energy spread of the reactant ion beam entering the collision chamber was about 1 eV, as indicated by retarding field measurements.

Relative reaction cross sections were determined as a function of kinetic energy for ion energies in the range 1.5–6.0 eV in the laboratory system. As described previously,[14-17] the shapes of the cross section *vs.* energy curves were used to differentiate between exothermic and endothermic reactions; the cross sections of endothermic reactions rise from zero at the energy threshold to a maximum several eV above threshold, while cross sections for exothermic processes decrease for all values of kinetic energy.

Phenomenological rate constants were determined at 2-eV ion energy (laboratory) by direct comparison of the relative reaction cross sections with that for (1), *viz.*

$$SiH_2^+ + SiH_4 \longrightarrow SiH_3^+ + SiH_3 \qquad (1)$$

The specific reaction rate of (1) has been determined previously[9] as $2.5 \pm 0.3 \times 10^{-10}$ cm^3/sec. The collision chamber pressure was measured with a capacitance monometer and was maintained at 1×10^{-3} Torr, a pressure sufficiently low to preclude the observation of third-order processes. Ionization chamber pressures of the order of $1\text{–}3 \times 10^{-3}$ Torr and an ionizing energy of 100 eV were employed.

Measurements of the dependence of ionic abundances in ionized disilane on ion-source pressure up to about 0.2 Torr were carried out in a Nuclide Associates 12-90G sector-field mass spectrometer. The energy of the ionizing beam was 100 eV, the trap current was very small and not measured, and the ion-accelerating voltage was 2500 V. In all experiments the repeller field was 6.25 V/cm leading to an ion-exit energy of 2.1 eV. The temperature of the ion source was 70°.

Ion-source pressures in the Nuclide mass spectrometer were monitored by a McLeod gauge that was connected *via* $\frac{5}{16}$-in. diameter tubing to the ion source. The fact that the McLeod gauge readings for disilane in the ion source were only about one-half of those for monosilane,[9] for equal pressures in the gas handling system, indicated that the McLeod gauge readings were not an absolute measure of the disilane pressure. van der Waals constants derived from the critical constants for disilane[18] indicate that deviations from ideal gas behavior cannot be the reason for the disparity between the absolute pressure and the McLeod gauge reading. While the detailed chemistry is not clear we must conclude that a chemical interaction of the disilane with the walls of the McLeod gauge and/or the mercury is occurring. Comparison of the decay curves of Si^+, SiH^+, SiH_2^+, and SiH_3^+ in disilane with the *total* rate constants for reaction of these ions with disilane, as determined by the tandem mass spectrometer, indicated that the McLeod gauge readings were lower than the actual ion-source pressures by a factor of 2.2 ± 0.2. While the collision energies in the tandem experiments and single-source experiments are not the same (2 eV and 0.7, respectively), this difference is much more likely to be re-

TABLE I: Reaction Products and Relative Cross Sections[a] of 2-eV Monosiliconium Ions with Disilane

Reactant ion	Relative cross section for formation of ion											
	Si_3H^+	$Si_3H_2^+$	$Si_3H_3^+$	$Si_3H_4^+$	$Si_3H_5^+$	Si_3H^+	$Si_2H_2^+$	$Si_2H_3^+$	$Si_2H_4^+$	$Si_2H_5^+$	$Si_2H_6^+$	$Si_2H_7^+$
Si^+		3.02	0.19		0.10		0.12		0.929			
SiH^+	0.42	0.24	1.28		0.27	0.05		0.705		1.48		
SiH_2^+		0.56		1.22	1.42				0.33		0.960	0.960
SiH_3^+			0.06		2.12					0.02		1.44

[a] Reaction cross sections are relative to that for the reaction $SiH_2^+ + SiH_4 \rightarrow SiH_3^+ + SiH_3$. At 2 eV the cross section for this reaction is $1.0 \pm 0.1 \times 10^{-16}$ cm^2.

flected in the product distribution for a given reactant ion than in the *total* rate constant for depletion of the reactant ion.

Disilane was prepared by the reduction of hexachlorodisilane (Peninsular Chemical Co.) with lithium aluminum hydride (Alfa Inorganics) using bis[2-(2-methoxyethoxy)-ethyl] ether as solvent.[19] Monosilane, purchased from the J. T. Baker Chemical Co., was subjected to several freeze-pump-thaw cycles before storage in a bulb on the vacuum line. The mass spectra of both gases indicated satisfactory purity.

Results and Discussion

1. Tandem Mass Spectrometric Studies. All primary ions in the mass spectrum of disilane are of significant intensity[19] and therefore a complete investigation of the ion–molecule reactions occurring in ionized disilane requires a study of the reactions of SiH_x^+ (x = 0,1,2,3) and $Si_2H_y^+$ (y = 0,1,2,3,4,5,6) with the disilane molecule.

Table I shows the ionic products of the reactions of 2-eV (lab) monosiliconium ions with disilane in terms of the reaction cross-sections relative to the cross section of (1) at the same laboratory energy. For convenience, the monosiliconium ions were produced in the ion source of the tandem mass spectrometer by electron impact on monosilane. In Tables II and III we show (similarly for 2-eV primary ions) the relative cross sections for the formation of tri- and tetrasiliconium ions by the reaction of disiliconium ions with disilane. We were unable to measure any H^- or H_2^- transfer reactions from disilane to the disiliconium ions because of the great disparity in intensity of the primary and secondary ion beams and the proximity of the masses for such reactions. The data in Tables I–III have been corrected for the isotope contributions from the beam and from the target gas using the values ^{28}Si(92.2%), ^{29}Si(4.7%), and ^{30}Si(3.1%).

As mentioned previously, the energy dependence of the relative cross sections for ionic product formation was used to determine whether the reaction forming that product was exothermic or endothermic. Typical such relationships are shown in Figure 1, from which we conclude that $Si_3H_5^+$ is formed in an exothermic reaction between $Si_2H_3^+$ and Si_2H_6 while Si_3H^+ is produced by an endothermic reaction involving the same two reactants. Also from Figure 1, we see that $Si_3H_7^+$ is formed in an exothermic reaction of SiH_3^+ with Si_2H_6, but that $Si_3H_5^+$ and $Si_3H_3^+$ are formed by endothermic reactions of the same two reactants.

The reactions found to be exothermic, on the basis of the energy dependence of cross section, are shown in Table IV. Also shown in Table IV are the enthalpy changes of the reactions forming disiliconium ion products, calculated from available thermochemical data;[19,20] in these cases, namely (2), (4), (5), (8)–(10), (14) in Table IV, the neutral products (and therefore the reactions) cannot be other than as written or else the reactions would be endothermic, in contradiction to the dependence of the cross section on kinetic energy. For those reactions forming tri- and tetrasiliconium ion products enthalpy changes could not be calculated, since standard enthalpies of formation are not available for these ionic products. In these cases, the neutral products are written such as to give the maximum exothermicity; the fact that the reactions are exothermic then permits assignment of upper limits to the standard enthalpies of formation of the tri- and tetrasiliconium ions. These thermochemical results are presented in a subsequent section.

Phenomenological rate constants of the exothermic reactions are also shown in Table IV. These values were obtained by measurement of the cross sections of the reactions shown in the table relative to that of (1), and the relationship

$$k_i = k_1 \frac{\sigma_i}{\sigma_1} \frac{V_{\text{reactant ion}}}{V_{SiH_2^+}}$$

in which the σ's represent cross sections and the V's are relative velocities.

Rate constants for the total exothermic reaction of the various primary ions may be obtained by summing the individual rate constants for each reactant ion in Table IV. Calculating the polarizability of disilane from the molar polarization,[21] it may be shown that the total rate constants for reaction of Si^+, SiH^+, and SiH_3^+ are in the range 0.5–0.8 of the Langevin orbiting rate constant.[22] The total rate constants for depletion of the disiliconium ions are lower; those for Si_2^+, Si_2H^+, $Si_2H_2^+$, and $Si_2H_3^+$ lie in the range of 0.3–0.4 of the Langevin orbiting rate constants while those for $Si_2H_4^+$ and $Si_2H_5^+$ are appreciably lower, being 0.15 and 0.06, respectively, of the Langevin orbiting values. Probably the major reason for the apparent low values for the disiliconium ions is that we were unable to measure disiliconium ion products from disiliconium ion reactants; therefore the rate constants of any such reactions are not included in the total reaction of each disiliconium ion. We would expect such reactions to be predominantly H^- transfer and it is noteworthy that the differences between the measured rate constant and the Langevin value are greatest for $Si_2H_5^+$ and $Si_2H_4^+$, suggesting a high probability of occurrence of the H^- transfer reactions

$$Si_2H_4^+ + Si_2H_6 \longrightarrow Si_2H_5^+ + Si_2H_5 \quad (37)$$

and

$$Si_2H_5^+ + Si_2H_6 \longrightarrow Si_2H_6 + Si_2H_5^+ \quad (38)$$

Reactions analogous to (37) and (38) involving SiH_2^+ and SiH_3^+ ions are known to be major processes in monosilane.[7-10]

The ions observed as products of endothermic reactions of the various primary ions are shown in Table V. Product ions shown in Table V that do not appear in Tables I–III

TABLE II: Relative Cross Sections[a] for Formation of Trisiliconium Ions from Reaction of 2-eV Disiliconium Ions with Disilane

	Relative cross section[a] for formation of ion							
Reactant ion	Si_3^+	Si_3H^+	$Si_3H_2^+$	$Si_3H_3^+$	$Si_3H_4^+$	$Si_3H_5^+$	$Si_3H_6^+$	$Si_3H_7^+$
Si_2^+	0.389	0.10	0.675	0.298				
Si_2H^+		0.421	0.050	0.278	0.056			
$Si_2H_2^+$			0.052		0.620			
$Si_2H_3^+$				0.374		0.655		
$Si_2H_4^+$					0.072		0.218	0.073
$Si_2H_5^+$						0.151		0.338
$Si_2H_6^+$								

[a] Reaction cross sections are relative to that for the reaction $SiH_2^+ + SiH_4 \rightarrow SiH_3^+ + SiH_3$. At 2 eV the cross section for this reaction is $1.0 \pm 0.1 \times 10^{-15}$ cm^2.

TABLE III: Relative Cross Sections[a] for Formation of Tetrasiliconium Ions from Reaction of 2-eV Disiliconium Ions with Disilane

	Relative cross section for formation of ion								
Reactant ion	Si_3^+	Si_3H^+	$Si_3H_2^+$	$Si_3H_3^+$	$Si_3H_4^+$	$Si_3H_5^+$	$Si_3H_6^+$	$Si_3H_7^+$	$Si_3H_8^+$
Si_2^+	0.40		1.72	0.84	0.74	0.27			
Si_2H^+		0.66		1.77		0.48			
$Si_2H_2^+$					1.23	0.13	0.42		
$Si_2H_3^+$				0.29		1.70		0.13	
$Si_2H_4^+$									0.76

[a] Reaction cross sections are relative to that for the reaction $SiH_2^+ + SiH_4 \rightarrow SiH_3^+ + SiH_3$. At 2 eV the cross section for this reaction is $1.0 \pm 0.1 \times 10^{-15}$ cm^2.

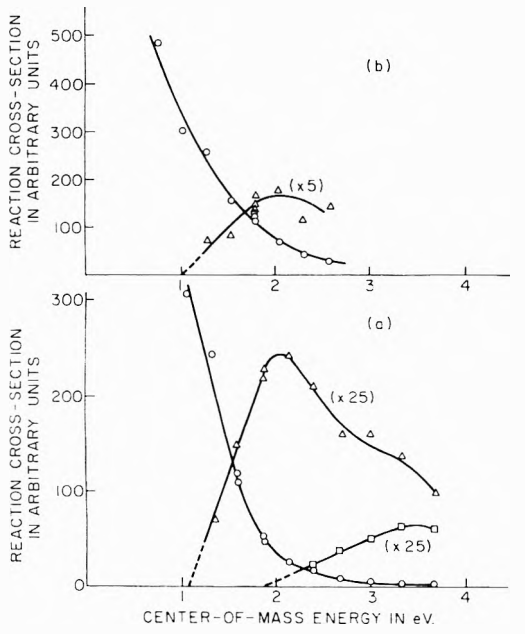

Figure 1. Dependence of reaction cross sections of center-of-mass energy: (a) $SiH_3^+ + Si_2H_6 \rightarrow Si_3H_7^+$, O; $Si_3H_5^+$, Δ; $Si_3H_3^-$, □; (b) $Si_2H_3^+ + Si_2H_6 \rightarrow Si_3H_5^+$, O; Si_3H^+, Δ.

have energetic thresholds above 2-eV laboratory energy of the reactant ion. In general, thresholds for the endothermic reactions were difficult to determine, partly because of mass interferences by isotopes of product ions from exothermic reactions. This was especially true for the tetrasiliconium ion products. However, a few reactions were free from such interference and provided sufficient intensity to measure the thresholds shown in Table V.

2. *High-Pressure Mass Spectrometry.* Single-source mass spectrometric studies of disilane are generally in accord with the tandem mass spectrometric results with regard to the relative total reaction cross sections of the primary ions and to the formation cross sections of the tri- and tetrasiliconium ions (secondary ions). What slight differences do exist in the relative cross sections for formation of the various secondary ions can be easily rationalized by the fact that the average reactant ion energy in the single-source experiments is of the order of 0.7 eV, while it is 2 eV in the tandem mass-spectrometric work.

In addition to exhibiting all of the secondary ion formation observed in the tandem mass-spectrometric experiments, the studies of the pressure dependence of ion abundance, carried out in the single instrument up to source pressures of about 0.2 Torr, showed numerous tertiary and higher order processes. In fact, as may be seen in Figures 2 and 3, the principal chemical result of ionizing disilane is a gaseous polymerization to higher silicon hydrides that is carried mainly by $Si_nH_{3n-2}^+$, $Si_nH_{2n}^+$, $Si_nH_{2n+1}^+$, and $Si_nH_{2n+3}^+$ ions. Also produced in this polymerization (Table IV) are SiH_4 and H_2.

Comparison of the semilogarithmic plots of the primary ion abundances *vs.* the ion-source pressure show that $Si_2H_6^+$ reacts with disilane in second-order processes having a total reaction rate constant of $5.8 \pm 0.7 \times 10^{-10}$ cm^3/sec. However, no tri- or tetrasiliconium ions were observed in the tandem mass-spectrometric studies when 2-eV (lab) $Si_2H_6^+$ ions impinged on disilane; we could not observe disiliconium ion products in such a reaction. One may note in Figure 3 that $Si_2H_7^+$ and $Si_3H_9^+$ are definitely formed in second-order reactions. Therefore, we conclude that in the single-source mass spectrometer $Si_2H_7^+$ and $Si_3H_9^+$ are formed by (39) and (40), respectively, *viz.*

$$Si_2H_6^+ + Si_2H_6 \longrightarrow Si_2H_7^+ + Si_2H_5 \quad (39)$$

$$Si_2H_6^+ + Si_2H_6 \longrightarrow Si_3H_9^+ + SiH_3 \quad (40)$$

We rationalize our failure to detect $Si_3H_9^+$ in the tandem mass-spectrometric experiment as being due to (39) most likely occurring *via* a direct mechanism (proton transfer and/or stripping) that is greatly favored over the probable complex process (40) at the higher energies in the tandem studies.

TABLE IV: Exothermic Ion–Molecule Reactions in Disilane

Reaction no.	Reaction	$\Delta H°$, kcal	$k \times 10^{10}$, cm³/sec
2	$Si^+ + Si_2H_6 \rightarrow Si_2H_2^+ + SiH_4$	−18	7.8 ± 0.9
3	$\rightarrow Si_3H_4^+ + H_2$	<0	2.4 ± 0.3
4	$SiH^+ + Si_2H_6 \rightarrow Si_2H^+ + SiH_4 + H_2$	−56	1.1 ± 0.1
5	$\rightarrow Si_2H_3^+ + SiH_4$	−65	3.3 ± 0.4
6	$\rightarrow Si_3H_3^+ + 2H_2$	<0	1.8 ± 0.2
7	$\rightarrow Si_3H_5^+ + H_2$	<0	3.7 ± 0.4
8	$SiH_2^+ + Si_2H_6 \rightarrow Si_2H_2^+ + SiH_4 + H_2$	−3	1.4 ± 0.2
9	$\rightarrow Si_2H_4^+ + SiH_4$	−25	3.1 ± 0.3
10	$\rightarrow Si_2H_5 + SiH_3$	−22	3.6 ± 0.4
11	$\rightarrow Si_3H_4^+ + 2H_2$	<0	0.82 ± 0.10
12	$\rightarrow Si_3H_6^+ + H_2$	<0	2.4 ± 0.3
13	$\rightarrow Si_3H_7^+ + H$	<0	2.4 ± 0.3
14	$SiH_3^+ + Si_2H_6 \rightarrow Si_2H_5^+ + SiH_4$	−21	5.2 ± 0.6
15	$\rightarrow Si_3H_7^+ + H_2$	<0	3.5 ± 0.4
16	$Si_2^+ + Si_2H_6 \rightarrow Si_3H_2^+ + SiH_4$	<0	1.2 ± 0.1
17	$\rightarrow Si_3H_3^+ + SiH_2$	<0	0.55 ± 0.07
18	$Si_2^+ + Si_2H_6 \rightarrow Si_4H_2^+ + 2H_2$	<0	3.1 ± 0.7
19	$\rightarrow Si_4H_3^+ + H_2 + H$	<0	1.5 ± 0.4
20	$\rightarrow Si_4H_4^+ + H_2$	<0	1.3 ± 0.3
21	$Si_2H^+ + Si_2H_6 \rightarrow Si_3H_3^+ + SiH_4$	<0	0.50 ± 0.06
22	$\rightarrow Si_4H_3^+ + 2H_2$	<0	3.2 ± 0.8
23	$\rightarrow Si_4H_5^+ + H_2$	<0	1.7 ± 0.4
24	$Si_2H_2^+ + Si_2H_6 \rightarrow Si_3H_4^+ + SiH_4$	<0	1.1 ± 0.1
25	$\rightarrow Si_4H_4^+ + 2H_2$	<0	2.2 ± 0.5
26	$\rightarrow Si_4H_6^+ + H_2$	<0	0.75 ± 0.18
27	$Si_2H_3^+ + Si_2H_6 \rightarrow Si_3H_3^+ + SiH_4 + H_2$	<0	0.67 ± 0.08
28	$\rightarrow Si_3H_5^+ + SiH_4$	<0	1.2 ± 0.1
29	$\rightarrow Si_4H_5^+ + 2H_2$	<0	3.1 ± 0.7
30	$\rightarrow Si_4H_7^+ + H_2$	<0	0.24 ± 0.06
31	$Si_2H_4^+ + Si_2H_6 \rightarrow Si_3H_4^+ + SiH_4 + H_2$	<0	0.13 ± 0.02
32	$\rightarrow Si_3H_6^+ + SiH_4$	<0	0.39 ± 0.05
33	$\rightarrow Si_3H_7^+ + SiH_3$	<0	0.13 ± 0.02
34	$\rightarrow Si_4H_8^+ + H_2$	<0	1.4 ± 0.3
35	$Si_2H_5^+ + Si_2H_6 \rightarrow Si_3H_5^+ + SiH_4 + H_2$	<0	0.27 ± 0.03
36	$\rightarrow Si_3H_7^+ + SiH_4$	<0	0.59 ± 0.07

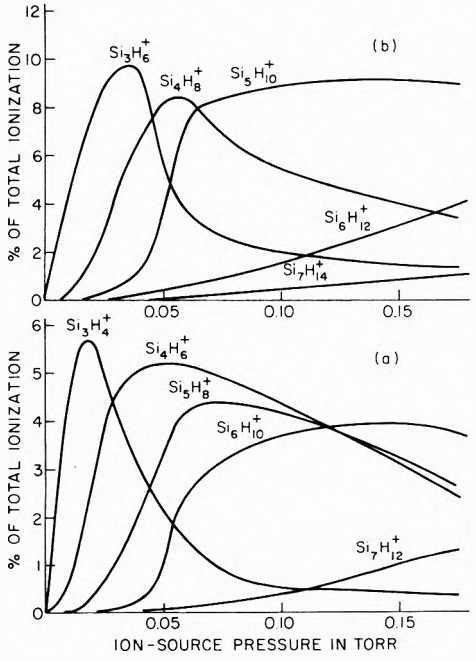

Figure 2. Dependence of ionic abundance in Si_2H_6 on ion-source pressure: (a) $Si_nH_{2n-2}^+$ ions; (b) $Si_nH_{2n}^+$ ions.

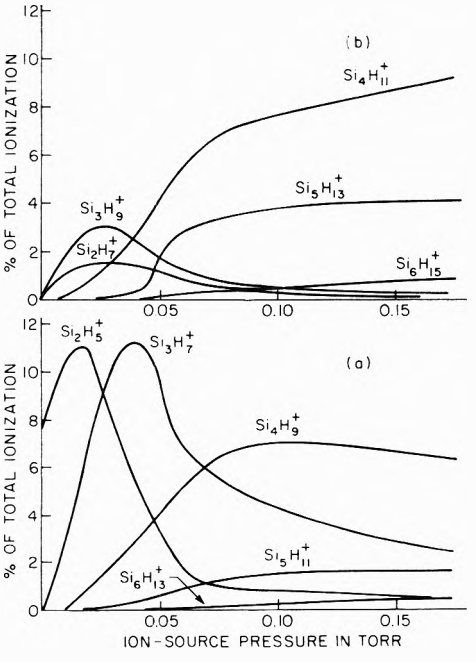

Figure 3. Dependence of ionic abundance in Si_2H_6 on ion-source pressure: (a) $Si_nH_{2n-1}^+$ ions; (b) $Si_nH_{2n-3}^+$ ions.

It is clear from Figure 3 that the secondary ions $Si_2H_7^+$ and $Si_3H_9^+$ are reactive toward disilane, probably contributing to the formation of $Si_4H_{11}^+$ and $Si_5H_{13}^+$ in second-order reactions. By analogy with the monosilane system,[9] and from inspection of the growth and decay curves of Figure 3 it seems very probable that third-order association reactions of $Si_2H_5^+$ and $Si_3H_7^+$ with Si_2H_6 contribute in a major way to formation of $Si_4H_{11}^+$ and $Si_5H_{13}^+$.

TABLE V: Endothermic Ion–Molecule Reactions in Disilane

Reactant ion	Product ions	Threshold in CM, eV	Reactant ion	Product ions	Threshold in CM, eV
Si^+	Si_2H^+		Si_2^+	Si_3^+	
	$Si_2H_3^+$			Si_3H^+	0.3 ± 0.1
	$Si_2H_5^+$			Si_4^+	
	Si_3^+	2.4 ± 0.2		$Si_4H_5^+$	
	$Si_3H_2^+$		Si_2H^+	Si_3H^+	
	$Si_3H_3^+$	2.8 ± 0.3		$Si_3H_2^+$	
SiH^+	$Si_2H_2^+$			$Si_3H_4^+$	
	$Si_2H_5^+$			Si_4H^+	
	Si_3H^+	0.9 ± 0.3		$Si_4H_4^+$	
SiH_2^+	$Si_2H_3^+$		$Si_2H_2^+$	$Si_3H_2^+$	
	$Si_3H_2^+$	2.6 ± 0.3		$Si_3H_5^+$	
	$Si_3H_5^+$			$Si_4H_5^+$	
SiH_3^+	$Si_2H_3^+$		$Si_2H_3^+$	Si_3H^+	1.0 ± 0.2
	$Si_3H_3^+$	1.9 ± 0.1		$Si_4H_3^+$	
	$Si_3H_5^+$	1.1 ± 0.1			

TABLE VI: Limits of Enthalpies of Formation of Tri- and Tetrasiliconium Ions

	$\Delta H_f°$, kcal/mol			$\Delta H_f°$, kcal/mol	
Ion	Upper limit	Lower limit	Ion	Upper limit	Lower limit
Si_3^+		59	Si_4H^+		−30
Si_3H^+		36	$Si_4H_3^+$	274	−39
$Si_3H_2^+$		104	$Si_4H_4^+$	309	126
$Si_3H_3^+$	265	160	$Si_4H_5^+$	273	153
$Si_3H_4^+$	279	17	$Si_4H_6^+$	309	
$Si_3H_5^+$	240	145	$Si_4H_7^+$	273	
$Si_3H_6^+$	279		$Si_4H_8^+$	287	
$Si_3H_7^+$	237				

A third-order association of SiH_3^+ with Si_2H_6, not observable in the tandem experiments, probably contributes also to formation of $Si_3H_9^+$. In the monosilane system,[9] third-order reactions become significant at about 0.15 Torr. With the increased complexity of the disilane system such stabilization reactions become significant at even lower pressures, namely, 0.02–0.03 Torr, a conclusion reached by inspection of the form and location of the growth curves of $Si_6H_{15}^+$ and $Si_7H_{17}^+$ being simple association reactions of are also compatible with the major mode of formation of $Si_6H_{15}^+$ and $Si_7H_{17}^+$ being simple association reactions of $Si_4H_9^+$ and $Si_5H_{11}^+$ ions, respectively, with the Si_2H_6 molecule.

3. Thermochemical Considerations. Standard enthalpies of formation of SiH_x^+ (x = 0,1,2,3) and $Si^2H_x^+$ (x = 1,2,3,4,5,6) ions, derived from a study of the electron-impact ionization and dissociation of monosilane and disilane, have been reported in the literature.[19,23] Such thermochemical information is not available for $Si_3H_x^+$ and $Si_4H_x^+$ ions and for this reason we cannot calculate the enthalpy changes of the reactions shown in Table IV. However, we do know that the reactions shown in Table V are exothermic or thermoneutral; therefore, by assuming that the reactions proceed by forming the most stable neutral products and that no internal excitation is involved in the reactants and products, we can calculate upper limits to the standard enthalpies of formation of the product ions. The values so obtained are shown in the second and fifth columns of Table VI.

If one writes the endothermic reactions indicated by the product ions shown in Table V in such a way as to yield the maximum endothermicity, one may calculate lower limits to the enthalpies of formation of the tri- and tetrasiliconium ions. The values so obtained are shown in the third and sixth columns of Table VI. For ions containing a small number of hydrogen atoms the lower limits obtained are obviously not very close to the true value, and, therefore, not very useful but they are presented in the table for completeness.

In the cases of $Si_3H_3^+$ formation (by the reaction of Si^+ and SiH_3^+ with Si_2H_6) and $Si_3H_5^+$ formation (by the reaction of SiH_3^+ with Si_2H_6) (Table V), we may use the measured threshold energies to compute $\Delta H_f°(Si_3H_3^+)$ and $\Delta H_f°(Si_3H_5^+)$ because in this case the actual reactions are unambiguous. In the case of $Si_3H_3^+$ formation from Si^+–Si_2H_6 collisions the threshold is 2.8 eV and the neutral products of the reaction must be H_2 + H or 3H. The former set of products lead to $\Delta H_f°(Si_3H_3^+)$ = 332 kcal/mol while the latter lead to $\Delta H_f°(Si_3H_3^+)$ = 228 kcal/mol. The upper limit to $\Delta H_f°(Si_3H_3^+)$ determined from the exothermic reactions (Table IV) is 265 kcal/mol which rules out the higher value above. Hence, we conclude that with no significant role of internal energy in reactants and products, $\Delta H_f°(Si_3H_3^+)$ = 228 kcal/mol. In an exactly similar manner, the threshold energies for formation of $Si_3H_3^+$ and $Si_3H_5^+$ in SiH_3^+–Si_2H_6 collisions result in the values $\Delta H_f°(Si_3H_3^+)$ = 198 kcal/mol and $\Delta H_f°(Si_3H_5^+)$ = 179 kcal/mol. The degree of agreement between the values of $\Delta H_f°(Si_3H_3^+)$, determined from the two different reactions, is probably as good as can be expected in view of the assumption of a negligible role of internal energy in these reactions. We, therefore, assign the following thermochemical values: $\Delta H_f°(Si_3H_3^+)$ = 211 ± 13 kcal/mol and $\Delta H_f°(Si_3H_5^+)$ = 179 ± 11 kcal/mol. No other endothermic processes in this system, for which a threshold energy could be determined, could be described by an unambiguous chemical reaction.

The reactions of Si^+ and SiH^+ with disilane to form $Si_2H_5^+$ are probably simple hydride ion transfer reactions as shown in (41) and (42), *viz.*

$$Si^+ + Si_2H_6 \longrightarrow SiH + Si_2H_5^+ \quad (41)$$

$$SiH^+ + Si_2H_6 \longrightarrow SiH_2 + Si_2H_5^+ \quad (42)$$

Both reactions are endothermic, as indicated by the energy dependence of the reaction cross section, so that if they occur as written we may use the known[19] enthalpy of formation of $Si_2H_5^+$ to derive lower limits to the enthalpies of formation of SiH and SiH_2. The values obtained are $\Delta H_f°(SiH) > 87$ kcal/mol and $\Delta H_f°(SiH_2) > 98$ kcal/mol.

From a spectroscopic study of the SiH molecule, Douglas[24] has shown that $D(Si-H) = 74$ kcal/mol; this leads to a value of $\Delta H_f°(SiH) = 87$ kcal/mol which is consistent with our result above. Saalfeld and McDowell,[25] from an electron impact study of $AsSiH_5$ have deduced $\Delta H_f°(SiH_2) = 81$ kcal/mol, and from a study of pyrolysis kinetics, Bowrey and Purnell[26] have reported $\Delta H°(SiH_2) = 59$ kcal/mol, both values being significantly lower than our lower limit. However, it may well be that our lower limit is high by at least 12 kcal/mol, and perhaps by as much as 25 kcal/mol, because of uncertainty in the standard enthalpy of formation of SiH^+. For this latter value we used 308 kcal/mol,[19] a value obtained from the appearance potential of SiH^+ from SiH_4. Electron-impact processes that involve the breakage of so many bonds are notorious for involving excess energy in some form and for leading to standard enthalpies of formation that are too high. In fact, Potzinger and Lampe[19] remark that the ionization efficiency curve of SiH^+ had a long tail, an indication of excess energy in its formation. Reasoning by analogy with ions derived from methane that the enthalpies of formation should show a monatonic decrease in the sequence M^+, MH^+, MH_2^+, and MH_3^+ leads us to conclude that the enthalpy of formation of SiH^+ should be in the range 283–296 kcal/mol. A value of $\Delta H_f°(SiH^+) = 290$ kcal/mol would be in accord with the value of $\Delta H_f°(SiH_2)$ reported by Saalfeld and McDowell[25] and with the fact that (42) is endothermic.

Acknowledgment. This work was supported by the U. S. Atomic Energy Commission under Contract No. AT(11-1)-3416.

References and Notes

(1) U. S. Atomic Energy Commission Document No. COO-3416-12.
(2) A. R. Anderson, "Fundamental Processes in Radiation Chemistry," P. Ausloos, Ed., Wiley, New York, N. Y., 1968, Chapter 5.
(3) G. G. Meisels in ref 2, Chapter 6.
(4) H. F. Calcote, "Ion-Molecule Reactions," J. L. Franklin, Ed., Plenum Press, New York, N. Y., 1972, Chapter 15.
(5) S. A. Studniarz in ref 4, Chapter 14.
(6) J. L. Franklin, ref 4 and references therein.
(7) G. G. Hess and F. W. Lampe, *J. Chem. Phys.*, **44**, 2257 (1966).
(8) J. M. S. Henis, G. W. Stewart, M. K. Tripodi, and P. O. Gaspar, *J. Chem. Phys.*, **57**, 389 (1972).
(9) T-Y. Yu, T. M. H. Cheng, V. Kempter, and F. W. Lampe, *J. Phys. Chem.*, **76**, 3321 (1972).
(10) J. M. S. Henis, G. W. Stewart, and P. P. Gaspar, *J. Chem. Phys.*, **58**, 3639 (1973).
(11) D. P. Beggs and F. W. Lampe, *J. Phys. Chem.*, **73**, 4194 (1969).
(12) G. W. Stewart, J. M. S. Henis, and P. P. Gaspar, *J. Chem. Phys.*, **57**, 1990 (1972).
(13) G. W. Stewart, J. M. S. Henis, and P. P. Gaspar, *J. Chem. Phys.*, **57**, 2247 (1972).
(14) T. M. H. Cheng, T-Y. Yu, and F. W. Lampe, *J. Phys. Chem.*, **77**, 2587 (1973).
(15) D. P. Beggs and F. W. Lampe, *J. Phys. Chem.*, **73**, 3307 (1969).
(16) D. P. Beggs and F. W. Lampe, *J. Phys. Chem.*, **73**, 3315 (1969).
(17) T. M. H. Cheng and F. W. Lampe, *Chem. Phys. Lett.*, **19**, 532 (1973).
(18) Landolt-Börnstein, "Zahlenwerte und Funktionen," II. Band, I. Teil, G. Auflage, Berlin, 1971, p 335.
(19) P. Potzinger and F. W. Lampe, *J. Phys. Chem.*, **73**, 3912 (1969).
(20) J. L. Franklin, J. G. Dillard, H. M. Rosenstock, J. T. Herron, K. Drexl, and F. H. Field, *Nat. Ref. Data Ser., Nat. Bur. Stand.*, **No. 26** (1969).
(21) H. E. Watson and K. L. Ramaswamy, *Proc. Roy. Soc., Ser. A*, **156**, 144 (1936).
(22) G. Gioumousis and D. P. Stevenson, *J. Chem. Phys.*, **29**, 294 (1958).
(23) W. C. Steele, L. D. Nichols, and F. G. A. Stone, *J. Amer. Chem. Soc.*, **84**, 4441 (1962).
(24) A. E. Douglas, *Can. J. Phys.*, **35**, 76 (1957).
(25) F. E. Saalfeld and M. V. McDowell, *Inorg. Chem.*, **6**, 96 (1967).
(26) M. Bowrey and J. H. Purnell, *Proc. Roy. Soc., Ser. A*, **321**, 341 (1971).

Polymer Concentration Dependence of Surface Electric Potential of Cylindrical Polyelectrolyte in Aqueous Salt Solutions

Katsutoshi Nitta* and Shintaro Sugai

Department of Polymer Science, Faculty of Science, Hokkaido University, Sapporo, Japan *(Received December 28, 1973)*

Publication costs assisted by Hokkaido University

The surface electric potential of cylindrical polyelectrolyte is calculated at finite dilution of polymer by use of the Poisson-Boltzmann equation with an electronic computer. Dependence of the potentiometric titration curve of poly(acrylic acid) or poly(glutamic acid) on its concentration is well explained by assuming its rod radius including counterion size to be 5.5 or 12.5 Å, respectively. Also the calculated dependence of pH on the polymer concentration is compared with theory of Maeda-Oosawa and Manning-Holtzer. In the presence of excess salts, the pH becomes independent of the polymer concentration as shown by Maeda-Oosawa. At any salt concentration and any degree of ionization, the pH is apparently linear *vs.* logarithm of the polymer concentration, if a change of the polymer concentration is caused by removal or addition of solvent. The slope is similar to that expected from these theories.

Introduction

Numerical calculation of surface electric potential of cylindrical polyelectrolyte in aqueous salt solution has been performed by solving the Poisson-Boltzmann equation with electronic computers.[1,2] The surface electric potential obtained from potentiometric titration and electrophoretic mobilities of various linear weak-acid polyelectrolytes have been compared with the theoretically

calculated values at infinite dilution of the polymers.[2-5] However, to compare with experimental data at finite dilution of the polymers, dependence of the surface electric potential on the polymer concentration should be taken into the theoretical consideration, because of long-range electrostatic interaction between the molecules. Indeed, the remarkable discrepancies between the theoretical surface electric potential at infinite dilution and the experimental at finite dilution have been pointed out, especially when the polymer concentrations were comparable or high as compared with the added salt concentrations.[2-4]

Recently, two groups of researchers have published theories of polymer concentration dependence of pH of the solutions of poly weak acids.[6,7] In their papers, the Poisson-Boltzmann equation has not been used, and the relationships of the theories to the Poisson-Boltzmann approach have been discussed, although few studies of the rigorous analytical or numerical calculation of the equation at finite dilution have been found.[8]

Here, the numerical calculation of the surface electric potential of a cylindrical polyelectrolyte in aqueous salt solution of the finite polymer concentration is presented by solving the Poisson-Boltzmann equation without the Debye-Hückel approximation. A model similar to Alexandrowicz and Katchalsky was used and the calculation has been performed, without any complicated assumptions used by them, with an electronic computer. The results are applied to interpretation of the polymer concentration dependence of potentiometric titration curve of some poly weak acids, and compared with other theories for the same problem.

Theory

Consider polyelectrolyte molecules in aqueous salt solution as an array of parallel rod-like cylinders at an average distance $2R$ between the molecular axes.[9-11] Then, the polymer concentration C_p (monomol/l.) is represented by the distance R as

$$1000/N_A C_p = \pi R^2 L \tag{1}$$

where L is length of a monomeric unit in the polymer and N_A Avogadro's number. The polyelectrolyte solution is assumed to be separated with a semipermeable membrane from an aqueous dialysate with the same salt, of which concentration is C_s'. The reduced electrostatic potential $\phi(= e\psi/kT)$ in the aqueous polymer solution can be determined from the Poisson-Boltzmann equation of cylindrical symmetry

$$\phi'' + \frac{1}{x}\phi' - \sinh\phi = 0 \tag{2}$$

where e, k, and T are defined in the usual manner, and ψ is the electric potential. Also, $x(= \kappa r)$ is the reduced distance, r the distance from the axis, and κ the Debye-Hückel parameter. An assumption of the uniform charge distribution on the cylinder leads to the following boundary conditions[9,10]

$$\phi'(\kappa a) = -Ze^2/DkT\kappa aL \tag{3}$$

$$\phi'(\kappa R) = 0 \tag{4}$$

where Z is the average number of charges on the monomeric unit, a distance of closest approach of mobile ions, and D the dielectric constant of medium. The electric potential in the outer dialysate solution at a distance sufficiently far from the membrane is defined to be zero, and therefore the Debye-Hückel parameter κ should be calculated with the salt concentration C_s'.

Assume ϕ may be expressed in the series

$$\phi = A\phi_1 + A^3\phi_3 + A^5\phi_5 + \cdots \tag{5}$$

where A is a constant to be determined from the boundary conditions. The function $\phi_n(x)$ can be obtained by the same method[2,9] as in the case of a spherical or rod-like polyelectrolyte at infinite dilution with the boundary condition eq 4 as

$$\phi_1 = I_0(x) + \frac{I_0(\kappa R)}{K_1(\kappa R)} K_0(x)$$

$$\phi_n = I_0(x)\int_{\kappa R}^{x} tK_0(t)g_n(t)\,dt - K_0(x)\int_{\kappa R}^{x} tI_0(t)g_n(t)\,d(t)$$

$$= \phi_1^{\,n} f_n(x)$$

$$(n = 3,5,7,\ldots) \tag{6}$$

where $I_n(x)$ and $K_n(x)$ are modified Bessel functions of the first and the second kinds, respectively, and the function $g_n(x)$ is defined in the literature.[12] Then ϕ can be written as

$$\phi = \sum_{i=1}^{\infty} A^{2i-1}\phi_1^{\,2i-1} f_{2i-1}(x)$$

$$(f_1(x) = 1) \tag{7}$$

Equations 3 and 7 determine the constant A in eq 5 or 7 with the same method as in the case of infinite dilution.[2]

The concentration of added 1-1 salt in the polyelectrolyte solution, C_s, is not equal to C_s' but represented in terms of C_s' as

$$C_s = \frac{C_s'}{V}\int_a^R \exp(-|\phi|)\,dV$$

$$= \frac{2C_s'}{(\kappa R)^2}\int_{\kappa a}^{\kappa R} x\exp(-|\phi|)\,dx \tag{8}$$

where V represents the volume of the polyelectrolyte solution per polymer molecule. To calculate ϕ in the polyelectrolyte solution, where the salt concentration is C_s, it may be necessary to take the following procedure: first, calculate a set of ϕ, *i.e.*, $\phi(1)$, $\phi(2)$, $\phi(3)$, ..., for a set of C_s' near the desired C_s, *i.e.*, $C_s'(1)$, $C_s'(2)$, $C_s'(3)$, ..., respectively. Second, calculate the salt concentration $C_s(i)$ in the polyelectrolyte solution in each case of the salt concentration $C_s(i)$ in the outer dialysate with eq 8. Finally the reduced electric potential ϕ in the polymer solution with the salt concentration C_s is determined by use of a suitable interpolation method with the sets of $\phi(i)$ and $C_s(i)$.

Application to Interpretation of the pH Titration Data

The potentiometric titration data are related in a direct way to the surface electric potential of the polyelectrolytes. The pH of a weak polyacid solution is given by[11]

$$pK = pH - \log\frac{\alpha}{1-\alpha}$$

$$= pK_0 - 0.434(\phi(\kappa a) - \phi(\kappa R)) \tag{9}$$

where pK_0 is the intrinsic dissociation constant and α the degree of ionization of ionizable group. Calculations were performed with an electronic computer FACOM 230-60 in the Hokkaido University Computing Center, as the same

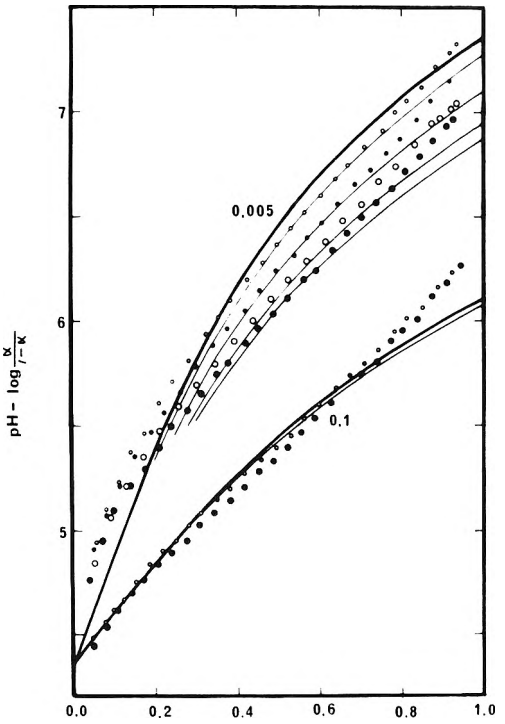

Figure 1. Theoretical and experimental titration curves for poly(acrylic acid) at 14°[3] with a = 5.5 Å and L = 2.54 Å. The numbers adjacent to the curves refer to the concentration of added 1-1 salt in M. The heavy lines are computed for infinite dilution and the light lines are for the corresponding polymer concentrations. The polymer concentrations are 0.00829 (small open circles), 0.193 (small filled circles), 0.0335 (large open circles), and 0.0419 monomol/l. (large filled circles).

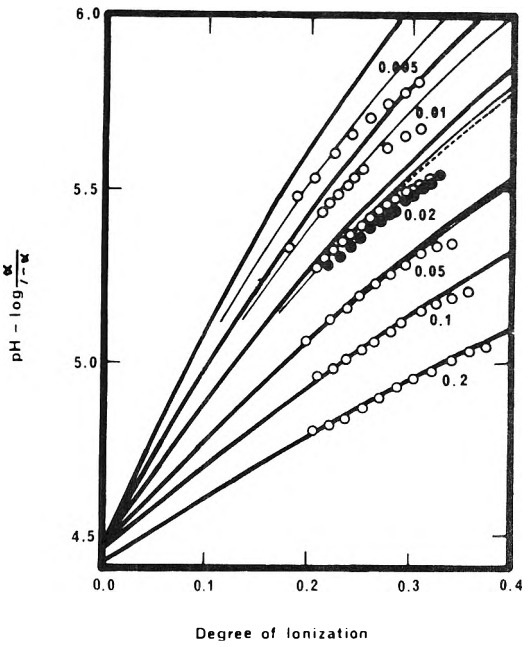

Figure 2. Theoretical and experimental titration curves for helical poly(glutamic acid)[13] with a = 12.5 Å and L = 1.5 Å. The numbers adjacent to the curves refer to the concentration of added 1-1 salt in M. The heavy lines are computed for infinite dilution, the light solid lines are for C_p = 0.0188 monomol/l., and the thin dashed line is for C_p = 0.0342 monomol/l. The open and the filled circles are experimental data for C_p = 0.0188 and 0.0342 monomol/l., respectively.

manner as that of infinite dilution.[2] The results are computed with potentiometric titration data of relatively high concentration of poly(acrylic acid) and of α-helical poly(glumatic acid) in Figures 1 and 2, respectively. The very precise data of Nagasawa, *et al.*,[3,13] were reproduced by enlarging photographs of the figures in their papers. Common pK_0 is employed for different C_p so far as C_s is common. The parameter a is assumed to be 5.5 or 12. 5 Å, respectively. The polymer concentration dependence of pH titration curve is fairly well explained by introducing the present concentration effect, especially at low added salt concentration. In Figure 3, the theoretical relationship between pK and $C_p^{1/2}$ is compared with the data of poly(acrylic acid). Although the experimental data seem to indicate the linearity of pK to $C_p^{1/2}$, linear extrapolation should not be done to evaluate the limiting pK at infinite dilution.

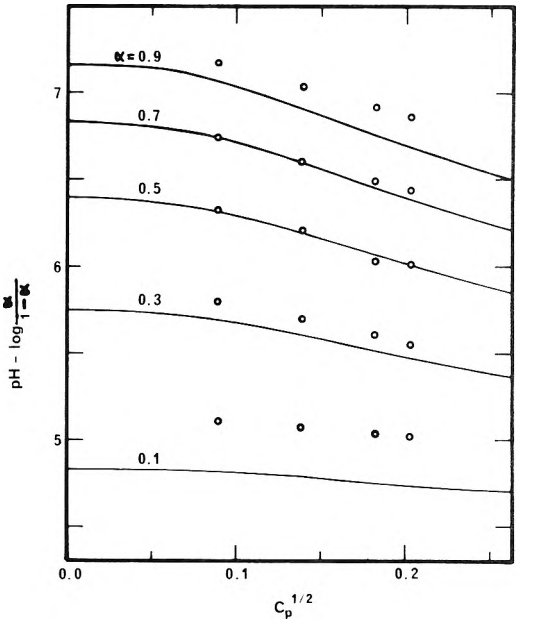

Figure 3. The relationship between pH − log (α/(1 − α)) and the root of polymer concentration (monomol/l.) at various degrees of neutralization α for poly(acrylic acid) at added salt concentration of 0.005 M. Open circles are experimental data[3] and solid lines are the values computed theoretically.

Discussions

Many previous theories of the titration curve have been based on solution of the Poisson–Boltzmann equation for a uniformly charged cylinder in a uniform dielectric, although its usual treatment is within the regime of the Born approximation. Nagasawa and the present authors have recently performed the numerical calculation for the rod-like poly weak acids at infinite dilution, and by adjusting the radii of polymers and counterions to coincide with the experimental data of their dilute solutions, they have found the radii of polymer rods including counterion sizes (Na or K ion) to be 5.5 and 14-15 Å in the cases of poly(methacrylic acid) and α-helical poly(glutamic acid), respectively.[2-4] However, few studies of the rigorous solutions of the Poisson–Boltzmann equation at finite dilution have been found. Alexandrowicz and Katchalsky used the same model as the present one, and their calculation was based on a subdivision of the potential into two parts corresponding to the close neighborhood region of the polyion and the screened-off region from the polyion, however, their skillful method included some intricate parameters.

Recently, Maeda and Oosawa have presented a thermo-

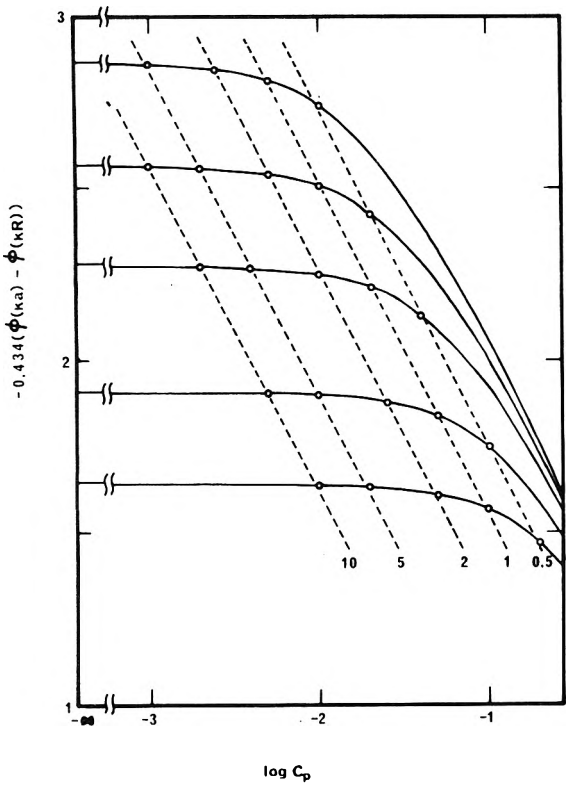

Figure 4. The relationship between the term $-0.434(\phi(\kappa a) - \phi(\kappa R))$ and the polymer concentration with a = 5.5 Å, L = 2.54 Å, and $Z = -0.9$. The added salt concentrations are (from top to bottom) 0.005, 0.01, 0.02, 0.05, and 0.1 M. The theoretical points at the same C_s/C_p ratio are indicated by open circles and joined with dashed lines. The numbers adjacent to each dashed line refer to the ratio C_s/C_p.

dynamic theory of the dependence of pH of polyelectrolyte solution on polymer concentration. Their theory has been based on both additivity of the osmotic pressure and the counterion activity in polymers containing salts and the invariability of the osmotic or activity coefficient with respect to the polymer concentration in salt-free solution. They have obtained the following relationship between the pH of the solution and C_p in terms of the present notations[6]

$$\left(\frac{\partial \mathrm{pH}}{\partial \log C_p}\right)_{C_s,\alpha} = 0 \qquad (C_s/C_p \gg 1) \tag{10}$$

$$\left(\frac{\partial \mathrm{pH}}{\partial \log C_p}\right)_{C_s/C_p,\alpha} = -1 + \frac{\partial}{\partial \alpha}(\alpha\phi_p) \tag{11}$$

where ϕ_p is the osmotic coefficient of salt free-solutions. Manning and Holtzer have also developed their polyelectrolyte theory based on counterion condensation and applied it to the same problem. From their calculations, the Poisson-Boltzmann theory with point counterion at infinite dilution has been found to be equivalent in their special case, and the Maeda-Oosawa theory for the concentration dependence of pK to be equivalent to their theory for nonsalt solutions. Also, their theory for the solution with salts gives the following relation in terms of the present notations[7]

$$\left(\frac{\partial \mathrm{pH}}{\partial \log C_p}\right)_{C_s/C_p,\alpha} = -g(\alpha) = \begin{cases} -1 & (\alpha > \alpha_1) \\ -\alpha/\alpha_1 & (\alpha < \alpha_1) \end{cases} \tag{12}$$

where α_1 is a critical charge density and equal to 0.35 for poly(acrylic acid).

TABLE I: Values of $-(\partial\ \mathrm{p}K/\partial \log C_p)_{C_s/C_p,\alpha}$ Evaluated from the Present Theory with a = 5.5 Å and L = 2.54 Å

C_s/C_p	α = 0.9	α = 0.7	α = 0.5
∞[a]	0.95	0.88	0.76
10	0.95	0.88	0.76
5	0.96	0.88	0.76
2	0.96	0.88	0.76
1	0.97	0.89	0.77
0.5	0.98	0.91	0.78

[a] Calculated from the results of the previous paper.[2]

The present calculation is based on the Poisson-Boltzmann equation for the uniformly charged cylinders at finite dilution in a uniform dielectric, however, only an adjustable parameter, the radius of polymer rod including the counterion size, is used without any other assumptions such as Alexandrowicz, *et al.* By use of essentially the same value of the radius of polymer as that obtained in infinite dilution,[2] the concentration dependence of the pH titration curve of poly(acrylic acid) or α-helical poly(glutamic acid) can be well explained as shown in Figures 1-3, except for the case of low degree of ionization (α = 0-0.3) of poly(acrylic acid), which may not be assumed to have the rod-like form.

To discuss the relationship between the present results and those of other authors, $-0.434(\phi(\kappa a) - \phi(\kappa R))(= \mathrm{p}K - \mathrm{p}K_0)$ is plotted against log C_p in Figure 4 for a = 5.5 Å, L = 2.54 Å, and α = 0.9. Clearly, eq 10 is very well satisfied. Also, at a glance, $(\partial\ \mathrm{p}K/\partial \log C_p)_{C_s/C_p,\alpha}$ is nearly independent of C_s/C_p and C_p in a range of C_s/C_p between 10 and 0.5. When α is considerably larger than α_1, the same conclusions can be obtained. In Table I, the values of $(\partial\ \mathrm{p}K/\partial \log C_p)_{C_s/C_p,\alpha}$ are given for various cases. The values for α = 0.9 or 0.7 agree well with Manning-Holtzer's results shown in eq 12. The values for α = 0.5, however, does not agree well. Manning's limiting law cannot rigorously be applied at near $\alpha = \alpha_1$ because of the oversimplification of his polyelectrolyte model. On the other hand, Maeda-Oosawa give also independence of $(\mathrm{p}K/\log C_p)_{C_s/C_p,\beta}$ on C_s/C_p and C_p as shown in eq 11 and the value should be considered to be between -1 and -0.7 for ϕ_p of poly(acrylic acid).[14] For low values of α, polymers such as poly(acrylic acid) must be flexible random coils and the cylindrical model is not adequate. The present treatment may not be applied to such cases.

In spite of the criticism on the application of the Poisson-Boltzmann equation,[7] the present conclusion on the dependence of pH of polyelectrolyte solution on its concentration may be identical with the results from thermodynamic[6] or counterion condensation theory.[7]

Acknowledgments. This work is supported in part by a Grant in Aid of the Ministry of Education in Japan. The authors are also grateful to Drs. N. Imai and H. Maeda of Nagoya University for enlightening discussions and helpful comments.

References and Notes

(1) L. Kotin and M. Nagasawa, *J. Chem. Phys.*, **36**, 873 (1962).
(2) S. Sugai and K. Nitta, *Biopolymers*, **12**, 1363 (1973).
(3) M. Nagasawa, T. Murase, and K. Kondo, *J. Phys. Chem.*, **69**, 4005 (1965).
(4) Y. Muroga, K. Suzuki, Y. Kawaguchi, and M. Nagasawa, *Biopolymers*, **11**, 137 (1972).
(5) T. Takahashi, I. Noda, and M. Nagasawa, *J. Phys. Chem.*, **74**, 1280 (1970).
(6) H. Maeda and F. Oosawa, *J. Phys. Chem.*, **76**, 3445 (1972).

(7) G. S. Manning and A. Holtzer, *J. Phys. Chem.*, **77**, 2206 (1973).
(8) A. D. MacGillivray, *J. Chem. Phys.*, **56**, 80, 83 (1972); **57**, 4071, 4075 (1972).
(9) R. M. Fuoss, A. Katchalsky, and S. Lifson, *Proc. Nat. Acad. Sci. U. S.*, **37**, 579 (1951).
(10) S. A. Rice and M. Nagasawa, "Polyelectrolyte Solutions," Academic Press, London, 1961, p 233.
(11) Z. Alexandrowicz and A. Katchalsky, *J. Polymer. Sci., Part A-1*, 3231 (1963).
(12) P. Pierce, Ph.D. Dissertation, Department of Chemistry, Yale University, 1950, cited in ref 10, p 142.
(13) M. Nagasawa and A. Holtzer, *J. Amer. Chem. Soc.*, **86**, 531 (1964).
(14) Z. Alexandrowicz, *J. Polym. Sci.*, **56**, 115 (1962).

Interaction of Hydrated Electrons with the Peptide Linkage

P. S. Rao and E. Hayon[1*]

Pioneering Research Laboratory, U. S. Army Natick Laboratories, Natick, Massachusetts 01670 *(Received November 26, 1973)*

Publication costs assisted by Natick Laboratories

The reaction rate constants k of e_{aq}^- with a wide range of peptides having terminal $-NH_3^+$ and *N*-acetyl groups have been determined in aqueous solutions, using the technique of pulse radiolysis. These rates were shown to be markedly dependent on the state of ionization of the terminal $-NH_3^+$ groups, the number of peptide linkages, and the overall charge on the peptide molecules. Amino groups in a β (or δ, γ) position are significantly less reactive than the corresponding α-amino peptides. The inductive effects on the peptide hydrogen -CONH- affect the reactivity toward e_{aq}^-, supporting previous suggestions that e_{aq}^- interacts with the carbonyl group. The rate constants k have been shown to be directly proportional to base-catalyzed rates for ionization of the peptide hydrogen of the same peptides, as determined by nmr. A similar correlation has been found between k and the ionization constants of the carboxylic acids of the corresponding peptides. Transient optical absorption spectra have been observed from the reaction of e_{aq}^- with the *N*-acetyl derivatives of triglycine, hexaalanine, and trisarcosine. These spectra are dependent upon pH and are suggested to be formed from the interaction of e_{aq}^- with the carbonyl group of the peptide linkage. The ketyl radicals formed can undergo acid-base equilibration $-C(O^-)NH- + H^+ \rightleftarrows -C(OH)NH-$, with pK_a(radical) $\geq$ 12.0. These ketyl radicals have very low (negative) redox potentials and are strong reducing agents.

Introduction

The principal linkage between the various amino acids making up a protein is the peptide bond -CONH-. Considerable experimental and theoretical studies have therefore been carried out on this linkage. The conductivity and electron transfer properties of proteins is also of particular importance, and hence the interest in studying the interaction of electrons with the peptide bond.

Nmr studies (see ref 2 for review up to 1969) have indicated the partial double-bond character of the amide bond

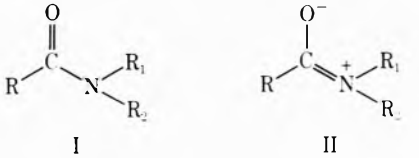

I II (1)

As a result[2,3] of this electronic delocalization, the linkage is planar and long-range spin coupling from R to R_1 and R_2 can be expected. The peptide hydrogen (R_1 = H) can undergo both base- and acid-catalyzed exchange reactions (see, *e.g.*, ref 4-6). Sheinblatt[4] has determined by nmr the rates of the base-catalyzed exchange, reactions 2 and 3, and established an acidity scale for the peptide hydrogen (see more below)

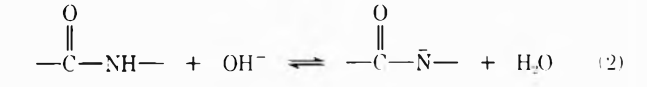

(2)

or, more generally

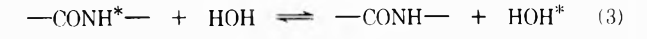

(3)

The k_2 rates were found[4] to be strongly dependent on the nature of R and R_1 (when R_2 = H).

The reaction rate constants for the interaction of hydrated electrons, e_{aq}^-, with amino acids and peptides were correlated by Braam[7] with the ionization constants of the terminal $-NH_3^+$ groups. This reactivity has since been correlated[8-12] with the presence and the number of carbonyl groups (*i.e.*, the number of peptide linkages). The cooperative effect of the peptide linkage(s), the amino and carbonyl groups, and the overall charge on the molecule have been suggested[11] to contribute to the reactivity toward e_{aq}^-.

The reaction of e_{aq}^- with simple amino acids[8,13] and oligopeptides[9,11,14,15] has been shown to *result* in reductive deamination

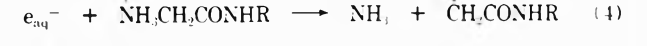

(4)

The CH_2CONHR radicals have been identified by pulse

TABLE I: Rate Constants for the Reaction of e_{aq}^- with Peptides

Peptide	Ionic form	pH	$k(e_{aq}^- + \text{peptide})$, M^{-1} sec^{-1} [a]
N-Acetylglycine	Ac-Gly-O$^-$	11.5	2.6×10^{6} [b]
N-Acetyldiglycine	Ac-Gly$_2$O$^-$	11.2	6.4×10^{7} [b]
N-Acetyltriglycine	Ac(Gly)$_3$O$^-$	9.2	4.4×10^{8}
N-Acetylalanine	Ac-Ala-O$^-$	7.0	1.2×10^{7}
N-Acetyltrialanine	Ac(Ala)$_3$O$^-$	9.2	6.8×10^{8}
N-Acetylhexaalanine	Ac(Ala)$_6$O$^-$	9.2	8.2×10^{8}
N-Acetylsarcosine	Ac-Sar-O$^-$	12.5	9.0×10^{6}
N-Acetyltrisarcosine	Ac(Sar)$_3$O$^-$	9.0	3.9×10^{8}
Glycine	$^+$H$_3$-Gly-O$^-$	6.4	8.2×10^{6} [c]
Alanine	$^+$H$_3$-Ala-O$^-$	7.4	1.2×10^{7}
β-Alanine	$^+$H$_3$-βAla-O$^-$	6.9	4.2×10^{6}
Sarcosine	$^+$H$_2$-Sar-O$^-$	7.0	1.6×10^{7}
Glycylglycine	$^+$H$_3$(Gly)$_2$O$^-$	6.4	3.7×10^{8} [b]
	H(Gly)$_2$O$^-$	13.1	4.9×10^{7} [b]
Glycylsarcosine	$^+$H$_2$-Gly-Sar-O$^-$	6.4	6.9×10^{8}
	H-Gly-Sar-O$^-$	11.3	1.0×10^{8}
Sarcosylglycine	$^+$H$_3$-Sar-Gly-O$^-$	5.8	8.8×10^{8}
	H-Sar-Gly-O$^-$	12.2	7.7×10^{7}
Glycyl-β-alanine	$^+$H$_3$-Gly-βAla-O$^-$	6.4	6.5×10^{8}
	H-Gly-βAla-O$^-$	11.3	6.3×10^{7}
Glycyl-β-alanine amide	$^+$H$_3$-Gly-βAla-NH$_2$	6.0	1.4×10^{9}
	H-Gly-βAla-NH$_2$	12.0	3.3×10^{8}
β-Alanyl-β-alanine	$^+$H$_3$-βAla-βAla-O$^-$	5.8	1.2×10^{8}
	H-βAla-βAla-O$^-$	12.2	4.5×10^{7}
Prolylglycine	$^+$H$_2$-Pro-Gly-O$^-$	6.2	9.6×10^{8}
	H-Pro-Gly-O$^-$	10.8	4.7×10^{7}
δ-Valylglycine	$^+$H$_3$-Val-Gly-O$^-$	6.2	1.3×10^{7}
γ-Aminobutyric glycine	$^+$H$_3$-γAmBut-Gly-O	6.0	3.4×10^{7}
β-Alanyldiglycine	$^+$H$_3$-βAla(Gly)$_2$O$^-$	6.4	2.8×10^{8}
	H-βAla(Gly)$_2$O$^-$	12.2	7.1×10^{7}
Diglycyl-β-alanine	$^+$H$_3$(Gly)$_2\beta$Ala-O$^-$	5.5	1.4×10^{9}
	H(Gly)$_2\beta$Ala-O$^-$	12.2	2.3×10^{8}
Triglutamic acid	$^+$H$_3$(Glu)$_3$O$^-$	6.3	2.3×10^{9}
	H(Glu)$_3$O$^-$	9.6	5.8×10^{8}
Tetraglycine	$^+$H$_2$(Gly)$_4$O$^-$	5.9	2.6×10^{9}
	H(Gly)$_4$O$^-$	10.2	3.9×10^{8}
Pentaglycine	$^+$H$_2$(Gly)$_5$O$^-$	6.1	4.0×10^{9}
	H(Gly)$_5$O$^-$	11.2	5.6×10^{8}

[a] Determined in ~1.0 *M* aqueous *tert*-butyl alcohol solutions by monitoring the decay kinetics of e_{aq}^- at 700 nm; values better than ±10%. [b] From ref 11. [c] From ref 24.

radiolysis[9-11] and confirmed by esr.[14,15] The *initial* site of reaction of e_{aq}^- is probably the peptide linkage.

The site of attack of e_{aq}^- with amides, imides, and peptides in aqueous solution has been found[12,16,17] to be the amide or peptide linkage. Characteristic transient optical absorption spectra have been observed (in the microsecond time scale) using the fast-reaction technique of pulse radiolysis. These spectra are pH dependent and were shown[17] to be a result of ionization of the radical, *e.g.*

$$—\dot{C}(OH)NH_2 \rightleftharpoons —\dot{C}(O^-)NH_2 + H^+ \qquad (5)$$

with pK_a(radical) values ranging from 3–13, dependent on the nature of R, R_1, and R_2 in structure I.

In this work, the reaction rate constants of e_{aq}^- with a number of oligopeptides including *N*-acetyl derivatives and β-alanine derivatives have been determined. These data have been correlated with certain physicochemical properties of these molecules, as determined in nmr studies. The ionization of the -Ċ(OH)NH- radical, reaction 6, has also been demonstrated.

$$—\dot{C}(OH)NH— \rightleftharpoons —\dot{C}(O^-)NH— + H^+ \qquad (6)$$

Experimental Section

The pulse radiolysis experimental set-up used has been described.[18,19] The reaction rate constants of e_{aq}^- with peptides were determined in presence of ~0.1–1.0 *M* *tert*-butyl alcohol (to scavenge the OH radicals produced in the radiolysis of water) by monitoring the decay kinetics of e_{aq}^- at 700 nm. From the pseudo-first-order-decay of e_{aq}^-, the second-order reaction rate constants were derived. Solutions were buffered using ~1 m*M* phosphate or borate buffers, and the pH was adjusted with perchloric acid and potassium hydroxide.

The chemicals used were the highest purity research grade commercially available, and were obtained from Cyclochemicals, Miles Laboratory, Fox Chemical Co., and Calbiochem. They were used as received.

Dosimetry was carried out using KCNS solution as described.[18] Extinction coefficients were derived based on $G(OH) = G(e_{aq}^-) = 2.8$.

Results and Discussion

Transient Species. The reaction of e_{aq}^- with simple peptides having terminal amino groups were shown to lead to reductive deamination,[8,9,11,13] reaction 4. The reaction of e_{aq}^- with *N*-acetyl derivatives of peptides leads to addition to the carbonyl group of the peptide linkages, with the rate constant increasing with increase in the number of -CONH- groups, see Table I. These

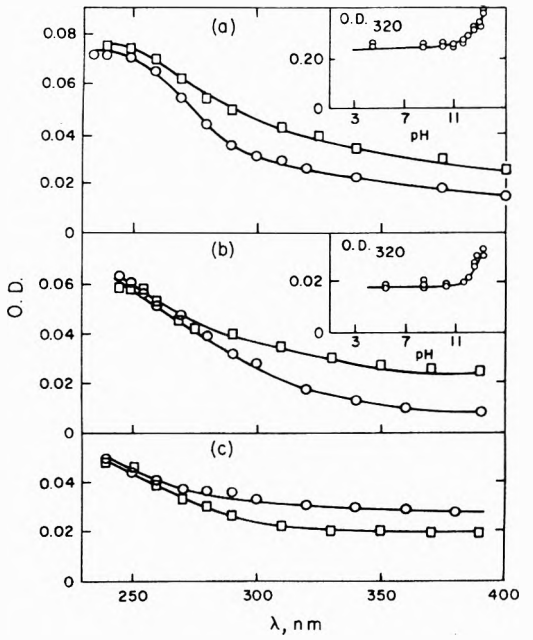

Figure 1. Transient optical absorption spectra produced from the reaction of e_{aq}^- with (a) 10^{-2} *M* *N*-acetyltriglycine at pH 5.2, O, and pH 13.3, □; (b) 10^{-2} *M* *N*-acetyltrisarcosine at pH 5.5, O, and pH 13.4, □; (c) 0.5 m*M* *N*-acetylhexaalanine at pH 6.2, O, and pH 13.3, □. In all cases 2.0 *M* *t*-BuOH was added to scavenge the OH radicals. Total dose ~4.0 krads/pulse. Inserts show change in absorbance at 320 nm with pH. OD measured ~0.2 μsec after electron pulse.

electron adducts have relatively low extinction coefficients and absorption maxima below ~240 nm. Figure 1 shows the transient spectra produced from *N*-acetyltriglycine, *N*-acetyltrisarcosine and *N*-acetylhexaalanine. These spectra are similar[12] to those formed by addition of e_{aq}^- to the cyclic dipeptides of glycine, alanine, and sarcosine.

Slight differences with pH are observed in the optical spectra of these transient species. Figure 1, and these are interpreted to be due to the acid-base properties of the radicals, reaction 6. The pK_a(radical) are ≥ 12.0, indicating that these radicals are very weak acids. Since *N*-acetyltrisarcosine produces similar transient absorptions which are also pH dependent, it is concluded that the peptide hydrogens are not involved in the ionization reaction 6.

The reaction of e_{aq}^- with polysarcosine (mol wt ~3000, 3.0×10^{-4} *M* solutions used in presence of 0.5 *M* *t*-BuOH) generated similar transient spectra (not shown) which were also dependent on pH. The maxima were below 240 nm, and ϵ_{250} 1300 M^{-1} cm^{-1} at pH 6.3 and ϵ_{250} 1500 M^{-1} cm^{-1} at pH 13.3.

It is interesting to note[20,21] that -Ċ(OH)NH- and -C(OH)NCH$_3$- radicals transfer an electron very efficiently to a range of acceptors, A

$$—\dot{C}(OH)NH— + A \longrightarrow \cdot A^- + —CONH— + H^+ \quad (7)$$

with k_7 values close to diffusion-controlled rates.[21] These rates are dependent upon the redox potentials of the acceptor molecules and the donor radicals. The -Ċ(OH)NH- radicals have been found[22] to have very low redox potentials, $E^{01} \leq -1.2$ V (where E^{01} notation is at pH 7.0 and 25°) making these peptide radicals powerful reducing agents. These results support the hypothesis of intramolecular electron transfer processes in proteins and peptides.

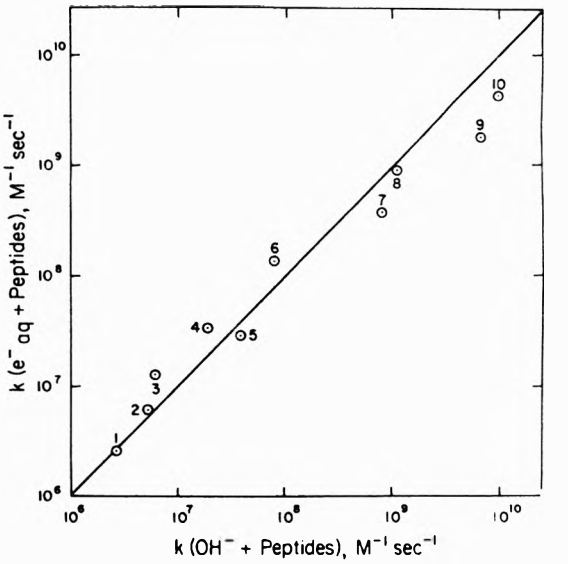

Figure 2. Correlation between the rate constants of e_{aq}^- with some peptides and the rate constants for base-catalyzed ionization of the peptide hydrogen of the same peptides as derived by Sheinblatt:[4] 1, *N*-Ac-Gly; 2, *N*-Me-acetamide; 3, δ-Val-Gly; 4, γ-Am-But-Gly; 5, *N*-Form-Gly; 6, β-Ala-Gly; 7, Gly-Gly; 8, Pro-Gly; 9, (Gly)$_3$; 10, Gly-Gly-NH$_2$.

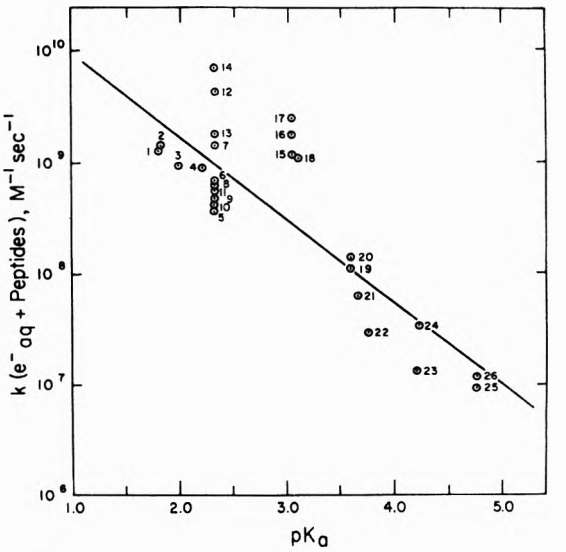

Figure 3. Correlation between the rate constants of e_{aq}^- with peptides and the pK_a of the carboxyl group of the corresponding acids (see text and ref 23): 1, His-His; 2, Phe-NH$_2$; 3, Pro-Gly; 4, Sar-Gly; 5, Gly-Gly; 6, Gly-Sar; 7, Gly-β-Ala-NH$_2$; 8, Gly-β-Ala; 9, Gly-Trp; 10, Gly-Tyr; 11, Gly-Phe; 12, Gly-Gly-NH$_2$; 13, (Gly)$_3$; 14, (Gly)$_3$-NH$_2$; 15, Gly-Gly-Phe; 16, Gly-Gly-β-Ala; 17, (Gly)$_4$; 18, Phe-Gly-Gly; 19, β-Ala-β-Ala; 20, β-Ala-Gly; 21, *N*-Ac-Gly-Gly; 22, *N*-Form-Gly; 23, δ-Val-Gly; 24, γ-Am-But-Gly; 25, *N*-Ac-Sar; 26, *N*-Ac-Ala.

Reactivity toward e_{aq}^-. The reaction rate constants of e_{aq}^- with a number of peptides and their derivatives have been determined as a function of the state of protonation of the terminal amino groups. The pK_a of -NH_3^+ groups are known.[23] These results and a few others from the literature[11,24] are presented in Table I. The following points can be made from this data.

(a) The rate constants decrease with ionization of the terminal amino groups, in agreement with results on other peptides.[7,11,24]

(b) The rate constants increase with the number of peptide linkages. Even in pentaglycine, however, ionization of the terminal $-NH_3^+$ group reduces k from 4.0×10^9 to $5.6 \times 10^8\ M^{-1}\ sec^{-1}$.

(c) Some correlation appears between the rate constants and the overall charge on the molecules. The amide or ester derivatives of the peptides are significantly more reactive (Table I and ref 11) than the corresponding $-COO^-$ derivatives.

(d) The β-amino derivatives have lower reactivities with e_{aq}^-, particularly when present in the terminal position. With δ- and γ-amino peptides, the rate constants decrease further.

(e) Sarcosyl peptides $-CON(CH_3)-$ appear to be slightly more reactive than the corresponding $-CONH-$ peptides.

Thus inductive effects on the peptide hydrogen, as well as on substituents on both sides of the peptide linkage (*i.e.*, the nature of R, R_1, and R_2 in structure I), affect the reactivity of the $-CONH-$ group to the attack by e_{aq}^-.

Many of the factors mentioned above to explain the reactivity of peptides toward e_{aq}^- appear to affect also the base-catalyzed rate constants, k_2, as determined by Sheinblatt.[4] The k_2 rates vary by about three orders of magnitude as do the rates for reaction of e_{aq}^- with the same compounds. Indeed a linear correlation can be demonstrated between these rates, and is represented in Figure 2. The agreement is remarkably good and would seem to support the acidity scale suggested[4] for the peptide hydrogen. Such a relationship can be used to predict k_2 and /or $k(e_{aq}^- + \text{peptide})$ rates.

The acidity of the peptide hydrogen has also been correlated[4,5] with the acidity (pK_a) of the carboxylic group of the corresponding peptides. Figure 3 shows a plot of $k(e_{aq}^- + \text{peptide})$ *vs.* the $pK_a(-COOH)$ of the corresponding peptide (*e.g.*, for glycylglycine, the $pK_a(COOH)$ of glycine was plotted). This correlation is in agreement with k_2 values as determined[4,5] by nmr.

Conclusions

This study shows that the inductive effects of substituents on the peptide linkage affect considerably the reactivity of peptides toward e_{aq}^-. Factors affecting the proton transfer[4] reactions of the peptide hydrogen, as can be described by a generalized Brønsted relationship, are the same as those which govern the interaction with e_{aq}^-.

Acknowledgment. We are grateful to Dr. M. Sheinblatt from Tel-Aviv University, Israel, for gifts of δ-valylglycine and γ-aminobutyric glycine.

References and Notes

(1) Author to whom correspondence should be addressed.
(2) W. E. Stewart and T. H. Siddall, III, *Chem. Rev.*, **70**, 517 (1970).
(3) B. Pullman and A. Pullman, "Quantum Biochemistry," Interscience, New York, N. Y., 1963.
(4) M. Sheinblatt, *J. Amer. Chem. Soc.*, **92**, 2505 (1970).
(5) R. S. Molday and R. G. Kallen, *J. Amer. Chem. Soc.*, **94**, 6739 (1972).
(6) R. S. Molday, S. W. Englander, and R. G. Kallen, *Biochemistry*, **11**, 150 (1972).
(7) R. Braam, *Radiat. Res.*, 27, 319 (1966); **31**, 8 (1967).
(8) W. M. Garrison in "Current Topics in Radiation Research," Vol. 4, M. Ebert and A. Howard, Ed., North-Holland Publishing Co., Amsterdam, 1968, p 43.
(9) M. Simic, P. Neta, and E. Hayon, *J. Amer. Chem. Soc.*, **92**, 4763 (1970).
(10) E. J. Hart and M. Anbar, "The Hydrated Electron," Wiley-Interscience, New York, N. Y., 1970.
(11) M. Simic and E. Hayon, *Radiat. Res.*, **48**, 244 (1971).
(12) E. Hayon and M. Simic, *J. Amer. Chem. Soc.*, **93**, 6781 (1971).
(13) P. Neta, M. Simic, and E. Hayon, *J. Phys. Chem.*, **74**, 1214 (1970).
(14) M. D. Sevilla, *J. Phys. Chem.*, **74**, 3366 (1970).
(15) P. Neta and R. W. Fessenden, *J. Phys. Chem.*, **74**, 2263 (1970).
(16) E. Hayon, T. Ibata, N. N. Lichtin, and M. Simic, *J. Amer. Chem. Soc.*, **93**, 5388 (1971).
(17) M. Simic and E. Hayon, *J. Phys. Chem.*, **77**, 996 (1973).
(18) M. Simic, P. Neta, and E. Hayon, *J. Phys. Chem.*, **73**, 3794 (1969).
(19) J. P. Keene, E. D. Black, and E. Hayon, *Rev. Sci. Instrum.*, **40**, 1199 (1969).
(20) M. Simic and E. Hayon, *Int. J. Radiat. Biol.*, **22**, 507 (1972).
(21) P. S. Rao and E. Hayon, *Biochim. Biophys. Acta*, **292**, 516 (1973).
(22) P. S. Rao and E. Hayon, to be submitted for publication.
(23) "Handbook of Biochemistry," Chemical Rubber Publishing Co., Cleveland, Ohio, 1968, p J-150.
(24) E. Hayon and M. Simic, *Intra-Sci. Chem. Rep.*, **5**, 357 (1971).

Effects of Tetraalkylammonium Salts on the Activity Coefficient of *N*-Acetyl Ethyl Esters of Phenylalanine, Norleucine, and Norvaline

Pradip K. Nandi[1]

Department of Physical Chemistry, Indian Association for the Cultivation of Science, Calcutta 32, India *(Received July 2, 1973; Revised Manuscript Received October 12, 1973)*

Activity coefficients of *N*-acetyl ethyl esters of phenylalanine, norleucine, and norvaline have been determined in tetraalkylammonium bromide salt solutions. The compounds generally show *salting in* in these salt solutions the magnitude of which increases with the increase in the size of the alkyl groups in the salt. The molar free energies, ΔF_{tr}, of transfer of the compounds from water to 1 *M* salt solution have been calculated. These values indicate that the contributions of the nonpolar and polar portion of the ester molecules toward the transfer process in these salt solutions are not additive in nature. The enthalpies, ΔH, and entropies, ΔS, which were calculated from the variation of the activity coefficients with temperature showed the importance of hydrophobic interaction in explaining the observed salting behavior of the compounds. An attempt has been made to apply these results to explain the mechanism of protein denaturation in tetraalkylammonium salt solution.

Tetraalkylammonium salts in aqueous solution occupy an interesting position in solution physical chemistry. Nearly 50 papers most of which have appeared during last 25 years reveal their uniqueness compared to simple salts as electrolytes in solvent water. The recent papers of Wen and Hung and Wirth and LoSurdo have documented the relevant references regarding physicochemical properties of these salts in aqueous solution and also their interaction with other solutes in water.[2] The unusual physicochemical properties, compared to ordinary electrolytes, which arise mainly due to the presence of nonpolar groups in these salts have drawn considerable attention to study their effects on the structural stability and reactivity of biological macromolecules. The effectiveness of these salts in denaturing proteins and DNA and affecting the activities of several enzymes, *viz.*, fumarase, lactate dehydrogenase, etc., has been demonstrated.[3-8] In general the effectiveness in causing above changes in the structure and reactivity increases from tetramethyl to tetrabutyl derivative.

The manner in which these salts effect the structure and activity of the macromolecules is not certain. It is still undecided whether an indirect effect *viz.* a change in the water "structure" caused by the tetraalkylammonium ions or a "direct binding" between these salts and macromolecules is responsible for the observed instability of the ordered structure of native protein molecules.[3,9]

Our recent studies have indicated how the groups which are mainly involved in the denaturation process of protein molecule would behave in concentrated salt solutions.[10,11] This information was obtained from the study of the activity coefficients of model compounds which are representative of the different groups present in protein. Here we report similar studies of a few model compounds in tetraalkylammonium bromide solution (R_4NBr). The compounds chosen are acetylamino acid ethyl esters (ARE), $CH_3CONHCH(R)COOC_2H_5$, R being phenyl alanyl, norleucyl, and norvalyl groups. Since temperature variation is often helpful to understand mechanism of reactions, the effect of temperature on the activity coefficient has been utilized to interpret the mechanism of interaction of R_4NBr salt with the model peptide and hence protein.

Experimental Section

Material and Methods. [^{14}C]*N*-Acetyl-L-norvaline ethyl ester (AnVE) and [^{14}C]*N*-acetyl-L-norleucine ethyl ester (AnLE) were prepared by the method of Wolf and Neeman.[12] Details of their preparation and characteristics have been reported elsewhere.[11]

N-Acetyl-L-phenylalanine ethyl ester (APE) obtained from Cyclo Chemical Corp. was recrystallized from water. A solubility phase curve showed the absence of any impurity. Experiments with nearly sevenfold change in the excess solid phase gave the same solubility values within ±1%.

Ammonium bromide used as Fishers Analytical Grade reagent. Tetramethyl- and tetraethylammonium bromides (Me_4NBr and Et_4NBr) were crystallized twice from methanol. Tetra-*n*-propyl- and tetra-*n*-butylammonium bromides (Pr_4NBr and Bu_4NBr) were twice crystallized from carbon tetrachloride. Glass distilled water was used throughout. *N*-Dibutyl ether was distilled twice, boiling point 141–142° (lit. 142°).[11] AR grade petroleum ether was used.

Radioactivity measurements were obtained with a Packard Model 3375 liquid scintillation spectrometer at 4°. Samples (0.1 ml) were added to the vials containing 10 ml of scintillation solution, the composition of which has already been described. The samples were counted for sufficient time to accumulate 20,000 counts in most cases reducing the standard errors of counting to 0.5%.[10,11]

The solutes were equilibrated with solvents in 12-ml capacity tube sealed with Teflon-lined screw caps, in both distribution and solubility measurements. The tubes were submerged in a water bath in a rotating rack, and mixing was accomplished by rotating tubes end-over-end and at 25–30 rpm. Temperatures were maintained at 0 ± 0.1, 25.0 ± 0.05, and 40.0 ± 0.1°.

Measurements of solubility with APE at three temperatures and distribution of AnVE and AnLE between aqueous and reference phase at 25 and 40° were carried out by

methods described in detail elsewhere.[10,11] Equilibrations for solubility experiments were carried out for 10 days at 0°, 3 days at 25°, and 2 days at 40°. The equilibration time for distribution measurements were 1 hr both at 25 and 40° for AnVE and AnLE. That the above periods of equilibration were adequate for the equilibrium to be attained were determined as described previously. Samples were removed for counting radioactivity from both phases of each tube to measure the concentration.

The concentration of APE was determined spectrophotometrically in a PMQ II Zeiss spectrophotometer, from the difference of absorption at 257.5 (λ_{max}) and 300 nm where the absorbance was small. Samples of the saturated solution were diluted by factors of 6 to 30 with water for absorbance measurements. This reduces the salt concentration to levels where no significant effects of salts on the uv spectra would be expected.

The solubility of APE in water at 25° and distribution coefficients of AnVE and AnLE between water and reference phases at 25 and 40° have been reported elsewhere.[11] The solubility values of APE at 0 and 40° are 2.59 ± 0.06 and 6.62 ± 0.10 g/l., respectively. Solubility and distribution coefficients were within ±5 and ±3%, respectively, of their mean values. We have assumed that these ranges of experimental error apply to determinations in salt solutions as well.

The degree of mutual solutions of the phases in the distribution experiments has been carried out as follows. Aqueous solutions of R_4NBr salts were shaken with reference phases. Aliquot of the reference phase was then shaken with fresh water, and this water phase was treated with silver nitrate solution. The absence of any recognizable amount of precipitate was considered to show the absence of any detectable mutual solubility of phases which could effect our distribution experiments.

Results

Equations 1 and 2 have been used to determine activity coefficients from solubility and distribution, respectively. Activity coefficients of the compounds in water have been assumed to be equal to one; f_i^s is

$$f_i^s = C_i^0/C_i^s \quad (1)$$

$$f_i^s = (C_i^{r,s}/C_i^s)(C_i^0/C_i^{r,0}) \quad (2)$$

the activity coefficient of the nonelectrolyte, i, in salt solution; C_i^0 and C_i^s are the molar concentrations of i in water and salt solution; $C_i^{r,0}$ and $C_i^{r,s}$ are concentrations in the reference phases corresponding to water and to salt solution, respectively.[13,14]

Figure 1 shows a semilogarithmic plot of the activity coefficient of APE as a function of salt concentration at 25°. The salting out of the compound in NH_4Br solution changes to salting in with the introduction of alkyl groups and the magnitude of the effect increases with the increase in the number of alkyl groups in the salt. Log f (i) increases linearly in NH_4Br solution, (ii) decreases linearly in Me_4NBr and Pr_4NBr solutions, and (iii) curves upward in Et_4NBr and slightly curves downward in Bu_4NBr solutions. AnLE shows similar solubility behavior in NH_4Br, Et_4NBr, and Bu_4NBr (Me_4NBr and Pr_4NBr effects were not carried out) and AnVE shows similar behavior in Bu_4NBr (where it has only been studied) solution. Effect of Bu_4NBr at 25° on the three solutes is shown in Figure 2.

Temperature has a marked effect on the activity coefficients of the compounds in R_4NBr solution. The decrease

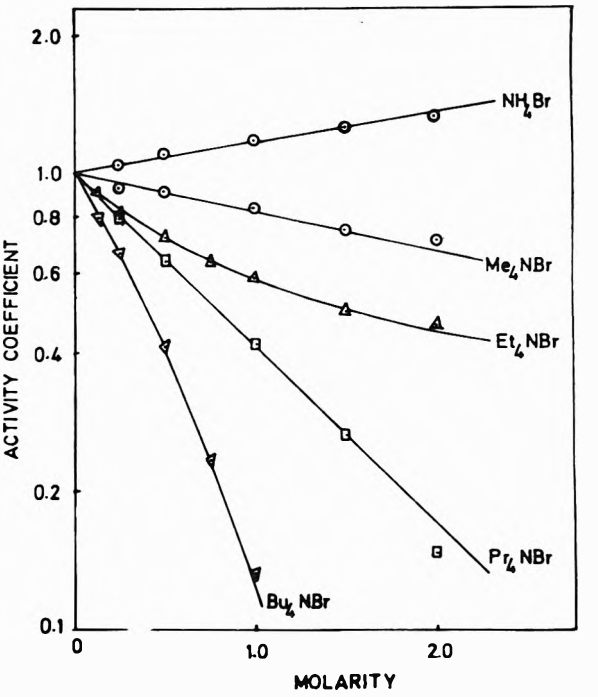

Figure 1. Effects of different salts on the activity coefficients of acetylphenylalanine ethyl ester at 25°.

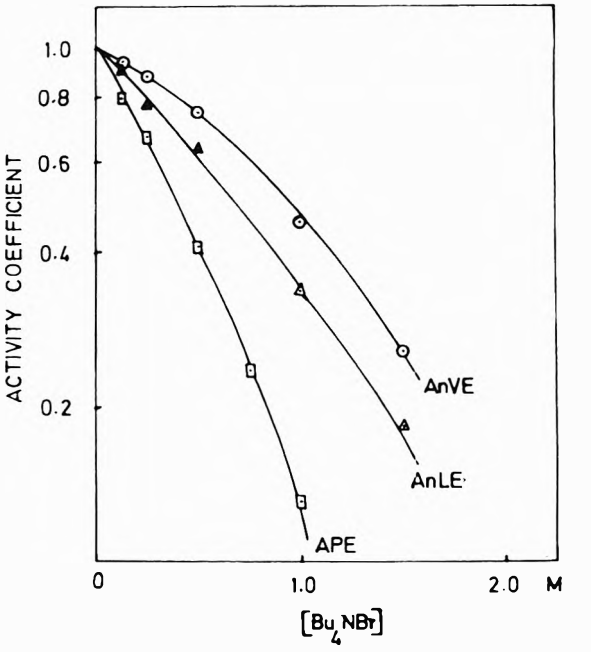

Figure 2. Effect of butylammonium bromide on the activity coefficients of acetylphenylalanine, acetylnorleuc ne, and acetylnorvaline ethyl esters at 25°.

in the activity coefficients increases with increase in the temperature from 0 to 40° (Figure 3). The curvature of the plot of log f *vs.* salt concentration decreases with increase in temperature. As with other simple electrolytes, the temperature effect on the activity coefficient in NH_4Br is not pronounced as in R_4NBr solution.[11]

The activity coefficient, f_i, of a nonelectrolyte is related to molar salt concentration, C_s, by the Setchenow eq

$$\log f_i = K_s C_s \quad (3)$$

K_s is the salting constant and is termed as *salting out* or

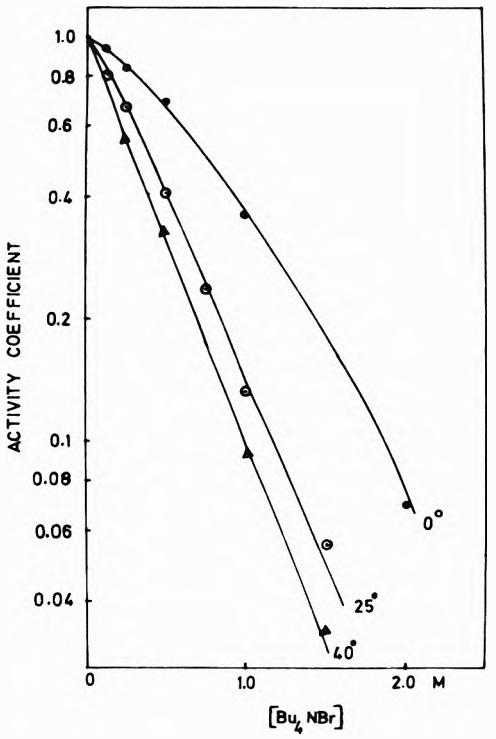

Figure 3. Effect of tetrabutylammonium bromide on the activity coefficients of acetylphenylalanine ethyl esters at different temperatures.

TABLE I: Salting Constants of the Amino Acid Ethyl Esters at Three Temperatures[a]

Compound	Salt	0°	25°	40°
	NH_4Br		0.07	0.09
	Me_4NBr	−0.05	−0.09	−0.08
APE	Et_4NBr	−0.14	−0.32	−0.31
	Pr_4NBr	−0.16	−0.39	−0.54
	Bu_4NBr	−0.31	−0.73	−1.08
AnLE	NH_4Br		0.10	0.11
	Bu_4NBr		−0.41	−0.57
AnVE	Bu_4NBr		−0.25	−0.44

[a] Calculated as described in the text.

TABLE II: Free Energy Transfer ΔF_{tr} (cal/mol) of the Amino Acid Ethyl Esters from Water to 1 *M* Salt Solution[a]

Compound	Salt	0°	25°	40°
APE	NH_4Br		100	120
AnLE			130	135
APE	Me_4Br	−65	−110	−115
AnLE[b]			0	0
APE	Et_4NBr	−140	−315	−310
AnLE			−80	−80
APE	Pr_4NBr	−200	−500	−770
APE	Bu_4NBr	−560	−1200	−1630
AnLE			−640	−945
AnVE			−465	−715

[a] Calculated from equation $\Delta F = RT \ln f_i$. [b] From single data at 1 *M*. Values are rounded to the nearest 5.

salting in constant respectively depending upon whether the activity coefficients of the nonelectrolyte *increases* or *decreases* in salt solution. The salting constant gives a convenient method for comparison of salt effects on various electrolytes.

The values of the salting constant in cases of linear plots were obtained by drawing the best straight line through all the points and determining the slope. In the case of curved plots, salting constants were estimated from initial slopes approximated by passing straight line visually through points below 1 *M*.[10] Salting out constants in NH_4Br and salting in constants of the esters in R_4NBr solutions are compared in Table I.

Another method of comparison of the effect of R_4NBr salts would be to compare the free energy of transfer, ΔF_{tr}, which can be calculated from the equation $\Delta F_{tr} = RT \ln f_i$ and represents the free energy of transfer of 1 mol of dilute solution of a given compound i, from water into the salt solutions at the same concentration in each solvent. The values of ΔF_{tr} of the compounds from water to 1 *M* salt solution are presented in Table II. ΔF_{tr} values at 0° for APE in Me_4NBr and Et_4NBr solution show considerable decrease than the values at 25°. There is, however, practically no differences in the values at 25 and 40° in these solutions. Temperature dependence of ΔF_{tr} is more pronounced in salts with larger alkyl groups.

Discussion

The aim of the present work is to study the behavior of compounds which contain a peptide group in tetraalkylammonium salt solution to understand the structural stability of the protein molecule in such solution. The model which has been used here for the denaturation process of proteins is the same as has been used previously.[10,11,15,16] Upon denaturation, the peptide (CHCONH) and nonpolar groups, which are buried in the interior of the native protein molecule, would be exposed to surrounding solvent with consequent increase in their concentration (decrease in the activity coefficient, salting in) in denaturing solvents compared to water. The studies of the model compounds in these solutions are expected to provide information which can be applied to the groups they represent in the protein molecule. Our previous work on model peptides showed the balance between the *salting in* of the newly exposed polar group (CHCONH) and the *salting out* (increase in the activity coefficient) of the simultaneously exposed nonpolar groups would determine the stability of one state or the other of a protein molecule in concentrated salt solution. This study also showed that nonpolar side chains are affected similarly to the hydrocarbons by salt solutions, although the magnitude of the salting out constant was appreciably higher for the hydrocarbons. At present no information is available about the behavior of peptide group in R_4NBr solution. We have chosen compounds $CH_3CONHCH(R)COOC_2H_5$ for this purpose. This study, however, would not give us any direct information about the behavior of peptide or ester groups themselves, but the combination of hydrocarbon side chain and polar group in these compounds might be considered as a model for the portion of the polypeptide chain present in protein. The compound where R represents the phenylalanyl group has been studied relatively thoroughly. The similarity of salting behavior of these types of compounds has been shown with compounds where R is norleucyl or norvalyl in a few R_4NBr solution.

The observed negative values of ΔF_{tr}, in general, for the transfer of 1 mol of ARE from water to 1 *M* R_4NBr salt solution show that the transfer process is spontaneous (Table II). Aliphatic and aromatic hydrocarbons show similar behavior in R_4NBr solution.[2,17] The values of ΔF_{tr} at maximum concentrations (shown in parentheses Table III) of R_4NBr at which Wen and Hung studied the alkanes

TABLE III: $-\Delta F_{tr}$ (cal/mol) for the Transfer of Different Solutes from Water to R_4NBr Solution at 25°[a]

Salt	Propane	AnVE	Butane	AnLE	Benzene	APE	Butane	Benzene
Bu_4NBr	170[b]	200(0.52)	115[b]	170(0.28)	1220[c] 1680[d]	900(0.77) 1185[e]	115[b]	685[c](0.31 *m*)
Pr_4NBr					935[e] 1240[d]	440(0.82) 510[e]	120[b]	650[c](0.40 *m*)
Et_4NBr	70[b]	50(0.40)	85[b]	60(0.38)	645[c] 765[d]	310(0.86) 320[e]	160[f]	410[f]
Me_4NBr			85[b]	0(0.77)	465[c] 480[d]	110(0.94) 115[e]	85[b]	365[c]

[a] Values in the parentheses are the maximum concentrations in molarity and molality (shown) of the salts for which data are available for the alkanes. ΔF_{tr} values for alkanes at these concentrations are compared with the interpolated values. ΔF_{tr} values of ARE and benzene at the same concentrations of R_4NBr. [b] Reference 2a. [c] Reference 2b. [d] From the salting constant values at 1 *M* (ref 17). [e] From the salting constant values at 1 *M*. [f] From salting constant data at 1 *M* from J. J. Morrison and N. B. B. Johnstone, *J. Chem. Soc.*, 3655 (1955).

have been compared with ΔF_{tr} values at the same interpolated salt concentrations for AnVE and AnLE. In absence of any similar solubility data of toluene in R_4NBr solution, the values of ΔF_{tr} for benzene obtained from salting constant of Desnoyers, *et al.*, have been compared with ΔF_{tr} values obtained for APE. In addition, ΔF_{tr} values of benzene around 1 *M* from recent studies of Wirth and LoSurdo have also been compared with the transfer values of APE at the same interpolated salt concentration (A. LoSurdo, personal communication).[18]

The results show that the transfer of AnVE and AnLE to larger tetraalkylammonium salt solutions is energetically more favorable than transfer of propane and butane, respectively, whereas in lower tetraalkyl salts (where AnLE has only been studied) the reverse is true. In contrast, APE is always energetically less favorable than benzene for the transfer to all R_4NBr solution by a considerable amount (by 350 to 700 cal/mol with the increase in the number of alkyl groups in the salt). The contribution due to the polar backbone $CH_3CONHCHCOOC_2H_5$, which would influence the overall ΔF_{tr} of the ester molecules, is not known with certainty. Saito, *et al.*, have shown that urea is salted in in R_4NBr solution.[19] Our previous result has shown that the (CH_2CONH) group is energetically favored by −30 cal/mol for the transfer from water to 1 *M* Me_4NBr solution although the transfer of acetylglycine ethyl ester, $CH_3CONHCH_2COOC_2H_5$, which is expected to resemble the backbone of the compounds studied here more than any other compound or group, is energetically unfavorable by 80 cal under similar condition.[10] This can possibly explain the value of ~0 cal/mol for the transfer of AnLE around 1 *M* Me_4NBr solution. Robinson and Jencks found that acetyltetraglycine ethyl ester is salted in with increase in the size of the alkyl groups in the salts.[16] The polar backbones of the compounds studied here may therefore find themselves salted in in a larger tetraalkyl salt solution, which probably explains the more negative ΔF_{tr} values of AnVE and AnLE than of propane and butane respectively in these solutions. The foregoing consideration, however, can not be applied to explain the results of APE and benzene. A transfer value of −300 cal more for benzene than APE in 1 *M* Me_4NBr can not be explained by the unfavorable contribution of 80 cal of the backbone in APE in this salt solution as mentioned above. Further, if it is assumed that the CH_2 group which links the phenyl group to the polar backbone in APE would make similar contribution as the CH_2 group obtained from the difference of transfer values of AnLE and AnVE, then ΔF_{tr} value of APE should have been at least 175 cal/mol more favorable than benzene molecule for the transfer to 1 *M* Bu_4NBr solution (where the relevant data are available), since as has been already pointed out, the backbone would be favorably disposed in Bu_4NBr solution. In fact benzene is 500 cal more favorable for the process at 1 *M*. These considerations indicate that the contributions of nonpolar and polar components in these compounds are not additive toward the transfer process in tetraalkylammonium salt solution.

Another significant observation in this study is that APE is transferred much more favorably than AnVE and AnLE. That this results primarily due to the difference in the aromatic and aliphatic groups is borne out by the comparison of the transfer values of alkane and benzene at comparable salt concentrations obtained from the studies of Wen and Hung, Wirth and LoSurdo, and LoSurdo (personal communication), also presented in the Table III.[2a,18] In addition a ΔF_{tr} value of −2500 cal/mol for the transfer of naphthalene to 1 *M* Bu_4NBr solution suggests that, in general, aromatic molecules or groups are responsible for the large favorable free energy of transfer to R_4NBr solution.[20]

Mechanism of Salt Effects

Qualitative similarity in the results between the esters ARE and nonpolar gases suggests that a similar mechanism is operative in both.[11] Electrostatic theories of salting behavior developed by Debye and Kirkwood and modified later by others, which relate change in the dielectric constant with the salting behavior, predict salting out of nonpolar compounds in all salt solutions and obviously fail to explain salting in of nonpolar gases in R_4NBr solution.[14] The internal pressure theory of McDevit and Long envisages a salt induced medium effect and predicts both salting in and its increase with the increase in the size of alkyl groups in the salt for both polar and nonpolar nonelectrolytes in R_4NBr solution. This has been explained as due to the negative electrostriction of the solvent water caused by the tetraalkyl ions.[21,22] However, Ben-Naim's observation that argon is salted *out* in tetraalkylammonium halide solution shows the limited applicability of the concept.[23] The third approach is the explanation based on the change in the water structure caused by the ions.[22,24] It is conceivable that any modification of water structure would be reflected in the salting parameters. The way in which R_4N^+ ions affect the water structure is still uncertain; the viscosity *B* coefficient and dielectric relaxation time show that these ions promote water structure; Kay, *et al.*, have concluded that Me_4N^+ breaks and Pr_4N^+ and Bu_4N^+ promote the structure whereas Et_4N^+ has no effect on water structure.[25] Recent pmr measurements by LoSurdo and Wirth show that all four R_4NBr salts are water structure breakers a conclusion arrived at earlier by

shift in proton resonance, proton relaxation rates, and ir measurements.[26-28] Therefore explanation of the effects of R_4NBr salts on the solubilities of solutes based on the effects of these salts on water structure can only be attempted when and if an unambiguous picture arises regarding the effects of these salts on the structure of water.

The inability of the indirect effect of the salts on the solvent water to explain the observed salting in behavior of the model peptides studied in tetraalkylammonium salt solutions suggests the phenomenon may be caused by some direct interaction. The increase in the solubility of the compounds may result from an association of these compounds with the salts. The thermodynamic parameters obtained from the temperature derivative of the activity coefficient are revealing about the mechanism of association and have been presented in Table IV.

The endothermic nature of the reaction suggests that the process is entropy driven with larger R_4NBr and at least in the temperature range 0-25° for the lower derivatives. These parameters suggest the presence of a hydrophobic bond between the salts and ARE. Limited studies at different temperatures led Wen and Hung to conclude the existence of a hydrophobic bond between alkanes and R_4NBr, the strength of bond increases with increase in the size of both salt and hydrocarbon.[2a] The micellization of nonionic detergents has been explained as hydrophobic bond formation between the nonpolar moieties and are associated with similar ΔH and ΔS values as we have observed in our study.[29] This indicates that most probably the nonpolar side chains of ARE are involved in hydrophobic bond formation with R_4NBr. The values of ΔH and ΔS in Me_4NBr solutions in the temperature interval 25-40° find similarity with the observation made by Schick who found that the enthalpy and entropy of micellization of detergents change from positive to negative values with increase in temperature.[30]

The hydrophobic interaction described above does not indicate whether an equilibrium of the type $a\text{ARE} + bR_4N^+ \rightleftharpoons \text{ARE}_a\text{-}R_4N_b^+$, having a definite stoichiometric interaction exists or whether ARE reacts with aggregates or micelles of R_4NBr.[31] The presence of micelles in R_4NBr solution except in Me_4NBr has been reported.[32,33] The relative rapid increase in the solubility of benzene above particulars concentrations of tetraethyl-, tetrapropyl-, and tetrabutylammonium bromide solutions has been suggested to result from its increased solubility in the micelles of these salts.[17,18] A similar rapid increase in the solubility, although to a reduced extent, is observed with the esters which suggests their possible interaction with the micelles in tetrapropyl and tetrabutyl salt solutions.

However, the following experimental observations remain inexplicable if the interaction of the compounds with only micelles is considered. It is known that added solutes affect the cmc values; although it may be expected that the same set of solutes *viz.*, esters and benzenes, would affect the cmc values of the micelles of these salts similarly, in Bu_4NBr the cmc value is observed to rise from 0.039 to 0.8-1 *M* where as in Pr_4NBr the cmc value either remain unaffected or decrease as indicated by the rapid rise in the solubilities of these compounds in these salt solutions. Secondly, comparison of the transfer values of alkanes and benzene from water to liquid paraffin, as compiled by Kauzmann, shows that the former is energetically more favorable than benzene for the transfer process.[34] Since the miceller core formed from the alkyl groups of R_4NBr would be expected to resemble liquid aliphatic hydrocarbon, the transfer of at least larger hydrocarbon butane to tetrapropyl- and tetrabutylammonium bromide solutions should have been energetically more favorable than the same process for benzene;[35] experimentally observed ΔF_{tr} values are just opposite to the above contention (Table III) which points out that the observed increased solubility of nonelectrolytes probably cannot be attributed to their interaction with micelles. Frank has argued that aggregated species which are formed from quasispherical R_4N^+ ions should not be described as micelles since they would structurally differ very much from the classical Hartley micelles.[36] Tamaki observed no break in the surface tension *vs.* molarity curves of Bu_4NBr solution which can be attributed to micelle formation as reported by Lindenbaum and Boyd.[33,37] Recently LoSurdo and Wirth from pmr and apparent molar volume data observed the presence of aggregates the composition of which varies with the concentration of tetraalkylammonium salts and suggest that these aggregates are established by "coulombic hydrophobic cation-cation" interaction.[26,28] From all this we suggest the interaction of the compounds studied here with the aggregates (particularly of the higher salts) is responsible for the observed salting behavior of the salts and the complex is stabilized by hydrophobic interaction.

TABLE IV: Enthalpy and Entropy of the Association Reaction between ARE and R_4NBr salts[a]

Compound	Salt	ΔH, kcal/mol		ΔS, eu at 25°	
		a	b	c	d
	Me_4NBr	3.5	−0.8	12.1	0
	Et_4NBr	4.5	0.9	16.1	4
APE	Pr_4NBr	5.3	4.7	19.5	17.4
	Bu_4NBr	4.3	2.1	18.4	11.1
AnLE	Bu_4NBr		5.8		21.5
AnVE	Bu_4NBr		4.6		16.8

[a] a and b are the values in the range 0–25 and 25–40°, respectively. c and d are the entropy values obtained by using a and b, respectively.

As has been mentioned earlier, the more favorable energetic of the transfer of the aromatic moieties compared to the aliphatic ones may arise from the interaction of the positive charge with the π electrons of the former in a relatively nonpolar environment (formed by the associated complex).[38] Further, a less restricted orientation of benzene molecules in the associated complex compared to the molecule with aromatic moiety attached to the peptide backbone may be responsible for more favorable free energy of transfer of benzene to R_4NBr solutions.

Application of the Observed Effects of R_4NBr on Model Peptides to Protein. von Hippel and Wong from their study of the effects of various chemical reagents, in which tetraalkylammonium bromide solutions were also included, suggested that a change in structure of solvent water surrounding the macromolecule rather than a direct binding between the denaturant and protein molecule is responsible for the observed unfolding of protein.[3] von Hippel and Wong view that denaturants by imposing their own brand of effect on water structure reduce the effective availability of water for "iceberg" formation (around the nonpolar groups, which originally prevented exposure of these groups to the surrounding solvent due to entropic reason), thereby facilitating the exposure of nonpolar groups and denaturing the protein. von Hippel and Schleich have extended the preceeding view where they suggest that the *extent* rather than the *type* of water

structure reorganization would determine the effect of chemical denaturants on the free energy of transfer of relevant groups from the interior of the protein to the solvent and hence the stability of the native protein molecule in these solutions.[39] Worley and Klotz from near-ir measurements showed that both $NaClO_4$ and Bu_4NBr at comparable concentrations change the water structure about the same extent, although in the opposite direction (the former breaks and the latter promotes the water structure; see, however, the mechanism section above); von Hippel and Schleich observed that both the salts affect melting temperature, T_m, of ribonuclease by the same amount at 1 M salt concentration.[39,40] Based on the von Hippel–Schleich concept one can expect the values of free energy of transfer of AnVE, AnLE, and APE from water would be same in 1 M $NaClO_4$ and Bu_4NBr; the values are ~75 cal/mol for all the esters for the process to 1 M $NaClO_4$ compared to −465, −640, and −1200 cal/mol, respectively, for AnVE, AnLE, and APE in 1 M Bu_4NBr solution which question the validity of the concept.[41]

Threlkeld, *et al.*, ultracentrifugally determined the binding of tetramethyl- and tetrabutylammonium bromides with gelatin and observed that the binding of R_4N^+ ions to the protein is primarily responsible for the denaturation of collagen in these salt solutions.[9] They did not, however, point out how R_4N^+ ions bind to the protein.

The present result of model peptides shows that R_4N^+ forms "hydrophobic bond" with the nonpolar aliphatic and aromatic side chains. It is suggested that these ions will interact with similar side chains in protein molecule, competing with the hydrophobic bond present in its interior, thereby stabilizing the denatured form of the protein by formation of a hydrophobic bond with the exposed side chains.

Acknowledgment. I am grateful to Dr. D. R. Robinson, Massachusetts General Hospital, Boston, for providing me necessary facilities to carry out most of the work. Financial assistance in the form of a Fulbright travel grant and Scientific Pool Officer, CSIR, India, is gratefully acknowledged.

References and Notes

(1) Address correspondence to the Protein Technology Discipline, Central Food and Technological Research Institute, Mysore 13, India.
(2) (a) W. -Y. Wen and J. H. Hung, *J. Phys. Chem.*, **74**, 170 (1970); (b) A. LoSurdo and H. E. Wirth, *ibid.*, **76**, 1333 (1972).
(3) P. H. von Hippel and K. Y. Wong, *Biochemistry*, **1**, 664 (1962); **2**, 1387 (1963); *J. Biol. Chem.*, **240**, 3909 (1965).
(4) K. Hamaguchi and E. P. Geiduschek, *J. Amer. Chem. Soc.*, **84**, 1329 (1962).
(5) K. M. Krupka, *Biochemistry*, **4**, 429 (1965); **5**, 1988 (1966).
(6) J. C. Warren, L. Stowring, and M. F. Morales, *J. Biol. Chem.*, **241**, 309 (1966).
(7) C. E. Smith and M. A. Lauffer, *Biochemistry*, **6**, 2457 (1967).
(8) J. T. Shapiro, B. S. Stannard, and G. Felsenfeld, *Biochemistry*, **8**, 3233 (1969).
(9) J. O. Threlkeld, J. J. Burke, D. Puett, and A. Cifferi, *Biopolymers*, **6**, 767 (1968).
(10) P. K. Nandi and D. R. Robinson, *J. Amer. Chem. Soc.*, **94**, 1299 (1972).
(11) P. K. Nandi and D. R. Robinson, *J. Amer. Chem. Soc.*, **94**, 1308 (1972).
(12) J. P. Wolf, III, and C. Nieman, *Biochemistry*, **2**, 493 (1963).
(13) F. A. Long and W. F. McDevit, *J. Chem. Soc.*, **74**, 1773 (1952).
(14) F. A. Long and W. F. McDevit, *Chem. Rev.*, **51**, 119 (1952).
(15) D. R. Robinson and W. P. Jencks, *J. Amer. Chem. Soc.*, **87**, 2462 (1965).
(16) D. R. Robinson and W. P. Jencks, *J. Amer. Chem. Soc.*, **87**, 2470 (1965).
(17) J. E. Desnoyers, G. E. Pelletier, and C. Jolicoeur, *Can. J. Chem.*, **43**, 3232 (1965).
(18) H. E. Wirth and A. LoSurdo, *J. Phys. Chem.*, **72**, 751 (1968).
(19) S. Saito, M. Lee, and W. Y. -Wen, *J. Amer. Chem. Soc.*, **88**, 5107 (1966).
(20) J. E. Gordon and R. L. Thorne, *J. Phys. Chem.*, **71**, 4390 (1967).
(21) N. C. Deno and C. H. Spink, *J. Phys. Chem.*, **67**, 1347 (1963).
(22) W. P. Jencks, "Catalysis in Chemistry and Enzymology," McGraw-Hill, New York, N. Y., 1969.
(23) A. Ben-Naim, *J. Phys. Chem.*, **71**, 1137 (1967).
(24) R. W. Gurney, "Ionic Processes in Solution," McGraw-Hill, New York, N. Y., 1953.
(25) R. L. Kay, T. Vituccio, C. Zawoyski, and D. F. Evans, *J. Phys. Chem.*, **70**, 2336 (1966).
(26) R. L. Kay, *Advan. Chem. Ser.*, **No. 73**, 14 (1968).
(27) K. A. Hartman, *J. Phys. Chem.*, **70**, 270 (1966).
(28) A. LoSurdo and H. E. Wirth, *J. Phys. Chem.*, **76**, 130 (1972).
(29) J. M. Corkill, J. F. Goodman, and J. R. Tate, *Trans. Faraday Soc.*, **60**, 996 (1964).
(30) M. J. Schick, *J. Phys. Chem.*, **67**, 1796 (1963).
(31) E. F. J. Duynstee and E. Grunwald, *Tetrahedron*, **21**, 2401 (1965).
(32) H. E. Wirth, *J. Phys. Chem.*, **71**, 2922 (1967).
(33) S. Lindenbaum and G. E. Boyd, *J. Phys. Chem.*, **68**, 911 (1964).
(34) W. Kauzmann, *Advan. Protein Chem.*, **14**, 1 (1959).
(35) After the completion of the manuscript some experimental results appeared which support the contention made. K. A. Robillard, Jr., and A. Wishnia (*Biochemistry*, **11**, 3835 (1972)) observed that free energy of transfer of butane, pentane, and toluene from water to sodium dodecyl sulfate micelle are −5.01, −5.82, and −4.84 kcal/mol, respectively. The transfer value of a CH_2 group obtained from differences of pentane and butane values when subtracted from the transfer value of toluene gives −4 kcal/mol for the free energy of transfer of benzene to sodium dodecyl sulfate micelle.
(36) H. S. Frank, *Z. Phys. Chem. (Leipzig)*, **228**, 364 (1965).
(37) K. Tamaki, *Bull. Chem. Soc. Jap.*, **40**, 38 (1967).
(38) P. Molyneux and H. P. Frank, *J. Amer. Chem. Soc.*, **83**, 3169, 3175 (1961).
(39) P. H. von Hippel and T. Schleich in "Structure and Stability of Biological Macromolecule," Vol. II, S. N. Timasheff and G. D. Fasman, Ed., Marcel Dekker, New York, N. Y., 1969.
(40) J. D. Worley and I. M. Klotz, *J. Chem. Phys.*, **45**, 2868 (1969).
(41) The values of the transfer to $NaClO_4$ solution have been taken from our previous data.[11]

Dielectric Polarization of Dilute Associating Solutions. V. Solvation of Alcohols in Nondipolar Solvents[1]

J. Małecki* and J. Jadżyn

Laboratory of Molecular Interactions, Institute of Physics, Polish Academy of Sciences, 60-179 Poznan, Smoluchowskiego 17/19, Poland *(Received November 12, 1973)*

Results on dipole polarization of solutions of alcohols in saturated hydrocarbons in the low concentration range up to 5 mol % are presented. In the range of 0.1 to 2 mol % a constant value of the polarization is observed. In this range, also, thermodynamic and nmr anomalies, observed by others, corroborate a strong deviation from the ideal association model. For an explanation of the experimental facts, a model is proposed which takes into account solvation of alcohol molecules by those of the nondipolar solvent (in addition to association). This model attempts to explain the dependence of the polarization on the concentration and temperature as well as the differences for the hydrocarbons investigated. The number of solvent molecules, solvating a molecule of alcohol, can be of the order of 10^2 near the melting temperature of the solvent pointing to the presence of two coordination spheres. At room temperature solvation is very well apparent in cyclohexane and *n*-tridecane, but nearly imperceptible in *n*-hexane.

Introduction

Research on association processes of alcohols and phenols in nondipolar solvents is proceeding in many places.[2-21] Notwithstanding the various techinques employed, the problem still remains unsolved. Opinions diverge widely as to the structure of the multimers arising in these processes and as to the values of the equilibrium constants accounting for the successive steps of the association process. Good agreement with experiment is in some cases achieved by assuming a single kind of multimers, *e.g.*, tetramers,[14,22] although a process of this kind would hardly appear plausible.

Parts I–IV[1] contain results concerning the dielectric polarization of dilute solutions of butanols in cyclohexane, *n*-hexane, and *n*-tridecane and of phenol in cyclohexane in the concentration range of $f_2 \leq 5$ mol % of the alcohol ($f_i = N_i/(N_1 + N_2)$, $i = 1,2$, is the nominal concentration of the ith component in mole fraction) at temperatures of 10, 20, 30, 40, and 50°. The experimental procedure is described in detail elsewhere.[1]

The earliest systematic investigation of the dielectric polarization of very dilute cyclohexane solutions of alcohols by Ibbitson and Moore[23] has already revealed certain unexpected properties. At concentrations ranging from 0.1 to 2 mol %, the polarization of the alcohol remained practically constant, independent of concentration, and equal to that of the monomers. These results, corroborated by ir absorption studies,[23] suggested the existence of a concentration range in which association is hindered. This conclusion, however, is at variance with the generally accepted model of ideal association.

Independently, in the same range of concentrations, such unusual properties were detected in solutions of alcohols by Wóycicka, *et al.*,[24,25] in thermodynamical studies, and by Dixon[22] in nmr measurements of chemical shift. The partial molar enthalpy as well as the chemical shift exhibit unexpectedly a point of inflection in the concentration range of 0.1–2 mol %.

Aiming at an explanation of this highly interesting behavior of the solutions, we propose here a model taking into account, besides equilibria between monomers, dimers, and trimers, solvation of the monomers of the alcohol by a nondipolar solvent.

Experimental Results

We shall express the dipolar polarization of the alcohol P_2^{dip} in units of polarization on the monomer

$$R_p = \frac{P_2^{dip}}{P_{mon}^{dip}} = \frac{\langle \mu^2 \rangle}{\mu_{mon}^2}$$

Values of P_2^{dip} are calculated from experimental data using Debye's formula which, for so highly dilute solutions, yields practically the same results as that of Onsager. The details of the calculations leading to P_2^{dip} and R_p are found in part I.[1]

Figure 1 shows the experimental concentration dependence of R_p for solutions of 1-butanol in cyclohexane at 10, 20, 30, 40, and 50°. The curves for 2-butanol and 2-methyl-2-propanol in cyclohexane[1] are similar. Figure 2 shows $R_p(f_2)$, at 20°, for 1-butanol in *n*-hexane, cyclohexane, and *n*-tridecane, whereas Figure 3 shows $R(f_2)$, at 20°, for the 1-butanol, 2-butanol, 2-methyl-2-propanol, and phenol in cyclohexane. The full experimental data as well as the concentration dependence of the dielectric permittivity and density of the solutions are given in parts I–IV.[1]

In all the systems investigated similar curves were obtained, revealing two distinct regions. The first region, defined in Figures 3 and 7 as comprising the concentrations $0 \leq f_2 \leq L$, is characterized to within experimental error by a constant value of the polarization. The second region, covering higher concentrations $f_2 > L$, is characterized by a decrease in polarization. The ensuing discussion will concern the width of the region L specific to the phenomenon under investigation and coincident with the inflection region of the concentration-dependent curves of partial molar enthalpy[24,25] and chemical shift.[22]

From the experimental results (Figures 1–4), the following conclusions can be drawn: (1) the width of the region L is strongly temperature dependent (Figures 1 and 4); (2) the width of the region L is strongly dependent on the solvent, notwithstanding the fact that all solvents used were saturated hydrocarbons (Figure 2); (3) the

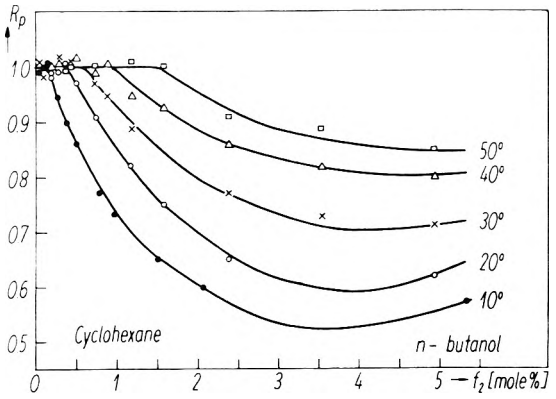

Figure 1. Dipole polarization R_p of solutions of 1-butanol in cyclohexane *vs.* concentration and temperature.

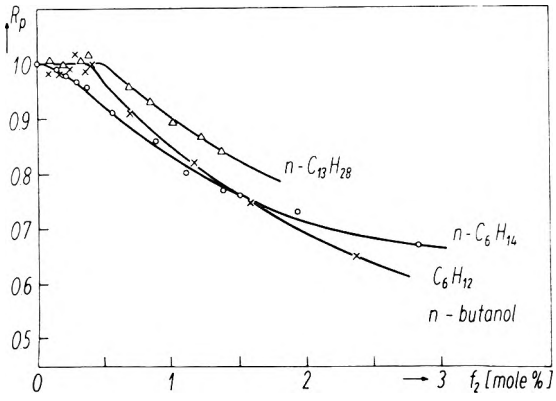

Figure 2. R_p *vs.* f_2, at 20°, for solutions of 1-butanol in *n*-hexane (O), *n*-tridecane (△), and cyclohexane (×).

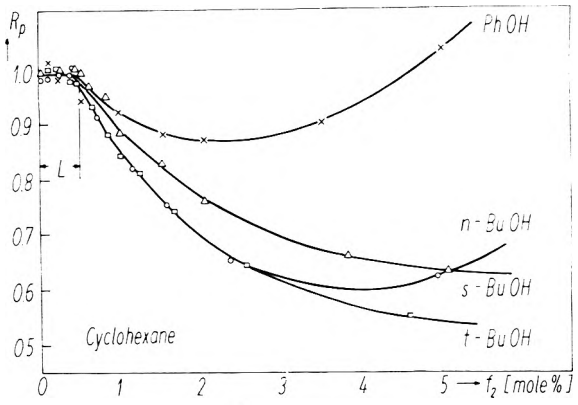

Figure 3. R_p *vs.* f_2, at 20°, for solutions of 1-butanol (O), 2-butanol (△), 2-methyl-2-propanol (□), and phenol (×) in cyclohexane.

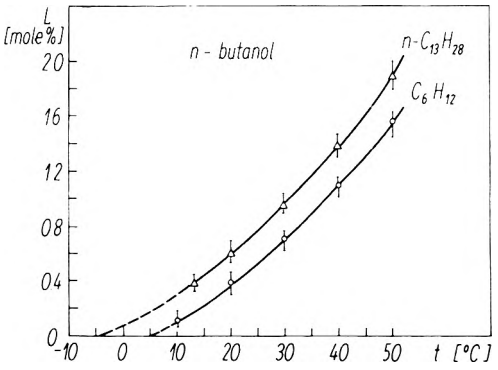

Figure 4. The region L (in units of the concentration f_2) as a function of temperature for solutions of 1-butanol in *n*-tridecane (△) and cyclohexane (O).

width of the region L is, to within experimental error, independent of the associating compound, notwithstanding the fact that the solutes used differed strongly in their ability to associate (1-butanol, 2-methyl-2-propanol, phenol, Figure 3).

Theoretical Model

The dipole polarization of an associating compound is usually considered to represent the polarization of a mixture of multimers; in our notation[8]

$$R_p = \frac{\langle \mu^2 \rangle}{\mu_{mon}^2} = \frac{1}{\mu_{mon}^2} \sum_{h,i} x_{hi} \frac{\mu_{hi}^2}{i} \tag{1}$$

where the summation extends over all the complexes present in the solution, μ_{hi} is the dipole moment of a complex of h molecules of the solvent and i molecules of the associating substance, whereas

$$x_{hi} = iN_{hi}/N_2$$

is the concentration of the h,i-fold complex, N_{hi} the number of such complexes in the solution, and $N_2 = \Sigma_{h,i} iN_{hi}$ that of molecules of the associating substance.

According to eq 1, the region L, characterized by a constant value of the polarization, can exist in the case of association only if the contributions to polarization from the open and ring multimers mutually cancel out to ensure fulfillment of the condition $\langle \mu^2 \rangle = \mu_{mon}^2$ throughout L. This, however, would appear to be an exception rather than the rule. Nor would such mutual compensation explain the thermodynamic anomalies[24] and nmr results.[22] A change in temperature ought to destroy the compensation, but no such effect is, in fact, observed. Finally, the fact that the width of region L is independent of the nature of the associating substance is a strong argument against compensation. One is thus led to the conclusion that *the association process of dilute solutions is subject to a perturbation by some additional factor* and that, contrary to expectation, dilute solutions deviate considerably from the ideal association model.

We propose, in order to explain the experimental facts, that the monomers of the alcohol are solvated by the nondipolar solvent. Since we are dealing with dilute solutions, we omit tetramers and higher multimers and restrict our considerations to the formation of dimers and trimers. We consequently write the following set of equilibrium equations between monomers, dimers, and trimers of the alcohol and molecules of the solvent

$$\begin{aligned} A_1 + nS &\rightleftharpoons S_nA_1 & K_s^n \\ A_1 + A_1 &\rightleftharpoons A_2 & K_2 \\ A_1 + A_2 &\rightleftharpoons A_3 & K_3 \end{aligned} \tag{2}$$

Since the number n of solvent molecules in a complex can be quite considerable, we shall henceforth be referring to it as *a solvate*.

The equilibrium constants are expressed in the usual way in terms of true molar fractions

$$\begin{aligned} K_2 &= \gamma a_2/a_1 \\ K_3 &= \gamma a_3/a_2 \\ K_s^n &= \delta^n a_n/a_1 \\ a_1 + 2a_2 + 3a_3 + a_n &= 1 \end{aligned} \tag{3}$$

The quantities a_i and the previously introduced concen-

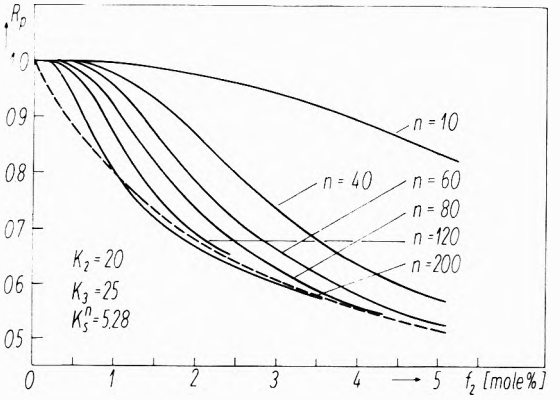

Figure 5. Theoretical curves of R_p *vs.* f_2 and n (the number of solvating molecules of the solvent), at constant $K_2 = 20$, $K_3 = 25$, and $K_s^n = 5.28$ ($\Delta F_s = -1$ kcal/mol). The dashed curve shows $R_p(f_2)$ for the traditional association model ($K_s = 0$, $n = 0$).

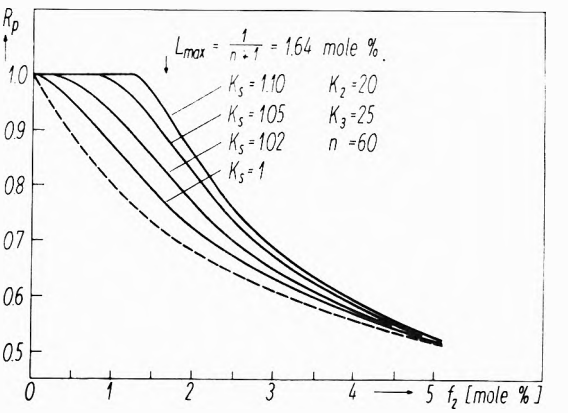

Figure 6. Theoretical curves of $R_p(f_2)$ at constant $K_2 = 20$, $K_3 = 25$, and $n = 60$. The variable parameter is K_s. The dashed curve has the same meaning as in Figure 5.

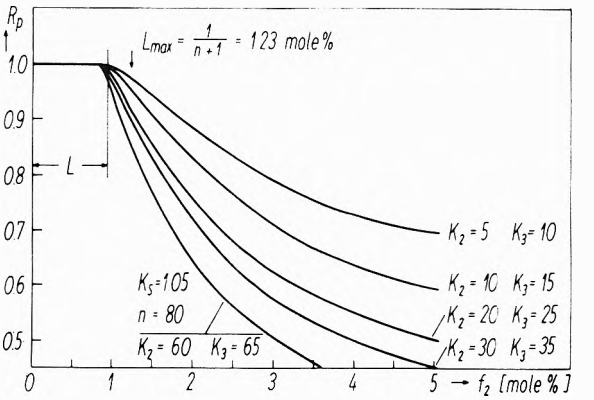

Figure 7. Theoretical curves of $R_p(f_2)$ at constant $K_s = 1.05$ and $n = 60$. Variable parameters are the association constants K_2 and K_3.

trations x_{hi} are related as follows

$$a_i = x_{0i}/i$$
$$a_n = x_{n1} \quad i = 1, 2, 3 \tag{4}$$

whereas

$$\gamma = \frac{\eta}{f_2 a_1}$$
$$\delta = \frac{\eta}{f_1 - n f_2 a_n}$$
$$\eta = f_1 + f_2[a_1 + a_2 + a_3 + (1 - n)a_n] \tag{5}$$

The set of eq 3, the parameters of which are given by the equilibrium constants K_1, K_2, and K_s as well as the number n of solvent molecules in the solvate, is resolvable numerically. The solutions a_i of eq 3 were used together with eq 1 and 4 for the calculation of theoretical $R_p(f_2)$ curves. To this aim, we assumed a dipole moment of the solvate $\mu_{n1} = \mu_{mon}$ and dimer and trimer moments amounting to $\mu_{02} = 0.8\mu_{mon}$ and $\mu_{03} = 0$. The calculations were performed by an Odra 1013 computer.

Figure 5 shows the theoretical curves $R_p(f_2)$ at the constant values $K_2 = 20$, $K_3 = 25$, and $K_s^n = 5.28$ ($\Delta F_s = -1$ kcal/mol), with n varying. The dashed curve is that of $R_p(f_2)$ for $K_s = 0$, $n = 0$, *i.e.*, for the traditional association model. Figure 6 shows curves of $R_p(f_2)$ with K_s as the variable parameter, the others being $K_2 = 20$, $K_3 = 25$, and $n = 60$. The meaning of the dashed curve is the same as in Figure 5. Finally, Figure 7 shows curves of $R_p(f_2)$ and their dependence on the association constants K_2 and K_3 at constant $n = 60$ and $K_s = 1.05$.

Conclusions

The preceding calculations, shown in the graphs of Figures 5–7, show that the model including solvation provides an explanation of the region L of constant polarization. In particular, these calculations permit the following statements: (1) the width of the region L depends strongly on n (Figure 5), and on K_s (Figure 6); (2) the width of the region L is practically independent of the association constants K_2 and K_3 even if the latter vary widely (Figure 7). These conclusions are readily put in correlation with the previously stated conclusions from the experimental facts. The experimental strong dependence of the region L on the temperature and solvent is a result of the dependence of L on K_s and n. The experimental fact that L is independent of the nature of the associating substance results directly from our model, in which L is practically independent of the association constants K_2 and K_3. Hence, in order to explain the experimental results, only the two parameters K_s and n have to be fitted. However, K_2 and K_3 were constant at 20 and 25, respectively, in most of our calculations. This choice of association constants was based on attempts to determine these quantities from the study of nonlinear dielectric effects.[8] With regard to the high error of that method, however, $K_2 = 20$ and $K_3 = 25$ are no more than rough assessments, though this is irrelevant to our conclusions because L is independent of K_2 and K_3.

It results from eq 5 that $nf_2a_n < f_1$. Hence, as a_n tends to unity with $K_s \rightarrow \infty$, the width of the region L has to satisfy the condition

$$L < 1/(n + 1) \tag{6}$$

Figures 6 and 7 show the maximal width of L. Thus, with growing n, the anomalous region L shrinks and becomes more difficult to detect experimentally. On the other hand, with decreasing n, the region L expands, simultaneously becoming increasingly diffuse, so that for $n \leq 10$ it is practically no longer distinguishable (Figure 5). There exists but one interval of n values where a region L is markedly present and experimentally detectable. Our calculations show that this is the case for the interval $20 < n < 200$. Such large values of n are astonishing and point to the presence of at least two solvation spheres.

We draw yet another conclusion from condition 6. Obviously, a decrease in temperature has to cause a rise in n,

and at the melting point $n \to \infty$. Hence, the point of intersection of the $L(T)$ curve and the temperature axis should define the melting temperature of the solvent. The curves of Figure 4 appear to confirm this. The lack of a well-defined L region in the case of n-hexane (Figure 2) is probably due to the fact that the measurements were carried out at temperatures considerably above the melting point, which in the occurrence amounts to $-94.3°$; consequently, the values of n and K_s are small, and the L region unapparent.

The model proposed here, by taking into account, in addition to association, solvation of the alcohol molecules by those of the nondipolar solvent, succeeds in explaining the anomalous shape of the dipole polarization of alcohols in the range of low concentrations (0-2 mol %). The model permits a qualitative explanation of the experimental temperature dependence of polarization as well as the differences observed for the alochols and hydrocarbons investigated. The number n of solvent molecules, solvating a dipolar molecule, can attain an unexpectedly high value of the order of 10^2, suggesting the presence of two coordination spheres. Such a situation exists near the melting temperature t_m of the solvent. At room temperature, solvation is very marked in the case of cyclohexane ($t_m = 6.5°$) and n-tridecane ($t_m = -6.2°$), but practically unobservable in that of n-hexane ($t_m = -94.3°$).

References and Notes

(1) Parts I-IV: J. Jadżyn, J. Małecki, K. Prafat, P. Kedziora, and J. Hoffmann, *Acta Phys. Polon.*, submitted for publication.
(2) P. Bamelis, P. Huyskens, and E. Meeusser, *J. Chim. Phys.*, **62**, 158 (1965).
(3) H. Wolff and H. E. Hoppel, *Ber. Bunsenges. Phys. Chem.*, **72**, 710, 722 (1968).
(4) G. E. Rajala and J. Crossley, *Can. J. Chem.*, **49**, 3617 (1971); 50 99 (1972).
(5) J. Crossley, L. Glasser, and C. P. Smyth, *J. Chem. Phys.*, **55**, 2197 (1971).
(6) L. Glasser, J. Crossley, and C. P. Smyth, *J. Chem. Phys.*, **57**, 3977 (1972).
(7) K. Sosnkowska-Kehiaian, W. Rečko, and W. Wóycicki, *Bull. Acad. Polon. Sci., Ser. Sci. Chim.*, **14**, 475 (1966).
(8) J. Małecki, *J. Chem. Phys.*, **43**, 1351 (1965); *Acta Phys. Polon.*, **28**, 891 (1965); **29**, 45 (1966).
(9) J. Biais, B. Lemanceau, and C. Lussan, *J. Chim. Phys.*, **64**, 1019, 1030 (1967).
(10) W. Storek and H. Kriegsmann, *Ber. Bunsenges. Phys. Chem.*, **72**, 706 (1968).
(11) J. J. Bellamy and R. J. Pace, *Spectrochim. Acta*, **22**, 525 (1966); J. J. Bellamy, K. J. Morgan, and R. J. Pace, *ibid.*, **22**, 535 (1966).
(12) P. Bordewijk, M. Kunst, and A. Rip, *J. Phys. Chem.*, **77**, 548 (1973).
(13) T. S. S. R. Murty, *Can. J. Chem.*, **48**, 184 (1970).
(14) A. N. Fletcher and C. A. Heller, *J. Phys. Chem.*, **71**, 3742 (1967).
(15) A. N. Fletcher, *J. Phys. Chem.*, **73**, 2217 (1969); **74**, 216 (1970).
(16) C. Brot, *J. Chim. Phys.*, **61**, 139 (1964).
(17) P. Huyskens and F. Cracco, *Bull. Soc. Chim. Belg.*, **69**, 422 (1960).
(18) P. Huyskens, G. Gillerot, and Th. Huyskens, *Bull. Soc. Chim. Belg.*, **72**, 666 (1963).
(19) P. Huyskens, R. Henry, and G. Gillerot, *Bull. Soc. Chim. Fr.*, 720 (1962).
(20) J. Malecki and Z. Dopierala, *Acta Phys. Polon.*, **36**, 385, 401, 409 (1969).
(21) A. Weisbecker, *J. Chim. Phys.*, **64**, 297 (1967).
(22) W. B. Dixon, *J. Phys. Chem.*, **74**, 1396 (1970).
(23) D. A. Ibbitson and L. F. Moore, *J. Chem. Soc. B*, 76, 80 (1967).
(24) K. M. Wóycicka and W. M. Rečko, *Bull. Acad. Polon. Sci., Ser. Sci. Chim.*, **20**, 783 (1972).
(25) K. M. Wóycicka and B. Kalinowska, *Bull. Acad. Polon. Sci., Ser. Sci. Chim.*, in press.

A Theory of Molecular Association in Cholesteric-Nematic Liquid Crystal Mixtures

John M. Pochan* and DarLyn D. Hinman

Xerographic Technology Department, Xerox Corporation, Webster, New York 14580

(Received January 17, 1974)

Publication costs assisted by Xerox Corporation

A theory based on molecular association is proposed to explain reflective pitch measurements in cholesteric-nematic mixtures. It is shown that pitch in a series of mixtures can be theoretically predicted using an inverse pitch relationship $[1/\lambda_T = \Sigma_i X_i/\lambda_i]$ with two variables; the number of nematic molecules associated with a given cholesteric molecule, and the reflective pitch of the pure complex material. Some mixtures are totally characterized by keeping the reflective pitch of the pure complex constant and varying the complex number. The method appears to be totally applicable for optically active nonmesomorphic materials in nematics as well as chiral nematics in nematics.

Introduction

Liquid crystals are a unique state of matter exhibiting optical properties of crystalline materials (birefringence) and rheological properties of liquids (relatively low viscosities). One liquid crystalline state, the cholesteric, also exhibits enhanced optical rotatory power over optically active monomeric units comprising the phase, *i.e.*, the ability to rotate a plane of polarized light is much greater than the additive sum of the individual components comprising the aggregated helical structure of this mesophase. In addition, the optical activity manifests itself in the ability of the Grandjean texture of the mesophase to selectively reflect one component of circularly polarized light.[1]

Saeva and Wysocki have recently shown[2] that the electronic transitions in these systems are affected by the asymmetric electronic field caused by the cholesteric helical aggregate which results in the observation of extrinsic circular dichroism (CD). It has also been shown[2,3] that the electronic transitions of molecules dissolved in the

cholesteric mesophase become circularly dichroic (liquid crystal induced circular dichroism (LCICD)). In addition, the reflective pitch band of the cholesteric system is altered by the addition of a nonactive component.

The most obvious case of this latter phenomena is the addition of (*p*-methoxybenzylidene)-*p*-*n*-butylaniline (MBBA), a room temperature nematic material, to a variety of cholesterol derivatives. One example of this is the MBBA-cholesteryl chloride system,[2] which exhibits a compensation point at intermediate compositions. This type of behavior indicates that the added nematic can not be considered as an inert diluent in these mixtures, but rather as a material whose optical activity is dependent on the second component in the mixture. Adams and Haas have shown[4] that the characteristic reflective pitch band of mixed cholesterics and nematic-cholesteric mixtures can be described by

$$\frac{1}{\lambda_T} = \sum_i \frac{\alpha_i}{\lambda_i} + f(\alpha_1, \alpha_2 \text{etc}) \qquad (1)$$

where λ_T is the reflective pitch of the mixture, α_i the weight fraction of each component, and λ_i the reflective pitch of the pure component i. Initially, it was felt that eq 1 with $f(\alpha_1, \alpha_2 \ldots) = 0$ could be used to describe all mixed systems; however, deviations from the expected linearity of such an equation led to the addition of $f(\alpha_1, \alpha_2 \ldots)$. The total equation adequately describes the functional dependence of the pitch band of mixtures. The use of weight fraction in such an equation remains puzzling. One would expect the helical aggregates of the cholesteric mesophase and, thus, the reflective pitch to be dependent upon the relative *numbers* of individual components. This type of interaction would require a *mole fraction* rather than *weight fraction* dependence. The following molecular model is proposed to explain the pitch phenomena for the mixed cholesteric-nematic mesophase.

Experimental Section

Reflective pitches of liquid crystalline mixtures were measured on thin films of the Grandjean texture of the cholesteric mesophase in the Cary 14 uv-visible spectrophotometer. Examples of typical reflective pitch *vs.* mole fraction of cholesteryl moiety in cholesteric-nematic mixtures of MBBA with cholesteryl chloride (CCL), $\Delta^{8,14}$-cholestenyl benzoate (DB), and allyl cholesteryl carbonate (ACC)[5,6] are shown in Figures 1 and 2. With the exception of the MBBA-CCL, the data for the mixtures show increasing pitch with increasing nematic concentration. The reflective pitch tends toward infinity at high MBBA concentrations.

Theory and Discussion

Saeva and Wysocki have suggested that electronic interactions within the cholesteric helix as well as the helicoidal ordering of the solute will produce induced optical activity in molecules dissolved in a cholesteric solvent.[2,3] We felt that a direct interaction between solute and solvent (somewhat analogous to a charge transfer complex) takes place which produces the shift in λ_0 that occurs when chiral solutes are added to the nematic mesophase. Thus an equilibrium between cholesteric molecules (C) and nematic molecules (N) is attained and a complex formed.

$$C + nN \rightleftharpoons CN_n \qquad (2)$$

The equilibrium of eq 2 is assumed to be far to the right.

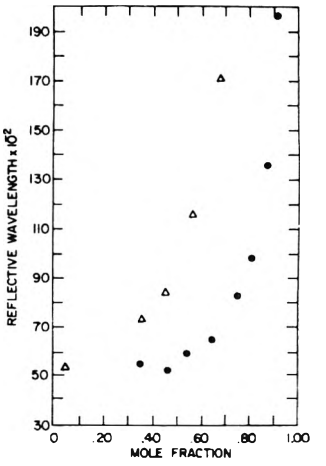

Figure 1. Reflective pitch band *vs.* mole fraction MBBA in MBBA-DB (O) and MBBA-ACC (Δ) mixtures.

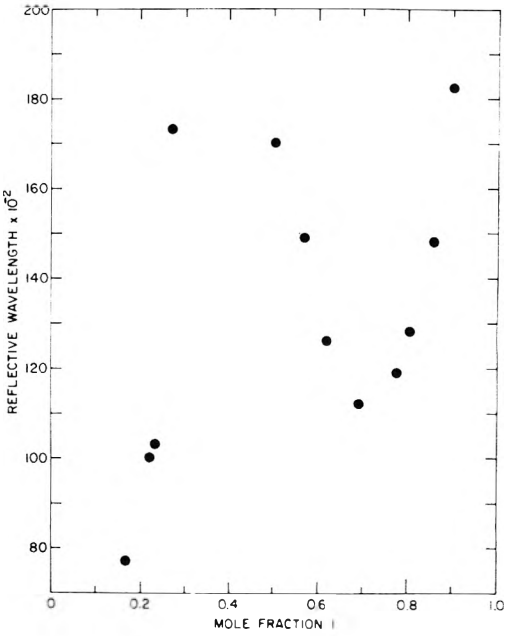

Figure 2. Reflective pitch band *vs.* mole fraction MBBA in an MBBA-CCL mixture.

The cholesteric and molecular complexes are assumed to have reflective pitches λ_C and λ_{CN}, respectively, while any unperturbed nematic molecules retain their infinite pitch. Equation 1 is now written

$$\frac{1}{\lambda} = \sum_i \frac{X_i}{\lambda_i} = \frac{X_C}{\lambda_C} + \frac{X_{CN}}{\lambda_{CN}} \qquad (3)$$

where X_i is the mole fraction of individual components, and the λ_i the wavelengths. X_C and X_{CN} are functions of the complex number n, and, thus, some method of attaining n from experimental data was sought.

Section A. DB, α-Cholesteryl Hexyl Carbonate (α-HXC), ACC, and Cholesteryl 2-Propyn-1-yl Carbonate (CPC) with MBBA. An initial value for λ_{CN} was chosen. Plots of λ_T (as obtained from eq 3) *vs.* initial mole per cent of MBBA were generated for a constant value of n. The value of n was then changed and the process repeated. In this way a series of theoretical reflective pitches as a function of n are generated. The results of such a calculation are seen in Figure 3 for an MBBA-CPC mixture.

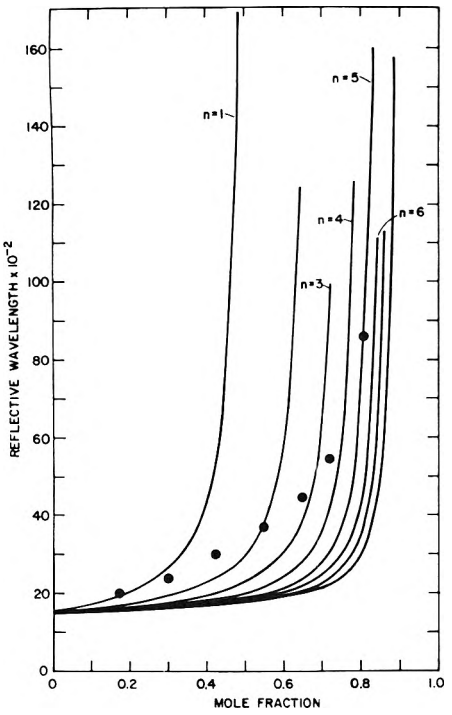

Figure 3. Theoretically produced pitch band as a function of composition for an MBBA-CPC mixture. Complex number n is varied. Experimental points (filled circles) are included: λ(CPC) 1538 Å, λ(complex) 30,000 Å.

The experimental data are also included. It is readily seen that none of the theoretical curves fit the experimental data. Theoretical values of n can, however, be extracted where the experimental curve crosses the theoretical curves. Values of n as a function of initial mole per cent active material can thus be obtained. Figure 4 is a plot of log n *vs.* log $X_{CPC(initial)}$. For the chosen complex reflective pitch, n is an approximate inverse logarithmic function of the initial mole fraction of active material in the mixtures. By using this correlation in the theoretical calculation of λ_T, an excellent fit of the experimental data is obtained (see Figure 5). A plot of concentration of the various components as a function of composition is shown in Figure 6.

The experimental data can also be fit with other values of λ_{CN}. The other values yield slightly different linear fits of log n with log X_C. Table I contains the theoretical fits of n with X_C for various complex reflective pitches and optically active materials. In all cases the fit is as good as that shown in Figure 5. It is interesting to note that in all cases the data can be described by keeping a constant reflective pitch and only varying the complex number with composition. At this time, there is no experimental method of determining λ_{CN} or n independently, and rather than speculate further, or produce empirical relationships between the variables, our data are presented as λ_{CN} constant with n as function of mixture composition. We would naturally assume that n and λ_{CN} are functionally dependent on X_C. This is even more obvious when the equation relating n and X_C is considered.

At high MBBA concentrations (>90%), the fitted data relating n and X_C indicate that the complex number becomes very large, *i.e.*, for MBBA-DB, λ_{CN} = 57000 Å at X_C = 0.06, n = 12.4. The sphere of influence of the cholesteric molecule's asymmetric electron clouds fall off as

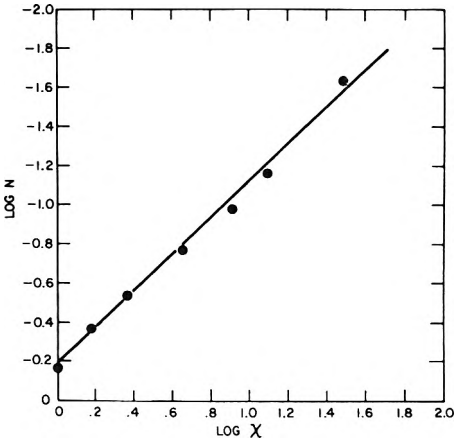

Figure 4. Log n *vs.* log X_{CPC}. Data interpolated from Figure 6. X is the initial CPC concentration.

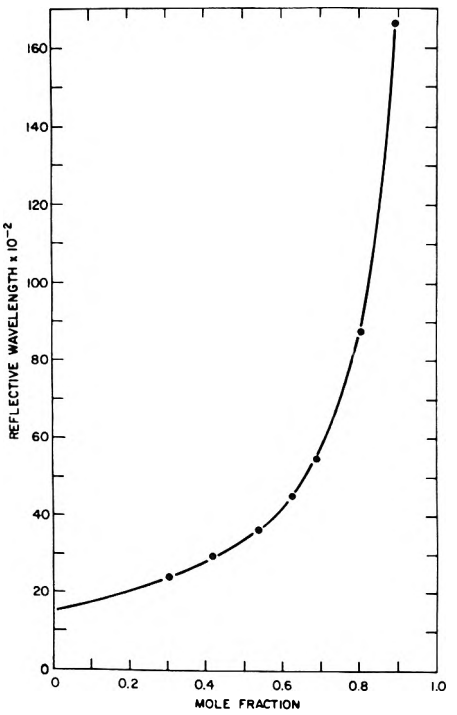

Figure 5. Theoretical and experimental reflective pitch *vs.* composition for MBBA-CPC mixtures: λ_{CN} 30,000 Å, λ_{CPC} 1538 Å; log n = −1.07 log X − 0.177.

R^{-6} and it would not be expected that the molecule's sphere of influence would extend beyond its nearest neighbors. In a close packing model this might lead to interactions with six other molecules. Complex numbers larger than this are, thus, unreasonable at high MBBA concentrations, and indicate the functional dependence of λ_{CN} as well as n on X_C.

The data in Table I may provide additional insight into interactions of the two systems. If our model is correct, it appears that the interaction between MBBA and the various test compounds differ. The log n relationship is approximately dependent on $X^{-1/2}$ for the DB derivatives, while the cholesterol derivatives vary, with two exhibiting inverse pitch relationships. This difference could be due to structural differences in the optically active molecules.

It is interesting to note that our reflective pitch bands for the above compounds follow the general form of the

TABLE I: Fit Parameters for Log n vs. Log X_C for Mixtures of MBBA with Cholesteryl and $\Delta^{8,14}$Cholestenyl Derivatives[a]

Active compound[b]	λ complex chosen	A	B
Cholesteryl 2-propyn-1-yl carbonate λ 6250 Å	15,000	−1.13 ± 0.03	−0.324 ± 0.030
	30,000	−1.04 ± 0.04	−0.177 ± 0.040
$\Delta^{8,14}$-Cholestenyl benzoate λ 2300 Å	125,000	−0.596 ± 0.070	0.422 ± 0.027
	57,000	−0.586 ± 0.060	0.423 ± 0.024
	100,000	−0.520 ± 0.023	0.467 ± 0.012
Allyl cholesteryl carbonate	100,000	−0.996 ± 0.047	−0.11 ± 0.02
	30,000	−1.104 ± 0.053	−0.17 ± 0.02
λ 4215 Å	70,000	−1.115 ± 0.060	−0.16 ± 0.02
α-Hexyl cholesteryl carbonate	100,000	−0.727 ± 0.081	0.744 ± 0.025
	50,000	−0.691 ± 0.107	0.782 ± 0.233
λ 1600 Å	30,000	−0.785 ± 0.040	0.571 ± 0.083

[a] Log $n = A \log X_C + B$. [b] Reflective wavelength given for pure material.

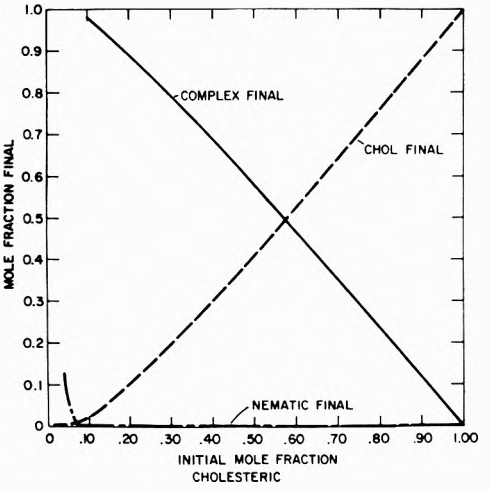

Figure 6. Final mole fraction of pure nematic, pure cholesteric, and cholesteric-nematic complex for CPC-MBBA as a function of initial cholesteric composition. Data based on parameters in Figure 5.

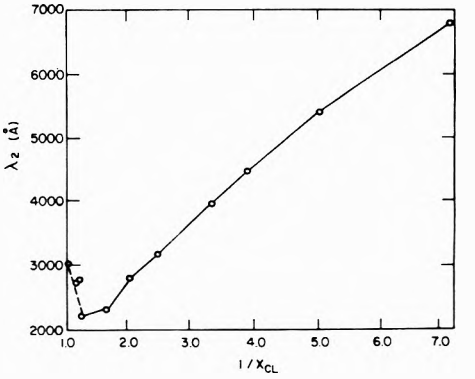

Figure 7. Complex reflective wavelength vs. $1/X_{CL}$ for MBBA-CCL mixtures.

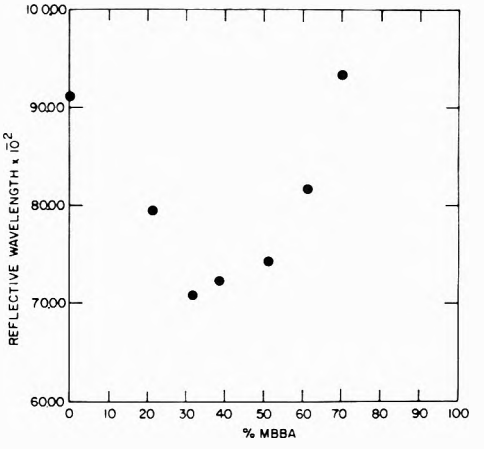

Figure 8. Reflective wavelength vs. mole per cent MBBA for a mixed (CCL, CN) cholesteric system with MBBA.

theoretical equations of Goossens[7] for a symmetric internal field interaction in the mixtures.

B. CCL-MBBA. The data for CCL-MBBA presented a different problem from the other mixtures shown, in that an actual pseudonematic (compensated) texture is obtained. This behavior is indicative of the fact that an optically active species other than CCL in the mixture has a sign opposite the negative −4880 Å pitch of CCL. A complete fit of the reflective data for this mixture was impossible using the techniques outlined above. Various attempts using λ_{CN} being both positive and negative failed. A method of overcoming this would be to have n and λ_{CN} vary with composition. Since we cannot anticipate the functional dependence of λ_{CN}, the following was done. Inspecting the data in Table I indicates that for two of the cholesteryl derivatives the dependence of n on X_C was inverse. The preexponential factor varied between −0.11 and −0.33, with most near −0.2. We, therefore, have assumed that $\log n = -\log X_C - 0.2$ in the CCL-MBBA mixture and have calculated (from eq 3) the λ_{CN} required to fit the experimental data. An attempt was then made to correlate λ_{CN} with X_C, in a variety of ways, the best of which is shown in Figure 7, a plot of λ_{CN} *vs.* $1/X_C$.

It would appear from this plot that the effective pitch of the cholesteric-nematic complex must be positive throughout the entire composition range of this mixture and that the functional dependence of $1/X_C$ reverses at compensation. A possible better choice of the parameters in the previous equation might produce more linear results. It appears that the effective pitch of the complex (1) decreases with increasing CCL concentration, (2) minimizes at compensation, and then (3) begins increasing near 100% CCL. This indicates that the more cholesteric in the mixture, the lower the effective pitch of the complex.

In the mixtures investigated, except for CCL-MBBA, plots of λ_T *vs.* composition increase with increasing MBBA concentration. In some mixtures of MBBA with cholesteric materials, the reflective pitch band minimizes with composition as seen in Figure 8. It is obvious in these cases that the theory could be used to fit the data by

varying n and λ_{CN} with composition as has been done with MBBA-CCL.

In conclusion, a simple model of molecular interactions in cholesteric-nematic mixtures has been proposed to characterize the reflective pitch of the mixtures. It is based on complexes of optically active cholesteric molecules with nematic molecules. Parameters involved in the theoretical model, namely, the degree of complexation and the helical structure of the complex materials, have been deduced from experimental data. It has been shown that some cholesteric-nematic mixtures can be totally characterized by keeping λ_{CN} constant and varying the complex number n. In the case of CCL-MBBA mixtures, it has been shown that both n and λ_{CN} can vary with composition. However, λ_{CN}, varies in a discontinuous fashion. We believe this method to be totally general for optically active nonmesomorphic materials in nematics as well as chiral nematics in nematics. This method, although more complicated, is also applicable to ternary or higher order mixtures of active materials in nematic mesophases.

This method of molecular complexing is not quantitative in that two variables which cannot be determined independently are presented. The method does present, however, cholesteric-nematic interactions in a easily pictured molecular framework.

Acknowledgment. The authors wish to thank J. J. Wysocki and F. Saeva for the reflective pitch measurements used in this work.

References and Notes

(1) J. L. Fergason, "Liquid Crystals," in the "Proceedings of the International Conference on Liquid Crystals," Gordcn & Breach, N. Y., 1967.
(2) F. D. Saeva and J. J. Wysocki, *J. Amer. Chem. Soc.*, **93**, 5928 (1971).
(3) F. D. Saeva, *Mol. Cryst. Liquid Cryst.*, **18**, 375 (1972).
(4) J. Adams and W. Haas, presented at the 166th National Meeting of the American Chemical Society, Chicago, Ill., Aug 26-31, 1973, Abstract.
(5) This data (MBBA-ACC, MBBA-DB, and MBBA-CPB) has been provided by J. Wysocki.
(6) MBBA-CCL reproduced by permission of the authors in ref 2.
(7) W. J. A. Goossens, *Mol. Cryst. Liquid Cryst.*, **12**, 237 (1971).

Field Dissociation Effect and Chemical Relaxation in Electrolyte Solutions of Low Polarity

André P. Persoons[1]

Laboratory of Chemical and Biological Dynamics, University of Leuven, Leuven, Belgium *(Received October 29, 1973)*

Publication costs assisted by Katholieke Universiteit te Leuven and F.K.F.O. Belgium

A stationary chemical method for the investigation of ionic equilibria in media of low permittivity is presented. The technique is based on the application of pulsed electric fields of high amplitude and high frequency to modulate the conductivity of the sample solution, representing a nonlinear resistance as a consequence of the field dissociation effect. The modulation depth or efficiency of the conductivity modulation is measured with superposed fields of low frequency and low intensity whereby the advantages of frequency-conversion methods are fully exploited. The efficiency of conductivity modulation at low modulation frequency is a measure of the field dissociation effect. The relation between modulation depth and field dissociation is derived. Measurements were carried out on solutions of tetrabutylammonium picrate in diphenyl ether at 50°. The value obtained for the field dissociation effect is in close agreement with the theoretical value given by Onsager and confirms the experimental data of Mead and Fuoss. At increasing modulation frequency the finite rate of ionic dissociation equilibria introduces a decrease in modulation efficiency. The relation between modulation depth, modulation frequency, field dissociation, and relaxation time of the ionic equilibrium is derived. Measurements on solutions of different electrolytes in weak polar media confirm these relation. From the dispersion of the field dissociation effect the relaxation time(s) of the ionic dissociation process(es) are calculated. Evidence was obtained for a dependence of the field dissociation effect on the frequency of the external electric fields used to modulate the conductivity of the electrolyte solutions. This effect may be related to the dynamics of the physical processes involved in the field dissociation effect. An extra advantage of the presented technique is the possibility of conductivity measurements in low conducting media without apparent interference of polarization effects.

Introduction

Kinetic investigations of association-dissociation equilibria of ions were made feasible by the advent of relaxation spectrometry.[2] These studies are mostly restricted to aqueous or aqueous-like media where ionic species are present in fairly high concentration. The study of chemical relaxation phenomena resulting from electrolyte equilibria in low-polar media is of interest. Such studies

should yield valuable information on ionic dissociation rates in nonaqueous media and lead to a better understanding of ion-pair formation, ionic aggregation, specific solvation effects, etc. These phenomena are of prime importance in the electrolyte theory of ionic solutions in organic solvents.

In this paper we present a relaxation method for the investigation of ionic dissociation and association rates in solutions of low dielectric permittivity. This new method uses the influence of high electric field strengths on ionic equilibria. As a consequence of the electric field dependence of ionic dissociation equilibria,[3] a solution of a weak electrolyte (and almost every electrolyte is weak in a low-polar media) behaves as a nonlinear resistance. It becomes feasible to use an electrolytic resistance as the nonlinear element in an appropriate modulator circuit. The extent and efficiency of modulation as a function of the frequency of the modulation signal will yield information on equilibrium shifts and chemical relaxation of the ionic equilibria. The extent and efficiency of this modulation may be detected from frequency components which are generated from the different intermodulation products related to the nonlinear behavior of the medium. As will be shown the amplitude of the intermodulation signals is proportional to the relative change in ionic concentration upon application of the electric field. The method is very sensitive and especially suited for low polar media where the concentration of free ions may be exceedingly small.

Theory

The increase of the conductivity of electrolyte solutions with increasing field strength was first discovered by Wien.[4] He showed that Ohm's law is only of limited applicability for electrolytic resistances. The enhancement of conductance for solutions of strong electrolytes (the first Wien effect) is rather small and can be explained as a consequence of modifications in the ionic atmosphere.[5] Deviations from Ohm's law in weak electrolytes[6] are much more pronounced. This field dissociation effect, or second Wien effect, is due to an increase in dissociation under the influence of the field. The second Wien effect was theoretically explained by Onsager[7] as a consequence of the anisotropy induced by the field upon the process of ionic dissociation from ion pairs. In the most general case the ionic dissociation equilibrium may be written as

$$AB \underset{k_{21}}{\overset{k_{12}}{\rightleftharpoons}} \underset{\text{ion pair}}{(A^+ B^-)} \underset{k_{32}}{\overset{k_{23}}{\rightleftharpoons}} A^+ + B^- \qquad (1)$$

According to Onsager's theory only the rate process from pairs to free ions (k_{23}) depends on the electric field strength. In solutions of weak electrolytes in high polar media the concentration of ion pairs can almost be neglected because the time average probability of having an oppositely charged ion within the Bjerrum distance (ion-pair interaction) is small compared to the probability of configurations with greater ionic separation. This situation is inverted in media polarity where interionic interaction is much more pronounced. As a consequence the main species in low polar media are ion pairs while the concentration of free ions is almost negligible. This is the case for most strong electrolytes dissolved in low polar solvents, where we only have to consider the equilibrium

$$\underset{\text{ion pair}}{(A^+ B^-)} \underset{k_{32}}{\overset{k_{23}}{\rightleftharpoons}} A^+ + B^- \qquad (2)$$

which is the equilibrium referred to in the Onsager theory. In a first approximation the field dependence of equilibrium 2 in a field of strength E is given according to Onsager

$$K(E)/K(0) = 1 + 2\beta q + \tfrac{1}{3}(2\beta q)^2 + \tfrac{1}{18}(2\beta q)^3 + \ldots \qquad (3)$$

This result was derived under the condition of infinite dilution; $K(0)$ is the thermodynamic dissociation constant. The quantity $q = |z_A z_B| e_0^2/2DkT$ (where z_i is the ionic valence) is known as the Bjerrum radius. At this distance the electrostatic interaction energy between two oppositely charged ions becomes equal to $2kT$; therefore the probability of the ions existing as an ion pair will increase when they are inside a shell of radius q. Obviously this energy cut-off limit of $2kT$ is rather arbitrary, even more so in low polar media where the critical distance for ion pair formation calculated on this becomes very large. The "exact" value of the limit is however of no critical importance in Onsager's theory.

As dimensionally required, the quantity 2β represents a reciprocal distance given by

$$2\beta = \frac{|Ee_0(z_A u_A - z_B u_B)|}{kT(u_A + u_B)} \qquad (4)$$

where u_A and u_B are the mechanical mobilities (reciprocal of the friction constant) of the ions. As can be seen from eq 4 the quantity 2β becomes independent of these mobilities in the case of symmetric electrolytes; $z_A = -z_B$. It should therefore be possible to give a theoretical description of the second Wien effect for these electrolytes without the need for parameters from transport theory, *i.e.*, if adequate boundary conditions could be given. For symmetric electrolytes, $(2\beta)^{-1}$ represents the distance at which two equal but opposite charges ze_0 form a dipole whose energy is $-kT$ if favorably aligned in the electric field.

In the linear approximation eq 3 can be written

$$\frac{\delta_c \ln K}{\delta |E|} = |z_A z_B| \frac{|z_A u_A - z_B u_B|}{u_A + u_B} \frac{e_0^3}{2Dk^2T^2} \qquad (5)$$

When eq 5 is multiplied by $\delta\alpha/\delta \ln K$ for the ionic equilibrium 2 we obtain a relation between the degree of ionic dissociation and field strength

$$\frac{\delta\alpha}{\delta |E|} = \frac{\alpha(1-\alpha)|z_A z_B||z_A u_A - z_B u_B|}{2-\alpha} \frac{e_0^3}{u_A + u_B} \frac{e_0^3}{2Dk^2T^2} \qquad (6)$$

The relative change in degree of dissociation upon the application of an electric field can be measured as a relative change in conductance σ

$$\frac{\overline{\Delta\alpha}}{\alpha} = \frac{1-\alpha}{2-\alpha}\frac{\Delta K}{K} = \frac{1-\alpha}{2-\alpha} 2\beta q = \frac{\overline{\Delta\sigma}}{\sigma} \qquad (7)$$

From these relations it can be seen that the relative change in conductance will be largest under conditions where dissociation in free ions is almost negligible, *i.e.*, when $\alpha \to 0$, a situation which is usually encountered in low polar media. Moreover the relative conductance change is directly proportional to the Bjerrum radius which is inversely dependent on the dielectric constant. The field dissociation effect will hence be most pronounced in low polar media, where the relative change in conductance is a direct measure of βq

$$\overline{\Delta\sigma}/\sigma = \beta q \simeq |E| \qquad (8)$$

In the preceding we have not considered temporal effects in the establishment of a new equilibrium state upon the application of the electric field. The increase in ionic dis-

sociation is not instantaneous but is determined by the relaxation time of the equilibrium between free ions and ion pairs. If the relaxation time of the one-step equilibrium 2 is τ the time dependence of a conductance change induced by the electric field may be determined from the general equation

$$\tau\frac{d\Delta\sigma}{dt} + \Delta\sigma = \overline{\Delta\sigma} \qquad (9)$$

whereby we implicitely assume that the relative change in conductance is very small (of the order of a few per cent) and the rate equations may be linearized. $\overline{\Delta\sigma}$ represents the equilibrium conductance change, *i.e.*, the conductance change which would be measured at each instant if ionization changes were instantaneous. $\overline{\Delta\sigma}$ is given by eq 8 and will have the same time dependence as the absolute value of the electric field which is used to perturb the ionic equilibrium.

In polar solvents the field dissociation effect is very small and ionic equilibria are only measurably perturbed by high fields. However, such fields produce considerable heating effects in polar media where the conductivity is rather high and therefore temperature-dependent changes in conductivity may occur. In highly conducting and polar media the field dissociation effect and its time dependence can therefore only be studied by impulse methods whereby electric fields are applied for a very short time.[9] In low polar media the conductivity is generally low and it becomes feasible to use stationary field methods which are more sensitive and accurate. The field strength necessary to provoke measurable conductance changes is moreover much smaller in media of low polarity. This reduces the experimental difficulty of producing repetitive field pulses of high amplitude.

A weak electrolyte solution behaves as a field dependent resistance under high field conditions. A cell containing such a solution subjected to electric field pulses may be used as the nonlinear element in a modulator circuit. Efficiency and frequency-dependent properties of such a modulator circuit are related to the dissociation field effect and its dispersion. In principle such a technique for the stationary measurement of the second Wien effect and its time dependence was already proposed by Eigen and De Maeyer.[10] By periodically switching on and off a high electric field between electrodes containing an ionic solution, the ionization of a weak electrolyte, and hence the conductance, can be modulated with the switching repetition frequency. This modulation can be detected by means of an alternating voltage (carrier) applied simultaneously to the same, or to other, electrodes. The presence of a nonlinear device (the electrolyte solution) introduces frequency components not originally present but generated from the different intermodulation products. If moreover modulation and carrier frequencies are the same, a dc signal will appear which, after adequate filtering of the ac signals, can be accurately measured. This dc intermodulation signal is a measure of the magnitude of the second Wien effect provided the frequency of modulation is low enough for an in-phase shift of the ionic equilibrium. Otherwise the intermodulation signals effectively disappears and one finds a dispersion in the amplitude of the dc signal when the high-field pulse repetition frequency is increased.

The repetitive electric field pulses used to modulate the conductance are preferably not of constant amplitude; experimentally this is difficult to realize. The relation between increase in ionization and applied electric field contains the absolute value of the electric field strength (eq 8); therefore high-frequency alternating electric field pulses can be used more efficiently to provoke the dissociation field effect. The frequency of these alternating fields is important because one may anticipate that at very high frequency the external field will no longer perturb the Brownian motion of the ions and the field dissociation effect will effectively vanish. (Although deviations from Onsager's theory may occur when we use ac fields of high frequency we know from symmetry considerations that the dissociation field effect will always be an even function of the electric field).

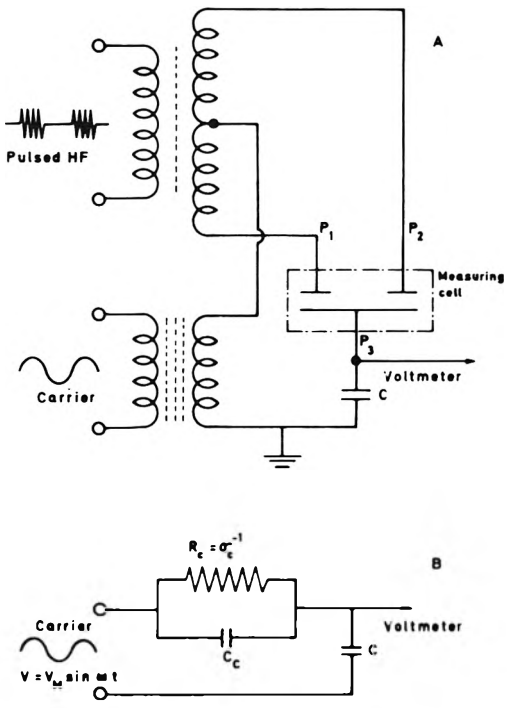

Figure 1. (A) Schematic circuit for the measuring technique. (B) Equivalent measuring circuit.

In Figure 1A a schematic arrangement is given of a modulator circuit which may be used in measurements of the second Wien effect and its frequency dependence. The dc intermodulation signal will charge the capacitor C and the dc voltage across this capacitor is a direct measure of the modulation depth or efficiency. This efficiency of modulation decreases when the pulse repetition frequency (frequency of the envelope or modulation frequency) increases and approaches the reciprocal relaxation time of the ionic equilibrium. Concomitant with the decrease in modulation efficiency, the charge on capacitor C decreases. The measurements of the dc voltage across C as a function of the modulation frequency will yield information about the dissociation field effect and its time dependence.

From the particular circuit arrangement we calculate the relation between the voltage across C, the modulation frequency, and the relaxation time τ of the ionic equilibrium. We consider the low-frequency equivalent measuring circuit (Figure 1B) where the resistance of the electrolyte solution in the cell is indicated as $R_c = \sigma_c^{-1}$. Parallel with this resistance we have the cell capacity C_c which is much smaller than the measuring capacity ($C_c << C$). The cell conductance changes upon the application of the

high-frequency field pulses and for simplicity we consider only the envelope of the absolute value of high-frequency pulses neglecting the internal time structure. This is equivalent to a description where we only take into account the on-off switching of a field of constant amplitude. The cell conductance σ_c is a function of time and modulation frequency which can be written as

$$\sigma(t,\omega) = \sigma_0\left[1+\frac{\Delta\sigma(t,\omega)}{\sigma_0}\right] \tag{10}$$

where σ_0 is the equilibrium conductance measured with low field intensities; $\Delta\sigma(t,\omega)$ is the shift in conductance at any moment for a modulation frequency ω. This shift may be calculated from eq 9 with $\Delta\sigma$ given by

$$\overline{\Delta\sigma} = \begin{cases} g\overline{\Delta\sigma} & \text{for } nT < t < (n+1/2)T \\ 0 & \text{for } (n+1/2)T < t < (n+1)T \end{cases} \tag{11}$$

where T is the modulation period ($T = 2\pi/\omega$). The parameter g should be equal to one if the change in conductance at low modulation frequencies is given by Onsager's theory (eq 8). However, g may be a function of ionic concentration, the high frequency in the pulses, and the "effective field strength" of the alternating electric field. By the use of Laplace transform methods eq 9 with the function $\Delta\sigma$ as given in eq 11 can be solved[11]

$$\Delta\sigma(t,\omega) = g\overline{\Delta\sigma}\left[\frac{1}{2}+\frac{e^{-t/\tau}}{1+e^{\pi/\tau\omega}}+\frac{2}{\pi}\sum_{n=1}^{\infty}\frac{\sin(2n-1)\omega t-(2n-1)\omega\tau\cos(2n-1)\omega t}{(2n-1)[1+(2n-1)^2\omega^2\tau^2]}\right] \tag{12}$$

After sufficient time, when transient terms have disappeared, the cell conductance as a function of time and modulation frequency is given by

$$\sigma(t,\omega) = \sigma_0\left[1+\frac{g\overline{\Delta\sigma}}{\sigma_0}+\frac{2g\overline{\Delta\sigma}}{\pi\sigma_0}\sum_{n=1}^{\infty}\frac{\sin(2n-1)\omega t-(2n-1)\omega\tau\cos(2n-1)\omega t}{(2n-1)[1+(2n-1)^2\omega^2\tau^2]}\right] \tag{13}$$

The voltage on capacitor C (Figure 1B) at a given modulation frequency ω may now be calculated from the differential equation which describes the equivalent measuring circuit of Figure 1B

$$\frac{dV}{dt}+\frac{\sigma(t,\omega)}{C}V = \frac{C_c}{C}\omega V_M\cos\omega t+\frac{\sigma(t,\omega)}{C}V_M\sin\omega t \tag{14}$$

In this equation it is important to note that we started with no phase shift between the carrier voltage and the envelope of the high frequency field pulses. We used the approximation that the cell capacitance is much smaller than the measuring capacitance and may be neglected with respect to the latter. To simplify the presentation of the results we will introduce some minor changes. Instead of considering the equilibrium conductance σ_0 we use the mean equilibrium conductance under field conditions $\bar{\sigma}$ given by $\sigma_0 + \frac{1}{2}\overline{\Delta\sigma}$. For all practical purposes the difference between the two values may be neglected. The conductance of the cell can thus be written as

$$\sigma(t,\omega) = \bar{\sigma}\left[1+m\sum_{n=1}^{\infty}\frac{\sin(2n-1)\omega t-(2n-1)\omega\tau\cos(2n-1)\omega t}{(2n-1)[1+(2n-1)^2\omega^2\tau^2]}\right] \tag{13b}$$

where the parameter m is equal to $2g\overline{\Delta\sigma}/\pi\bar{\sigma}$. Equation 14 can be rewritten as

$$\frac{dV}{dt}+\frac{\bar{\sigma}}{C}[1+m\Sigma]V = \frac{C_c\omega V_M}{C}\cos\omega t+\frac{\bar{\sigma}V_M}{C}[1+m\Sigma]\sin\omega t \tag{14b}$$

where Σ is the summation given in eq 13.

This is a nonhomogeneous linear differential equation with periodic (time-dependent) coefficients. To solve the equation it is important to note that $m << 1$; this allows us to use a perturbation method and to write for the solution

$$V = V_0 + mV_1 \tag{15}$$

neglecting all but the linear term in m. We can substitute eq 14b with a set of two other differential equations where the first describes the cell circuit in the absence of any perturbation while the second yields the superimposed harmonic components generated from the modulation effect

$$\frac{dV_0}{dt}+\frac{\bar{\sigma}}{C}V_0 = \frac{C_c\omega V_M}{C}\cos\omega t+\frac{\bar{\sigma}}{C}V_M\sin\omega t \tag{16a}$$

$$\frac{dV_1}{dt}+\frac{\bar{\sigma}}{C}V_1 = \left(\frac{\bar{\sigma}}{C}V_M\Sigma\right)\sin\omega t-\frac{\bar{\sigma}}{C}V_0\Sigma \tag{16b}$$

The solution of these equations is straightforward and we obtain for V_1 a series in harmonic components containing a frequency-independent term which represents a dc voltage measured on the capacitor C. This dc component is given by

$$V_{dc} = g\frac{\overline{\Delta\sigma}}{\bar{\sigma}}\frac{V_M}{\pi}\frac{1}{1+\omega^2\tau^2}\frac{(\bar{R}C\omega)^2}{1+(\bar{R}C\omega)^2}\left(1-\frac{C_c}{C}\right)\left(1-\frac{\omega\tau}{\bar{R}C\omega}\right) \tag{17}$$

$\bar{R}$ is the mean equilibrium cell resistance under field conditions ($\bar{R} = \bar{\sigma}^{-1}$) which is of the order of several Mohms for the systems under consideration. For values as low as 50 sec^{-1} for ω and for reasonable values of C(>50 nF) we note that $\bar{R}C\omega$ is much larger than 1; hence we can neglect the dispersion effect introduced by the time-dependent properties of the electric circuit. Generally we have that τ is much smaller than 1 sec and $C_c << C$; this permits us to neglect the last two terms in parentheses. We finally find, for reasonable experimental conditions, that the dc voltage measured on C is given by

$$V_{dc} = \left(g\frac{V_M}{\pi}\frac{\overline{\Delta\sigma}}{\bar{\sigma}}\right)\frac{1}{1+\omega^2\tau^2} = \frac{V_{dc\,max}}{1+\omega^2\tau^2} \tag{18}$$

The amplitude of this dc voltage signal across the capacitor C shows a simple dispersion from which the relaxation time is readily determined. After normalization, a theoretical curve is made to coincide with the experimentally measured dispersion curve merely by a displacement parallel to the abscissa. The amplitude of the dc voltage at modulation frequencies which are much smaller than the reciprocal relaxation time of the ionic equilibrium is a measure of the field dissociation effect, given by $g\overline{\Delta\sigma}/\sigma$. $\overline{\Delta\sigma}/\sigma$ is the relative conductance increase as calculated from the Onsager theory, while g measures the experimental deviations from the theoretical predictions. In the foregoing calculations it was always assumed that there was only one ionic equilibrium resulting in one simple relaxation process. If there are more ionic equilibria in the solution we may obtain more relaxation processes and the am-

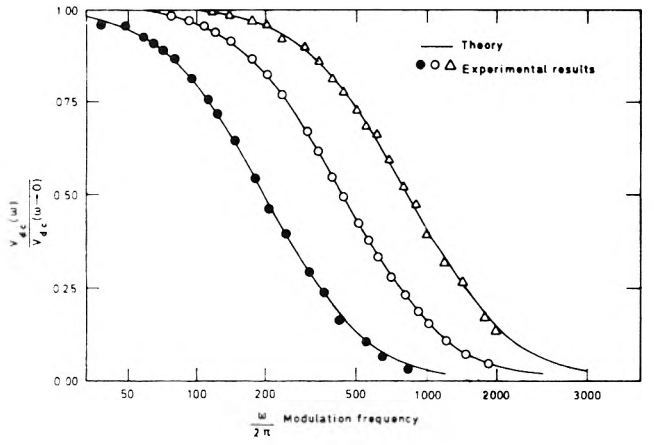

Figure 2. Dispersion of the field dissociation effect with the modulation frequency (as given by expression 18): experimental conditions 1, (●) 2.1 × 10^{-6} *M* lithium picrate in dipropyl ether at 25°, effective field strength E_0 = 3.8 kV cm^{-1} and $\omega_{HF}/2\pi$ 60 kHz, the reciprocal relaxation time τ^{-1} (equal to ω_{mod} at V_{dc} $(\omega_{mod})/V_{dc}(0)$ = 0.50) is 1225 sec^{-1}; 2, (○) 1.75 × 10^{-4} *M* tetrabutylammonium picrate in a mixture chlorobenzene–benzene (20/80 by volume) at 25°, effective field strength E_0 = 1.3 kV cm^{-1} and $\omega_{HF}/2\pi$ = 100 kHz, the reciprocal relaxation time τ^{-1} is 2800 sec^{-1}; 3, (△) 5 × 10^{-4} *M* tetrabutylammonium picrate in a mixture chlorobenzene–benzene (20/80 by volume) at 25°, effective field strength E_0 = 1.3 kV cm^{-1} and $\omega_{HF}/2\pi$ = 100 kHz, the reciprocal relaxation time τ^{-1} is 5160 sec^{-1}.

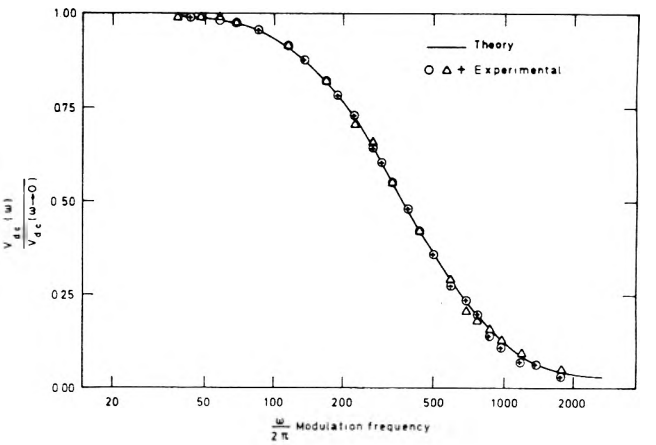

Figure 3. Influence of the frequency (ω_{HF}) and amplitude of the alternating fields on the dispersion of the field dissociation effect for a solution of tetrabutylammonium picrate (9 × 10^{-6} *M*) in diphenyl ether at 50°: experimental conditions (○) effective field strength E_0 = 3.8 kV cm^{-1} and $\omega_{HF}/2\pi$ = 100 kHz; (△) effective field strength E_0 = 3.8 kV cm^{-1} and $\omega_{HF}/2\pi$ = 35 kHz; (+) effective field strength E_0 = 1.9 kV cm^{-1} and $\omega_{HF}/2\pi$ = 100 kHz. For all conditions the reciprocal relaxation time τ^{-1} is 2390 sec^{-1}.

plitude of the dc signal will contain a summation over different dispersion terms each with its own relaxation time

$$V_{dc} = V_{dc\,max}\sum_i \frac{b_i}{1+\omega^2\tau_i^2} \quad \text{with} \quad \sum_i b_i = 1 \qquad (19)$$

According to Onsager's theory the quantity V_{dcmax} in eq 19 is the same as in eq 18 because the stationary dissociation effect caused by a constant electric field is independent of ionic concentration for a small degree of ionization. It is also independent of the nature of the ions as long as symmetric electrolytes are considered.

From the concentration dependence of the relaxation time(s) details of the mechanism of the ionic association–dissociation process(es) are obtained. For example, a simple ionic equilibrium, when ionic dissociation is very small, will show a square-root dependence of the relaxation time upon the total electrolyte concentration.

Experimental Verification and Discussion

The predictions of the theoretical considerations and the validity of the assumptions made were investigated with an experimental set-up which closely follows the schematic circuit given in Figure 1A.[12] A square-wave, modulated high-frequency voltage is obtained from the secondary of a center-taped ferrite-core step-up transformer (1:10) driven from a modulated power oscillator. To tune the secondary winding with the capacitive load of the sample cell the ferrite core has an adjustable air gap. The sample cell consists of a symmetric arrangement of two electrodes (P_1 and P_2) against a common third electrode P_3. This central electrode is in thermal contact with the thermostated and grounded cell body, while electric insulation is obtained by interposing a mylar sheet between the electrode and the cell body. The electrodes P_1 and P_2 are connected to the high-voltage transformer output terminals. Between the center tap terminal of the high-voltage secondary and the central electrode P_3 a series capacitor C is connected as well as the secondary of an isolation transformer (1:1) which is driven from a low-power, low-frequency sinusoidal oscillator. The square-wave signal modulating the high-frequency voltage is locked in frequency and phase to this oscillator, this ensures a good synchronism between high voltage and low voltage (carrier). In the range of the modulation frequencies used the series capacitor has a low impedance compared with the impedance of the two halves of the sample cell, which are connected in parallel for the signal path of the low-voltage source.

The dc intermodulation signal which appears over the capacitor C is measured with a high-input impedance voltmeter after filtering out the carrier and other ac intermodulation signals. The dc voltage on C is a direct measure of the conductance change upon application of the high field. The kinetic information is obtained from the dependence of this dc voltage upon the modulation frequency. The measured dc values are plotted relative to the dc values measured at low modulation frequencies yielding normalized dispersion curves as shown in Figures 2 and 3.

Analysis of Temperature Effects

Every stationary relaxation technique which makes use of electric fields should first be analyzed for possible temperature effects which may invalidate the interpretation of the measurement. This applies to our method since, in principle, we use a conductance method for the measurement of the adjustments of the ionic equilibria to the electric field perturbations. Our results show convincingly that the measured effects cannot be ascribed to heating effects provoked by the high electric fields. If the conductance increased as a result of the warming of the solution after the field is applied, the measured signal would increase with increasing electrolyte concentration at constant field strength. An increase in electrolyte concentration would result in a decrease of cell resistance and hence a stronger Joule dissipation at a given field strength. The increase of the relative conductance change with a temperature increase can easily be derived from eq 7. With α

→ 0 as is the case, we have

$$\overline{\Delta\alpha}/\alpha = \Delta \ln K = \overline{\Delta\sigma}/\sigma \qquad (7')$$

Now $\Delta \ln K$ is given by Van't Hoff's relation and we obtain for the variation of $\overline{\Delta\sigma}/\sigma$ on a slight temperature increase

$$\overline{\Delta\sigma}/\sigma = (\Delta H/RT^2)\Delta T \qquad (20)$$

The results presented in Figure 4 show that an increase in electrolyte concentration and the concomitant increase of conductance actually give rise to a smaller signal at a given field strength. As will be shown quantitatively, the effects measured are in good agreement with the values given by Onsager's treatment of the field dissociation effect. We therefore argue that the influence of heating effects may be completely neglected in the systems studied. From the cell resistance and from the amplitude of the applied fields an estimate of the temperature increase can be obtained. It shows that in the systems studied this increase is indeed negligible, even without thermostating (usually about 10^{-2} deg and smaller).

Other arguments against heating effects having a major influence on the results are found in the values of the relaxation times measured. These relaxations are far too fast to be explained by heating-cooling cycles that occur as the electric fields are switched on and off. Moreover Figure 3 shows that the relaxation effects are independent of the amplitude of the alternating fields used. The slight effect on the amplitude of the field dissociation effect which is observed upon a change in electrode area may entirely be ascribed to changing stray effects of the electrode edges. No effect is observed on the relaxation times while the dynamics of heating-cooling cycles should be pronouncedly influenced by a change in cell geometry.

From all the arguments presented we may infer that the measured field dissociation effects are undisturbed by possible temperature changes, caused by the application of high electric fields on weakly conducting electrolyte solutions.

Measurements of the Field Dissociation Effect

The conductance change measured at low modulation frequencies is the field dissociation effect and can in principle be calculated from the theory given by Onsager. This theory is based on derivations where only dc fields are considered while our technique make use of ac fields with a rather high frequency. We therefore must define an "effective field strength E_0" which is equivalent to the dc field used in the theoretical equations. Onsager showed that the field dissociation effect is proportional to the absolute value of the field strength; we therefore use the linear average over the absolute value of the alternating field as the effective field strength E_0

$$E_0 = \frac{1}{T}\int_0^T |E_M \sin \omega t| \, dt = \frac{2E_M}{\pi} = \frac{E_{pp}}{\pi} \qquad (21)$$

where E_M is the amplitude of the high-intensity high-frequency field and E_{pp} the peak-to-peak value which is easiest to measure with sufficient accuracy. The field strength E_{pp} is obtained from dividing the peak-to-peak value of the high voltage by the electrode distance.

Measurements of the field dissociation effect were carried out on solutions of tetrabutylammonium picrate in diphenyl ether at 50°. The choice of this system and of the particular conditions was dictated by the need for a reference system with known field dissociation effects. This system was thoroughly investigated by Mead and Fuoss[13] who carefully measured the dependence of conductance on field strength. In accordance with their results, we note a dependence on electrolyte concentration for the second Wien effect which was not predicted by the Onsager theory. This may be explained by the formation of ionic aggregates, *e.g.*, triple ions, at higher electrolyte concentration. Only at low electrolyte concentrations, where the phenomena can be described completely by a simple ionic dissociation, are the assumptions of Onsager's theory fulfilled. Furthermore, the complete neglect of the screening effects of the ionic atmosphere results in a discontinuity at low field strength, which cannot be a physical reality. The change of conductance with field strength can therefore be described by Onsagers theory only at relatively high field strengths and for very dilute electrolyte solutions. As can be seen in Figure 4, we find a linear dependence of the conductance on field strength above ~3 kV cm^{-1}. The relative increase of conductance for the lowest electrolyte concentration is given by 1.1×10^{-2} cm kV^{-1} at high fields, *e.g.*, a conductance increase of 1.1% per kV cm^{-1} change in the electric field strength. The same quantity calculated from the linear approximation of eq 3 is equal to 1.32×10^{-1} cm kV^{-1} for the given conditions. The agreement between these two figures clearly shows the applicability of the method for measurements of the field dissociation effect and, more generally, for the measurement of nonlinear resistances. The slight discrepancy between experimental and theoretical value of the conductance increase can be explained from the uncertainty in the electrode distance and from stray effects at the edges of the electrodes. The new cell designs currently

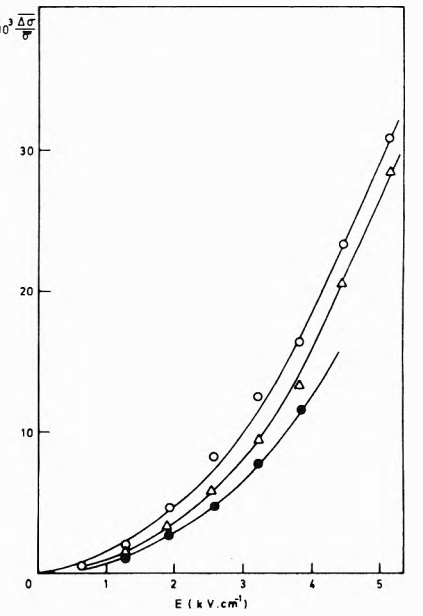

Figure 4. Field dissociation effect as a function of the effective field strength E_0 (as given by eq 21) for solutions of tetrabutylammonium picrate (TBAP) in diphenyl ether at 50° and measured at low modulation frequencies. The relative conductance increase ($\overline{\Delta\sigma}/\bar{\sigma}$) was calculated from the maximal voltage signal on C as expressed by eq 18: experimental conditions (○) 3.9×10^{-5} *M* TBAP, $\omega_{HF}/2\pi$ = 40 kHz and $\omega/2\pi$ = 100 Hz; (△) 1.5×10^{-3} *M* TBAP, $\omega_{HF}/2\pi$ = 40 kHz and $\omega/2\pi$ = 200 Hz; (○) 3.9×10^{-5} *M* TBAP, $\omega_{HF}/2\pi$ = 100 kHz and $\omega/2\pi$ = 100 Hz. Due to the capacitive loading of the power oscillator by the cell it was not possible to realize higher field strengths at the frequency of 100 kHz.

studied permit variations and refined measurements of the electrode distance in order to determine the influence of stray effects.

Another and very important reason for a possible discrepancy between the theoretical predictions of Onsager's theory and the measured conductance change may be an influence of the frequency of the alternating field. Although the absolute value of an alternating field is on the average constant, the dissociation field effect may actually vanish if the frequency of the applied alternating field becomes too high. We assume that the upper limit of this frequency will be approached when the period is of the order of the time needed for two ions to diffuse out of each others electrostatic influence. From the results presented in Figure 4 we clearly see that at a frequency of 100 kHz for the alternating field the field dissociation effect is measurably attenuated. We therefore conclude that the second Wien effect undergoes a dispersion when the frequency of the alternating field is increased. It is also noted from the data that the relaxation of the field dissociation effect in the given conditions takes place at rather low frequency. Although this relaxation as well as the dynamic process behind it are not very well understood we have an experimental approach toward the very complex and as yet unsolved problem of the time dependence of the field dissociation effect. It is almost certain that a thorough investigation of this "high-frequency" relaxation will yield new insights into the physicochemical behavior of electrolyte solutions. Some preliminary experiments already carried out (although limited by the possibilities of our experimental set-up) indicate a strong influence of viscosity which denotes possibly a relation with diffusion processes.

Our results indicate that the parameter g, introduced in eq 11 as a measure for the deviations of the theoretical equations given by Onsager, is a function of the ionic concentration C_i at low fields and of the frequency ω_{HF} of the alternating fields which modulate the conductance

$$g = g(C_i, \omega_{HF}) \tag{22}$$

The deviations of g from unity at a given electrolyte concentration contain information on the nature of charged species in solution and of their activity coefficients. The dispersion of g with the high frequency in the field pulses is related to the dynamics of physical interactions between ion in solution.

Kinetic Measurements

As stated in the theoretical derivations a frequency increase of the square-wave modulation signal (synchronous with the sinusoidal measuring voltage) will lower the modulation efficiency in the time domain where the ionic equilibria undergo relaxation. In Figure 2 measurements on some low-polar electrolyte solutions under different conditions are presented.[14] The agreement between the theoretical dispersion curves and the experimental measurements is excellent. A clear influence of the electrolyte concentration on the relaxation time is shown by the experimental dispersion curves 2 and 3.

We may legitimately ask whether the frequency of the high-frequency alternating field also has an influence on the value of the relaxation time, as it had upon the magnitude of the field dissociation effect. Measurements made on a very dilute solution of tetrabutylammonium picrate in diphenyl ether are presented in Figure 3. The important variation in the frequency and in the amplitude of the high-frequency alternating field yields pronounced differences in the experimental data with respect to the magnitude of the relative conductance increase. There is however no influence at all on the dynamic characteristics of the dispersion of the (normalized) relative conductance change with modulation frequency as presented in Figure 3. The frequency and amplitude of the alternating field have therefore no influence on the evaluation of the relaxation time, which is the kinetically important quantity. Therefore even with an alternating electric field of relatively low frequency and amplitude we are able to measure chemical relaxation phenomena in low polar media. These conditions substantially lighten the experimental requirements of alternating fields of high amplitude and high frequency. At least it becomes possible to use the technique as a method for the kinetic study of ionic dissociation in the reaction media considered.

Conductivity Measurements[15]

The dc signal on the measuring capacitor (see Figure 1 and eq 18) does not appear, or disappear, instantaneously when the high field is switched on or off, but it is characterized by a time constant determined by the cell resistance and by the capacitance of the measuring capacitor. The measurement of this time constant, which is generally of the order of seconds, will give the cell resistance and hence the conductance of the solution. Surprisingly we had no difficulties at all with polarization effects which are the main cause of erratic results in conductance measurements in low conducting media. This may be due to some "cleaning" effects of the electrode surfaces by the high-frequency alternating field. We were able to reproduce, in a short time and with good agreement, the conductivity results of Mead and Fuoss on the tetrabutylammonium picrate solutions in diphenyl ether at 50°. From such conductivity measurements we can determine dissociation equilibria constants which will be very helpful supplementary data for explaining the measured kinetic phenomena.

Conclusion

The measurement of the field dissociation or second Wien effect and its dynamics, caused by chemical relaxation phenomena, can be carried out by perturbing the ionic association equilibria with alternating fields. The technique described allows for an accurate determination of the field dissociation effect in media of low dielectric permittivity. However the results are to be considered with caution because the frequency of the alternating fields has a large influence. The dispersion of the field dissociation effect with the frequency of the alternating electric field is demonstrated for the first time. Further experiments will permit a thorough study of the physical aspects of the time dependence of the field dissociation effects.

Kinetic measurements of the association-dissociation equilibria of ions can be carried out easily and accurately with the proposed method, which may be called a "field-modulation-relaxation" method. Preliminary experiments clearly indicated that the experimental requirements are much less stringent for kinetic investigations than for the accurate measurement of the field dissociation effect.

A supplementary advantage of the technique is the possibility of a simple measurement of the conductance of low conducting media without interference of polarization effects.

Acknowledgments. It is a pleasure to thank Professor L. De Maeyer and Dr. L. Hellemans for numerous stimulating discussions and helpful comments. Thanks are due to Mr. F. Nauwelaers for his excellent experimental work and to Mr. J. Rijckenberg, Mr. J. Meurrens, and Mr. M. Van de Mosselaer for help in the construction of mechanical and electronic parts of the equipment.

Financial support of the Fonds voor Kollektief Fundamenteel Onderzoek, Belgium (Grant No. 10.040), is gratefully acknowledged.

References and Notes

(1) Correspondence should be addressed to the Laboratory of Chemical and Biological Dynamics, Celestijnenlaan 200 D, B-3030-Heverlee, Belgium.
(2) (a) M. Eigen, *Discuss. Faraday Soc.*, **17**, 194 (1954); (b) M. Eigen and L. De Maeyer, "Techniques of Organic Chemistry," Vol. VIII, Part II, 2nd ed, S. L. Friess, E. S. Lewis, and A. Weissberger, Ed., Interscience, New York, N. Y., 1963; (c) M. Eigen and L. De Maeyer, "Theoretical Basis of Relaxation Spectrometry" in "Techniques of Chemistry," Vol. 6, Part 2, A. Weissberger and G. Hammes, Ed., Interscience, New York, N. Y., 1973.
(3) H. C. Eckstrom and G. Schmelzer, *Chem. Rev.*, **27**, 367 (1939), and references given here.
(4) (a) M. Wien, *Ann. Phys.*, **83**, 327 (1927); (b) *Phys. Z.*, **28**, 334 (1927).
(5) W. S. Wilson, Dissertation, Yale University, 1936, as given in ref 8.
(6) M. Wien and J. Schiele, *Phys. Z.*, **32**, 545 (1931).
(7) (a) L. Onsager, *J. Chem. Phys.*, **2**, 599 (1934); (b) L. Onsager and C. T. Liu, *Z. Phys. Chem.* (Leipzig), **228**, 428 (1965).
(8) (a) H. S. Harned and B. B. Owen, "Physical Chemistry of Electrolyte Solutions," 3rd ed, Reinhold, New York, N. Y., 1958; (b) H. Falkenhagen, "Theorie der Elektrolyte," Hirzel Verlag, Stuttgart, 1971.
(9) (a) M. Eigen and J. Schoen, *Z. Elektrochem., Ber. Bunsenges. Phys. Chem.*, **59**, 483 (1955); (b) M. Eigen and L. De Maeyer, *ibid.*, **59**, 986 (1955).
(10) M. Eigen and L. De Maeyer, *Ber. Bunsenges. Phys. Chem.*, **59**, 1024 (1955).
(11) The formalism of complex exponential functions often used in electric circuit theory is only applicable to linear problems; we therefore used trigonometric functions.
(12) (a) L. De Maeyer and A. Persoons, "Electric Field Methods" in ref 2c; (b) F. Nauwelaers, L. Hellemans, and A. Persoons, manuscript in preparation.
(13) (a) D. J. Mead and R. M. Fuoss, *J. Amer. Chem. Soc.*, **61**, 2047 (1939); (b) *ibid.*, **61**, 3589 (1939), correction of ref 13a.
(14) In an unpublished investigation, Spatz (1963, Max-Planck-Institut fur Physikalische Chemie-Gottingen) also observed relaxation phenomena in solutions of aluminum chloride in benzene with an analogous modulation method (L. De Maeyer, personal communication).
(15) The author is much indebted to Dr. L. Hellemans for drawing his attention to this useful application of the described technique.

Apparent Molal Volumes, Heat Capacities, and Excess Enthalpies of *n*-Alkylamine Hydrobromides in Water as a Function of Temperature

Paul-André Leduc, Jean-Luc Fortier, and Jacques E. Desnoyers*

Department of Chemistry, Université de Sherbrooke, Sherbrooke, Québec, J1K 2R1, Canada *(Received November 29, 1973)*

Publication costs assisted by the National Research Council of Canada

The enthalpies of dilution of the homologous salts RNH_3Br, where R varies from H to *n*-octyl, and ammonium acetate were measured in water at 25° for initial concentrations between 0.01 and 1 *m* with a flow microcalorimeter. The densities and volumetric specific heats were also determined for the same systems with a flow densimeter and a flow microcalorimeter between 15 and 55°; with *n*-octylamine hydrobromide, data were also obtained at 5°. Expansibilities were calculated from the temperature dependence of the apparent molal volumes. The infinite dilution apparent molal volumes ϕ_V^0, expansibilities ϕ_E^0, and heat capacities ϕ_C^0 of RNH_3Br and the change in volume and heat capacity during micellization of *n*-$HepNH_3Br$ and *n*-$OctNH_3Br$ are all consistent with an increasing hydrophobic character of the homologous salts with increasing chain length. However, the concentration dependence of the two higher homologs are out of line with the others and these anomalies are accentuated when their temperature dependence are examined. Also ϕ_C^0 passes through a maximum when plotted against temperature and this maximum is shifted toward lower temperatures as the chain length increases. These results suggest that the structural hydration effects in aqueous solutions may be more complicated than previously believed.

Introduction

Previous studies in this laboratory on the apparent molal volumes,[1] conductivities and viscosities[2] in H_2O, and enthalpies of transfer[3] from H_2O to D_2O of *n*-alkylamine hydrobromides have shown that this homologous series is an excellent model system for the study of hydrophobic interactions in the premicellar region and of hydrophobic bonding. An extension of this study to relative apparent molal enthalpies ϕ_L and apparent molal heat capacities ϕ_C at different temperatures, we felt, would be useful in characterizing the energetics of these interactions. Since accurate densities are required to calculate ϕ_C,[4] the densities of this series[1] were also extended to other temperatures (5 to 55°) and apparent molal expansibilities ϕ_E were derived from the data. Ammonium bromide and acetate (NH_4Ac) were also studied for comparison.

Experimental Section

The RNH_3Br salts, where R varies from methyl (Me) to *n*-octyl (Oct), were prepared by titrating the correspond-

ing amine, dissolved in anhydrous ethanol, with a nearly saturated alcoholic solution of HBr gas. The addition of the HBr solution at room temperature was followed with a combination glass electrode up to the equivalence point. The salt was precipitated by concentrating the solution through evaporation of the ethanol; the crystals were washed thoroughly with anhydrous ethyl ether, filtered, and recrystallized twice with the usual solvents.[1] They were finally dried under vacuum at room temperature for 48 hr.

The gases, HBr, methylamine, and ethylamine (Matheson Gas Co.), were used without further purification. The remaining liquid normal amines up to *n*-octylamine (Fisher) were redistilled before use and the collected fractions were shown to be pure from vpc. To minimize possible oxidation, the distillation of the two higher homologs were performed under reduced pressure. Reagent grade NH_4Br (ACS Fisher) was recrystallized once from anhydrous ethanol and dried under vacuum for 48 hr at 100°. A freeze-drying technique was used to deal with the hygroscopy of NH_4Ac (ACS Fisher), as previously described.[5]

All solutions were prepared by weight with water redistilled from an alkaline permanganate solution and kept in equilibrium with atmospheric CO_2. The molalities m were converted to molarities c whenever necessary using the measured densities of the solutions.

Density Measurements. Density data at different temperatures were obtained with a digital densimeter (Anton Paar, Model DMA02C). Problems were encountered with the thermal equilibration of the cell which, in the worse cases, led to an uncertainty of $\pm 1 \times 10^{-5}$ g cm^{-3} in the determination of $(d - d_0)$, the difference between the density of the solution and that of water. For *n*-$OctNH_3Br$ solutions at 5 and 45°, a flow densimeter[6] was used, which is capable of reproducing differences in density to $\pm 3 \times 10^{-6}$ g cm^{-3}. The densities at 25° were taken from the literature.[1]

The apparent molal volumes were calculated from

$$\phi_V = \frac{M}{d_0} - \frac{1000(d - d_0)}{cd_0} \quad (1)$$

where M is the salt molecular weight. The solvent densities d_0 at various temperatures were taken from the literature.[7] Apparent molal expansibilities ϕ_E were derived from the temperature dependence of ϕ_V

$$\phi_E = (\partial\phi_V/\partial T)_p \quad (2)$$

Enthalpies of Dilution Measurements. The integral enthalpies of dilution ΔH_{ID} of most salts were measured at 25° with a flow microcalorimeter,[8] which is an improved version of the one previously described.[9] The dilution ratio was kept close to 1. The overall precision on ΔH_{ID} (J mol^{-1}) is ±0.5% up to the limit of sensitivity, $\pm 1 \times 10^{-6}$. Since with some of the earlier measurements the mixing of *n*-$HepNH_3Br$ and *n*-$OctNH_3Br$ was shown to be incomplete at the higher concentrations ($m > 0.7$), ΔH_{ID} were checked or complemented with measurements with a static microcalorimeter[10] with a similar precision. The mixing cell of the flow microcalorimeter has now been modified to improve the mixing process.

The treatment of the data is given elsewhere.[11] Essentially ϕ_L is expressed as a power series in m

$$\phi_L = A_L(d_0m)^{1/2} + B_Lm + C_Lm^{3/2} + D_Lm^2 + \ldots \quad (3)$$

where the parameter A_L is the known Debye-Hückel limiting slope and has the value 1975 J l.$^{1/2}$ mol$^{-3/2}$ for 1:1 electrolytes in water at 25°.[12] The experimental enthalpy of dilution is given by

$$\Delta H_{ID} = Q/n = \phi_L(m_f) - \phi_L(m_i) \quad (4)$$

where $\phi_L(m_f)$ and $\phi_L(m_i)$ refer to the final and initial solutions ($m_f < m_i$), Q is the measured heat, and n the number of moles of solute. Combining eq 3 and 4 gives a parametric equation for ΔH_{ID} in terms of m from which B_L, C_L, ... can be obtained through a weighted least-squares analysis.

Heat Capacity Measurements. The volumetric specific heats σ (J K^{-1} cm^{-3}) were determined with a differential flow microcalorimeter[4] capable of measuring differences in σ to $\pm 7 \times 10^{-5}$ J K^{-1} cm^{-3} during a temperature rise of 1.6 K and a liquid flow rate of 0.7 cm^3 min^{-1}. The same temperature rise and flow rate were maintained at all temperatures. From the measured ratio $(\sigma - \sigma_0)/\sigma_0$, where σ_0 is the volumetric specific heat of the solvent ($\sigma_0 = c_p^0 d_0$), the apparent molal heat capacity can be derived

$$\phi_C = \phi_V\sigma_0 + \frac{1000(\sigma - \sigma_0)}{c} \quad (5)$$

The weight specific heats c_p (J K^{-1} g^{-1}) can also be derived from σ ($\sigma = c_p d$) and used to calculate ϕ_C

$$\phi_C = Mc_p + \frac{1000(c_p - c_p^0)}{m} \quad (6)$$

The ratio $\Delta\sigma/\sigma_0$ is obtained to ±0.3% up to the limit of sensitivity.[13] For pure water, σ_0 was calculated from c_p^0 at different temperatures.[14]

Temperature Control. The temperature of all instruments was kept constant by means of a closed-loop thermostat.[15] Their stability, ±0.0005° at 25°, decreased to ±0.005° at 5°. The absolute value of each experimental temperature was measured with a calibrated thermistor probe (Yellow Spring) and believed to be accurate to ±0.03°.

Results

The experimental $(d - d_0)$, ΔH_{ID}, and $\Delta\sigma/\sigma_0$ in the region $0.01 < m_i < 1$ are given in the Appendix (see paragraph at end of text regarding supplementary material). All data obtained with flow instruments are the average of at least triplicate measurements. At low concentrations in the premicellar region, ϕ_V and ϕ_C are given by

$$\phi_V = \phi_V^0 + A_Vc^{1/2} + B_V'c \quad (7)$$

and

$$\phi_C = \phi_C + A_Cc^{1/2} + B_C'c \quad (8)$$

where ϕ_V^0 and ϕ_C^0 are the standard apparent molal values (infinite dilution) equal to the standard partial molal values $\bar{V}^0$ and C_p^0; A_V and A_C are the Debye-Hückel limiting slopes and B_V' and B_C' are adjustable parameters which measure the deviations from the limiting law. (The parameters B_V and B_C refer to the corresponding equations $\phi_V = \phi_V^0 + A_V(d_0m)^{1/2} + B_Vm$ and $\phi_C = \phi_C^0 + A_C(d_0m)^{1/2} + B_Cm$, where d_0 is the density of the solvent). The calculated A_V and A_C are given in Table I for 1:1 electrolytes.

Recent literature values for d_0[7] and the dielectric constant[17] of water were used in the expression for the limiting slope of the Debye-Hückel law.[12] The present calculated A_C are comparable with those suggested by Lewis and Randall[18] and by Harned and Owen.[12] The small difference between the different calculations can be traced to

TABLE I: Parameters A_V and A_C of Eq 7 and 8 for 1:1 Electrolytes in Water at Various Temperatures

T, °C	A_V,[a] cm³ l.$^{1/2}$ mol$^{-3/2}$	A_C, J K^{-1} l.$^{1/2}$ mol$^{-3/2}$
5	1.529	22.52
15	1.697	25.85
25	1.868	28.99
35	2.046	32.22
45	2.234	35.74
55	2.435	39.58

[a] Reference 16.

the uncertainty of the second derivative of the dielectric constant of water with respect to the temperature.

Plots of $\phi_C - A_C c^{1/2}$ *vs.* c for the homologous series at 25° are shown in Figure 1. A similar plot for *n*-OctNH$_3$Br will be shown later. A similar plot for ϕ_V has been given previously.[1] In the region where $\phi_C - A_C c^{1/2}$ and $\phi_V - A_V c^{1/2}$ were linear in c, the parameters ϕ_C^0, B_C', ϕ_V^0, and B_V' were determined at different temperatures from a weighted least-squares analysis[19] and are given in Tables II and III. At temperatures other than 25°, the number of data points in the linear region are sometimes small (as few as three in some cases), and the derived B_C' and B_V' should not be considered too reliable, as indicated by the number of significant figures given in Tables II and III. The smooth variation of these parameters with temperature suggests that they are of the right order of magnitude. The sudden decrease in ϕ_C observed with the two higher homologs occurs in the region where micelles begin to form.

Individual ϕ_C values are usually measurable to ±0.5 J K^{-1} mol^{-1} above 0.1 *M*.[13] At 25°, ϕ_C^0 should be reliable to about 1 J K^{-1} mol^{-1} or better since eq 8 is obeyed over a reasonable range of concentration. At 5 and 55°, the uncertainty may increase to about 5 J K^{-1} mol^{-1}, mostly as a result of increased difficulty in controlling the temperature. As seen from Figure 2, ϕ_C^0 at 25° increases linearly with the number of carbon atoms in the chain. A similar behavior[1] was observed for ϕ_V^0.

The only values of ϕ_C^0 in the literature that can be compared with the present results are those of MeNH$_3$Cl[20,21] and EtNH$_3$Cl.[20] Correcting for the difference between Cl$^-$ and Br$^-$,[13] the corresponding MeNH$_3$Br would be 15 and −11 J K^{-1} mol^{-1} as compared with the present value of 7.7 J K^{-1} mol^{-1}, while the corresponding EtNH$_3$Br, with a value of 58 J K^{-1} mol^{-1} is quite far from 101.6 presently found. The large scatter in the data taken from the literature results mostly from the experimental technique used for the determination of ϕ_C^0, *i.e.*, specific heat measurements on concentrated solutions. On the other hand, the average incremental group contribution of each $-CH_2$ can be found, from Figure 2 and Table II, to be 88 ± 3 J K^{-1} mol^{-1} at 25°. This is in good agreement with the corresponding values obtained from homologous carboxylic acids,[22] 84 ± 2, amines,[22] 90 ± 2, *N*-substituted amines,[22] 86 ± 2, and alcohols, 95 ± 4,[23] 96 ± 4,[24] 100.[25]

The ϕ_V^0 appear in general to be precise to ±0.05 cm^3 mol^{-1} or better at all temperatures; the values of ϕ_V^0 and B_V' at 25° in Table III were recalculated from previously published ϕ_V[1] using a weighted least-squares analysis. The ϕ_V and ϕ_C of NH$_4$Ac and the ϕ_C of NH$_4$Br at 25° have been reported elsewhere.[1,5]

The variation of ϕ_C^0 and ϕ_V^0 with temperature is given in Figures 3 and 4. The standard apparent molal expansibilities ϕ_E^0, derived from the slopes in Figure 4, are, inside the experimental uncertainty, independent of temperature. They are given in Table IV along with the other derived parameters B_E' (= $\partial B_V'/\partial T)_p$, $(\partial \phi_C^0/\partial T)_p$, and $(\partial B_C'/\partial T)_p$. These ϕ_E^0 (= E^0) are all positive and become more so the longer the chain. The ϕ_C^0 (= $\bar{C}_p^0$) are also relatively independent of temperature, the lower members showing a slight increase with temperature and the higher homologs passing through a maximum. This maximum which is outside the experimental uncertainty occurs at lower temperatures with the longer-chain salts and is also observed with salts such as *n*-nonyltrimethylammonium bromide[26] and tetraalkylammonium bromide.[27]

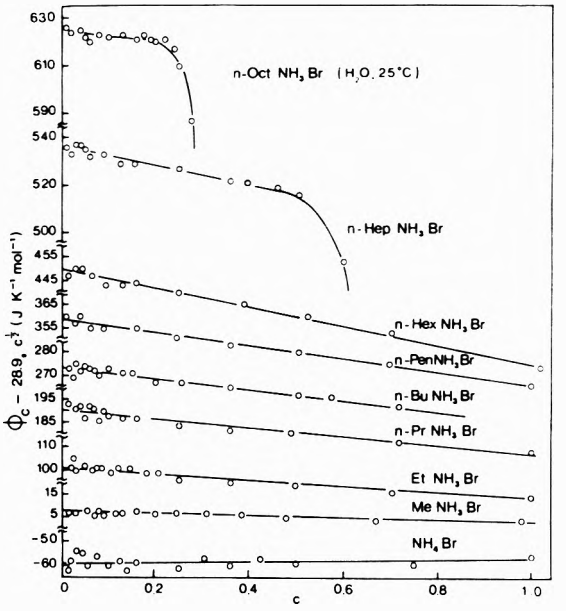

Figure 1. Apparent molal heat capacities of *n*-alkylamine hydrobromides in water at 25°.

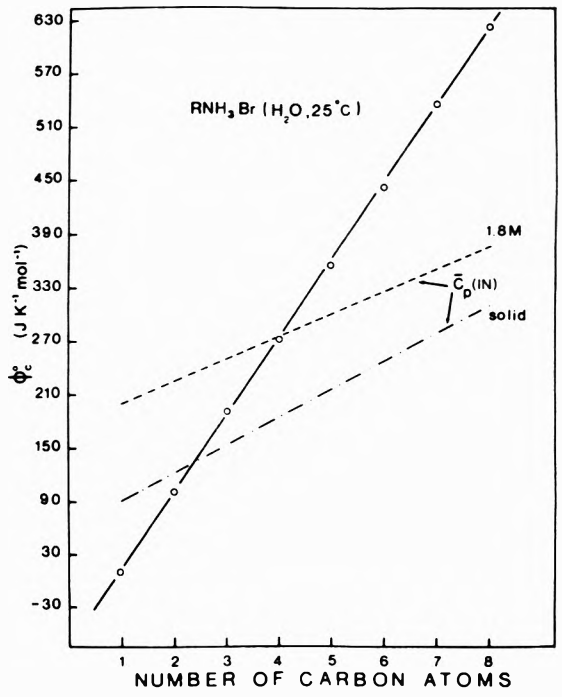

Figure 2. Apparent molal heat capacity at infinite dilution of *n*-alkylamine hydrobromides in water at 25°.

TABLE II: Apparent Molal Heat Capacities of *n*-Alkylamine Hydrobromides in Water at Various Temperatures[a]

Electrolytes	5°	15°	25°	35°	45°	55°
NH_4Ac[b]		88(21)[c]	105.4(−12.7)		120(12)	133(−40)
NH_4Br[b]		−72(1.1)	−60.8(5.2)	−52(3.9)	−46(−5.8)	−41(−22)
$MeNH_3Br$		−7.2(0.7)	7.7(−3.7)	13.2(−6.1)	18.9(−16)	17.1(−9.9)
$EtNH_3Br$		99.5(−20)	101.6(−14.3)	109.9(−20)	110.7(−20)	108.3(−19)
n-$PrNH_3Br$		184.6(−23)	191.6(−20.7)	194.1(−28)	195.3(−33)	192.5(−30)
n-$BuNH_3Br$			273.7(−23.4)			
n-$PenNH_3Br$			359.4(−31.2)			
n-$HexNH_3Br$			447.7(−33.6)			
n-$HepNH_3Br$		533(−25)	534.8(−35.7)	536(−71)	531(−97)	521(−116)
n-$OctNH_3Br$	608(40)	622(−11)	624.3(−16)	614(−45)	616(−130)	591(−110)

[a] Parameters ϕ_{C^0} ($= \bar{C}_p^0$) and B_C' of eq 8. Units of ϕ_C on J K^{-1} mol^{-1}. [b] Values at 25° are taken from ref 5. [c] Values of B_C' are given in parentheses.

TABLE III: Apparent Molal Volumes of *n*-Alkylamine Hydrobromides in Water at Various Temperatures[a]

Electrolytes	5°	15°	25°	35°	45°	55°
NH_4Ac[b]		58.05(1.4)[c]	58.55(0.15)	58.68(1.7)	58.89(0.2)	59.08(−1.3)
NH_4Br		42.13(−0.5)	42.52(−0.48)[d]	42.84(−0.07)	43.21(−0.9)	43.13(−0.8)
$MeNH_3Br$		59.98(−0.3)	60.80(−0.51)[d]	61.12(−0.5)	61.40(−0.6)	61.59(−0.6)
$EtNH_3Br$		77.63(−0.9)	77.61(−0.78)[d]	78.65(−1.0)	78.80(−0.9)	79.18(−1.1)
n-$PrNH_3Br$		93.56(−1.6)	94.11(−1.15)[d]	94.78(−1.6)	95.39(−1.8)	95.73(−1.7)
n-$BuNH_3Br$			110.15(−1.48)[d]			
n-$PenNH_3$			126.13(−1.85)[d]			
n-$HexNH_3Br$			142.05(−2.16)[d]			
n-$HepNH_3Br$		156.52(−3.9)	157.83(−2.19)[d]	159.77(−3.0)	161.44(−2.9)	162.65(−1.9)
n-$OctNH_3Br$	169.40(−2.2)	171.64(−2.1)	173.79(−2.39)[d]	175.18(−0.5)	177.67(−1.8)	178.84(1.7)

[a] Parameters ϕ_{V^0} ($= \bar{V}^0$) and B_V' of eq 7. Units of ϕ_V are cm^3 mol^{-1}. Values at 25° are taken from ref 5. [c] Values of B_V' are given in parentheses. [d] Values obtained from a weighted least-squares fitting of original data.[1]

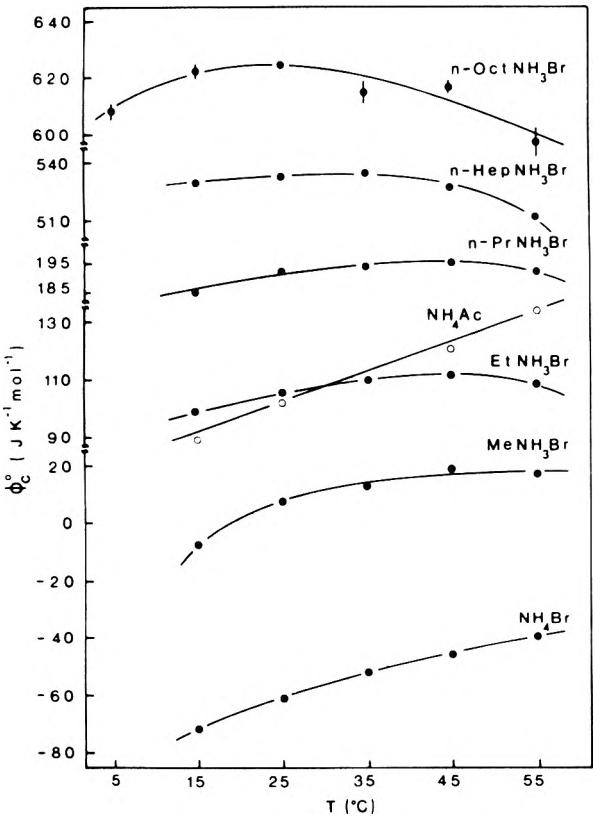

Figure 3. Temperature dependence of the apparent molal heat capacities at infinite dilution of *n*-alkylamine hydrobromides and ammonium acetate in water.

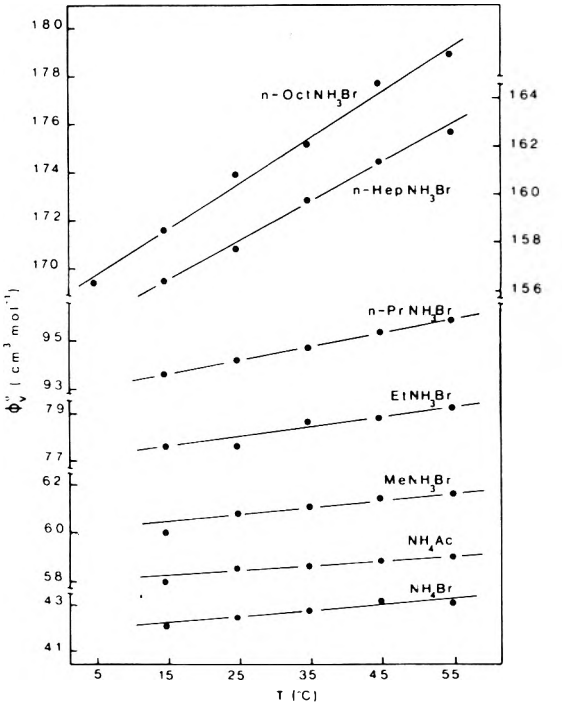

Figure 4. Temperature dependence of the apparent molal volumes at infinite dilution of *n*-alkylamine hydrobromides and ammonium acetate in water.

The thermodynamic excess parameters B_V' and B_C', which reflect solute–solute interactions other than the long-range Debye–Hückel type (limiting law), are given as a function of temperature in Figure 5 for NH_4Br, *n*-Pr, *n*-Hep, and *n*-$OctNH_3Br$. For *n*-$PrNH_3Br$ and the lower members of the series, B_C' and B_V' vary very little with temperature. On the other hand, B_C' of the two micellar salts (*n*-Hep and *n*-$OctNH_3Br$) show a marked decrease with temperature. The parameters B_V' of these long-chain salts also vary with temperature but in a nonlinear fashion, suggesting that the excess expansibilities B_E' are not constant.

The integral enthalpies of dilution are given in the Appendix. The parameters of eq 3, describing the concentra-

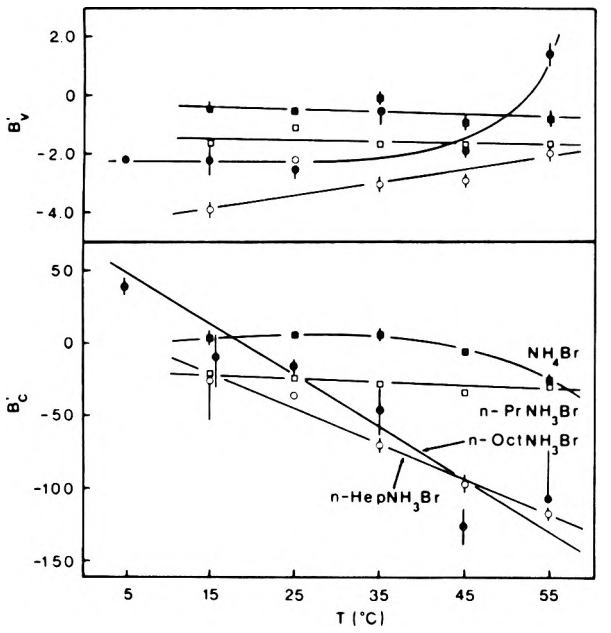

Figure 5. Effect of temperature on the deviation from the Debye-Hückel limiting law of the apparent molal volume (B_V') and heat capacity (B_C') for some *n*-alkylamine hydrobromides in water.

TABLE IV: Expansibilities and Variation with Temperature of the Heat Capacities of *n*-Alkylamine Hydrobromides and Ammonium Acetate in Water at 25°

Electrolyte	ϕ_E^0, cm³ K⁻¹ mol⁻¹	B_E'	$(\partial\phi_C^0/\partial T)_p$, J K⁻² mol⁻¹	$(\partial B_C'/\partial T)_p$
NH_4Ac	0.024		1.05	
NH_4Br	0.036	−0.010	1.00	−0.57
$MeNH_3Br$	0.026	−0.007	0.30	−0.33
$EtNH_3Br$	0.038	−0.005	0.52	−0.047
n-$PrNH_3Br$	0.056	−0.08	0.47	−0.26
n-$HepNH_3Br$	0.159	0.05	0.15	−2.4
n-$OctNH_3Br$	0.190	0.1	≃0	−6.8

tion dependence of ϕ_L, are given in Table V with the standard error on each parameter. The deviations (see Appendix) between the experimental ΔH_{ID} and those calculated from eq 3 and 4 are within experimental error. With *n*-$OctNH_3Br$, ΔH_{ID} for initial concentrations above 0.3 *m* could not be fitted with a polynomial equation. The values of $\phi_L(m_i)$ were calculated from ΔH_{ID} and $\phi_L(m_f)$; below 0.3 *m*, $\phi_L(m_f)$ was calculated from eq 3 and above 0.3 *m* interpolated from a large graph of ϕ_L *vs.* *m*. The derived values of $\phi_L(m_i)$ are given in Table VI.

The variation of $\phi_L - A_L(d_0m)^{1/2}$ with *m* is shown in Figure 6 for NH_4Ac, NH_4Br, and the homologous series RNH_3Br. In all cases, there is an initial negative deviation from the Debye-Hückel limiting law (DHLL). With the lower members, ϕ_L remains negative, but with the longer-chain salts ϕ_L eventually becomes positive at higher concentration.

Discussion

Most of the recent work on aqueous solutions seems to indicate that structural interactions (changes in the hydrogen bond distribution caused by the presence of the solute) are present in all solutions and affect both the solute-solvent and solute-solute interactions. However, their importance varies from property to property. With

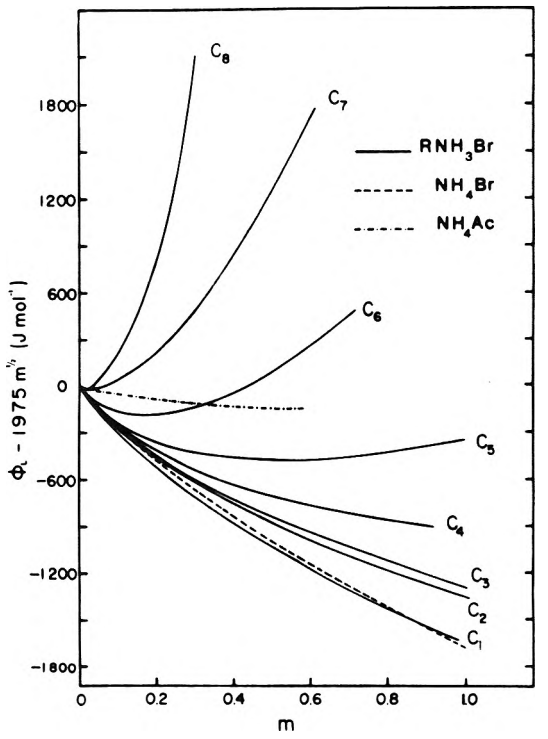

Figure 6. Relative apparent molal enthalpies of *n*-alkylamine hydrobromides and ammonium acetate in water at 25°.

enthalpies of hydration, the structural interactions are evident only when transfer functions from H_2O to D_2O[3,28,29] or from H_2O to urea-water mixtures[30,31] are examined. On the other hand, properties related to the second derivative of the chemical potential with respect to temperature or pressure, such as ϕ_C and ϕ_E, are much more sensitive to structural effects.[13] A careful examination of ϕ_V^0, ϕ_C^0, and ϕ_E^0 (solute-solvent interactions) and ϕ_L, B_V', B_V', and B_E' (solute-solute interactions) as well as the heat, volume, expansibility, and heat capacity of micellization (hydrophobic bonding) should throw some light on the importance of structural effects with these systems.

Solute-Solvent Interactions. The standard apparent molal quantities of aqueous organic ions can be divided into four main contributions[32,33]

$$\phi_Y^0 = \bar{Y}(\mathrm{IN}) + \bar{Y}(\mathrm{COUL}) + \bar{Y}(\mathrm{STR}) + \bar{Y}(\mathrm{HB}) \quad (9)$$

where $\bar{Y}$(IN) is the intrinsic property, *i.e.*, the molar property of the (liquid) solute before interactions take place, $\bar{Y}$(COUL) is the coulombic contribution arising from charge-dipole, charge-quadrupole and other similar interactions, $\bar{Y}$(STR) is the overall structural part which includes any cavity contribution, and $\bar{Y}$(HB) is the contribution arising from hydrogen bonding of the solute with the solvent.

The intrinsic heat capacity $\bar{C}_p$(IN) is not known for these solutes. For a monatomic ion, it is probably close to that of an ideal gas $5R/2$,[13,20,34] but with polyatomic solutes it also includes all contributions from the internal degrees of freedom. Two indirect methods can be used to estimate these $\bar{C}_p$(IN). First, $C_p(\mathrm{IN}) \simeq c_p M$, where c_p is the average specific heat of similar organic liquids, *i.e.*, approximately 1.8 J K⁻¹ g⁻¹, and *M* is the salt molecular weight. These estimated $\bar{C}_p$(IN) are shown in Figure 2. On the other hand, C_p(IN) may be assumed to be equal to the molar heat capacity of the corresponding pure crystalline salt. These heat capacities are known for the solid

TABLE V: Relative Apparent Molal Enthalpies of RNH_3Br and Related Solutes in Water at 25°[a]

Electrolytes	B_L	C_L	D_L	E_L	F_L	Range[c]
NH_4Ac	−962(71)[b]	1,634(219)	−903(172)			$0.06 \leq m_i \leq 0.6$
NH_3Br	−3481(39)	3,209(145)	−1,891(191)	484(84)		$0.015 \leq m_i \leq 1.0$
$MeNH_3Br$	−4239(362)	5,212(1284)	−3,903(1631)	1,284(700)		$0.015 \leq m_i \leq 1.0$
$EtNH_3Br$	−4500(75)	7,316(297)	−6,503(409)	2,332(181)		$0.038 \leq m_i \leq 1.0$
n-$PrNH_3Br$	−4799(70)	7,657(261)	−6,131(347)	2,027(155)		$0.015 \leq m_i \leq 1.0$
n-$BuNH_3Br$	−3682(26)	4,364(69)	−1,613(50)			$0.1 \leq m_i \leq 0.72$
n-$PenNH_3Br$	−4377(148)	7,217(798)	−2,335(1711)	−2,761(1655)	1,926(597)	$0.02 \leq m_i \leq 1.0$
n-$HexNH_3Br$	−9072(243)	42,283(1636)	−88,438(4324)	91,736(5082)	−35,776(2206)	$0.02 \leq m_i \leq 0.7$
n-$HepNH_3Br$	−3194(315)	23,722(2186)	−61,031(5880)	82,954(6976)	−38,732(3040)	$0.02 \leq m_i \leq 0.7$
n-$OctNH_3Br$	−2598(1153)	11,214(12424)	58,211(52726)	−202,296(99659)	199,500(69542)	$0.01 \leq m_i \leq 0.28$

[a] Parameters of eq 3. Units of ϕ_L in J mol^{-1}. [b] Values in parentheses are the standard error. [c] Range of validity of the corresponding parameters.

TABLE VI: α_L of n-$OctNH_3Br$ in Water at 25° for Concentrations above 0.3 m

m_i	ϕ_L, J mol^{-1}
0.35023	3122[a]
0.42961	3803[a]
0.59955	4090[a]
0.7615	4230[b]
1.0016	4304[b]

[a] $\phi_L(m_f)$ calculated with eq 4. [b] $\phi_L(m_f)$ estimated graphically.

$MeNH_3Cl$[35] and n-$PenNH_3Cl$.[36] From the difference in heat capacities of solid Me_4NBr and Me_4NCl,[37] the corresponding heat capacity of the alkylammonium bromides can be estimated ($MeNH_3Br$, 90.8 and n-$PenNH_3Br$, 216.4 J K^{-1} mol^{-1}). Assuming $\bar{C}_p(IN)$ to be linear with chain length or with the number of carbon atoms in the chain, all the other $\bar{C}_p(IN)$ can be predicted. These latter values, shown in Figure 2, probably underestimate $\bar{C}_p(IN)$ since liquids usually have larger heat capacities than the corresponding solids. Still, these two methods of estimating $\bar{C}_p(IN)$ probably set limits to the real values and show that $\phi_C^0 - \bar{C}_p(IN)$ changes signs between n-$PrNH_3Br$ or n-$BuNH_3Br$; it is negative for the lower homologs and positive for the higher ones.

It has been suggested[13] that $\bar{C}_p(COUL)$ does not contribute much to ϕ_C^0 compared to $\bar{C}_p(STR)$ with alkali halides. This should therefore be more so with the present salts. Also, by analogy with urea and substituted ureas[38] $\bar{C}_p(HB)$ should not contribute much to the ϕ_C^0 of RNH_3^+. Consequently, we would expect $\phi_C^0 - \bar{C}_p(IN)$ to be mostly a measure of $\bar{C}_p(STR)$. With the smaller homologs, the structure-breaking effect near $-NH_3^+$ and Br^- are the leading interactions while, with the higher homologs, the hydrophobic interactions of the alkyl chain take over.

The origin of $\bar{C}_p(STR)$ can be visualized as follows. With ordinary liquids the heat capacity results from the molecular translations, rotations, and vibrations and the intermolecular interactions. The high heat capacity of liquid water compared with other liquids results from the partly crystalline nature of water. In addition to the intrinsic heat capacity of the different species (monomers, dimers, ..., clusters) in the liquid, there is a further contribution arising from the shift in equilibrium between the species. If the clusters are considered ice like, then, for a unit increase in temperature, there will be an absorption of some heat of fusion due to the melting of the clusters, and the heat capacity of the bulk water becomes much larger.[18,39] By definition, there are less clusters to melt in the structure-broken region around the ions and the molar heat capacity of the water therein should be significantly smaller. Therefore $\phi_C^0 - \bar{C}_p(IN)$ should be negative for structure breakers.

The extra heat capacity, $\phi_C^0 - \bar{C}_p(IN)$, observed with most nonpolar groups or molecules in water, is usually attributed to an overall increase in the structure of water.[40] By analogy with the structure-breaking effect, the hydrophobic cosphere is probably not a rigid frozen-in network in the sense that it must be more structured than bulk water at 25° and at the same time more sensitive to temperature changes. The total absorption of some heat of fusion of clusters during a unit change in temperature must be larger than in the absence of solutes. D_2O is more structured than H_2O at ordinary temperatures in the same sense and ϕ_C^0 of hydrophobic solutes are more positive in D_2O.[41] Similarly, it was concluded that urea–water mixtures are less structured than pure water since ϕ_C^0 of tetrabutylammonium bromide is less positive[32] and that of alkali halides less negative[42] in the solvent mixture than in pure water.

Some evidence that the large ϕ_C^0 of organic solutes is related to hydrophobic hydration comes from the changes in ϕ_C during micelle formation. The interior of a micelle being lyophilic, most of the hydrophobic hydration must have been eliminated. For example, ϕ_C^0 of n-$OctNH_3Br$ drops from 620 in the premicellar region to 350 J K^{-1} mol^{-1} after micellization. This latter value can be compared with the two estimates of $\bar{C}_p(IN)$, 311 and 378 J K^{-1} mol^{-1}. This indicates that whatever hydrophobic hydration is left in the system is now largely compensated by the structure-breaking effect of the $-NH_3^+$ group and Br^-.

Further evidence that the interpretation of $\phi_C^0 - \bar{C}_p(IN)$ is self-consistent comes from the B_η viscosity coefficient and from the enthalpies of transfer from H_2O to D_2O of this homologous series. It has been shown[43] that the deviation from Einstein's theory, $B_\eta - 0.0025\bar{V}^0$, can be used as a criterion for the overall structural influence of a so-

lute. This function[44] and ΔH_{tr}^0 ($H_2O \rightarrow D_2O$)[3] change sign at about *n*-$BuNH_3Br$ in agreement with $\phi_V^0 - \bar{C}_p(IN)$. Similarly, nmr[45] and esr[46] studies on this systems are consistent with hydrophobic bonding during micellization.

It must be borne in mind however that thermodynamic properties do not give any direct information on the nature of the molecular structure, and it is only through models and theories that some insight may be obtained. In that respect, it should be mentioned that the theories of Eley[44] and of the scaled-particle[47] predict remarkably well the heat capacity of nonelectrolytes in water. This could mean that the large ϕ_C^0 of hydrophobic solutes is related to cavity formation and not to an increase in structure, or else it could mean that hydrophobic hydration is primarily an interfacial phenomena; at an air–water or cavity–water interface, the water molecules show a preferential orientation, and the above calculations indirectly include the structural effects. Therefore, even if the existence of hydrophobic hydration seems well established, its exact nature is still an open question.

The expansibility should also be useful in characterizing structural hydration effects. As with ϕ_C^0, $\bar{E}$(COUL) and $\bar{E}$(HB) can probably be taken as zero. With monatomic solutes, $\bar{E}$(IN) is also zero since $\bar{V}$(IN) does not change with temperature. However, with polyatomic solutes, we would expect some small intrinsic expansibility. On the other hand both the structure-breaking effect and hydrophobic hydration seem to cause a positive contribution to ϕ_E^0.[13] As with heat capacities, one of the main contributions to the expansibility of pure water is the liberation of the volume of fusion of "ice" (negative) during an increase in temperature. This effect being reduced in the structure-broken region, $\bar{E}$(STR) is positive. We would expect the opposite to be true with structure makers. However, with alkali and tetraalkylammonium halides the expansibilities[39,49] and compressibilities[39,50] do not change signs when going from structure breakers to structure makers. This is probably related to the fact that $\phi_V^0 - \bar{V}$(IN) is negative for hydrophobic solutes even though structure is promoted; the increase in ice likeness ($\Delta V > 0$) is more then compensated by the loss in free space between the solute surface and hydrophobic shell ($\Delta V < 0$).[1] In other words, the molar expansibility of the water molecules in the hydrophobic cosphere must be larger than that of the molecules in the bulk, and this difference in molar expansibility of the molecules must exceed the decrease in volume for the fusion of ice in the cosphere during a unit change in temperature. The observed large and positive ϕ_E^0 of *n*-$HepNH_3Br$ and *n*-$OctNH_3Br$ are therefore normal when compared with other hydrophobic systems.

Solute–Solute Interactions. Information on solute–solute interactions can be obtained from the concentration dependence of the thermodynamic functions. Since the Debye–Hückel limiting law, and probably the distance of closest approach, are the same for all the homologous salts, the extra ion–ion interactions in the premicellar region are given by the parameters B_V', B_C', and B_E'. With ϕ_L, it is impossible to represent the deviation from the DHLL with a single adjustable parameter. With all solutes, there is an initial decrease in $\phi_L - A_L(d_0m)^{1/2}$, and with the hydrophobic solutes there is an eventual increase. The initial negative contribution seems to be present with all solutes (hydrophobic or hydrophilic)[13,30] and is probably not structural in origin; it seems to disappear when transfer functions from H_2O to D_2O[3,51] or from H_2O to urea–water mixtures[30] are considered. One suggestion that has been put forward[52] is that it is related to the repulsive forces (core potential or distance of closest approach). Levine and Wood,[53] on the other hand, prefer to attribute the negative deviation from the Debye–Hückel law to pairwise interactions. It is difficult however to see how these shorter-range electrostatic interactions will lead to a negative contribution to ϕ_L while the long-range coulombic forces (Debye–Hückel limiting law) lead to a positive contribution.

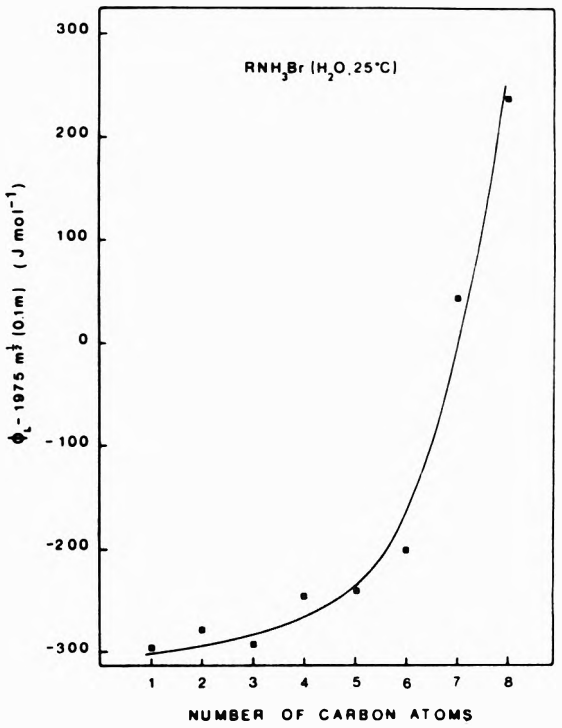

Figure 7. Excess enthalpies at 0.1 *m* for *n*-alkylamine hydrobromides and ammonium acetate in water at 25°.

Despite the complexity of ϕ_L, relative trends can be still studied by comparing $\phi_L - A_L(d_0m)^{1/2}$ at a fixed concentration (0.1 *m*). Such a plot is shown in Figure 7.

The concentration dependence of the thermodynamic properties hydrophobic solutes can be interpreted through the overlap of cospheres.[54] The hydrophobic hydration per ion is decreased if the solutes share part of their cospheres. Therefore, the excess functions should be of opposite sign to those at infinite dilution. This implies that, as the chain length of the RNH_3Br salts increases, B_V',[1] B_C', and B_E' should become more negative and the excess enthalpy more positive. This is generally observed at 25° (see Tables II and III and Figure 7). However, with the higher members of the series, B_V' and B_C' seem to become relatively constant (B_E' of *n*-$OctNH_3Br$ is even much less negative than the others). Despite the larger uncertainty, B_E' of *n*-$HepNH_3Br$ and *n*-$OctNH_3Br$ is positive. On the other hand, the excess enthalpies in Figure 7 increase only slowly with chain length up to *n*-$HexNH_3Br$, then rapidly with the higher homologs. The regularity in the standard apparent molal quantities with chain length is therefore not observed with the excess functions. This could mean that the solute–solute interactions of the higher homologs are different than the others, that new interactions occur (*e.g.*, dimerization), or that the model used for the interpretation of hydrophobic–hydrophobic interactions is wrong. It will be necessary to examine the

temperature dependence of these functions before drawing any further conclusion.

Temperature Effects. If structural interactions are the main contribution to $\phi_C^0 - \bar{C}_p(IN)$ and ϕ_E^0, then we would expect a decrease of these effects as the temperature increases. The temperature dependence of ϕ_C^0 is shown in Figure 3. With the structure-breaking solutes, NH_4Br, NH_4Ac, and the three lower members of the homologous series, ϕ_C^0 does in fact increase with temperature, but with the higher homologs it goes through a maximum rather than decrease as expected. A similar behavior is also observed with tetraalkylammonium halides[27] and with nonyltrimethylammonium bromide.[26] It could be that the decrease in $\bar{C}_p(STR)$ is compensated to some extent by an increase in $\bar{C}_p(IN)$, but it is difficult to explain why $\bar{C}_p(STR)$ should not have a large temperature dependence.

A clue to the interpretation of $(\partial\phi_C^0/\partial T)_p$ might come from the high temperature behavior of simple electrolytes in water. The ϕ_C^0 of most alkali halides go through a maximum in the region 60 to 80°.[20,55,56] The behavior of the hydrophobic salts are therefore similar to those of hydrophilic salts except that the maximum in ϕ_C^0 occurs at lower temperatures. However, to our knowledge, no satisfactory explanation has yet been given to account for the $(\partial\phi_C^0/\partial T)_p$ of aqueous alkali halides at high temperatures.

Another possible approach to the interpretation of the temperature dependence of $\bar{C}_p(STR)$ could be through an analogy with transfer functions. The main contribution to $\bar{C}_p(STR)$ is the passage of water molecules from the bulk to the solute cospheres.[13,42] On the other hand, for the transfer from H_2O to D_2O[13] or from H_2O to urea-water mixtures,[42] the heat capacity of transfer is reflecting primarily the difference between the heat capacities of the pure solvents or mixed solvents. Transposing this to $(\partial\phi_C^0/\partial T)_p$, it could be that this function is reflecting primarily the variation of the heat capacity of pure water with temperature. If the high heat capacity of water was correctly attributed to the shift in water equilibrium during a rise in temperature, then the heat capacity of liquid water should be higher at 0 than at 100°. Experimentally the heat capacity of water goes through a minimum and is approximately the same at 0 and 100°. Therefore, until we reach a better understanding of the temperature dependence of the heat capacity of pure water, it might be difficult to interpret $(\partial\phi_C^0/\partial T)_p$.[57]

The volumes ϕ_V^0 vary linearly with temperature, as seen from Figure 4. This implies that, within experimental uncertainty, ϕ_E^0 is independent of temperature. Therefore, as with $\bar{C}_p(STR)$, $\bar{E}(STR)$ hardly changes with temperature. Here again, no simple explanation can be offered.

The temperature dependence of B_V' and B_C' is shown in Figure 5. At high temperatures, the parameter B_C' follows the order expected from the structural interaction model.[54] However, at low temperatures, the opposite order is observed. At 5°, B_C' of n-$OctNH_3Br$ even becomes positive. Similar trends occur with tetraalkylammonium bromides.[27] Positive B_C' parameters are also observed with hydrophobic solutes having hydrogen bonding groups such as $-OH$[33] and COO^-.[5,33] The effect observed therefore seems general even though there is no obvious explanation for this behavior. A plausible explanation is that there are extra weak interactions between the solutes that are masked by stronger interactions with most functions.

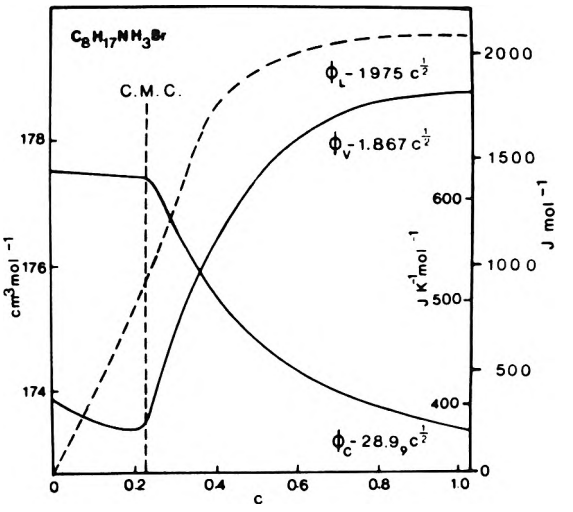

Figure 8. Concentration dependence of ϕ_V, ϕ_C, and ϕ_L less the DHLL slopes of n-octylamine hydrobromide in water at 25°.

However, if these interactions, although small, are very temperature dependent, they may become very important with functions related to the third temperature derivative of the chemical potential.

Hydrophobic Bonding. Micelle formation is often used as a model system for hydrophobic bonding.[58] The alkyl chains will come together in order to minimize the overall hydrophobic hydration. The volumes, heat capacities, and enthalpies of n-$OctNH_3Br$ are compared up to 1 M in Figure 8. Micelles begin to form at about 0.2 M;[1] this corresponds to the minimum in $\phi_V - A_V c^{1/2}$ as well as to the region where $\phi_L - A_L c^{1/2}$ increases more sharply and where $\phi_C - A_C c^{1/2}$ drops very rapidly. Therefore, the heat of micellization is positive (endothermic), the heat capacity of micellization negative, and the volume of micellization positive.[1]

It is not easy to evaluate these thermodynamic functions of micellization since the micellization region is not sharp. Micelles are being formed or grow in size, over a wide concentration range (0.2-1 M). The order of magnitude of these functions can be approximated from the functions at 1 M minus those at 0.2 M and give $\Delta V_m = +5.2$ cm³ mol⁻¹,[1] and $\Delta C_m = -278$ J K⁻¹ mol⁻¹. On the same basis ΔH_m would be about 1000 J mol⁻¹, but its value is more doubtful in view of the large concentration dependence of ϕ_L in the premicellar region. The signs of these functions are all consistent with the decrease in hydrophobic hydration during association; there are fewer hydrogen bonds being formed ($\Delta H > 0$, $\Delta S > 0$), the free space around the solute reappears ($\Delta V > 0$), and the positive contribution of $C_p(STR)$ to ϕ_C^0 of hydrophobic monomers is lost. It should be noted also that ΔC_m is large compared with ΔH_m. This means that ΔH_m is very temperature dependent and is in fact positive only at low temperature; it would probably become negative above 30°.

Acknowledgment. We would like to thank P. Picker for his collaboration in the initial part of this project, C. Jolicoeur for useful discussion of the interpretation, and A. Hade of Université du Québec à Montréal for the loan of a digital densimeter. We are grateful to the National Research Council of Canada and to the Quebec Ministry of Education for financial support of this project. One of us,

J. -L. F., is also thankful to the National Research Council for the award of a scholarship.

Supplementary Material Available. The Appendix, which will appear following these pages in the microfilm edition of this volume of the journal, contains tables of the actual density, enthalpy of dilution, and volumetric specific heat data of the systems studied. Photocopies of the supplementary material from this paper only or microfiche (105 × 148 mm, 24× reduction, negatives) containing all of the supplementary material for the papers in this issue may be obtained from the Journals Department, American Chemical Society, 1155 16th St., N.W., Washington, D. C. 20036. Remit check or money order for $5.00 for photocopy or $2.00 for microfiche, referring to code number JPC-74-1217.

References and Notes

(1) J. E. Desnoyers and M. Arel, *Can. J. Chem.*, **45**, 359 (1967).
(2) J. E. Desnoyers, M. Arel, and P.-A. Leduc, *Can. J. Chem.*, **47**, 547 (1969).
(3) J. E. Desnoyers, R. Francescon, P. Picker, and C. Jolicoeur, *Can. J. Chem.*, **49**, 3460 (1971).
(4) P. Picker, P.-A. Leduc, P. R. Philip, and J. E. Desnoyers, *J. Chem. Thermodyn.*, **3**, 631 (1971).
(5) P.-A. Leduc and J. E. Desnoyers, *Can. J. Chem.*, **51**, 2993 (1973).
(6) P. Picker, E. Tremblay, and C. Jolicoeur, *J. Solution Chem.*, in press.
(7) G. S. Kell, *J. Chem. Eng. Data.*, **12**, 66 (1967).
(8) P. Picker and J.-L. Fortier, manuscript in preparation; see also P. Picker, *Can. Res. Develop.*, **7**, No. 1, 11 (1974).
(9) P. Picker, C. Jolicoeur, and J. E. Desnoyers, *J. Chem. Thermodyn.*, **1**, 469 (1969).
(10) P. Picker, C. Jolicoeur, and J. E. Desnoyers, *Rev. Sci. Instrum.*, **39**, 676 (1968).
(11) J.-L. Fortier, P.-A. Leduc, P. Picker, and J. E. Desnoyers, *J. Solution Chem.*, **2**, 467 (1973).
(12) H. S. Harned and B. B. Owen, "The Physical Chemistry of Electrolytic Solutions," Reinhold, New York, N. Y., 1958, Chapters 3 and 8.
(13) J.-L. Fortier, P.-A. Leduc, and J. E. Desnoyers, *J. Solution Chem.*, in press.
(14) H. F. Stimson, *Amer. J. Phys.*, **23**, 614 (1955).
(15) P. Picker, C. Jolicoeur, and J. E. Desnoyers, *J. Chem. Educ.*, **45**, 614 (1968).
(16) L. A. Dunn, *Trans. Faraday Soc.*, **64**, 2951 (1968).
(17) C. G. Malmberg and A. A. Maryotte, *J. Res. Nat. Bur. Stand.*, **56**, 1 (1956).
(18) G. N. Lewis and M. Randall, "Thermodynamics," K. S. Pitzer and L. Brewer, Ed., McGraw-Hill, New York, N. Y., 1961, Chapter 25 and Appendix 4.
(19) P. H. Bevington, "Data Reduction and Error Analysis for the Physical Sciences," McGraw-Hill, New York, N. Y., 1969.
(20) H. Ruterjans, F. Schreiner, U. Sage, and Th. Ackermann, *J. Phys. Chem.*, **73**, 986 (1969).
(21) E. P. Whitlow and W. A. Felsing, *J. Amer. Chem. Soc.*, **66**, 2028 (1964).
(22) J. Konicek and I. Wadso, *Acta Chem. Scand.*, **25**, 1541 (1971); see also K. Kusano, J. Suuskuusk, and I. Wadso, *J. Chem. Thermodyn.*, in press.
(23) D. M. Alexander and D. J. T. Hill, *Aust. J. Chem.*, **22**, 347 (1969).
(24) E. M. Arnett, W. B. Kover, and J. V. Carter, *J. Amer. Chem. Soc.*, **91**, 4028 (1969).
(25) R. Arnaud, L. Avédikian, and J.-P. Morel, *J. Chim. Phys.*, **76**, 45 (1972).
(26) G. M. Musbally, G. Perron, and J. E. Desnoyers, *J. Colloid Sci.*, submitted for publication.
(27) G. Perron and J. E. Desnoyers, manuscript in preparation.
(28) C. V. Krishnan and H. L. Friedman, *J. Phys. Chem.*, **74**, 2356 (1970).
(29) J. Greyson and H. Snell, *J. Phys. Chem.*, **73**, 3208 (1969).
(30) R. B. Cassel and W.-Y. Wen, *J. Phys. Chem.*, **76**, 1369 (1972).
(31) T. S. Sarma and J. C. Ahluwalia, *J. Phys. Chem.*, **76**, 1366 (1972).
(32) P. R. Philip, J. E. Desnoyers, and A. Hade, *Can. J. Chem.*, **51**, 187 (1973).
(33) J. E. Desnoyers, R. Pagé, G. Perron, J.-L. Fortier, P.-A. Leduc, and R. F. Platford, *Can. J. Chem.*, **51**, 2129 (1973).
(34) C. de Visser and G. Somsen, *J. Chem. Soc., Faraday Trans. 1*, **69**, 1440 (1973).
(35) J. G. Aston and C. W. Ziemer, *J. Amer. Chem. Soc.*, **68**, 1405 (1946).
(36) J. C. Southard, R. T. Milner, and S. B. Hendricks, *J. Chem. Phys.*, **1**, 95 (1932).
(37) S. S. Chang and E. F. Westrum, Jr., *J. Chem. Phys.*, **36**, 2420 (1962).
(38) P. R. Philip, G. Perron, and J. E. Desnoyers, *Can. J. Chem.*, in press.
(39) H. S. Frank and N. W. Evans, *J. Chem. Phys.*, **13**, 507 (1945).
(40) H. S. Frank and W.-Y. Wen, *Discuss. Faraday Soc.*, **24**, 133 (1957).
(41) P. R. Philip and J. E. Desnoyers, *J. Solution Chem.*, **1**, 353 (1972). In the two-state water model presented, the shift in equilibrium contribution to the structural interaction was unfortunately overlooked.
(42) N. Desrosiers, G. Perron, J. J. Mathieson, B. E. Conway, and J. E. Desnoyers, *J. Solution Chem.*, accepted for publication.
(43) J. E. Desnoyers and G. Perron, *J. Solution Chem.*, **1**, 199 (1972).
(44) D. D. Eley, *Trans. Faraday Soc.*, **35**, 1281 (1939).
(45) B. Lindman, H. Wenmerstrorm, and S. Forsen, *J. Phys. Chem.*, **74**, 754 (1970).
(46) C. Jolicoeur and H. L. Friedman, *Ber. Bunsenges. Phys. Chem.*, **75**, 248 (1971).
(47) R. A. Pierotti, *J. Phys. Chem.*, **67**, 1840 (1963); **69**, 281 (1965).
(48) D. N. Glew, *J. Phys. Chem.*, **66**, 605 (1962); see also M. Lucas, *ibid.*, **76**, 4030 (1972).
(49) B. E. Conway and L. H. Laliberté, *J. Phys. Chem.*, **72**, 4317 (1968); see also *Trans. Faraday Soc.*, **66**, 3032 (1970).
(50) B. E. Conway and R. E. Verrall, *J. Phys. Chem.*, **70**, 3952 (1966).
(51) R. H. Wood, R. A. Rooney, and J. N. Braddock, *J. Phys. Chem.*, **73**, 1673 (1969).
(52) J.-L. Fortier, P.-A. Leduc, P. Picker, and J. E. Desnoyers, *J. Solution*, in press.
(53) A. S. Levine and R. H. Wood, *J. Phys. Chem.*, **77**, 2390 (1973).
(54) J. E. Desnoyers, M. Arel, G. Perron, and C. Jolicoeur, *J. Phys. Chem.*, **73**, 3346 (1969).
(55) M. Eigen and E. Wicke, *Z. Electrochem.*, **55**, 354 (1951).
(56) C. M. Criss and J. W. Cobble, *J. Amer. Chem. Soc.*, **83**, 3223 (1961).
(57) It has been pointed out by one of the referees that the anomalous temperature dependence of ϕ_C^0 could arise from the difference between C_p and C_v. It seems that C_v may be more directly related to structural effects than C_p since C_v of pure water decreases monotonically with increasing temperature as expected from a decrease in structure. Unfortunately, the conversion of ϕ_{Cp}^0 to ϕ_{Cv}^0 requires knowledge of ϕ_E^0 and ϕ_K^0. While approximate ϕ_E^0 have been measured in the present paper, ϕ_K^0 are not known for the present systems. However, such measurements are presently under study in our laboratory and this possible approach to the treatment of heat capacities will certainly be investigated.
(58) P. Mukerjee, *Advan. Colloid Interface Sci.*, **1**, 241 (1967).

Orientation Behavior of Adsorbed Pyridine and Pyrazine at the Mercury–Water Interface in Relation to Solution Thermodynamic Properties

B. E. Conway,* J. G. Mathieson, and H. P. Dhar

Chemistry Department, University of Ottawa, Ottawa, Canada *(Received May 4, 1973; Revised Manuscript Received February 4, 1974)*

Publication costs assisted by the University of Ottawa

An experimental procedure for evaluation of the orientation of solvent molecules at the Hg–H_2O interface is described, based on the study of adsorption of pyrazine and pyridine. The adsorption and orientation behavior is investigated in relation to the solution properties of these two molecules, characterized by partial molal volume and compressibility measurements in H_2O and D_2O. The free energies of adsorption are substantially coverage dependent, even in the case of pyrazine, which, overall, is a nonpolar molecule. This behavior is discussed in terms of intermolecular H bonding with water in the interphase. The orientation effects are indicated by evaluation of surface dipole potential changes caused by displacement of oriented solvent by the organic adsorbate. The orientation effects are examined in relation to the surface pressure behavior at the Hg electrode–water interface. In the case of pyridine and pyrazine, the charge dependence of water orientation at the Hg electrode can be quantitatively evaluated while, with pyridine, the extent of orientation of the organic molecule itself can be calculated in terms of its own surface dipole potential contribution.

Introduction

Electrochemical adsorption of organic molecules involves (a) interaction with the metal electrode surface; (b) displacement of previously adsorbed solvent molecules oriented to an extent dependent on the electrode surface charge q_M or corresponding local field; (c) interaction with remaining solvent molecules; and (d) interaction between the adsorbate molecules, including their modified solvent cospheres, at finite coverage θ.

A little examined feature in previous work on adsorption involving solvent displacement is the quantitative evaluation of the extent of solvent orientation R in relation to q_M and θ of the adsorbate. In the present paper, a method is proposed for derivation of R from the experimental adsorption behavior of a neutral, overall nonpolar molecule, pyrazine.

Factors c and d are related to analogous interactions in the bulk phase but, hitherto, in electrochemical adsorption studies of neutral molecules, little attention has been given to specificity of adsorption behavior in relation to solution properties of the adsorbate. In the case of organic molecules in water, this factor must be taken into account in interpreting adsorption behavior since H bonding and solvent-structure factors[1] are important both in the bulk phase and the interphase. Accordingly, in the present paper, the solution properties of pyrazine and pyridine have also been studied in relation to the adsorption behavior of these molecules.

Interactions in the interphase may be characterized at a given metal surface charge, q_M, either (a) by fitting the adsorption data (surface excess, Γ, or θ) to an isotherm in which an interaction term of a previously assumed form is included (*e.g.*, see ref 2) or (b) evaluation of the apparent standard free energy of adsorption,[3,4] $\Delta G^\circ_{ads}{}'$, in an isotherm of the form

$$\frac{\theta}{x(e^{x-1})(1-\theta)^x} = \frac{C_o}{C_w}\exp\left(-\frac{\Delta G^\circ_{ads}{}'}{RT}\right) \qquad (1)$$

where C_o and C_w are the concentrations of organic substances and water in the bulk phase and x is the ratio of effective areas of adsorbate and solvent. Equation 1 is the proper form (*cf.* ref 5) of the Flory–Huggins isotherm for substitutional adsorption at an electrode in contact with a solvent. In eq 1, $\Delta G^\circ_{ads}{}'$ is usually a function of θ or C_o, and its θ dependence, which can be evaluated from the experimental data,[3] corresponds to any nonideal free energy associated with nonideality of the two-dimensional interphase. Evaluation of $\Delta G^\circ_{ads}{}'$ as $f(\theta)$ is in some ways more satisfactory than fitting Γ or θ data to a preconceived isotherm, as the latter procedure usually implies an assumed and simple form for the molecular interaction forces in the interphase and in many previous papers, neglect of the size factor x. In the presence of coadsorbed water, such interaction effects are usually complex, involving solvent-structure[1,6] cosphere overlap, H bonding, as well as previously considered intermolecular dipole–dipole interactions,[4] so that evaluation of $\Delta G^\circ_{ads}{}'$ as $f(\theta)$ is a preferable initial procedure in reducing experimental adsorption results.

Experimental Section

1. Methods. In the present work, the adsorption of 1,4-pyrazine and pyridine was studied at the Hg–water interface by both capillary electrometry and droptime measurements using recently described improvements[7] of experimental technique. Special attention was given to evaluation of changes of surface pressure and surface potential. Complementary measurements of the solution properties of these two molecules were made by apparent molal volume, (ϕ_V), and adiabatic compressibility, ($\phi_{K,S}$), measurements in H_2O and D_2O.[8] These measurements, and the comparison of the infinite-dilution values $\phi_V{}^0$ and $\phi_{KS}{}^0$ (equal to the partial molal values $\bar{V}^0$ and $\bar{K}^0$ in H_2O and D_2O[8,9]), have previously been shown[9,10] to give diagnostic information on the types of interaction which neu-

tral and ionized organic molecules undergo with the water solvent, *e.g.*, in relation to local changes of the relaxation properties[11] of solvent molecules near the organic solute, *i.e.*, so-called "structure-breaking" and "structure-making" effects.

Previously considered aspects of the adsorption of pyrazine and pyridine, *e.g.*, the dependence of free energy of adsorption on charge q_M and solvent orientation are described in ref 12.

2. Choice of Compounds. Pyridine and pyrazine were chosen as adsorbates owing to their simple rigid structures (no field dependence of conformations[13]) and because of previous interest in the orientation of the former molecule, which has its dipole located in the ring structure. Pyrazine is almost exactly the same size as pyridine and is also rigid but has no *overall* dipole moment. It should not, therefore, be oriented in the electrode field as is pyridine,[4,14] especially at more negative q_M and high θ.[4] The rigid, overall nonpolar character of the pyrazine molecule makes it ideal as a probe for evaluation of changes of water orientation in the interface by examining the Esin and Markov effect, the dependence of $\Delta G^{\circ\prime}$ on q_M (reported elsewhere[12,15]) and the dependence of $\Delta G^{\circ\prime}$ on θ.

Most other adsorbates studied at the Hg–H_2O interface are more flexible and can exhibit a field-dependent conformation (*cf.* ref 2 and 19), so that distinction between solvent and functional group orientation is difficult to make and interaction effects are correspondingly more difficult to interpret.

3. Adsorption Measurements. Electrocapillary measurements were made at 20 and 25 ± 0.1° by means of the recently developed procedure described in detail elsewhere.[6,7] Aqueous $NaClO_4$ (0.03 *M*) was used as the supporting electrolyte with a 0.03 *M* aqueous NaCl–calomel reference electrode. Concentrations of the organic adsorbates were as follows: *pyridine* 0.003, 0.006, 0.008, 0.012, 0.020, 0.035, 0.05, 0.09, 0.13, 0.18, 0.25, 0.35, and 0.50 *M*; *pyrazine* 0.001, 0.002, 0.003, 0.005, 0.009, 0.016, 0.025, 0.040, 0.065, 0.110, 0.170, 0.240, 0.340, and 0.460 *M*. Adsorption results were identical in solutions of 0.03 *M* $NaClO_4$ + 0.01 *M* NaOH employed to eliminate significant ionization of the N bases.

Although previous comparisons of surface tension and adsorption behavior at Hg by electrocapillary and droptime or sessile drop dimension[16] measurements have indicated that electrocapillary determinations are essentially reliable under most conditions in aqueous medium, the possibility that potential-dependent variations of contact angle may introduce systematic errors has been recognized.[16-18] Accordingly, in the present work on pyrazine, measurements of surface tension γ were made independently by both the capillary electrometer and droptime methods (the latter in collaboration with Professor F. Kimmerle, University of Sherbrooke). While small differences in γ (0.2–0.3 dyn cm^{-1}) do arise between the two methods, they do so throughout the curve of γ *vs.* log *c* so that the derived surface excess values, Γ, are in very good agreement and show no systematic charge-dependent deviations.

The droptime procedure employed has recently been described in detail elsewhere[19] and droptimes reproducible to better than 0.3 msec in 3 sec are readily obtained. Surface tension values were derived from the droptimes after making the necessary, previously discussed corrections.[19,20]

Shifts of the Hg electrode potential ΔE with increasing surface excess Γ[13,21] (*cf.* ref 22) were derived[23,24] for various q_M, including $q_M = 0$, and were measured in order to evaluate adsorbate and solvent orientation.

Saturation values of Γ, for expressing some of the results in terms of fractional coverage θ, were estimated from Courtauld space-filling models.

4. Apparent Molal Volumes. Density measurements down to 0.01 *m* were made with a differential buoyancy balance using 100-ml floats as described previously.[25] Apparent molal volume data were calculated by the standard procedure and extrapolated linearly with respect to molal concentration *m* to obtain $\bar{V}^0$. Densities were accurate to ±0.000003[25] and temperature constant to ±0.001°.

5. Adiabatic Compressibilities. Apparent molal adiabatic compressibilities, $\phi_{K,S}$, were derived by means of the "sing-around" technique described previously[26,27] using the apparatus shown in those papers; temperature was controlled to ±0.0005°.[26,27] $\phi_{K,S}$ was measured[8] down to 0.01 *m* and extrapolated linearly to infinite dilution to obtain $\phi_{K,S}{}^0$ values accurate to $\pm 0.2 \times 10^{-4}$ ml mol^{-1} bar^{-1}.

In both the volume and compressibility work, measurements were made in H_2O and 99.8% D_2O in order to obtain the solvent-isotope effects[9] $\Delta V_{D_2O\text{-}H_2O}{}^0$ and $\Delta \bar{K}_{S,D_2O\text{-}H_2O}{}^0$ in $\bar{V}^0$ and $K_S{}^0$, respectively.

Results and Discussion

1. Nature of the Adsorption Behavior of Pyrazine. Except at low Γ ($<0.8 \times 10^{-10}$ mol cm^{-2}) where Γ values are hard to obtain with sufficient accuracy, Figure 1 shows that the ΔE *vs.* Γ plots for pyrazine are essentially linear. Since, thermodynamically, $(\partial E/\partial \mu)_q$ is equivalent to $(\partial E/\partial \Gamma)_{qM}(\partial \Gamma/\partial \mu)_{qM}$ and because plots of E_{qM} *vs.* log *c* were also found to be linear, it follows that the adsorption isotherm for pyrazine should be logarithmic (over the range of Γ and μ covered in the experiments). This is well supported by the data of Figure 2 for several q_M values obtained by *both* electrocapillary *and* droptime measurements. The ΔE–Γ behavior is probably a result of the symmetrical rigid and nondipolar nature of the pyrazine molecule that makes it an especially interesting molecule for electrochemical adsorption studies, *e.g.*, the standard free energy of adsorption $\Delta G^\circ_{ads}{}'$ varies with charge[12,15] in a very symmetrical way about $q_M = -2$ μC cm^{-2} (see below).

If the molecule itself is unoriented (as expected since its overall dipole moment is zero), the symmetrical variation of $\Delta G^\circ_{ads}{}'$ with q_M must originate from a symmetrical increase of solvent orientation[28,29] polarization about $q_M = -2$ μC cm^{-2}. This can be examined by evaluating the solvent orientation as described in the following section.

2. Shifts of Potential at Constant Charge due to Adsorption. With neutral molecule adsorption, an effect analogous to the Esin and Markov effect[13,21,22] can arise (a) by orientation of the adsorbate dipole in the metal-solution double-layer field, and/or by specific chemical affinity of one end of molecule for the metal surface (*e.g.*, as with thiourea) and (b) by substitution of already oriented solvent molecules by an unoriented or oriented adsorbate molecule. Effect b will always arise in substitutional adsorption if solvent orientation is $f(q_M)$, as is usually the case, *e.g.*, as treated in the solvent orientation theory of Watts-Tobin and Mott[28] and that of Bockris, Devanthan, and Müller[29] for adsorption. Effect a will be significant if the adsorbate has a permanent net dipole moment or is otherwise electronically anisotropic (*e.g.*,

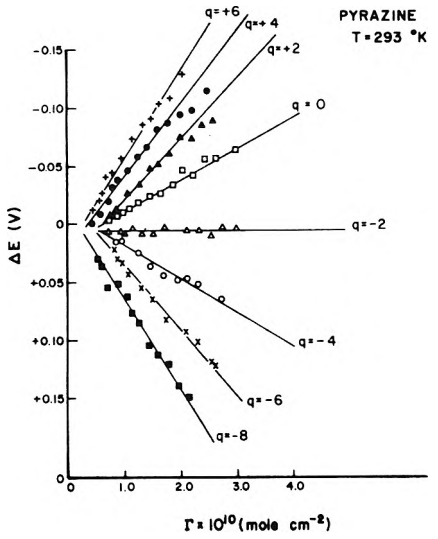

Figure 1. Plots of potential shifts ΔE *vs.* Γ for pyrazine adsorption at Hg at various q_M as a function of Γ (0.03 *M* aqueous $NaClO_4$, 298°K).

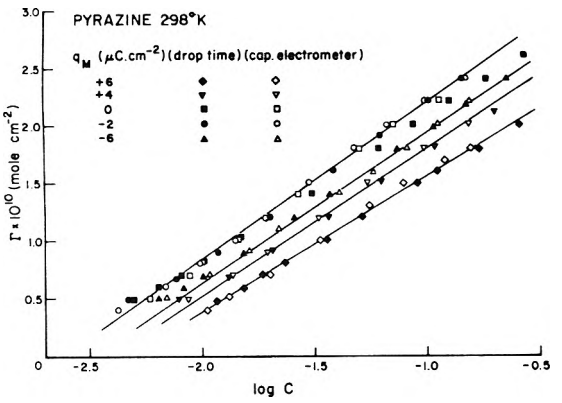

Figure 2. Plots of surface excess Γ for pyrazine adsorption at Hg at 25° from 0.03 *N* aqueous $NaClO_4$ by electrocapillary and droptime measurements for various q_M values.

with aromatic hydrocarbons) and thus may be indirectly oriented by changing solvent interactions as q_M is changed. We have previously demonstrated[12] the importance of displacement of oriented solvent molecules by showing that an appreciable shift of E_M with Γ (*cf.* ref 13 and 21) arises with adsorption of the nonpolar molecule naphthalene from methanolic solution at Hg.

By employing the "flat" and rigid molecule pyrazine in aqueous solution, it is possible to measure quantitatively the charge-dependent water dipole orientation by evaluating the shift ΔE as a $f(\Gamma)$ for various q_M, since pyrazine itself will not tend to be oriented in the electrode field. It seems reasonable to suppose that pyrazine lies on the Hg surface with its π orbitals interating with the Hg; this supposition is supported by the results shown below.

By means of similar experiments with pyridine, the role of both effects a and b may be evaluated and the lateral dipole interaction energy[29] derived as a $f(\theta)$.

Figure 1 shows the potential shifts ΔE (V) for pyrazine adsorption in aqueous solution as $f(\Gamma)$ for various q_M values. Values of Γ at given q_M values were evaluated by differentiation of Parsons ξ function.[23] Linear relations are observed over the accessible range of Γ and the slopes $d(\Delta E)/d\Gamma$ are strongly dependent on q_M. Since the adsorbate itself has no dipole moment, the ΔE shifts must be due mainly (see below) to replacement of adsorbed solvent previously oriented to an extent dependent[28,29] on q_M. The finite slope for $q_M = 0$ shows[30] that water is specifically oriented at the potential of zero charge and only becomes randomly oriented at *ca.* $q_M = -2\ \mu C\ cm^{-2}$ (see Figure 1). This q_M also corresponds to the charge for maximum adsorption (minimum $\Delta G^{\circ\prime}$) evaluated elsewhere,[12] *i.e.*, for the condition of maximum ease of displacement of solvent molecules when they interact minimally with the metal surface in the absence of field due to net charge.

The inner layer potential displacement E will be determined by two components: the potential displacement due to q_M and the dipole potential displacement χ; *i.e.*

$$E = 4\pi q_M d/\epsilon_s + 4\pi(N\uparrow - N\downarrow)\bar{\mu}_{H_2O} \qquad (2)$$

In the above equation for E, $N\uparrow$ and $N\downarrow$ are the populations of solvent molecules oriented in "up" ($\uparrow$) or "down" ($\downarrow$) directions[28,29] in the electrode field out of a total N_T of water molecules cm^{-2}; $\bar{\mu}_{H_2O}$ is the dipole moment (or mean normal component thereof) of H_2O, d is the thickness of the inner layer and ϵ the local dielectric constant of water in the inner layer at the electrode interface. (According to Levine, *et al.*,[31] ϵ does not enter the second term since the orientation of solvent implicit in $N\uparrow - N\downarrow$ corresponds already to the orientation dielectric polarization. In the representation of Kir'yanov, *et al.*,[32] however, ϵ_s is retained in both terms, seemingly incorrectly.[31] References 33 and 34 give a useful discussion of the significance of dielectric constant in considerations of solvent orientation at electrodes but the subject is still contraversial.)

At constant q_M, ΔE shifts will arise primarily from displacement of oriented solvent dipoles determined by the q_M dependent $N\uparrow - N\downarrow$ of eq 2. In the representation of Kir'yanov, *et al.*,[32] a component of ΔE could arise from change of d/ϵ_s upon adsorption of organic. However, for flat orientation of pyrazine, d would be little changed from that for a water layer and ϵ_s is normally low in the inner layer so it seems reasonable to suppose that the main change of ΔE with adsorption of pyrazine will arise from the solvent displacement term. This seems to be borne out by the form of the experimental results (Figure 1).

Then the change of surface dipole potential, $\Delta\chi$, corresponding to ΔE for solvent replacement by pyrazine will be

$$\Delta\chi_{H_2O} \doteq \Delta E = x\Gamma \frac{(N\uparrow - N\downarrow)}{N_T} 4\pi\bar{\mu}_{H_2O} \qquad (3)$$

If ΔE is defined as $(E_0 - E)_{q_M}$, *i.e.*, the difference of potentials on the electrocapillary curve at a given q_M in the supporting electrolyte (E_0), and in the adsorbate solution (E), then the shifts of E in Figure 1 as $f(\Gamma)$ for various q_M are seen to be consistent with progressively more orientation of O atoms in H_2O toward the electrode as q_M is made more positive and more orientation in the reverse direction as q_M is made more negative. Replacement of x H_2O molecules associated with a net orientation $x(N\uparrow - N\downarrow)/N_T$ by the nonpolar organic adsorbate pyrazine causes a decrease of $\Delta\chi$ due to water dipoles or an apparent ΔE shift for pyrazine in a direction opposite to that corresponding to the $\Delta\chi$ of the water molecules before displacement.

The observed effects (Figure 1) are symmetrical about $q_M = -2\ \mu C\ cm^{-2}$, for reasons mentioned above. Similar ΔE shifts are observed at temperatures above and below 25°, except that the slopes $dE/d\Gamma$ decrease somewhat with

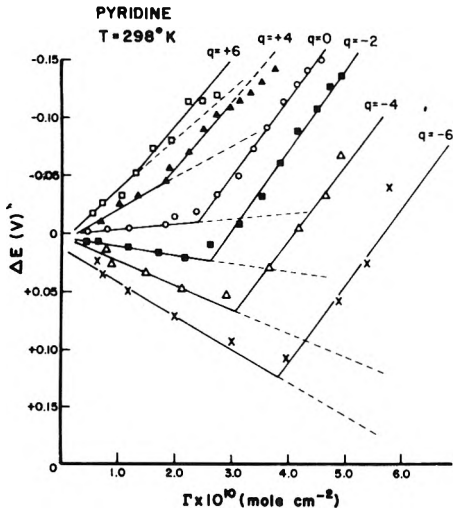

Figure 3. Plots of ΔE *vs.* Γ for pyridine adsorption at Hg at various q_M as a function of Γ (0.03 *M* aqueous $NaClO_4$, 293°K). Dashed lines show initial solvent orientation contribution in ΔE.

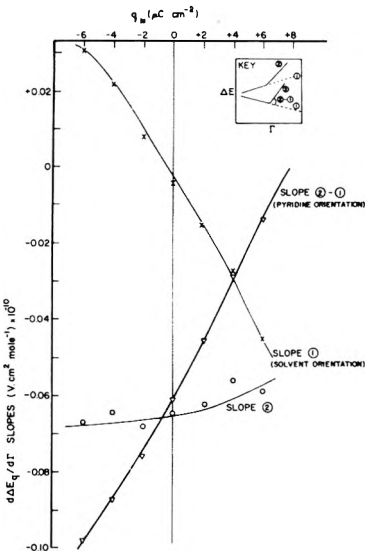

Figure 4. Resolution of slope components in the plots of Figure 3, based on water and pyridine orientation contributions.

increasing temperature as expected on account of thermal disorientation of H_2O.

Figure 3 shows corresponding ΔE *vs.* Γ plots for pyridine. In contrast to Figure 1, the $\Delta E - \Gamma$ plots show sharp inflections, especially as q_M becomes more negative. While the slopes of the initial parts of the $\Delta E - \Gamma$ plots of Figure 3 change with q_M in a way similar to the whole lines of Figure 1, the slopes of the second lines of Figure 3 at higher Γ's are all in the same direction, more or less independent of q_M. This strongly suggests an orientation transition[14,15] and the sharpness of the effect is reminiscent of a phase change.

When orientation of the adsorbate itself occurs, the overall $\Delta\chi$ will be composed of two main contributions: (a) due to solvent displacement (as with pyrazine) and (b) due to adsorbate dipole orientation. Then, for pyridine (Py)

$$\Delta E = \Delta\chi_{H_2O} = \Delta\chi_{Py} = x\Gamma \frac{(N\uparrow - N\downarrow)}{N_T} 4\pi\bar{\mu}_{H_2O} + 4\pi\Gamma\bar{\mu}_{Py} \quad (4)$$

where μ_{py} is the normal component of moment of pyridine when the latter molecules become oriented and ϵ_s, following Levine, *et al.*,[31] is not included.

The progressive change of slopes of the lines in Figure 3 for the ΔE shift with pyridine is accounted for by the two terms of eq 4. As q_M becomes more negative, orientation of water with H atoms nearest to the Hg surface increases, causing a positive change of ΔE due to solvent replacement in the interphase while pyridine itself becomes increasingly oriented. If the two effects can be assumed to be independent, the difference of slopes of the two regions would give the contribution due to pyridine orientation. This is shown in Figure 4, as a function of q_M, together with the initial solvent orientation effect. It is clear that at $+6\ \mu C\ cm^{-2}$ pyridine orientation, while significant beyond $\Gamma = 1.3 \times 10^{-10}$ mol cm^{-2}, is quite small as indicated by the slope differences in Figures 3 and 4. However, as q_M becomes more negative, pyridine orientation increases and the effect is almost linear in q_M. Since the changes of slopes arise suddenly at critical Γ values, dependent on q_M (Figure 3), it seems that a certain fraction of pyridine molecules in the surface must become more or less *completely* oriented and this fraction increases with more negative q_M; a sudden transition of the type shown by the ΔE *vs.* Γ plots could hardly arise if all pyridine molecules at a given Γ were oriented to some mean but smaller extent, dependent on q_M.

The above interpretation suggests that pyridine orientation involves a two-state equilibrium in the interphase between unoriented and oriented, possibly associated (see section 2) pyridine molecules, with the relative quantities of the two species depending on Γ and q_M. This is consistent with previously expressed views[14,35] that pyridine orientation is a cooperative phenomenon, involving a two-dimensional phase transition.

The θ dependence of $\Delta G^{\circ\prime}$ for pyridine and pyrazine is shown in Figures 5 and 6. $\Delta G^{\circ\prime}$ is quite dependent on θ, even for pyrazine which is unoriented and has no net dipole moment. The observed variation of $\Delta G^{\circ\prime}$ must therefore be attributed largely to hydration cosphere effects[6] connected with the surface concentration dependence of the interaction of pyrazine with water and corresponding changes of state of the water in the interphase as Γ increases.[6] These interactions will also be a function of q_M since that quantity determines the water dipole orientation.

Congruency Relations for Pyrazine Adsorption. It is of interest to examine how changes of q_M, for given E values (Figure 7), as a function of Γ compare with changes of E for given q_M values also as a function of Γ. Both are linear over the experimental range of Γ values determined. The question of congruency in electrochemical adsorption behavior has been the subject of discussion in various papers[36-39] and congruency in *both* E and q_M has previously been found for neutral molecule adsorption at Hg, *e.g.*, for 2-butyne-1,4-diol by Parsons, *et al.*,[39] and for acetonitrile by Battisti and Trasatti.[38] The above observations are not thermodynamically inconsistent since the E *vs.* q_M plots do not cross exactly at a common value of q_M corresponding to maximum adsorption (the q_M for maximum adsorption is seen from a previously published figure[12] to vary to a small but significant extent about the value $-2\ \mu C\ cm^{-2}$). At present,[38,39] it seems that the available results for neutral molecule adsorption, including pyrazine, do not clearly distinguish between congruency in E or q_M.

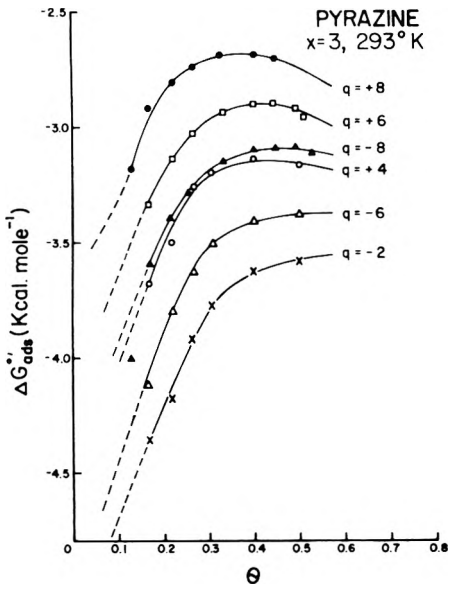

Figure 5. Coverage dependence of apparent standard free energy of adsorption, $\Delta G^{\circ}_{ads}{}'$, of pyrazine at Hg in 0.03 *M* aqueous $NaClO_4$, 293°K.

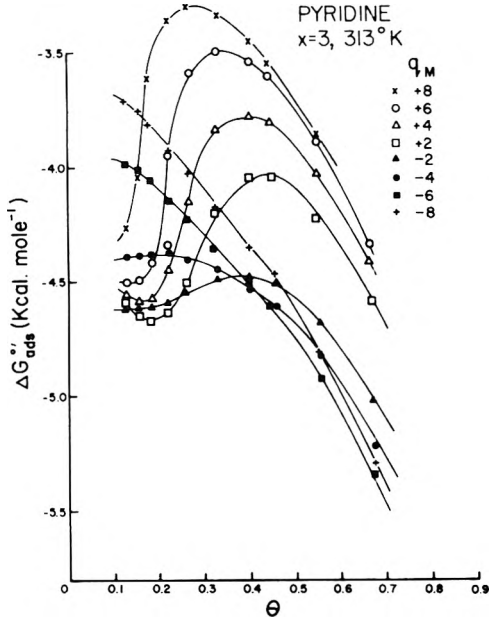

Figure 6. Coverage dependence of apparent standard free energy of adsorption, $\Delta G^{\circ}_{ads}{}'$, of pyridine at Hg in 0.03 *M* aqueous $NaClO_4$, 313°K.

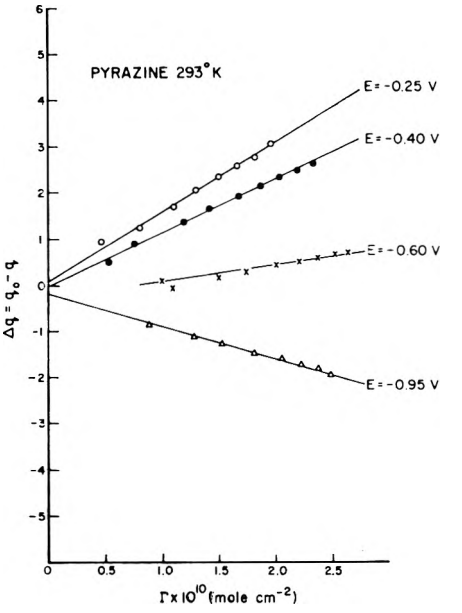

Figure 7. Changes of q_M for given *E* values with increasing surface excess Γ of pyrazine adsorbed at Hg (25°, 0.03 *N* aqueous $HClO_4$) (compare Figure 1).

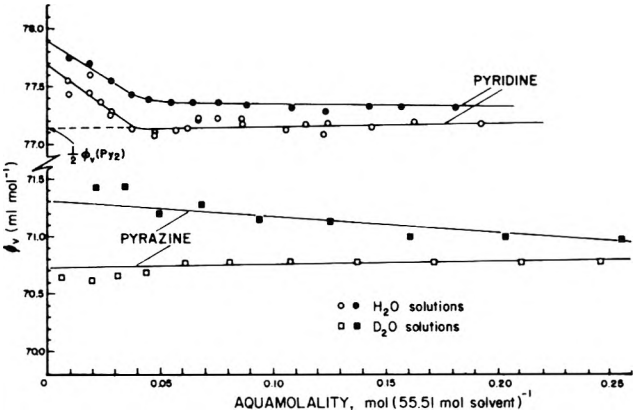

Figure 8. Concentration dependence of ϕ_V for pyridine and pyrazine in H_2O and D_2O at 298°K.

The observed congruency probably arises because pyrazine, more than most uncharged adsorbates previously studied, meets the requirements of rigidity (no conformation-dependent dipole moment) and lack of a permanent dipole moment (no field-induced orientation of the adsorbate itself). Thus its adsorption behavior and effects on surface dipole potential in the double layer arise primarily from displacement of water oriented to an extent dependent on q_M.

2. Partial Molal Volume and Compressibility Behavior. Figures 8 and 9 show the concentration dependence of ϕ_V and $\phi_{K,S}$ for pyrazine and pyridine. The ϕ_V values for pyridine are those previously published.[9] Table I shows the extrapolated infinite dilution values of these properties in H_2O and D_2O and the corresponding solvent isotope effects. b_V and $b_{K,S}$ are the empirical slopes for the concentration dependence of ϕ_V and $\phi_{K,S}$.

Previous partial molar volume work on tetraalkylammonium salts in relation to smaller, more electrostricting ions has shown[9,10] that a positive difference $\Delta\bar{V}_{D_2O\text{-}H_2O}{}^0$ for a solute indicates predominance of a structure-forming, hydrophobic-type interaction with water and corresponds to a lengthening of the nmr relaxation time[11] brought about by the presence of the organic ion. On the other hand, negative $\Delta\bar{V}_{D_2O\text{-}H_2O}$ is observed for electrostricting and structure-breaking ions, and from these observations it has been proposed[8,9] that any structural effect of a solute in H_2O is enhanced in the more structured D_2O solvent, so that the isotope effect can be used as a diagnostic test[10] for the predominant type of hydration (as it affects volume). With nonelectrolytes, electrostriction is absent and volume changes must be due to more subtle structural and H-bonding effects.

For interpretation of the measured partial molal volumes shown in Table I, intrinsic molar volumes (V_{int}) of the molecules are first required. The molecular van der Waals volumes (V_W), estimated from the data of Bondi,[40]

TABLE I: Partial Molal Volumes and Adiabatic Compressibilities of Pyrazine and Pyridine in H_2O and D_2O at 25°

	V^0, ml mol^{-1}			$10^4 \times K_S^0$, ml mol^{-1} bar^{-1}		
Compound	H_2O	D_2O	Isotope effect D_2O–H_2O	H_2O	D_2O	Isotope effect D_2O–H_2O
Pyrazine	70.72 $b_V = +0.32$	71.30 $b_V = -1.44$	+0.58	6.3 $b_{K,S} = 4.8$	3.9 $b_{K,S} = 5.0$	−2.4
Pyridine	77.70 $b_V = -12$, $0 < m < 0.05$; $b_V = 0.2$ $m > 0.05$	77.90 $b_V = -10$ $0 < m < 0.05$; $b_V = 0.2$ $m > 0.05$	+0.20	5.3 $b_{K,S} = 7.8$ $m > 0.05$	0.0 $b_{K,S} = 11.6$ $m > 0.05$	−5.3

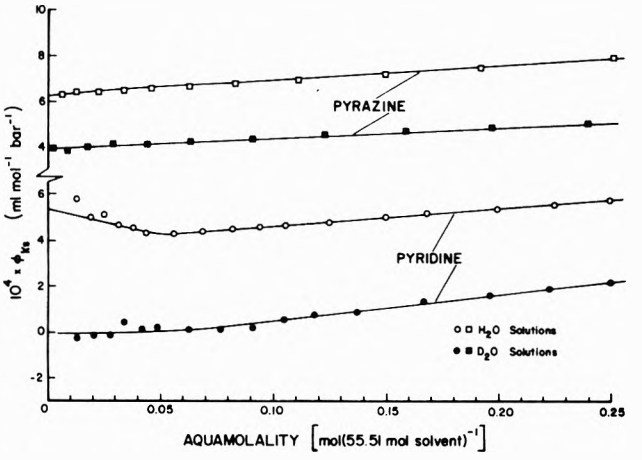

Figure 9. Concentration dependence of $\phi_{K,S}$ for pyridine and pyrazine in H_2O and D_2O at 298°K.

for benzene, pyridine, and pyrazine are 48.4, 45.6, and 43.4 ml mol^{-1}, respectively. These values are much smaller than the effective volumes in the liquid state. The measured volumes for these compounds in *n*-hexane, benzene, and water are compared in Table II.

Actual V_{int} values probably correspond most closely to the volumes in the least polarizable solvent, *i.e.*, *n*-hexane, and it is in this solvent that $\bar{V}^0$ are in a simple relation to the van der Waals volumes, *viz.*, $\bar{V}^0 = (1.83 \pm 0.02)V_W$, and further, the same volume difference of 5.3 ml mol^{-1} is found for the successive loss of each H atom across Table II. Stokes and Robinson[41] used volume fraction statistics to calculate the contribution of the void space to the intrinsic volume associated with randomly packed spheres and found the value $1.73 \times V_{spheres}$, a factor close (5%) to that for V_W in *n*-hexane.

The volume changes encountered on going from *n*-hexane to benzene are surprizingly large for pyridine and pyrazine, and must presumably arise from dipole π-electron interactions. The volumes of pyridine and pyrazine in benzene are similar to those in the corresponding pure liquids $\bar{V}^0(C_6H_5N)$ = 80.5 ml mol^{-1} and $V^0(C_4H_4N_2)$ = 74.5 ml mol^{-1} (the latter being estimated at 25° from the density at 61° and the molar expansibility). Thus, the cohesive dipole–dipole and dipole–π-electron forces must be similar in both the pure liquids and in the C_6H_6 solutions. For H_2O solutions, a considerable volume change for benzene arises since now water dipole π interactions are possible and additionally, since water has an open structure, some of the volume decrease can arise from hole-filling, diminished by hydrophobic structure enhancement. Although the difficulties concerned with interpretation of specific effects must not be underestimated,[9,42-44] the

TABLE II: Infinite Dilution Molal Volumes (ml mol^{-1}) at 25°[a]

	Solute		
Solvent	Benzene	Pyridine	Pyrazine
n-Hexane	89.8 — 5.3 →	84.5 — 5.3 →	79.2
	0.4 ↓	4.4 ↓	5.2 ↓
Benzene	89.4 — 9.3 →	80.1 — 6.5 →	73.6
	8.7 ↓	2.4 ↓	2.9 ↓
Water	80.7 — 3.0 →	77.7 — 7.0 →	70.7

[a] Values in arrows show differences in volume between indicated systems.

principal structural effects expected in water on going from pyridine to pyrazine are (a) a *decrease* in hydrophobic structure making due to the two N atoms tending to make $\Delta\bar{V}_{st}^0$(pyridine) > $\Delta\bar{V}_{st}^0$(pyridine); (b) a doubling of the N-water interaction. Then (i) solute dipole–water dipole interactions yield $\Delta\bar{V}_{st}^0$(pyridine) > $\Delta\bar{V}_{st}^0$(pyrazine) while (ii) a *positive* change in volume due to H-bond formation and structure making at the N atom will give a contribution $\Delta\bar{V}_{st}^0$(pyridine) < $\Delta\bar{V}_{st}^0$(pyrazine).

Experimentally, if $\bar{V}^0$ (solute in *n*-C_6H_{14}) = $\bar{V}_{int}^0$ is estimated, then $\bar{V}_{st}^0 = \bar{V}^0 - \bar{V}_{int}$ = 6.8 ml mol^{-1} for pyridine and 8.1 ml mol^{-1} for pyrazine, so that interactions a and b,i predominate in causing the volume change. A significant and negative part of $\bar{V}_{st}^0$ will be due to hole filling in water.

$\Delta\bar{V}_{D_2O\text{-}H_2O}^0$ is positive for both compounds and greater for pyrazine, indicating[9,42] structure formation; however, since $\Delta\bar{V}_{D_2O\text{-}H_2O}^0$ is greater for pyrazine, it seems that formation of H bonds at the N centers is more effective in producing a positive isotope effect than is hydrophobic hydration.

The b_V terms indicate the net effect of solute–solute cosphere interaction[45] as measured by volume. Negative b_V indicates predominance of an attractive interaction, *e.g.*, with pyridine due to elimination of hydrophobic hydration. In water, pyridine dimers appear to exist through sharing H bonds with an H_2O molecule as directly indicated by the vapor pressure,[46] nmr relaxation,[47] activity,[48] and volume[9] behavior. The nmr relaxation studies[47] indicate long-lived structures containing pairs of pyridine molecules hydrogen bonded through one or more interlinking water molecules. $Py_2(H_2O)_6$ can be inferred[46,47] as the stoichiometry of the complex. The ϕ_V behavior at high dilutions[9] may be interpreted in terms of dissociation of this dimer and the equilibrium constant K estimated (*cf.* ref 49) as $(3.5 \pm 1)\ M^{-1/2}$ or $\Delta G^\circ = -0.74$ kcal mol^{-1}. The limiting volume change for dimerization being *ca.*

-0.56 ml mol^{-1} demonstrates that loss of hydrophobic hydration is the dominant factor in the dimerization volume change (*cf.* ref 50). The attractive forces involved in dimerization probably imply, for adsorption, a decrease in $\Delta G^{\circ\prime}$ with coverage (Figure 6).

Positive b_V for nonelectrolytes implies, on the other hand, net cooperative structure building. We find this for pyrazine in water and since pyrazine is bifunctional, chain-like hydrogen bonding of water molecules between pyrazine N atoms appears to be an important basis for cosphere interactions about molecules adsorbed at the Hg surface leading to the observed $\Delta G^{\circ\prime}$ behavior.

Intrinsic compressibilities of solutes in water are probably small[42] and $\bar{K}_S^0$ results therefore principally reflect changes in local solvent compressibility. The $\bar{K}_S^0$ data for pyrazine indicate that it swims in a locally slightly more compressible solvent than does pyridine. For both molecules, $\bar{K}_S^0$ is positive and close to the value for pure water (+8.1 ml mol^{-1} bar^{-1}); hence, these solutes have little net compressibility effect. Since hydrophobic structure building yields locally a "stiffer" water structure[11,42] (negative change in $\bar{K}_S^0$), this implies that hydrogen-bond interaction has a compensating positive effect. The fact that $\bar{K}_S^0$(pyrazine) > $\bar{K}_S^0$(pyridine) conforms with this observation which is also consistent with interpretations of $\bar{V}$ and $\bar{K}_S$ isotope effects[8,9] for the solute HOD which indicated that the isotope effect for H bonding to the solvent is positive.[8]

The compressibility isotope effects indicate that the hydrophobic interaction with pyridine is quite sensitive to solvent structural change, while the effect is much more positive for pyrazine because of H bonding, as mentioned above, but it remains negative due to remaining ring hydrophobic effects. Positive $b_{K,S}$ is found in each case and implies that relatively incompressible cosphere structures are being broken, the effect being greater for pyridine than pyrazine. Spectroscopic studies[51] on uv shifts of $\pi \rightarrow \pi^*$ bands give information on H-bonding effects but, unfortunately, this approach is not possible for pyridine since suitable bands are not present[52] in the uv spectrum.

3. Relation to Free Energies of Adsorption and Surface Pressure Behavior. Orientation effects in adsorption should be reflected in (a) the free energies of adsorption and (b) in the surface pressure ϕ_{qM} behavior. Figure 10 shows the dependence of ϕ_{qM} on Γ for pyrazine and pyridine at various q_M values. The ϕ_{qM} data for the pyrazine are almost independent of q_M confirming the relative absence of adsorbate orientation effects and the congruency[36] of corresponding isotherms for pyrazine adsorption at various q_M. On the other hand, for pyridine, the $\phi_{qM} - \Gamma$ relations show inflections beyond $q_M = 0$ corresponding to those in the plots of Figure 3. The similarity of the ϕ_{qM} behavior for pyrazine and pyridine up to $q_M = 0$ suggests that the latter molecule is oriented flat at Hg, like pyrazine, at positive q_M. This is consistent with the low Γ regions of Figure 3. However, ϕ_{qM} for pyridine is less than that for pyrazine when q_M is negative and $\Gamma > ca.\ 3 \times 10^{-10}$ mol cm^{-2}.

In the case of pyridine, it appears (relative to the behavior of pyrazine) that a greater coverage can be accommodated, especially at higher negative q_M, without (or with less) repulsive interaction under conditions where neither type of molecule is oriented (as indicated from the low Γ regions of Figures 1 and 3). This observation is also in agreement with the cosphere effects found in the solution properties (see section 2). Pyridine is a monofunctional H-bonding molecule, so less interference with other H-bonded pyridine molecules attached to water will arise in comparison with pyrazine. Also, as q_M becomes more negative, the strength of H bonding between oriented water molecules and pyridine N centers can become stronger due to an inductive effect through the π orbitals (in the "flat" orientation) from the negative metal surface (making N more basic). This would lead to relatively less easy orientation as q_M is made larger, except as the ratio of pyridine to water becomes greater at higher Γ, whereupon (Figure 3) relatively sudden orientation arises, possibly with two molecules carrying a water molecule between them at the N centers.[47] Also, some relief of hydrophobic interaction[1] with the water, indicated by the value of $b_{K,S}$ for pyridine in relation to that for pyridine and the isotope effect in $\bar{K}_S^0$ for these two solutes, would tend to be achieved in the side-by-side orientation of the rings shown in Figure 11.

The high Γ sections of the inflected $\phi_{qM} - \Gamma$ relations of Figure 12 for pyridine show a diminishing slope, $d\phi_{qM}/d\Gamma$, as q_M becomes more negative. In relation to the slopes of the main parts of the $\phi_{qM} - \Gamma$ lines for $q_M > 0$, and to

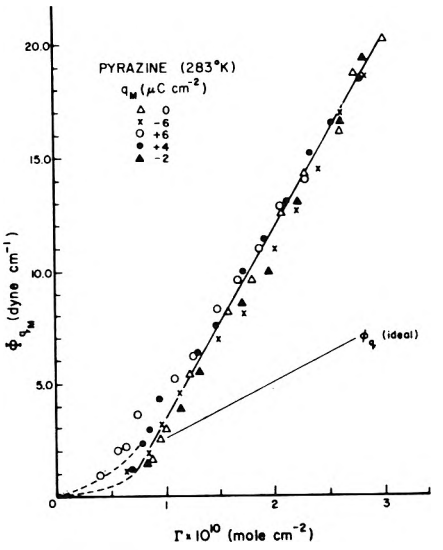

Figure 10. Surface pressure ϕ_{qM} as a function of Γ for pyrazine adsorption at Hg for various q_M values (0.03 *M* aqueous $NaClO_4$, 283°K). ϕ_{qM}(ideal) is the ideal surface pressure relation.

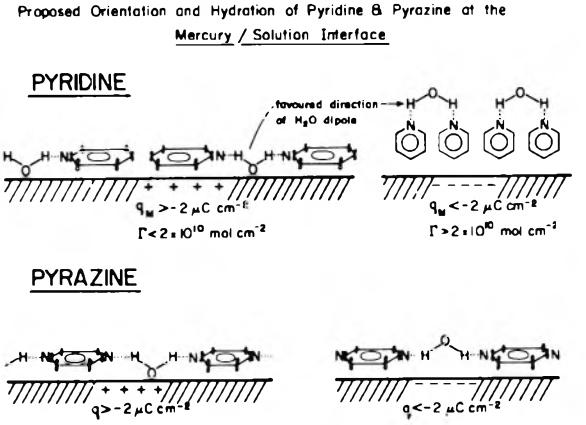

Figure 11. Schematic representation of pyrazine and pyridine orientation at a Hg surface with H bonding to oriented water molecules.

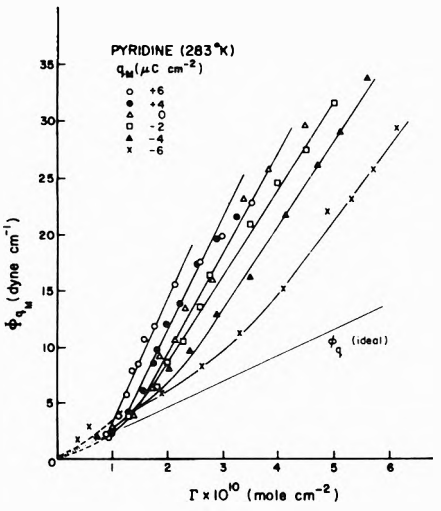

Figure 12. Surface pressure ϕ_{qM} *vs.* Γ relations for pyridine at various q_M values at Hg (0.03 *M* aqueous $NaClO_4$, 283°K). ϕ_{qM}(ideal) is the ideal surface pressure relation.

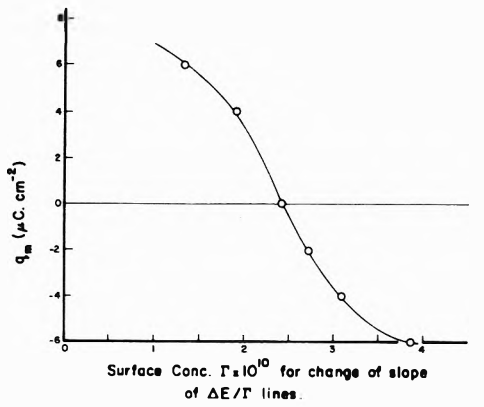

Figure 13. Surface "concentration" Γ required for orientation of pyridine at the Hg electrode as a function of q_M.

the slopes of the ϕ_{qM} − Γ lines for all q_M values in the case of pyrazine (Figure 10), it is of interest to establish first if the lower slopes of the ϕ_{qM} − Γ lines for pyridine originate because of attractive interactions or if the higher slope lines originate because of repulsive or equivalent interactions (*e.g.*, hydration cosphere overlap). For ideal behavior in the interface, $\phi_{qM} = RT\Gamma$ or $d\phi_{qM}/d\Gamma = RT = 2.476 \times 10^{10}$ erg mol^{-1}. Inspection of Figures 10 and 12 shows that for pyrazine and for the high Γ sections of the pyridine behavior, the slopes $d\phi_{qM}/d\Gamma$ are some four times *larger* than the value for ideal behavior beyond $\Gamma = 0.8 \times 10^{-10}$ mol cm^{-2} indicating an appreciable second virial coefficient.[36] For $q_M > 0$, the lower slope regions for pyridine (Figure 12) therefore indicate relatively *less* repulsive interactions which persist to higher Γ values, the more negative is q_M. This is entirely consistent with the results of Figure 3 where pyridine orientation sets in only at progressively higher Γ's as q_M becomes more negative (see Figure 13).

The above effects of q_M on orientation of pyridine (*e.g.*, in the ΔE − Γ or the ϕ_{qM} − Γ relations) do not arise in the case of pyrazine since there is no double-layer field effect tending to promote net orientation of this molecule and the bifunctional H bonding with water helps to keep the molecule in the "flat" orientation.

In the case of pyrazine, the repulsive interaction inferred from the ϕ_{qM} values becomes appreciable, but independent of q_M (Figure 10), as $\Gamma \times 10^{10} >$ *ca.* 0.8, *i.e.*, about one-quarter coverage. Construction of a model of the surface shows that pyrazine molecules each with one water molecule H bonded to each N atom can just be accommodated without overlap up to *ca.* one-quarter coverage of the surface by pyrazine. Beyond that coverage, interference among the H-bonded water molecules must arise, giving the diminished $-\Delta G_{ads}^{\circ}$ as ϕ_{qM} increases (Figure 5) and the higher slopes of the ϕ_{qM} − Γ relations for pyrazine above the ideal value. The independence of $d\phi_{qM}/d\Gamma$ on q_M, and the lack of an orientation contribution due to pyrazine in the ΔE − Γ plots of Figure 1, shows that pyrazine itself is not oriented and that the interaction effect is not very sensitive to water orientation in the double layer.

Since ϕ_{qM} at negative q_M values is lower when $\Gamma > 1.5 \times 10^{-10}$ mol cm^{-2} than it is at more positive q_M, it follows that the course of the ϕ_{qM} plots must correspond to two more or less independent contributions to the dependence of ϕ_{qM} on Γ. This effect corresponds to the inflections in the ϕ_{qM} − Γ plots of Figure 12 and the behavior is thus similar to that leading to the inflected ΔE − Γ plots of Figure 3, *i.e.*, the ϕ_{qM} regions of higher slope in Figure 12 are superimposed on continuing ϕ_{qM} − Γ lines of lower slope, presumably corresponding to unoriented pyridine behaving more ideally with respect to surface pressure. Were all the pyridine layer to become suddenly oriented as Γ increased (for negative q_M), ϕ_{qM} values would suffer a stepwise increase at a critical value of Γ. Possibly, for the negative q_M values, hydrogen-bonded dimers of pyridine, with bridging water,[47] constitute the unoriented state with consequent elimination of interference between hydration cospheres about the pyridine N atoms previously in the surface layer adjacent to the Hg.

4. Relation to Orientation and θ Dependence of ΔG°_{ads}'. The orientation of pyridine we have shown (Figure 13) seems critically dependent both on Γ and q_M. At low Γ, even when q_M is appreciably negative (Figures 3 and 12), orientation is not indicated. This suggests that the pyridine N atom can be held among a system of H-bonded interphase water molecules, even when the latter are appreciably oriented. The orientation function[12,29] $(N\uparrow - N\downarrow)/N_T$ as $f(q_M)$ has been previously calculated,[12] based on an interaction parameter[29] $Uc/kT = 2$ for pyrazine and a larger value for pyridine, evaluated[15] from the breadth of the $\Delta G^{\circ}_{ads}'$ − q_M relations experimentally observed for pyrazine and pyridine (positive q_M branch). As Γ increases, however, the H bonding between interphase water molecules (Figure 11) must decrease and pyridine molecules become freer to orient in the field determined by q_M. This orientation may be assisted by intermolecular H bonding with water as shown in Figure 11. Since the slopes of the ΔE − Γ relations for pyridine at the high Γ end are little dependent on q_M (Figure 3), it must be supposed that once orientation sets in, it does so in a cooperative way (as in a phase change[35]) aided more by H bonding with the solvent than by interaction with the field due to q_M. The effect of q_M is more on the critical value of Γ at which (see Figure 13) orientation sets in; this is presumably due to the effect of field on orientation of water which tends to diminish the lateral H bonding between pyridine molecules.

In the case of pyrazine, the molecules can be involved in bifunctional H bonding (Figure 11), which is consistent

with the difference of solution thermodynamic properties of pyrazine and pyridine described earlier. Thus, even when θ = 50–60%, corresponding to the limits of Γ in Figure 1 or 10, there is still a tendency for the molecules to be held in a network in the interphase, parallel with the Hg surface; also, in the pyrazine case, there is no net field effect tending to orient them.[53]

Acknowledgment. Grateful acknowledgment is made to the Department of Energy, Mines and Resources, Canada (Inland Waters Branch), for support of this work on a research contract. We have also appreciated the interest of Drs. M. C. B. Hotz and W. A. Adams in this work. We also acknowledge the cooperation of Professor F. Kimmerle, Université of Sherbrooke, in arranging for the drop-time measurements to be carried out, which will be published in more detail elsewhere.

References and Notes

(1) G. Némethy and H. A. Scheraga, *J. Chem. Phys.*, **36**, 3401 (1962).
(2) E. Dutkiewicz, J. D. Garnish, and R. Parsons, *J. Electroanal. Chem.*, **16**, 505 (1968).
(3) E. Blomgren and J. O'M. Bockris, *J. Phys. Chem.*, **63**, 1475 (1959).
(4) B. E. Conway and R. G. Barradas, *Electrochim. Acta*, **5**, 319, 349 (1961).
(5) H. P. Dhar, B. E. Conway, and K. M. Joshi, *Electrochim. Acta*, **18**, 789 (1973).
(6) B. E. Conway and L. G. M. Gordon, *J. Phys. Chem.*, **73**, 3609 (1969).
(7) L. G. M. Gordon, J. Halpern, and B. E. Conway, *J. Electroanal. Chem.*, **21**, 3 (1969).
(8) J. G. Mathieson and B. E. Conway, *J. Solution Chem.*, in press.
(9) B. E. Conway and L. H. Laliberté, *Trans. Faraday Soc.*, **66**, 3032 (1970).
(10) B. E. Conway and L. H. Laliberté, *J. Phys. Chem.*, **72**, 4317 (1968).
(11) G. Engel and H. G. Hertz, *Ber. Bunsenges. Phys. Chem.*, 72, 808 (1968).
(12) B. E. Conway and H. P. Dhar, Proceedings of the Summer School of Surface Chemistry, Rovinj, Yugoslavia, June 1972; *Croat. Chem. Acta*, **45**, 109 (1973).
(13) R. G. Barradas, P. G. Hamilton, and B. E. Conway, *J. Phys. Chem.*, **69**, 3411 (1965).
(14) L. Gierst in "Transactions of the Symposium on Electrode Processes, 1959," E. Yeager, Ed., Wiley, New York, N. Y., 1961.
(15) B. E. Conway, H. P. Dhar, and S. Gottesfeld, *J. Colloid Interface Sci.*, **43**, 303 (1973).
(16) J. N. Butler, *J. Phys. Chem.*, **69**, 3817 (1965).
(17) B. E. Conway, in "Techniques of Electrochemistry," Vol 1, E. Yeager and A. J. Salkind, Ed., Wiley-Interscience, New York, N. Y., 1972, Chapter 5, p 389.
(18) D. M. Mohilner and J. Lawrence, *J. Electrochem. Soc.*, **118**, 1596 (1971).
(19) H. Menard and F. Kimmerle, *J. Electroanal. Chem.*, **47**, 375 (1973).
(20) E. Verdier, R. Grand, and P. Vanel, *J. Chim. Phys.*, **66**, 376 (1969).
(21) R. Parsons, *Trans. Faraday Soc.*, **55**, 999 (1959); see also E. Mackor, *Recl. Trav. Chim. Pays-Bas*, **70**, 747 (1951); F. W. Schapink, M. Oudeman, K. W. Leu, and J. N. Helle, *Trans. Faraday Soc.*, **70**, 747 (1951).
(22) O. A. Esin and B. F. Markov, *Acta Physiochim. URSS*, **10**, 353 (1939).
(23) R. Parsons, *Trans. Faraday Soc.*, **51**, 1518 (1955).
(24) R. Parsons, *Proc. Int. Congr. Surface Activity, 2nd*, **38**, 147 (1957).
(25) H. E. Wirth, *J. Amer. Chem. Soc.*, **59**, 2549 (1937); *cf.* F. Vaslow, *J. Phys. Chem.*, **70**, 2286 (1966); R. E. Verrall and B. E. Conway, *ibid.*, **70**, 3901 (1966); B. E. Conway, R. E. Verrall, and J. E. Desnoyers, *Trans. Faraday Soc.*, **62**, 2738 (1966).
(26) J. G. Mathieson and B. E. Conway, *Anal. Chem.*, **44**, 1517 (1972).
(27) R. Garnsey, R. J. Boe, R. Mahoney, and T. A. Litovitz, *J. Chem. Phys.*, **50**, 5222 (1969).
(28) R. J. Watts-Tobin and N. F. Mott, *Electrochim. Acta*, **4**, 79 (1961); *Phil. Mag.*, **6**, 133 (1961).
(29) J. O'M. Bockris, M. A. V. Devanthan, and K. Müller, *Proc. Roy. Soc., Ser. A*, **274**, 55 (1963).
(30) Part of the ΔE change could arise by displacement of specifically adsorbed anions. However, in the 0.03 *M* $NaClO_4$ used here, this effect, we believe, will be negligible.
(31) S. Levine, G. M. Bell, and A. L. Smith, *J. Phys. Chem.*, **73**, 3534 (1969).
(32) V. A. Kir'yanov, V. S. Krylov, and B. B. Damaskin, *Sov. Electrochem.*, **6**, 521 (1970).
(33) K. Müller, *J. Res. Inst. Catal., Hokkaido Univ.*, **14**, 224 (1967).
(34) B. E. Conway, D. J. MacKinnon, and B. V. Tilak, *Trans. Faraday Soc.*, **66**, 1203 (1970).
(35) R. Armstrong, *J. Electroanal. Chem.*, **20**, 168 (1969).
(36) R. Parsons, *Proc. Roy. Soc., Ser. A*, **261**, 79 (1961).
(37) R. Payne, *J. Electroanal. Chem.*, **47**, 265 (1973).
(38) A. de Battisti and S. Trasatti, *J. Electroanal. Chem.*, **48**, 213 (1973).
(39) E. Dutkiewicz, J. D. Garnish, and R. Parsons, *J. Electroanal. Chem.*, **16**, 505 (1968).
(40) A. Bondi, *J. Phys. Chem.*, **68**, 441 (1964).
(41) R. H. Stokes and R. A. Robinson, *Trans. Faraday Soc.*, **53**, 301 (1957).
(42) B. E. Conway and R. E. Verrall, *J. Phys. Chem.*, **70**, 3952 (1966).
(43) L. H. Laliberté and B. E. Conway, *J. Phys. Chem.*, **74**, 4116 (1970).
(44) A. Holtzer and M. F. Emmerson, *J. Phys. Chem.*, **73**, 26 (1969).
(45) R. W. Gurney, "Ionic Processes in Solution," McGraw-Hill, New York, N. Y., 1953.
(46) R. J. L. Andon, J. D. Cox, and E. F. G. Herington, *Trans. Faraday Soc.*, **53**, 410 (1957).
(47) E. von Goldammer and H. G. Hertz, *J. Phys. Chem.*, **74**, 3734 (1970).
(48) S. Cabani, G. Conti, and L. Lepori, *Trans. Faraday Soc.*, **67**, 1933 (1971).
(49) J. G. Mathieson, Ph.D. Thesis, University of Newcastle, N.S.W. Australia 1970; J. G. Mathieson and G. Curthoys, submitted for publication.
(50) T. C. Broadwater and D. F. Evans, *J. Phys. Chem.*, **73**, 164 (1969); F. Franks, M. J. Quickenden, J. R. Ravenhill, and H. T. Smith, *ibid.*, **72**, 2668 (1968); L. Benjamin, *ibid.*, **70**, 3790 (1966).
(51) A. S. N. Murthy and C. N. R. Rao, *Appl. Spectrosc. Rev.*, **2**, 69 (1968).
(52) F. Halverson and R. C. Hirt, *J. Chem. Phys.*, **19**, 711 (1951).
(53) If the double-layer field were very heterogeneous, then some quadrupole orienting effect with pyrazine might be observed. Over the q_M range covered, this does not seem experimentally to be the case.

Angular Overlap Model Description of the Electronic and Magnetic Properties of Copper(II) Complexes

Robert C. Marshall and David W. James*

Chemistry Department, University of Queensland, St. Lucia, Brisbane, Australia, 4067 *(Received February 20, 1973; Revised Manuscript Received February 19, 1974)*

The molecular orbital orientation of the angular overlap model has been developed to describe the d-d electronic spectra, anisotropic molecular magnetic susceptibilities, and esr g values of orthorhombically distorted octahedral copper(II) complexes. By systematically varying the σ and π perturbation energy parameters good agreement is reached between the experimental properties and the corresponding calculated values with particular reference to the potassium copper Tutton's salt ($K_2Cu(H_2O)_6(SO_4)_2$).

Introduction

Magnetic properties of transition metal complexes have previously been discussed in terms of a crystal field model in which the formation of molecular orbitals between the central metal ion and ligands is accounted for by the inclusion of the anisotropic orbital reduction parameter. Much work has been reported on the first transition series ions in cubic fields, *i.e.*, octahedral and tetrahedral,[1] but only recently has there been any extensive investigation of the effect of low symmetry crystal fields,[2,3] and then only of tetragonal nature.

With a crystal field model, anisotropic magnetic properties for tetragonally distorted octahedral copper(II) salts have been evaluated when a number of parameters involving orbital energy levels, orbital reduction factors, temperature, and spin orbit coupling are varied.[2] The d → d electronic transitions and anisotropic magnetic susceptibilities and esr g values were successfully described for potassium copper Tutton's salt ($K_2Cu(H_2O)_6(SO_4)_2$) when the experimental data were analyzed assuming a tetragonal crystal field. A recent neutron diffraction study[4] shows that this analysis is invalid as the chromophore is orthorhombic (D_{2h}). If the above model is extended to the lower symmetry case (D_{2h}), there is an increase in the number of parameters which are not readily interpretable from a chemist's point of view. We report a description of the d orbital energy levels and associated magnetic properties using the angular overlap model which produces a chemically more satisfying analysis.

The molecular orbital orientation of the angular overlap model (AOM) utilizes the full symmetry splitting of the partially filled d shell.[5] It has successfully described the d → d electronic spectra of transition metals in cubic fields including the cases of tetragonal and trigonal bipyramidal perturbation in copper(II) systems.[6] We have used this model to describe the orbital energy levels of orthorhombically distorted octahedral copper(II) complexes and extended it for a description of anisotropic magnetic susceptibilities and esr g values. The theme of this paper is the general development of the model and its method of application with reference to a particular system, $M_2Cu(H_2O)_6(SO_4)_2$ (M = K, Cs, or NH_4).

The Model

(I) Defining the System. We consider only the nearest neighbors (L) to the copper(II) ion (M) as providing the ligand field potential of D_{2h} symmetry. If the ligands are the same and the specific symmetry arises from different bond lengths, the axes XYZ of the ML_6 moiety are defined by the following: the origin of the rectangular Cartesian coordinate system XYZ coincides with M, the Z axis is coincident with the M-L bond of greatest length, the Y axis with the shortest bond, and the X axis with the intermediate bond length. A subsidiary set of Cartesian coordinates $X'Y'Z'$ are localized on each ligand and these are shown in Figure 1 along with the numbering system of the ligands.

(II) Perturbation Matrix. The ligand field potential on the d electrons consists of the sum of a spherical potential and a specific symmetry potential and it is the latter which we consider in AOM. We take account of the symmetry of the field by the specification of the rotation operator $R(\phi,\theta,\psi)$. According to Schäffer,[5] whose notation is used here, the coordinate system $X'Y'Z'$ initially coinciding with the XYZ system is rotated around Z through angle ϕ then around Y through θ and finally around Z through ψ. The irreducible representation matrices $D(R(\phi,\theta,\psi))$ are now formulated knowing from Figure 1 that (ϕ,θ,ψ) for ligands 1, 2, and 3 are respectively $(0,\pi,\pi)$, $(0, \pi/2, 3\pi/2)$, and $(\pi/2, 3\pi/2, \pi)$. Assuming for a general case that the perturbation from each ligand consists of a σ and two π interactions, the perturbation matrix shown in Chart I can be derived as shown by Schäffer.[5] Here e_i^p are the perturbation energies from the ligand positions 1, 2, and 3 (superscript on e), and the subscripts σ, πc, and πs refer to the ligand potentials along the Z', X', and Y' axes, respectively.

Partitioning of this matrix yields three 1 × 1 matrices and a 2 × 2 matrix. Solution of the latter gives the eigenvalues of the $a_g(1)$ and $a_g(2)$ wave functions (see below) along with the mixing coefficients for the linear combination of (z^2) and $(x^2 - y^2)$ orbitals, *i.e.*, the values of a and b discussed in the next section.

(III) Molecular Orbital Formation. To simplify the formation of molecular orbitals, we form symmetry adapted orbitals of the ligand orbitals available for σ and π bonding to the metal ion. So that the notation of orbitals is not too formidable, let σ_i (i = 1, 2,. . .,6 denotes ligand position) denote the σ bonding ligand orbital, *i.e.*, the one along the Z' axis, πc_i and πs_i the π bonding orbitals corresponding to the X' and Y' axes. The notation of the gerade normalized symmetry adapted ligand molecular orbitals are self explanatory and are shown in Table I. The an-

Chart I

(z^2)	(yz)	(zx)	(xy)	$(x^2 - y^2)$
$e_\sigma{}^1 + {}^1/_4(e_\sigma{}^2 + e_\sigma{}^3)$	0	0	0	$(-\sqrt{3}/4)(e_\sigma{}^2 - e_\sigma{}^3)$
0	$e_{\pi 2}{}^3 + e_{\pi s}{}^1$	0	0	0
0	0	$e_{\pi c}{}^1 + e_{\pi s}{}^2$	0	0
0	0	0	$e_{\pi c}{}^2 + e_{\pi s}{}^3$	0
$(\sqrt{3}/4)(e_\sigma{}^2 - e_\sigma{}^3)$	0	0	0	$(3/4)(e_\sigma{}^2 + e_\sigma{}^3)$

TABLE I: Gerade Normalized Symmetry Adapted Ligand Orbitals

σ bonding	πc bonding	πs bonding
$a_g(z) = \frac{1}{\sqrt{2}}(\sigma_1 + \sigma_6)$	$b_{1g}(\pi c) = \frac{1}{\sqrt{2}}(\pi c_2 + \pi c_5)$	$b_{1g}(\pi s) = \frac{1}{\sqrt{2}}(\pi s_3 + \pi s_4)$
$a_g(x) = \frac{1}{\sqrt{2}}(\sigma_2 + \sigma_5)$	$b_{2g}(\pi c) = \frac{1}{\sqrt{2}}(\pi c_1 + \pi c_6)$	$b_{2g}(\pi s) = \frac{1}{\sqrt{2}}(\pi s_2 + \pi s_5)$
$a_g(y) = \frac{1}{\sqrt{2}}(\sigma_3 + \sigma_4)$	$b_{3g}(\pi c) = \frac{1}{\sqrt{2}}(\pi c_3 + \pi c_4)$	$b_{3g}(\pi s) = \frac{1}{\sqrt{2}}(\pi s_1 + \pi s_6)$

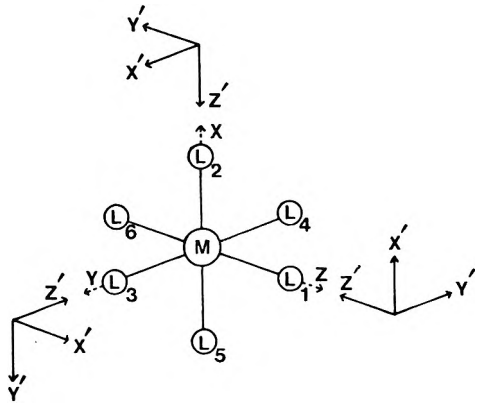

Figure 1. The rectangular Cartesian coordinate system XYZ of the ML_6 moiety. A subsidiary set of Cartesian coordinates $X'Y'Z'$ are localized on each ligand whose numbering system is shown.

tibonding orbitals ψ^*, whose major contributions are the d orbitals (phased according to Condon and Shortley[7]), are

$$\psi_{a_g}{}^*(1) = N_{a_g}(1)\{[a(z^2) + b(x^2 - y^2)] + c_1(a_g(z)) + c_2(a_g(x)) + c_3(a_g(y))\}$$
$$= \alpha_1(z^2) + \alpha_2(x^2 - y^2) + \alpha_3(a_g(z)) + \alpha_4(a_g(x)) + \alpha_5(a_g(y))$$
$$\psi_{a_g}{}^*(2) = N_{a_g}(2)\{[-b(z^2) + a(x^2 - y^2)] + c_4(a_g(z)) + c_5(a_g(x)) + c_6(a_g(y))\}$$
$$= \beta_1(z^2) + \beta_2(x^2 - y^2) + \beta_3(a_g(z)) + \beta_4(a_g(x)) + \beta_5(a_g(y))$$
$$\psi_{b_{1g}}{}^* = N_{b_{1g}}\{(xy) + c_7(b_{1g}(\pi c)) + c_8(b_{1g}(\pi s))\}$$
$$= \gamma_1(xy) + \gamma_2(b_{1g}(\pi c)) + \gamma_3(b_{1g}(\pi s))$$
$$\psi_{b_{2g}}{}^* = N_{b_{2g}}\{(zx) + c_9(b_{2g}(\pi c)) + c_{10}(b_{2g}(\pi s))\}$$
$$= \epsilon_1(zx) + \epsilon_2(b_{2g}(\pi c)) + \epsilon_3(b_{2g}(\pi s))$$
$$\psi_{b_{3g}}{}^* = N_{b_{3g}}\{(yz) + c_{11}(b_{3g}(\pi c)) + c_{12}(b_{3g}(\pi s))\}$$
$$= \delta_1(yz) + \delta_2(b_{3g}(\pi c)) + \delta_3(b_{3g}(\pi s))$$

It is now necessary to determine the admixture coefficients of the symmetry adapted ligand orbitals to the metal orbitals. Consider the general case where the metal d orbital is ϕ_M and the linear combination of the ligand orbitals of the same symmetry type as ϕ_M is ϕ_L (ϕ_M and ϕ_L are each separately normalized). The resultant molecular orbital ψ is

$$\psi = N(\phi_M + \lambda\phi_L)$$

where λ is the admixture coefficient and N is the normalizing coefficient. Coulson[8] has shown the method by which the value of λ can be obtained by solving the secular equations in the variation method. If the Wolfsberg-Helmholtz[9] approximation is incorporated, and because the Coulomb integral for the ligand is much more negative than that for the metal, then λ can be approximated as

$$\lambda \approx -(k/2)S$$

where k, arising in the Wolfsberg-Helmholtz approximation, lies between 1.6 and 2. Within the angular overlap model, the overlap integral S is the product of the angular factor D (discussed above) and a radial factor $S_t{}^*$[5] (t designates whether the overlap is σ, πc, or πs in origin).

$$S = DS_t{}^*$$

Jorgensen,[10] by applying second-order perturbation theory to the Wolfsberg-Helmholtz equation, deduced the destabilization energy associated with the metal d orbital on the formation of molecular orbitals with ligand orbitals. This energy derives from the sum of spherical and specific symmetry potential energies of the ligand field. Because the spherical term is small compared with H_M, it can be absorbed into H_M and hence the specific symmetry potential e_t can be equated to the destabilization energy, *i.e.*

$$e_t \approx [({}^1/_2k - 1)H_M + {}^1/_2kH_L]^2(S_t{}^*)^2/(H_M - H_L) \approx -{}^1/_4k^2H_L(S_t{}^*)^2 \quad (H_L \ll H_M < 0)$$

where H_M and H_L are the core potentials for the metal and ligand orbitals, respectively. Thus λ can be formulated in terms of the σ, πc, and πs energy parameters as

$$\lambda \approx -D\sqrt{e_t/(-H_L)}$$

(IV) Spin Orbit Coupling Perturbation. The effect of spin orbit coupling in copper is significant and its perturbation has to be included. The operator for spin orbit coupling, $\zeta\,\hat{l}\cdot\hat{s}$ (ζ is the single electron spin orbit coupling parameter), has to be degraded into its components in the X, Y, and Z directions because of the orthorhombic nature of the ligand field, *i.e.*

$$\zeta\hat{l}\cdot\hat{s} = \zeta_Z\hat{l}_Z\cdot\hat{s}_Z + \zeta_X\hat{l}_X\cdot\hat{s}_X + \zeta_Y\hat{l}_Y\cdot\hat{s}_Y$$

Chart II

$\psi_{a_g}^*(1)[+1/2]$	$\psi_{a_g}^*(2)[+1/2]$	$\psi_{b_{2g}}^*[-1/2]$	$\psi_{b_{1g}}^*[+1/2]$	$\psi_{b_{3g}}^*[-1/2]$
$E_{a_g}(1)$	0	$\frac{\zeta_0\epsilon_1}{2}(-\sqrt{3}\alpha_1 + \alpha_2)$	$i\alpha_2\gamma_1\zeta_0$	$\frac{-i\zeta_0\delta_1}{2}(\sqrt{3}\alpha_1 + \alpha_1)$
0	$E_{a_g}(2)$	$\frac{\zeta_0\epsilon_1}{2}(-\sqrt{3}\beta_1 + \beta_2)$	$i\beta_2\gamma_1\zeta_0$	$\frac{-i\zeta_0\delta_1}{2}(\sqrt{3}\beta_1 + \beta_2)$
$\frac{-\epsilon_1\zeta_0}{2}(\sqrt{3}\alpha_1 - \alpha_2)$	$\frac{-\epsilon_1\zeta_0}{2}(3\beta_1 - \beta_2)$	$E_{b_{2g}}$	$\frac{-i\epsilon_1\gamma_1\zeta_0}{2}$	$\frac{-i\epsilon_1\delta_1\zeta_0}{2}$
$-i\gamma_1\alpha_2\zeta_0$	$-i\gamma_1\beta_2\zeta_0$	$\frac{i\gamma_1\epsilon_1\zeta_0}{2}$	$E_{b_{1g}}$	$\frac{\gamma_1\delta_1\zeta_0}{2}$
$\frac{i\delta_1\zeta_0}{2}(\sqrt{3}\alpha_1 + \alpha_2)$	$\frac{i\delta_1\zeta_0}{2}(\sqrt{3}\beta_1 + \beta_2)$	$\frac{i\delta_1\epsilon_1\zeta_0}{2}$	$\frac{\delta_1\gamma_1\zeta_0}{2}$	$E_{b_{3g}}$

Out of necessity to keep the number of parameters at a minimum and also as the anisotropic variation of the spin orbit coupling is unknown, ζ_Z, ζ_X, and ζ_Y have been approximated as being equal. As we have shown previously,[2] the isotropic spin orbit coupling parameter can be reasonably approximated by the free ion single electron spin orbit coupling parameter ζ_0 (= 830 cm^{-1}). It may be noted that the orbital reduction factor necessary in previous calculations is not required here.

The 10 × 10 perturbation matrix obtained by the operation of the spin orbit coupling on the ten antibonding wave functions, predominantly of metal d orbital character, can now be set up. The spin orbit coupling arising from the ligand is small and is considered to be negligible compared with ζ_0. Also overlap of orbitals on different ligands has been neglected because it would be extremely small due to the ligands considered subsequently. The 10 × 10 matrix can be factorized into two similar 5 × 5 matrixes, one of which is shown in Chart II. The eigenvectors of this matrix indicate the contribution of the original molecular orbital (ψ^*) to the new molecular orbital ψ.

(*V*) *Application of a Magnetic Field.* The magnetic susceptibility may be calculated using Van Vleck's equation[11] for the situation where the wave functions, ψ, are perturbed by a magnetic field.

Application of the Model

(*I*) *General Description.* The molecular orbital orientated angular overlap model has been developed in order to describe anisotropic magnetic data and d → d electronic spectra of magnetically dilute, orthorhombically distorted octahedral copper(II) complexes. Such compounds are the copper Tutton's salts ($M^I_2(Cu(H_2O)_6(SO_4)_2$, M^I = Cs, K, or NH_4). The energies of d → d electronic transitions, magnetic susceptibilities, and esr g values have been calculated for certain values of the σ, πc, and πs energy parameters when ζ_0, H_L, and the temperature are stated. The parameters e_i are varied until a best fit between the experimental data and the calculated corresponding value is obtained. The systematic fitting procedure was by Powell's method of conjugate directions[12] in which values of the n energy parameters approximating a fit are given along with n independent vectors as search directions. After each complete sweep, a conjugate direction is obtained and consequently all the parameters are varied simultaneously in the fitting. We define the criterion for best fit as the minimization of the sum of the square of the difference between the calculated and experimental values divided by the standard deviation of that experimental measurement, *i.e.*, F is minimized where

$$F = \sum\left(\frac{\text{experimental} - \text{calculated}}{\text{standard deviation}}\right)^2$$

(*II*) *Structure of the Copper Tutton's Salts.* Evidence for the orthorhombic distribution of the H_2O ligands about the Cu(II) ion in the cesium, potassium, and ammonium copper Tutton's salts has been obtained from esr spectroscopy[13] and neutron diffraction.[4] The latter investigations indicate that the water is of the tetrahedral type which Chidambaram, *et al.*,[14] call type J. The two lone pairs of electrons on the oxygen atom are considered to occupy two of the tetrahedral positions around this atom and the two hydrogen atoms are at the remaining two positions. Because of this tetrahedral nature, the bonding in H_2O is best described by the equivalent orbital approach[15] where the nonbonding orbitals θ_{11} and θ_{12} are

$$\theta_{11} = -0.009(1s) + 0.680(2s) - 0.192(2p_z) + 0.707(2p_x)$$
$$\theta_{12} = -0.009(1s) + 0.680(2s) - 0.192(2p_z) - 0.707(2p_x)$$

Either of these orbitals, lying along any of the Z' axes of Figure 1, can σ bond to copper(II) ion. The s orbital contributions to the remaining lone-pair orbital have no net π bonding, but the $(2p_x)$ contribution can form a π bond with the appropriate metal d orbital. It is found from the crystal structure analysis that the X' axes (Figure 1) correspond with the p_x contribution direction. The value of H_L has been assumed to be the same in both the σ and π directions and has been approximated as −100,850 cm^{-1}. In the description of the model it was assumed that the overlap between ligands was negligible. This is a reasonable approximation for the Tutton's salt because of the nature of the ligands and the interligand distance (≃ 3 Å).

Fitting of the Angular Overlap Model to Experimental Results

The angular overlap model has been fitted by the variation of the perturbation energy parameters to the experimental d → d electronic energies, magnetic susceptibilities, and g values reported elsewhere[16] and summarized in Table II.

(*a*) *Estimation of Standard Deviations.* Before the fitting procedure can be started, it is necessary to have an estimate of the standard deviation of each experimental measurement.

The standard deviations for the d → d electronic energies were estimated by inspection, taking into account agreement between single crystal and diffuse reflectance

TABLE II: Electronic Spectral Band Positions,[a] Magnetic Susceptibility,[a] and g Values[b] for Some Copper Tuttons Salts

	$Cs_2[Cu(H_2O)_6]SO_4$	$K_2[Cu(H_2O)_6]SO_4$	$(NH_4)_2[Cu(H_2O)_6]SO_4$
d–d band positions,[c] cm^{-1}	9,820	9,980	10,110
	10,650	11,770	11,660
	12,530	12,660	12,350
	13,200	14,170	13,390
Magnetic susceptibility,[d]	1,689(48)	1,610(50)	1,775(40)
10^{-11} m^3 mol^{-1}	1,860(118)	1,994(94)	2,077(80)
	2,471(78)	2,378(76)	2,407(74)
Esr g value[c]	2.075	2.055	2.058
	2.149	2.157	2.208
	2.407	2.384	2.358

[a] Reference 16. [b] References 13 and 17. [c] Estimated maximum errors for d ← d band positions are 300 cm^{-1} and for esr g values are 0.08. [d] Numbers in parentheses are estimated maximum errors.

TABLE III: Results Obtained at 293 K from the Fitting of the Angular Overlap Model to the Experimental Data for $Cs_2Cu(H_2O)_6(SO_4)_2$ with $e_{\pi c} = (1/3)e_{\pi s}$[a]

	Perturbation energy, cm^{-1}			
	Run a		Run b	
Bond length, pm	e_σ	$e_{\pi s}$	e_σ	$e_{\pi s}$
196.6	0	60	0	1,600
200.4	5,620	1,620	9,190	3,390
231.5	11,760	2,610	12,190	5,170

		Calculated value	
	Experimental value[b]	Run a	Run b
d → d energy, cm^{-1}	9,820(150)	9,930	9,840
	10,650(150)	11,590	10,700
	12,530(150)	12,400	12,350
	13,200(150)	13,340	13,370
Magnetic susceptibility, 10^{-11} m^3 mol^{-1}	1,689(24)	1,636	1,688
	1,860(59)	1,924	1,796
	2,471(39)	2,435	2,489
Esr g value	2.075(0.04)	2.011	2.036
	2.149(0.04)	2.148	2.088
	2.407(0.04)	2.380	2.404

[a] The perturbation energies have been corrected so that the minimum value is zero. $(z^2) \rightarrow (x^2 - y^2)$ is (a) first transition, (b) second transition. [b] The estimated standard deviation is in parentheses.

results and the positions of absorptions for different polarizations and different crystal faces. As this method was very approximate individual standard deviations were not determined but an "average" standard derivative was estimated as 150 cm^{-1}. For the principal molecular susceptibilities, the errors include random errors which are estimated from a least-squares analysis, alignment errors arising when the crystal is transferred to the suspension, and a systematic error of 0.5% arising from calibration of the magnetic field. These errors are discussed in more detail elsewhere.[16] The standard deviation is estimated to be half the maximum error shown in Table II.

The accuracy of the principal g values calculated by Bose, *et al.*,[13] and Pal, *et al.*,[17] depends only upon that of the measuring apparatus.[13] On this assumption, the g values have a greatest possible error of 0.04. The actual error must be greater than this since the deduced direction cosines[13,17] differ appreciably from the more accurate ones calculated from the neutron diffraction data.[4] Probably a more realistic estimate of the maximum error in the principal g values would be 0.08, thus giving a standard deviation of 0.04.

(*b*) *Results Obtained from Fitting Analyses.* As discussed previously, the major π bonding contribution from the tetrahedral water ligand derives from the oxygen ($2p_x$) orbital with a possible smaller π contribution from the ($2p_y$) orbital. As no estimates of the amount of the latter contribution can be made, one of the fitting procedures assumed that it was equal to one-third of that from the major π contribution. Another of the fitting procedures was carried out with the minor π contribution equal to zero. However, there is little effect on the values of the perturbation energies obtained from the fitting procedure when the minor π interaction is changed from zero to one-third of the major π interaction. Generally, the perturbation energies changed by less than 500 cm^{-1} which is considered to be negligible (*vide infra*). Only the results obtained when the minor π interaction is one-third of the major π interaction are further considered.

The fitting procedure revealed that to obtain physically reasonable values for the perturbation energy parameters, the electronic transition from the (z^2) orbital to the ($x^2 - y^2$) orbital may have the smallest or second smallest energy (*i.e.*, $(z^2) \rightarrow (x^2 - y^2)$ may be the first or second transition). Tables III–V show the "best-fit" perturbation energy parameters when the $(z^2) \rightarrow (x^2 - y^2)$ is the first or second transition. Also in these tables are the calculated values for the d → d electronic energies, the principal molecular susceptibilities, and the principal molecular g values which arise from the tabulated perturbation energies. Excellent correspondence between the experimental and the calculated properties has been obtained independent of whether $(z^2) \rightarrow (x^2 - y^2)$ is the first or second transition.

During the fitting procedure, it was observed that a change in the perturbation energies by a few hundred wave numbers affected the energies of the electronic transitions but had little effect on the magnetic susceptibilities of g values.

The linear combinations of the metal ion d orbitals which correspond to the "best-fit" values of Tables III–V are shown in Table VI.

Discussion of the Angular Overlap Model Results

Figures 2 and 3 show the variation of the σ and π perturbation energies with Cu–OH_2 bond lengths (from Tables III–V) when $(z^2) \rightarrow (x^2 - y^2)$ is the first and second transition, respectively. The results indicate that the σ perturbation energies decrease more sharply with increase in the Cu–OH_2 bond length than the π perturbation ener-

TABLE IV: Results Obtained at 293 K from the Fitting of the Angular Overlap Model to the Experimental Data for $K_2Cu(H_2O)_6(SO_4)_2$ with $e_{\pi c} = (1/3)e_{\pi s}$[a]

Bond length, pm	Perturbation energy, cm^{-1} Run a e_σ	Run a $e_{\pi s}$	Run b e_σ	Run b $e_{\pi s}$
227.7	370	0	0	1,210
206.7	6,250	2,340	6,010	3,330
194.3	12,150	1,700	14,190	5,030

	Experimental value[b]	Calculated value Run a	Calculated value Run b
d → d energy, cm^{-1}	9,980(150)	9,970	10,090
	11,770(150)	11,620	11,760
	12,660(150)	12,730	12,890
	14,170(150)	14,230	13,940
Magnetic susceptibility, 10^{-11} m^3 mol^{-1}	1,610(25)	1,644	1,621
	1,994(47)	1,908	1,891
	2,378(38)	2,347	2,404
Esr g value	2.055(0.04)	2.015	2.004
	2.157(0.04)	2.142	2.134
	2.384(0.04)	2.342	2.367

[a] The perturbation energies have been corrected so that the minimum value is zero. $(z^2) \rightarrow (x^2 - y^2)$ is (a) first transition, (b) second transition. [b] The estimated standard deviation is in parentheses.

TABLE V: Results Obtained at 293 K from the Fitting of the Angular Overlap Model to the Experimental Data for $(NH_4)_2Cu(H_2O)_6(SO_4)_2$ with $e_{\pi s} = (1/3)e_{\pi c}$[a]

Bond length, pm	Perturbation energy, cm^{-1} Run a e_σ	Run a $e_{\pi c}$	Run b e_σ	Run b $e_{\pi s}$
223.0	0	910	0	2940
207.3	5,990	1440	8,500	3040
196.6	12,040	1910	13,690	5700

	Experimental value[b]	Calculated value Run a	Calculated value Run b
d → d energy, cm^{-1}	10,110(150)	10,160	10,080
	11,660(150)	11,490	11,670
	12,350(150)	12,560	12,160
	13,390(150)	13,350	13,580
Magnetic susceptibility, 10^{-11} m^3 mol^{-1}	1,775(20)	1,642	1,662
	2,077(40)	1,969	1,914
	2,407(34)	2,328	2,282
Esr g value	2.058(0.04)	2.015	2.025
	2.208(0.04)	2.171	2.146
	2.358(0.04)	2.334	2.312

[a] The perturbation energies have been corrected so that the minimum value is zero. $(z^2) \rightarrow (x^2 - y^2)$ is (a) first transition, (b) second transition. [b] The estimated standard deviation is in parentheses.

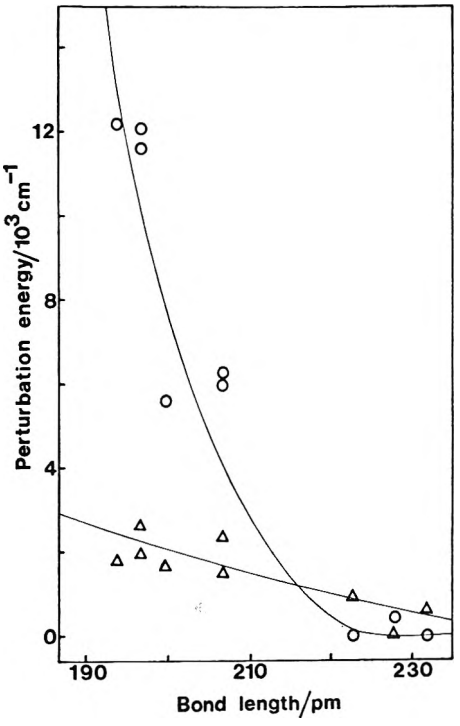

Figure 2. Variation in the perturbation energy parameters with $Cu-OH_2$ bond length when $(z^2) \rightarrow (x^2 - y^2)$ is the first transition (O represents the σ perturbation energy and Δ represents the π perturbation energy).

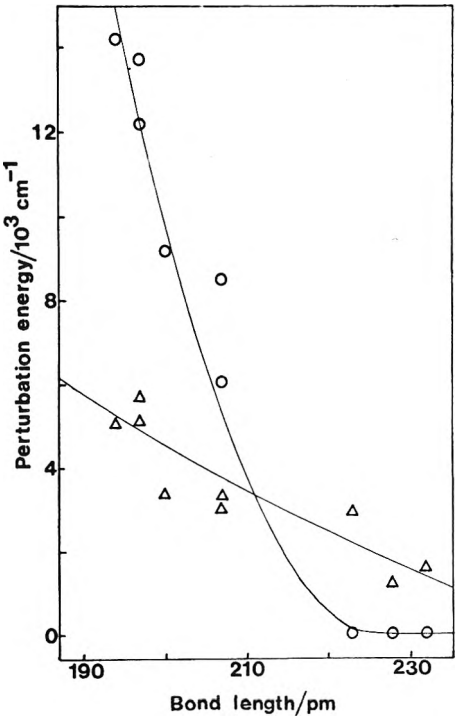

Figure 3. Variation in the perturbation energy parameters with $Cu-OH_2$ bond length when $(z^2) \rightarrow (x^2 - y^2)$ is the second transition (O represents the σ perturbation energy and Δ represents the π perturbation energy).

gies. For $(z^2) \rightarrow (x^2 - y^2)$ as the second transition (Figure 3), both the σ and π perturbations energies are larger than when $(z^2) \rightarrow (x^2 - y^2)$ is the first transition (Figure 2). Near 214 pm, the σ and π interactions are similar, and at larger bond lengths the π interaction dominates.[18] This is not consistent with the results reported by Smith[19] who found that the π overlap integrals fall off much more sharply with increasing bond lengths than σ overlaps, and that π interaction with axial ligands is probably negligible. These results by Smith[19] derive from calculations of

TABLE VI: Wave Functions Relevant to the "Best-Fit" Values in Tables III–V for the Cesium, Potassium, and Ammonium Copper Tutton's Salts[a]

Copper Tutton's salt	Run	Energy, cm^{-1}, relative to $(x^2 - y^2)$	(z^2)	$(x^2 - y^2)$	(zx)	(xy)	(yz)
Cs	a	0	$0.226i$	$0.805i$	$0.012i$	0.060	−0.033
		9,930	$-0.856i$	$0.232i$	$0.228i$	0.196	0.150
		11,590	$0.118i$	$-0.072i$	$-0.316i$	0.909	0.172
		12,400	−0.171	0.088	−0.773	$0.339i$	$-0.423i$
		13,340	−0.230	0.041	−0.426	$-0.049i$	$0.816i$
Cs	b	0	$0.097i$	$0.815i$	$0.018i$	0.063	−0.025
		9,840	$-0.054i$	$-0.040i$	$-0.153i$	0.944	0.138
		10,700	$0.851i$	$-0.101i$	$-0.327i$	0.018	−0.161
		12,350	−0.175	0.058	−0.747	$0.217i$	$-0.483i$
		13,370	−0.311	0.024	−0.443	$-0.029i$	$0.744i$
K	a	0	$0.216i$	$0.805i$	$0.013i$	0.054	−0.032
		9,970	$-0.866i$	$0.230i$	$0.267i$	0.059	0.103
		11,620	$-0.093i$	$0.003i$	$-0.558i$	0.765	0.244
		12,730	−0.209	0.097	−0.701	$0.624i$	$-0.106i$
		14,230	−0.153	0.0010	−0.199	$-0.135i$	$0.924i$
K	b	0	$0.246i$	$0.781i$	$0.009i$	0.059	−0.030
		10,090	$-0.086i$	$-0.019i$	$-0.139i$	0.952	0.130
		11,760	$0.704i$	$-0.218i$	$-0.582i$	−0.014	−0.089
		12,890	−0.379	0.153	−0.594	$0.213i$	$-0.553i$
		13,940	−0.410	0.111	−0.416	$-0.008i$	$0.709i$
NH_4	a	0	$0.219i$	$0.811i$	$0.013i$	0.052	−0.037
		10,160	$-0.862i$	$0.233i$	$0.204i$	0.102	0.242
		11,490	$0.128i$	$-0.036i$	$0.434i$	0.598	0.626

[a] $(z^2) \rightarrow (x^2 - y^2)$ is (a) first transition, (b) second transition.

diatomic σ and π overlap integrals between the copper(II) ion d orbitals and the np orbitals of various ligator atoms including oxygen. The use[19] of the radial wave functions of Clementi[20] and Richardson, *et al.*,[21] for the ligand atoms and Cu^+, respectively, and the assumption that the charge on the copper was +1, would affect the calculations but should not alter the relative importance of the σ and π overlap. Thus it appears that the disagreement arises from the results of the angular overlap model, probably from a combination of the various approximations made in the present adaptation.

For the potassium salt, the orbital containing the unpaired electron which is deduced by the angular overlap model agrees with that calculated by Hitchman.[22] The angular overlap model predicts that the probability of the unpaired electron being found along the Z, X, and Y axes is approximately 5, 32, and 63% while Hitchman found the probabilities to be about 2, 38, and 60%. Similar probabilities to those for the potassium salt are found from the angular overlap model for the cesium and ammonium salts.

The position of the (z^2) orbital cannot be unequivocally ascertained, but the polarized crystal spectral results tentatively suggested that $(z^2) \rightarrow (x^2 - y^2)$ is the second transition. The interchange of $(z^2) \rightarrow (x^2 - y^2)$ from the first to the second transition may arise from stronger π bonding, and this has been observed for a tetragonally distorted octahedral complex.[23] Since the π bonding from tetrahedral water is less than trigonal water,[24] it would not be expected that the π bonding in the Tutton's salts would be sufficient to cause $(z^2) \rightarrow (x^2 - y^2)$ to be the second transition. Thus, it seems more realistic for the $(z^2) \rightarrow (x^2 - y^2)$ transition to be the lowest energy one.

The predicted ordering of the d orbitals for the cesium and potassium salts, *viz.* $(x^2 - y^2) > (z^2) > (xy) > (zx) > (yz)$, is consistent with that proposed by Billing and Hathaway[25] for orthorhombic distortion. The ordering for the ammonium salt is different, being $(x^2 - y^2) > (z^2) > (zy) > (xy) > (zx)$. This change arises as a consequence of the direction of π interaction. To the knowledge of the author, the interchange of the "t_{2g}" orbitals by the type of π interaction has not been reported previously. Further experimental work should be done to investigate this.

Evaluation of Usefulness of the Angular Overlap Model

To explain magnetic susceptibilities and g values, magnetochemists have generally used the crystal field model in which the formation of molecular orbitals is accounted for by the inclusion of the orbital reduction factor. The interpretation of the orbital reduction factor does not easily afford a description of σ and π bonding.[26] In contrast, the perturbation energy parameters of the angular overlap model which satisfactorily explains the electronic spectra, magnetic susceptibilities, and g values are readily interpretable in terms of σ and π bonding.

The perturbation energy parameters vary according to the metal–ligand bond lengths. Thus, if tetrahedral water is bonded to copper(II) ion and the Cu–OH_2 bond length is known, the relevant perturbation energy can be obtained from Figures 2 or 3. If similar graphs could be determined for other types of ligands, it should be possible to predict the electronic and associated magnetic properties of the Cu(II) ion complex.

Acknowledgments. Dr. C. E. Schäffer and Professor C. K. Jorgensen are thanked for helpful suggestions during the development of this work. A grant from the Australian Research Grants Committee enabled construction of the Faraday magnetic balance. One of us (R. C. M.) acknowledges receipt of a Commonwealth Postgraduate Award.

References and Notes

(1) B. N. Figgis, *Trans. Faraday Soc.*, **57**, 198, 204 (1961); B. N. Figgis, J. Lewis, F. E. Mabbs, and G. A. Webb, *J. Chem. Soc. A*, 1411 (1966); 442 (1967); B. N. Figgis, M. Gerloch, J. Lewis, F. E. Mabbs, and G. A. Webb, *ibid.*, 2086 (1968).

(2) R. C. Marshall and D. W. James, *J. Inorg. Nucl. Chem.*, **32**, 2543 (1970).
(3) B. N. Figgis, *Trans. Faraday Soc.*, **56**, 1553 (1960); E. Konig and A. S. Chakravarty, *Theor. Chim. Acta*, **9**, 151 (1967); M. Gerloch, *J. Chem. Soc. A*, 2021 (1968); B. N. Figgis, M. Gerloch, and R. Mason, *Proc. Roy. Soc., Ser. A*, **279**, 210 (1964).
(4) D. J. Robinson and C. H. L. Kennard, *Cryst. Struct. Commun.*, **1**, 185 (1972); K. G. Shields and C. H. L. Kennard, *ibid.*, **1**, 189 (1972).
(5) C. E. Schaffer, *Structure Bonding*, **5**, 68 (1968).
(6) D. W. Smith, *J. Chem. Soc. A*, 1708, 2529 (1969); 176 (1970).
(7) E. U. Condon and G. H. Shortley, "Theory of Atomic Spectra," Cambridge University Press, New York, N. Y., 1951.
(8) C. A. Coulson, "Valence," 2nd ed, Oxford University Press, London, 1961.
(9) M. Wolfsberg and L. Helmholtz, *J. Chem. Phys.*, **20**, 837 (1952).
(10) C. K. Jorgensen, "Orbitals in Atoms and Molecules," Academic Press, London, 1962.
(11) J. H. Van Vleck, "Theory of Electric and Magnetic Susceptibilities," Oxford University Press, London, 1932.
(12) M. J. D. Powell, *Computer J.*, **7**, 155 (1964).
(13) A. Bose, U. S. Ghosh, R. N. Bagchi, and A. K. Pal, *Ind. J. Phys.*, **38**, 361 (1964).
(14) R. Chidambaram, A. Sequeira, and S. K. Sikha, *J. Chem. Phys.*, **41**, 3616 (1964).
(15) F. O. Ellison and H. Shull, *J. Chem. Phys.*, **23**, 2348 (1955).
(16) D. W. James and R. C. Marshall, to be submitted for publication.
(17) A. K. Pal, R. N. Bagchi, P. R. Saha, and R. K. Shaha, *Ind. J. Phys.*, **41**, 856 (1967).
(18) For the situation when $(z^2) \rightarrow (x^2 - y^2)$ is the first transition, the difference between the σ and π perturbation energies is almost inconsequential with regards to the magnetic properties because the maximum difference of 900 cm^{-1} would not significantly alter the calculated magnetic susceptibilities and g values.
(19) D. W. Smith, *J. Chem. Soc. A*, 1498 (1970).
(20) E. Clementi, IBM Technical Report, No. R.J.-256 (1963).
(21) J. W. Richardson, W. C. Niewpoort, R. R. Powell, and W. F. Edgell, *J. Chem. Phys.*, **36** 1057 (1962); J. W. Richardson, R. R. Powell, and W. C. Niewpoort, *ibid.*, **38**, 796 (1963).
(22) M. A. Hitchman, *J. Chem. Soc. A*, 4 (1970).
(23) D. E. Billing, B. J. Hathaway, and P. Nicholls, *J. Chem. Soc. A*, 316 (1969).
(24) C. K. Jorgensen, "Inorganic Complexes," Academic Press, London, 1963.
(25) D. E. Billing and B. J. Hathaway, *J. Chem. Soc. A*, 1516 (1968).
(26) M. Gerloch and J. R. Miller, *Progr. Inorg. Chem.*, **10**, 1 (1968).

COMMUNICATIONS TO THE EDITOR

Notes on the Intermolecular Energy of Fluids at the Critical Temperature and Its Dependence on the Temperature

Publication costs assisted by the American Petroleum Institute

Sir: It is well known that the second virial coefficient derived from the hard-sphere equation of state with a van der Waals attraction term is

$$\beta = 4b(T) - a(T)/(RT) \tag{1}$$

where $b(T) = \frac{1}{6}\pi N_0 \sigma_e^3$, N_0 is the Avogadro number, and σ_e is the effective collision diameter that varies with the temperature. $a(T)$ and σ are related to the critical temperature T^c and the *corrected* liquid molar volume V^* at $T/T^c = 0.6$ as follows[1,2]

$$\frac{1}{6}\pi N_0 \sigma^3 = 0.434 V^* \qquad a^c = 4.65 R T^c V^* \tag{2}$$

where σ is the value of σ_e at $T = 0$ and a^c is the value of $a(T)$ at $T = T^c$. Analogous relations are obtained by using the critical volume V^c instead of V^*. Thus, the values of β/V^* of different substances at the critical temperature, β^c/V^*, should be identical. This is, however, not true.

Recently, Lal and Spencer[3] obtained the values of σ_e and the pair potentials $u(r)$ for n-alkanes (C_1 to C_5) by the Monte-Carlo simulation of chain molecules. The values of $(\sigma_e)^3$ are surprisingly small and they vary approximately linearly with $(V^*)^{2/3}$, not with V^*. The line passes through the origin and this result implies that $b(T)_{MC} \sim (V^*)^{2/3}$ and

$$\beta^c/(V^*)^{2/3} = c_1 - c_2(V^*)^{1/3} \tag{3}$$

where the constants evaluated by the method of least squares for 12 substances are $c_1 = 3.41$ and $c_2 = 4.121$. The values of β^c were taken from the recently published tables.[4] The results shown in Figure 1 confirm the validity of eq 3.

This result also implies that the product $T^c V^*$ in eq 2 is in fact $T^c(V^*)^{1/3}(V^*)^{2/3}$, where $T^c(V^*)^{1/3}$ is proportional to the minimum value of $u(r)$. It has been shown elsewhere[5] for several substances that $T^c(V^*)^{1/3}/T_0^c(V_0^*)^{1/3} \approx \bar{u}/\bar{u}_{00}$, where $\bar{u}/k$ are the minimum values of $u(r)$ obtained for the Kihara potential and subscript 00 denotes a reference substance (argon, $\bar{u}_{00}/k = -166$ K).

Equation 3 is valid at $T = T^c$ only. According to Rowlinson's theory of noncentral forces,[6] in general $\bar{u} = \bar{u}_0(1 + \eta/(kT))$ and η/k can be estimated from Pitzer's acentric factor[7] ω

$$\eta/k \approx 0.833 \omega T^c \tag{4}$$

Accordingly

$$a(T) = 4.65 R T_0^c \left(1 + \frac{\eta}{kT}\right) V^* \tag{5}$$

where $T_0^c = T^c(1 + \eta/(kT^c))^{-1}$ and eq 5 simplifies to eq 2 for $T = T^c$. Equations 4 and 5 were recently applied to the evaluation of the excess functions of mixtures[2] with satisfactory results. Below, the values of η/k obtained from observed energies of vaporization of liquids U^* at $T/T^c = 0.6$ are compared with η/k calculated from eq 4. U^* is equal to the residual energy $(U - U_{id})$ where U_{id} is that of a perfect gas. The part due to attraction is obtained from the relations

$$U - U_h = U^* - (U_h - U_{id}) \tag{6}$$

where $(U_h - U_{id})$ is the residual energy of hard spheres

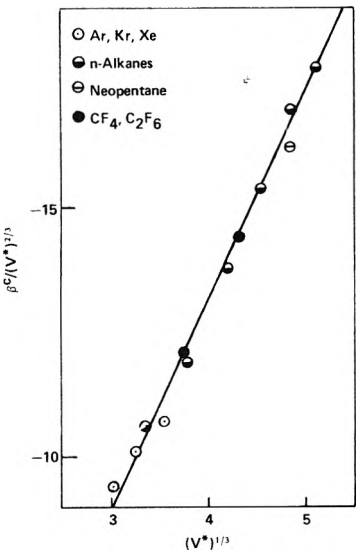

Figure 1.

TABLE I: Some of the Intermolecular Energy Parameters (in Kelvins)

	η/k (eq 4)	η/k (eq 8)	$(U_h - U_{id})/R$ (eq 7)[a]
Argon	−0.3	6.9	45
Krypton	−0.3	3.8	63
Xenon	+0.5	4.2	81
Methane	2.1	7.1	55
Ethane	27	26	79
Propane	47	50	81
n-Butane	71	71	81
n-Pentane	99	102	77
n-Hexane	123	136	73
Neopentane	70	73	70
Tetrafluoromethane	36	38	58
Perfluoro-*n*-hexane	183	281	46
Methanol	237	263	152
Ethanol	273	388	129

[a] For the liquid at $T/T^c = 0.6$.

(for references see ref 1)

$$(U_h - U_{id})/(RT) = -2T(\partial\xi/T)_v[(1 - \xi)^{-2} + (1 - \xi)^{-3}] \quad (7)$$

$$-(U - U_h)/(RT) = 4.65V^*T_0^c(1 + 2\eta/(KT))/(TV) \quad (8)$$

where $\xi = b(T)/V$ and $(\partial\xi/\partial T)_v$ were evaluated as before.[1] V was set equal to the observed liquid molar volume at $T/T^c = 0.6$ that for small molecules is slightly larger than V^*. The values of η/k obtained from eq 8 are given in Table I. $(U_h - U_{id})$ is positive and increases the absolute value of $(U - U_h)$ so that the values of η/k of the rare gases are positive. They are certainly better than the values of η/k obtained from vapor pressures and P^c (*i.e.*, from ω) where the hard-sphere correction cannot be evaluated.

It is known that the Kihara potential fails to reproduce well the values of β for fluorocarbons and other gases with specific interactions. The above results suggest the following relation for $\bar{u}/k$ suitable in application of the Kihara potential

$$\bar{u}/k = -0.3635T^c(V^*)^{1/3}(1 + \eta/(kT))(1 + \eta/(kT^c))^{-1} \quad (9)$$

fitting $\bar{u}/k = -166$ K for argon[8] ($(V^*)^{1/3} = 3.028$ cm $mol^{-1/3}$).

These results show that the hard-sphere equation of state with a van der Waals attraction term is suitable at high densities of a fluid. It is unclear why $\phi(\xi)$ "degenerates" to the form of eq 3 at very low densities.

References and Notes

(1) A. Kreglewski, R. C. Wilhoit, and B. J. Zwolinski, *J. Chem. Eng. Data*, **18**, 432 (1973); *J. Phys. Chem.*, **77**, 2212 (1973).
(2) A. Kreglewski and R. C. Wilhoit, prepared for publication.
(3) M. Lal and D. Spencer, *J. Chem. Soc., Faraday Trans. 2*, 1502 (1973).
(4) B. J. Zwolinski, *et al.*, "Selected Values of Properties of Hydrocarbons and Related Compounds," API Research Project 44, TRC Data Project, Texas A & M University, College Station, Tex.
(5) A. Kreglewski, "Mixtures of Fluids," API44-TRC Publications, Thermodynamics Research Center, Texas A & M University, College Station, Tex. 1973.
(6) J. S. Rowlinson, "Liquids and Liquid Mixtures," Butterworths, London, 1959.
(7) The values of acentric factors are given by R. C. Reid and T. K. Sherwood, "The Properties of Gases and Liquids," McGraw-Hill, New York, N. Y., 1966.
(8) G. A. Pope, P. S. Chappelear, and R. Kobayashi, *J. Chem. Phys.*, **59**, 423 (1973).

Thermodynamics Research Center **Aleksander Kreglewski**
Texas A & M University
College Station, Texas 77843

Received February 21, 1974

Equivalent Conductances of Univalent Counterions and Coions in Polyelectrolyte Solutions

Sir: Nagasawa, Noda, Takahashi, and Shimamoto[1] have recently published detailed data on the equivalent conductances of Na^+ and Cl^- in solutions of poly(acrylic acid) neutralized to various degrees by NaOH. Their results, which contain several interesting features, including a transition with decreasing NaCl concentration from positive to negative equivalent sodium conductances, have motivated us to extend a previous calculation[2-4] of counterion transport in a solution of polyelectrolyte salt to a solution which contains an additional component of simple salt. We will restrict attention to univalent counterions and coions and reserve for another context the extension to multivalent species.

Extension of the theory to the case of added salt is straightforward, since this problem has already been solved for the tracer diffusion coefficients of counterion and coion.[2] We recall the starting point of the diffusion theory

$$j_i = (-kT/\zeta_i^0)[\nabla n_F^i + n_F^i z_i \nabla\phi_F - n_F^i F_i/kT)] \quad (1)$$

In this equation j_i is the local flux of counter- or coions of species i with valence z_i, ζ_i^0 is the friction constant of such ions at infinite dilution in the pure solvent, F_i is an externally imposed uniform force on each ion i, n_F^i is the local concentration of i as perturbed by this external force, and $\phi_F = e\psi_F/kT$, where e is the protonic charge and ψ_F is the locally inhomogeneous electrostatic potential set up by the polyions and perturbed by the influence of the external force on the ionic atmospheres. In the diffusion theory the introduction of F_i is merely a device to allow later ap-

plication of the Einstein relation between friction constants and tracer diffusion constants. For the conductance problem, however

$$F_i = z_i e E \tag{2}$$

where E is the external electric field. Equation 1 then describes the local flux of counter- and coions as due to diffusion along local concentration gradients and drift velocities caused by the locally inhomogeneous polyion field and the uniform external field.

It remains to describe the perturbations in terms of the equilibrium distribution of all species and then to perform the appropriate averages to convert the local flux to the macroscopically observable one. This problem was solved in detail for tracer diffusion in ref 2. For conductance, the procedure is parallel, but the equation of continuity is different[3]

$$\nabla(j_i - n_F{}^i v_p) = 0 \tag{3}$$

where

$$v_p = u_p E \tag{4}$$

is the uniform drift velocity of the polyions under the influence of the external field, and u_p is the electrophoretic mobility of the polyion (positive for a polycation, negative for a polyanion). This form of the equation of continuity simply recognizes that the appropriate frame of reference for eq 1 is on the moving polyion.

We recall further[2] that the model chosen for the polyion and used to obtain the equilibrium structure of the solution is an infinitely long line charge characterized by a dimensionless charge density ξ

$$\xi = e^2/\epsilon kTb \tag{5}$$

where ϵ is the dielectric constant of the bulk solvent and b is the average charge spacing along the axis of the real polyion chain (*i.e.*, contour length divided by number of charged groups). For univalent counterions, the value $\xi = 1$ is critical. If $\xi < 1$ no counterions are associated with the polyion and eq 1 gives the total local flux of counterions. However, if $\xi > 1$, the fraction $1 - \xi^{-1}$ of the total polyion charge is neutralized by condensation of counterions, so that the net polyion charge density corresponds to $\xi = 1$. In this case eq 1 describes the local flux of the uncondensed counterions only, whereas the total observed counterion flux includes that of the condensed counterions. The latter is obtained by neglecting the mobility along the polyion chain of a condensed counterion, so that each condensed counterion has the velocity v_p given by eq 4.

At this point we forego further detail and state the final results

$$\lambda_1 = \lambda_1{}^0(D_1/D_1{}^0) - \lambda_p[1 - (D_1/D_1{}^0)] \tag{6}$$

$$\lambda_2 = \lambda_2{}^0(D_2/D_2{}^0) + \lambda_p[1 - (D_2/D_2{}^0)] \tag{7}$$

The counterion is designated as species 1, the coion as species 2, the polyion as species p. The quantity λ_i is the equivalent conductance of species i (based on stoichiometric charge and concentration, not on net values after counterion condensation). The quantity $\lambda_i{}^0$ is the limiting equivalent conductance of species i in pure solvent; it is derived from the friction constant $\zeta_i{}^0$ in eq 1. The ratio $D_i/D_i{}^0$ is that of the self-diffusion constant D_i of species i in the polyelectrolyte solution to its value $D_i{}^0$ in pure solvent. Expressions for $D_i/D_i{}^0$ are given in ref 2 in terms of rapidly converging infinite series (see eq 33 of ref 2 for $\xi < 1$ and eq 39 and 40 for $\xi > 1$).

TABLE I: Comparison of Calculated Counterion Equivalent Conductances with Observed Values

α	x_e	$\lambda_1{}^0$	$\lambda_p{}^{obsd}$	$(D_1/D_1{}^0)_{calcd}$	$\lambda_1{}^{calcd}$	$\lambda_1{}^{obsd}$
1.00[a]	0.30	42.3	30.0	0.79	26.9	27.7
1.00[a]	0.47	44.4	29.8	0.68	20.6	19.7
1.00[a]	0.81	47.9	40.9	0.44	−1.9	−1.2
0.90[b]	1.00	50.1	43.5	0.34	−11.7	−11.8
0.60[a]	0.21	42.3	27.6	0.90	35.1	33.1
0.60[a]	0.34	44.4	32.5	0.82	30.7	29.9
0.60[a]	0.72	47.9	37.8	0.64	17.0	7.2
0.60[b]	1.00	50.1	45.2	0.51	3.4	−2.1

[a] Data from ref 1. [b] Data from ref 5.

TABLE II: Comparison of Calculated Coion Equivalent Conductances with Observed Values[a]

α	x_e	$\lambda_2{}^0$	$\lambda_p{}^{obsd}$	$(D_2/D_2{}^0)_{calcd}$	$\lambda_2{}^{calcd}$	$\lambda_2{}^{obsd}$
1.00	0.30	64.5	30.0	0.98	63.8	60.4
1.00	0.47	66.7	29.8	0.96	65.2	70.2
1.00	0.81	70.6	40.9	0.91	68.0	70.6
0.60	0.21	64.5	27.6	0.98	63.7	65.9
0.60	0.34	66.7	32.5	0.96	65.4	65.5
0.60	0.72	70.6	37.8	0.91	67.7	91.7[b]

[a] All data from ref 1. [b] This value appears to be inconsistent with the other observed values in this column.

There are only two parameters in the theoretical expressions for $D_i/D_i{}^0$ in ref 2, the charge parameter ξ, and the ratio $X = n_e/n_s$, where n_e is the stoichiometric equivalent polyion concentration and n_s the concentration of uni-univalent salt. Instead of X, we will here use equivalent fractions

$$x_e = n_e/(n_e + n_s) \quad x_s = n_s/(n_e + n_s) \tag{8}$$

since the restriction of x_e to values between zero and unity provides a more compact description of the solution composition. Since $X = x_e/x_s = x_e/1 - x_e$, we trust that no confusion will arise from this minor shift in notation. We recall some important qualitative features of $D_i/D_i{}^0$

$$D_1/D_1{}^0 = D_2/D_2{}^0 < 1 \qquad \xi < 1 \tag{9}$$

$$D_1/D_1{}^0 < D_2/D_2{}^0 < 1 \qquad \xi > 1 \tag{10}$$

Equations 6 and 7 are of some interest for the understanding of the structure of polyelectrolyte solutions. The motion of the polyion is seen to diminish the conductance of the counterion but to augment that of the coion. The polyion "carries along" its diffuse ionic atmosphere, which consists of both counterions and coions. The participation of coions in the ionic atmosphere of polyions (*i.e.*, the significant electrostatic interaction of coions with the polyion) is often not appreciated in the polyelectrolyte literature. Moreover, for $\xi < 1$, eq 9 indicates that the interaction of the counterion with the polyion is no stronger than that of the coion; therefore, on no account should the diminution of λ_1 be ascribed to "ion binding." For $\xi > 1$, of course, part (but not all) of the term proportional to λ_p is due to the condensed counterions which travel with the polyion because they are bound to it.

In Tables I and II we have compared eq 6 and 7 with the data of Nagasawa, *et al.*[1] The calculated values of λ_1 and λ_2 were obtained by using *theoretical* values of $D_i/D_i{}^0$ from ref 2 and *measured* values of λ_p from ref 1. since the present theory does not treat the electrophoretic mobility of the polyion, but only of the small ions. The first col-

umn gives the degree of neutralization α of the polyacid; the value of ξ is given by 2.85α at 25°, since the charge spacing b for a fully charged vinylic chain is 2.5 Å, or ξ = 2.85. Note that ξ is fixed by structural knowledge of the chain; hence D_i/D_i^0 is calculated on a purely *a priori* basis with no flexible parameters. A minor problem is presented by λ_i^0. Since eq 6 and 7 are limiting laws, strictly valid only at infinite dilution, it is clear that in the theory λ_i^0 is the ionic conductance in pure solvent. However, it is also seen from eq 6 and 7 that λ_i^0 is the value of λ_i when $x_e = 0$ (since then $D_i/D_i^0 = 1$). Therefore it is reasonable to take λ_i^0 as the equivalent conductance of i in a solution with $n_e = 0$ (no polyelectrolyte) and n_s equal to the uni-univalent salt concentration present in the polyelectrolyte solution for which λ_i is measured. This procedure forces agreement of theory and observation at $x_e = 0$; it is, of course, strictly empirical, since interactions of small ions with the polyion (counterion condensation, Debye-Hückel cylindrical atmosphere) continue to be treated by a theory rigorously valid only in the limit of zero concentration. A rigorous method would be to use λ_i^0 as the limiting value in pure solvent for the theory and to extrapolate the data at fixed x_e to $n_s = 0$; however, the measurements of Nagasawa, *et al.*, were not so designed.

Agreement of the last two columns in each table is quite good. In particular, for $\alpha = 1.0$, the transition of λ_1 from positive to negative values as x_e increases is predicted correctly, including the value of x_e at which $\lambda_1 = 0$ (x_e somewhat less than 0.80). To round out the picture in Table I, we included two entries at $x_e = 1$ from the data of Wall and Hill.[5] From Table II it is seen that λ_2 is almost insignificantly different from λ_2^0. It may not thereby be inferred that the coion does not interact significantly with the polyion. Equation 7 indicates that the interaction should be measured by D_2/D_2^0, which, as indicated in Table II, deviates by as much as 9% from unity. (Actually, the self-diffusion theory gives the value of D_2/D_2^0 = 0.87 as x_e tends to unity, a value which has recently been closely confirmed by Menezes-Affonso and Ander.[6]) The reason that $\lambda_2 \approx \lambda_2^0$ in this case is that the diminution caused by attraction of the coion into the ionic atmosphere of the polyion (first term in eq 7) is balanced by the augmentation due to the directed motion of the polyion (second term).

Incidentally, Schmitt and Varoqui[7] have demonstrated that the requirement of mechanical equilibrium during conductance experiments implies that λ_1 cannot be negative unless some of the counterions are associated with the polyion. This requirement is consistent with the results in Table I, since all values of α correspond to $\xi > 1$ so that counterion condensation occurs. We repeat, however, that the negative contribution to λ_1 in eq 6 is only *partly* accounted for by the condensed counterions when $\xi > 1$, the other contribution being due solely to diffuse atmosphere effects. It may also be noted that Schmitt and Varoqui[7] have derived eq 6 for salt-free polyelectrolyte solutions by a phenomenological approach.

References and Notes

(1) M. Nagasawa, I. Noda, T. Takahashi, and N. Shimamoto, *J. Phys. Chem.*, **76**, 2286 (1972).
(2) G. S. Manning, *J. Chem. Phys.*, **51**, 934 (1969).
(3) G. S. Manning, *J. Chem. Phys.*, **47**, 2010 (1967).
(4) G. S. Manning, *Biopolymers*, **9**, 1543 (1970).
(5) F. T. Wall and W. B. Hill, *J. Amer. Chem. Soc.*, **82**, 5599 (1960).
(6) S. Menezes-Affonso and P. Ander, *J. Phys. Chem.*, in press.
(7) A. Schmitt and R. Varoqui, *J. Chem. Soc., Faraday Trans. 2*, **69**, 1087 (1973).

School of Chemistry
Rutgers University
The State University
New Brunswick, New Jersey 08903

David I. Devore
Gerald S. Manning*

(*Received January 10, 1974*)

lege

Prof.
Prof.
Prof.
Prof.
st. Prof.

:y

8-2261

hD, Professor
D, Professor
ofessor
D, Assoc. Prof.
Assoc. Prof.
Assoc. Prof.
hD, Assoc. Prof.
Assoc. Prof.
, Assoc. Prof.
H., MS, Assoc. Prof.
PhD, Assoc. Prof.
D, Asst. Prof.
hD, Asst. Prof.
, Asst. Prof.
hD, Asst. Prof.
, Asst. Prof.
, PhD, Asst. Prof.
hD, Asst. Prof.

orgia

try,

stry
., PhD, Professor
., PhD, Professor
hD, Professor
rt A., PhD, Professor
, PhD, Professor
n J., PhD, Res. Prof.
liam L., PhD, Res. Prof.
M., PhD, Assoc. Prof.
V. Scott, PhD, Assoc. Prof.
n, Daniel V., PhD, Assoc. Prof.
d V., BS, Assoc. Professor
., PhD, Assoc. Prof.
n, PhD, Assoc. Prof.
Lars G., PhD, Assoc. Prof.
bert E., PhD, Assoc. Prof.
, Joseph F., PhD, Assoc. Prof.
mes, PhD, Assoc. Prof.
ald S., PhD, Asst. Prof.
chard J., PhD, Asst. Prof.
Norman G., PhD, Asst. Prof.
va, Prakash N., PhD, Asst. Prof.
er, John E., PhD, Asst. Prof.

y of Georgia
0602
y Dept., (404) 542-2626
Chemistry
on, Charles E. (H), PhD, Professor
Richard K., PhD, Professor
etier, S. William, PhD, Professor
brook, George E., PhD, Professor
nger, Norman L., PhD, Res. Prof.
ng, R. Bruce, PhD, Res. Prof.
aldwin, Winfield M., PhD, Assoc. Prof.
ox, Richard H., PhD, Assoc. Prof.
st, John F., PhD, Assoc. Prof.

P Handler, George S., PhD, *Assoc. Prof.*
P Hercules, David M., PhD, *Assoc. Prof.*
O Heric, Eugene L., PhD, *Assoc. Prof.*
P Janzen, Edward G., PhD, *Assoc. Prof.*
I Johnston, Francis J., PhD, *Assoc. Prof.*
P King, Allen D., PhD, *Assoc. Prof.*
O Ruff, John K., PhD, *Assoc. Prof.*
G Smith, Darwin W., PhD, *Assoc. Prof.*
O Stammer, Charles H. PhD, *Assoc. Prof.*
A Waggoner, William H., PhD, *Assoc. Prof.*
A Whitten, Kenneth W., PhD, *Assoc. Prof.*
O Carr, Peter W., PhD, *Asst. Prof.*
P Cassen, Tom, PhD, *Asst. Prof.*
I Hautala, Richard R., PhD, *Asst. Prof.*
P Kelly, Patrick C., PhD, *Asst. Prof.*
P Klatt, Leon N., PhD, *Asst. Prof.*
A Nelson, Robert F., PhD, *Asst. Prof.*
A Newton, Gary M., PhD, *Asst. Prof.*
A Schelly, Zoltan A., PhD, *Asst. Prof.*
A Wynne, Kenneth J., PhD, *Asst. Prof.*
A Bobbio, Stephen M., PhD, *Instructor*
A Carreira, Nionel A., PhD, *Instructor*
A Kutal, Charles R., PhD, *Instructor*
A Leyden, Donald E., PhD, *Instructor*
A Seitz, William R., PhD, *Instructor*

University of Georgia

Athens 30602
Dept. of Medicinal Chemistry,
(404) 542-3077
B, M, D, Medicinal Chemistry

X LaRocca, Joseph P. (H), PhD, *Professor*
OX Blanton, DeWitt C., Jr., PhD, *Assoc. Prof.*
OX Honigberg, Irwin L., PhD, *Assoc. Prof.*
AX Stewart, James T., PhD, *Assoc. Prof.*
BX Thompson, Bobby B., PhD, *Assoc. Prof.*
BX Martinelli, Louis C., PhD, *Asst. Prof.*
AX Sternson, Larry A., PhD, *Asst. Prof.*

Gordon Junior College (2)

Barnesville 30204
Dept. of Math-Science, (205) 358-1700,
Ext. 72

AGO Smith, Maurice R., MS, *Instructor*

LaGrange College

LaGrange 30240
Dept. of Chemistry, (404) 882-2911,
Ext. 71
B, Chemistry

ABGO Hicks, Arthur M. (H), PhD, *Professor*
AIPX Hicks, Patrick M., MS, *Assoc. Prof.*
ABOP Cooper, Kenneth, PhD, *Asst. Prof.*

Macon Junior College (2)

Macon 31206
Div. of Natural Sciences and Mathematics,
(912) 745-8551, Ext. 262, 263

G Dever, David F., PhD, *Assoc. Prof.*

Mercer University

Macon 31207
Dept. of Chemistry, (912) 743-1511,
Ext. 287
B, Chemistry

AG James, Franklin W. (C), PhD, *Professor*
AIG Furse, Clare T., PhD, *Professor*
GP Marquart, John R., PhD, *Assoc. Prof.*
OX Wiesler, Donald P., PhD, *Asst. Prof.*
GO Taylor, Robert E., MEd, *Instructor*

Mercer University in Atlanta

Atlanta 30341
Dept. of Science and Mathematics,
(404) 451-0331, Ext. 46
B, Chemistry

AIGO Edwards, Henry L. (C), PhD, *Professor*

A New ACS Audio Course

ACS AUDIO COURSES

The Use of Chemical Abstracts

by O. Bertrand Ramsay

THE COURSE

This ACS Audio Course is designed to teach the effective use of **Chemical Abstracts**. The tutorial portion of the course is presented on either a sound/slide or sound/filmstrip combination and is organized as follows:

Part 1: Format and organization of **Chemical Abstracts**

Part 2: Content and use of **CA** Indexes: Author, Numerical Patent, Patent Concordance, Keyword, Subject, Formula, HAIC, Registry Number, Ring Systems

Part 3: Content and use of: Ring Index and Supplements; Decennial and Collective Indexes; Index Guide; **Chemical Abstracts Service Source Index**

A workbook is included to aid the listener in actual hands-on experience with **CA** volumes and indexes.

THE LECTURER

O. Bertrand Ramsay received his B.S. from Washington and Lee University in 1955 and his Ph.D. from the University of Pennsylvania in 1960. Dr. Ramsay has had post-doctoral fellowships at Georgia Institute of Technology and Northwestern University and has served on the faculty of the University of the Pacific. He is now Associate Professor of Chemistry at Eastern Michigan University, where he has been since 1965.

THE UNIT

The complete unit includes the following:

3 audio cassettes (total length, 50 min.)
131 transparencies (either 131 plastic-mounted 35-mm slides **or** 3 filmstrips)
1 workbook (problems, hints, answers, supplementary problems; 47 pp.)
1 booklet of answers to supplementary problems (12 pp.)
1 script, complete with reproductions of all transparencies (49 pp.)

PURCHASE/ APPROVAL

Complete unit: $160.00 (slide)
$125.00 (filmstrip)
Additional workbooks: $3.00 (1-9 copies)
$2.25 (10 or more copies)

All purchases may be returned within 10 days for full refund or invoice cancellation.

OTHER TOPICS AVAILABLE

Technical Writing • Orbital Symmetry • Liquid Chromatography • Infrared Spectra • Acids/Bases • Fluorescence/ Phosphorescence • Organic Synthesis • R & D Management • NMR • Raman Spectroscopy • Gel Permeation Chromatography • Ion-Selective Electrodes • Crystalline Polymers • Organometallic Compounds • Organofluorine Compounds

Send coupon below for complete information.

ORDER FORM — **CHEMICAL ABSTRACTS**

Department of Educational Activities, American Chemical Society
1155—16th Street, N.W., Washington, D.C. 20036

Please allow 3 to 5 weeks for delivery.

☐ Please send _____ complete slide units at $160 per unit.

☐ Please send _____ complete filmstrip units at $125 per unit.

☐ Please send _____ extra copies of the workbook.

☐ Please send an invoice. ☐ Payment is enclosed.

NOTE: Payment must accompany orders of less than $10.

☐ Please send brochure describing all ACS Study Units currently available.

Organization _____

Address _____

Authorized Individual _____ Phone _____